12-2012

PVT Study of Selected UAE Reservoir Fluids

Rashid Sher Mohammad

جامعة الإمارات العربية المتحدة
United Arab Emirates University

UAEU College of Engineering

PVT Study of Selected UAE Reservoir Fluids

By

Rashid Sher Mohammad
Department of Chemical and Petroleum Engineering
Faculty of Engineering
United Arab Emirates University

A thesis submitted in partial fulfillment of the requirements for the
Degree of Master of Science in Petroleum Engineering

Master Program of Petroleum Engineering
Department of Chemical and Petroleum Engineering
Faculty of Engineering
United Arab Emirates University

December 2012

United Arab Emirates University
Faculty of Engineering
M.Sc. Program in Petroleum Science & Engineering

PVT Study of Selected UAE Reservoir Fluids

By
Rashid Sher Mohammad

Submitted to
United Arab Emirates University in Partial Fulfillment of the Requirements for the Degree of Master of Science in Petroleum Science & Engineering

December 2012

United Arab Emirates University

Faculty of Engineering

M.Sc. Program in Petroleum Science & Engineering

Thesis Title: PVT Study of Selected UAE Reservoir Fluids

Author Name: Rashid Sher Mohammad

Supervisor(s):

Name	Position
Dr. Samir I. Abu-Eishah (Supervisor)	Associate Professor, Chemical Engineering
Dr. Mohamed A. Nakoua (Ex-Supervisor)	Assistant Professor, Chemical Engineering

December 2012

Thesis of Rashid Sher Mohammad

Title: **PVT Study of Selected UAE Reservoir Fluids**

Submitted in Partial Fulfillment for the Degree of

Master of Science in Petroleum Science & Engineering

Chair of Examination Committee

Dr. Samir I. Abu-Eishah

Chemical & Petroleum Engineering Department

United Arab Emirates University

External Examiner:

Prof. Georgios Kontogeorgis

DTU Chemical Engineering
Department of Chemical and Biochemical Engineering CERE
Technical University of Denmark

Internal Examiner:

Prof. Abdurazak Zekri

Chemical & Petroleum Engineering Department

United Arab Emirates University

Program Director (Petroleum Science & Engineering):

Dr. Sulaiman Al-Zuhair

Chemical & Petroleum Engineering Department

United Arab Emirates University

Associate Dean for Research & Graduate Studies:

Dr. Ali Al-Marzouqi

United Arab Emirates University

December 2012

Abstract

Phase behavior modeling in crude oil includes prediction of thermodynamic properties (such as saturation pressure, density, viscosity, thermal conductivity, etc.) for the vapor and liquid phases. The aim of phase behavior modeling is to establish the accuracy and reliability of the developed equation of state model to predict various other fluid phase behavior properties at high pressure and temperature conditions.

In the first part of this work, a new and reliable phase behavior apparatus designed in Brazil was used for the two-stage recombination process and phase behavior measurements. The recombination of the surface sample fluids (first-stage separator gas and stock-tank oil) was used in this work in order to reproduce the original oil composition. Initially, a precise amount of stock-tank oil is introduced into the PVT cell, and then a pre-calculated amount of the gas from the first-stage separator was injected to the PVT cell. The test was started at a pressure well above the bubble point until getting a monophasic fluid, and then it was reduced stepwise until the first bubble was observed. The observed bubble point pressure was almost the same as that of the field reservoir pressure (2277 psia for well A#22 and 2377 psia for well #33, United Arab Emirates). But the composition of the recombined fluid was found a little far from the required reservoir fluid composition; therefore, the vapor molar ratio was varied until a monophasic fluid was obtained with a fluid composition of minimum deviation from the under test reservoir fluid composition. The optimized vapor molar ratio was 0.5183 and 0.5603 for wells A#22 and A#33, respectively, which are almost the same values given by the service provider. Also the value of the vapor molar ratio with minimum deviation in the methane concentration was found to be about 0.42 for each well when compared to that of the reservoir methane.

In the second part of this work, another experimental setup for both recombination and phase behavior of CO_2 measurements is described. After recombination process, a precise amount of CO_2 was injected into the PVT cell and then the mixture saturation pressure and the swelling factor were measured. The influence of CO_2 addition on crude oil properties was investigated using several molar ratios of CO_2/crude oil at conditions close to the oil well mixture conditions.

The static-synthetic principles method, which consists of preparing a mixture of known overall composition, was used to observe the fluid phase behavior by changing the pressure of the PVT cell at constant temperature. A vapor-liquid-liquid transition was observed at CO_2 mass fractions above 0.3. For CO_2 mass fractions between 0.0 and 0.6, the swelling factor ranged from 1.0 to 1.74. All the measurements in the above mentioned tests were performed using an infrared device which allows phase transition detection with a precision of less than 1 bar and 3-4 % error.

Lastly, a phase behavior modeling was carried out using the PVTi [1] and PVTpro [2] modules from commercial (Schlumberger) simulators. The recombination process was simulated using the Soave-Redlich-Kwong (SRK) and Peng-Robinson (PR) equations of state including binary-interaction coefficient and volume-shift corrections. The fluid composition and the reservoir saturation pressure and temperature are the main inputs to the phase behavior simulators. The simulation task for compositional analysis was performed and results compared to available field data. After conversion to the bubble point pressure (to be the same as that of field data), and by comparing the results of both EOS, the PR EOS was selected since it gives more accurate results when compared to the experimental results and field data. The other fluid properties such Z-factor, specific volume, density, viscosity, oil formation volume factor, etc., were found to match well with experimental data, except the saturated liquid molar density, therefore, the Rackett equation was used to estimate the liquid saturated volume and gave very close values when compared to the corresponding field values.

The PVTpro simulator was also used to recombine the surface fluids (first-stage separator gas and stock-tank oil) at the reservoir conditions. The predicted recombined fluid composition from the PVTpro was found in very good agreement with the reservoir fluid composition; with an absolute error of 0.17% and 3.11% for wells A#22 and A#33, respectively. The PVTpro simulator was also used to perform the swelling test by injecting CO_2 gas to the recombined fluid (to investigate how much oil is going to swell and to establish the relation between CO_2 concentration and saturation pressure). The error in the predicted saturation pressure relative to the experimental values was 8.4% for well A#22 and 6.3% for well A#33.

Acknowledgements

At the beginning and before everything I would thank my God, because my success is due to Allah, I express my deepest gratitude to all whose help in various ways enabled me to complete my thesis research. I would like to thank, in particular, Dr. Samir Abu-Eishah (Supervisor) and for his support, follow up and encouragement. His enthusiasm and drive kept me motivated to keep striving forward towards completion of the degree. I also like to express my deep gratitude and appreciation to Dr. Mohamed Nakoua (Ex-Supervisor) and Dr. Papa Matar Ndiaye for their help during my thesis research work.

Thanks to my mother for her help and moral support, from my first day in the primary school, I am grateful to my father for his financial support, during the many years of my continued education. I pray to Allah to grant them forgiveness and paradise. I am also indebted to my brothers and sisters for their love, support and encouragement all the time. Finally, thanks to my friends for everything.

Table of Contents

Description	Page
Abstract	4
Acknowledgemetns	6
Table of Contents	7
List of Figures	8
List of Tables	9
Chapter One: Background and Literature Review	10
1.1 Introduction	10
1.2 Literature Review	11
1 3 Research Objectives	13
Chapter Two: Theory and Methodology	14
2.1 Phase Behavior of Hydrocabon Fluids	14
2.1.1 Phase Behavior of Single Component System	15
2.1.2 Phase Behavior of Multi-Component System	15
2.1.3 Phase Behavior of Low Shrinkage Reservoir Fluid	16
2.1.4 Phase Behavior of Retrograde Condensate Reservoir Fluid	16
2.1.5 Phase Behavior of Dry Gas Reservoir Fluid	18
2.1.6 Phase Behavior of Wet Gas Reservoir Fluid	18
2.1.7 Phase Behavior of Crude Oil System	18
2.3 The Corresponding States Theorem	20
2.4 Z-factor Correlation	22
Chapter Three: Sampling and Laboratory Analysis	23
3.1 Sampling	23
3.1.1 Well Testing	23
3.1.2 Conditioning	24
3.1.3 Down Hole Sampling	25
3.1.4 Surface Sampling	26
3.2 Laboratory Analysis	27
3.2.1 Compositional Determination	28
3.2.2 Saturation Pressure Determination	29
3.2.3 The Constant Mass Study (CMS) Test	30
3.2.4 The Separator Test (SEP)	31
Chepter Four: Experimental Setup & Procedures	34
4.1 Experimental Setup	34
4.2 Experimental Procedure for Phase Equilibrium Measurement	38
4.3 Experimental Porcedure for Swelling Measurement	39
4.4 Recombination of the Reservoir Fluid	41
Chapter Five: Field Data and Related Calculations	42
5.1 Field Data	42
5.2 Compositional Analysis	42
5.3 Calculation for Recombination Process	46
5.4 The modified Peng-Robinson Model	48
Chapter Six: Results and Discussion	52
6.1 Simulation Results	52
6.2 Experimental Results	62
Chapter Seven: Conclusion and Recommendations	71
7.1 Conclusions	71
7.2 Recommendations	72
References	73
Appendix A	77
Appendix B	108
Nomenclature	135
الملخص باللغة العربية	137

List of Figures

Description	Page
Figure 1.1: A schematic diagram of the total oil production system	10
Figure 2.1: *P-T* curves for a binary equimolal mixture	16
Figure 2.2: *P-T* phase diagram of a low shrinkage reservoir fluid	17
Figure 2.3: *P-T* phase diagram of a retrograde condensate reservoir gas	17
Figure 2.4: *P-T* phase diagram of a dry gas reservoir fluid	18
Figure 2.5: *P-T* phase diagram of a wet gas reservoir fluid	19
Figure 2.6: Compressibility of natural gas as a function of reduced pressure and temperature (Based on Standing and Katz, 1942)	21
Figure 3.1: Reservoir fluid and sampling	24
Figure 3.2: A schematic of a gas chromatographic system	28
Figure 3.3: Expected V_{rel}-*P* curves of crude oil around the bubble point	29
Figure 3.4: Schematic representation of the Constant Mass Study (CMS) test and the corresponding *V-P* curves	31
Figure 3.5: A schematic diagram of a 2-stage separator test	32
Figure 4.1: A schematic drawing of the experimental setup used in this work	35
Figure 4.2: The equilibrium cell used in this work	36
Figure 4.3: Details of the piston components	37
Figure 4.4: The PVT cell experimental setup used in this work	37
Figure 4.5: A schematic diagram of the swelling test procedure	40
Figure 4.6: A schematic diagram of the surface separator metering and sampling	41
Figure 5.1: Compositional analysis of well A#22 fluid, recombined oil at β = 0.5183 and recombined oil at β = 0.4199 (0% deviation in methane composition)	45
Figure 5.2: Compositional analysis of well A#33 fluid, recombined oil at β = 0.5603 and recombined oil at β = 0.4196 (0% deviation in methane composition)	45
Figure 6.1: Simulated 2-stage recombined fluid, 1-stage flash, and 2-stage flash vs. field individual component compositions for well A#22	54
Figure 6.2: Simulated 2-stage recombined fluid, 1-stage flash, and 2-stage flash vs. field individual component compositions for well A#33.	54
Figure 6.3: Experimental (reservoir fluid) vs. predicted (recombined fluid using PVTpro) compositions for well A#22.	58
Figure 6.4: Experimental (reservoir fluid) vs. predicted (recombined fluid using PVTpro) compositions for well A#33.	58
Figure 6.5: Monophasic live oil at 257 °F for well A#33	62
Figure 6.6: Initial phase formation in live oil at 257 °F for well A#33	62
Figure 6.7: Monophasic fluid of the CO_2/live oil system at 257 °F for well A#33	63
Figure 6.8: Phase transition in the CO_2/live oil system at 257 °F for well A#33	63
Figure 6.9: Swelling factor of CO_2/live oil system as function of saturation pressure at 235 °F for well A#22.	65
Figure 6.10: Swelling factor of CO_2/live oil system as function of saturation pressure at 257 °F for well A#33.	65
Figure 6.11: Measured saturation pressure vs. CO_2 mass fraction at 235 °F for well A#22.	66
Figure 6.12: Measured saturation pressure vs. CO_2 mass fraction at 257 °F for well A#33.	67
Figure 6.13: Experimentally observed vapor-liquid-liquid transition at 257 °F for well A#33.	67
Figure 6.14: Proposed mechanism of phase formation at low CO_2 mass fractions as a function of saturation pressure.	68
Figure 6.15: Proposed mechanism of phase formation at high CO_2 mass fractions as a function of saturation pressure.	69
Figure 6.16: Experimental vs. simulated (using PVTpro) swelling test results for well A#22.	70
Figure 6.17: Experimental vs. simulated (using PVTpro) swelling test results for well A#33.	70

List of Tables

Description	Page
Table 5.1: Reservoir Fluid Compositions from Service Provider	43
Table 5.2: Phase properties of $C_{20}+$ and fluid for flashed and monophasic fluids from wells A#22 and A#33	43
Table 5.3: Critical properties and composition of the gas mixture of wells A#22 and A#33	47
Table 5.4: Calculated Z and V^v of the gas injected into the PVT cell for wells A#22 and A#33	47
Table 6.1: Comparison between SRK and PR EOS predictions (using the PVTi Simulator) for wells A#22 and A#33	52
Table 6.2: Comparison between 2- and 3-parameters PR EOS for wells A#22 and A#33	53
Table 6.3: Comparison between PVTi & PVTpro in calculating fluid properties of well A#22	55
Table 6.4: Comparison between PVTi & PVTpro in calculating fluid properties of well A#33	56
Table 6.5: Experimental composition (reservoir fluid field) vs. predicted (recombined fluid using PVTpro) composition for wells A#22 and A#33	57
Table 6.6: Calculated saturated liquid volume and density using the Rackett equation for well A#22 at 2277 psia and 235 °F	60
Table 6.7: Saturated liquid volume calculation using Rackett equation for well A#33	61
Table 6.8: Saturation pressure and swelling data for the CO_2/live oil system for well A#22 at 235 °F	64
Table 6.9: Saturation pressure and swelling data for the CO_2/live oil system for well A#33 at 257 °F	64
Table 6.10: Comparison between experimental and simulated (using PVTpro) swelling test results for wells A#22 and A#33.	69

Chapter One

Background and Literature Review

1.1 Introduction

In order to perform flow simulation in the reservoir and oil production systems, one requires knowledge of several physical properties of the fluid system. Firstly, what phases are present: gas, oil, or water? What are the comparative quantities of these phases? What are the common phase properties, i.e., density, viscosity, thermal conductivity, etc.? [3]

In principle, we can take samples of the reservoir fluid and measure the quantities of interest at certain pressure and temperature. However, these experiments are both difficult and costly and cannot hope to cover the range of pressures, temperatures and compositions likely to encounter [4]. A schematic diagram of the total production system is shown in Figure 1.1.

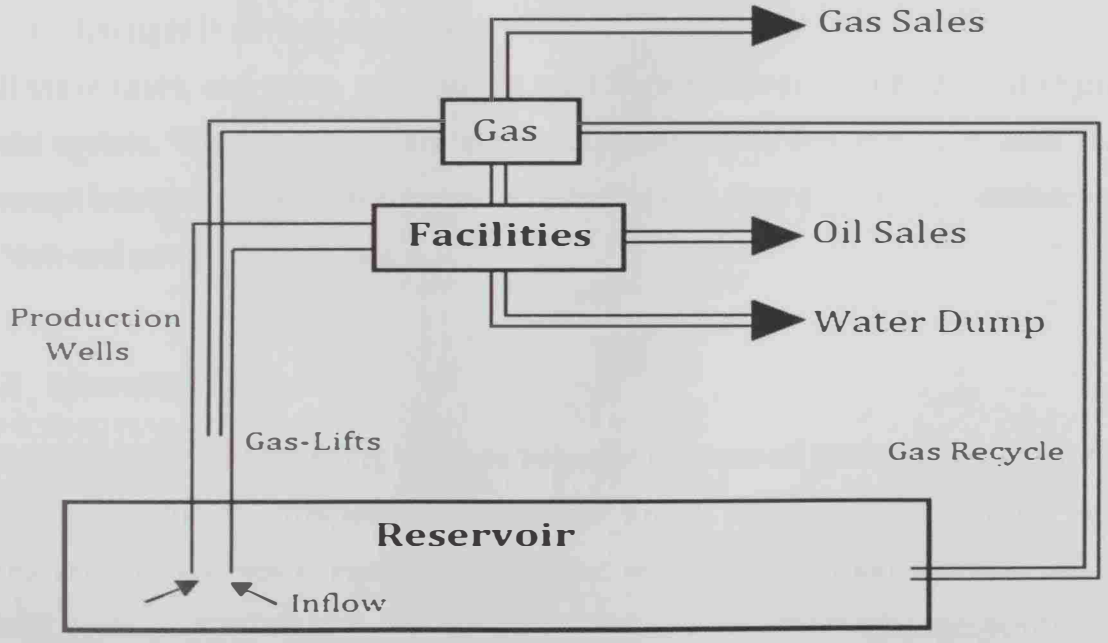

Figure 1.1: A schematic diagram of the total oil production system

In mature areas of petroleum accumulations it is now common to find reservoirs at 20,000 ft (6,096 m) or more. At such depths, pressures can approach 16,000 psia (~109 MPa) and temperatures are close to 400 °F (477.6 K). Pressure can take any value between reservoir initial static pressure and one atmosphere in the stock

tank, if one exists. Temperature will also vary between reservoir temperature and standard temperature (60 °F).

If the fluid composition is fixed, a set of pre-defined look-up tables could handle temperature and pressure variability. Generally, the fluid composition within the production system is not fixed for a variety of reasons [5].

(i) Within the reservoir, the following changes can take place:

- Composition varies with depth and areal location. The presence of high permeability streaks can then allow different fluids to mix.
- As fluid drops below its saturation pressure, one phase, generally the gas will flow in favorite to the oil so the produced well composition changes with time. This effect is mainly important for near critical fluids.
- Gas injection for pressure maintenance or miscibility processes.

(ii) Within the production system:

- Fluids from different parts of the reservoir or reservoirs can mix.
- Gas injection for gas-lift.
- Changes in surface separation.

All these cases, and more, point to the need for a compositional treatment of the fluid system. These methods are computationally expensive. However, with the prompt increase in computer power at reducing cost, they are all now possible on a high-end personal computer.

1.2 Literature Review

The study and understanding of phase behavior in crude oil systems play a central role in predicting compositional changes under varying temperatures and pressures in reservoirs, surface separations, and production and transportation facilities. In particular, they are critical for reliable and successful compositional reservoir simulation. How the fluids behave within the reservoir, within the wells, at surface conditions, in the network, and at the refinery is a complex question usually made in the ambient of exploration, production and refining [6].

The fluid properties must be known over a wide range of temperatures and pressures. When a gas is injected into the reservoir, it is also important to know

how the properties of the original reservoir fluid will change as the composition of the mixture changes. The *PVT* properties are also needed to predict:-

a) The composition of the well stream as a function of time,
b) completion design, which depends on the properties of well-bore liquids,
c) The effect of injecting or re-injecting gas,
d) The amount and composition of the liquid left behind in the reservoir and their properties (density, surface tension, viscosity, etc.),
e) Equilibrium ratios, more commonly known as *k*-values; (= vapor phase mole fraction to liquid phase mole fraction) at equilibrium.

Several articles have addressed the procedures for evaluating and improving the *k*-values. In a fluid mixture consisting of different chemical species at high pressure, *k*-values are dependent on the pressure, temperature, and composition of the mixture. This extra dependency on the fluid composition, for high-pressure systems compared to low-pressure systems, has limited the ability to predict high pressure *k*-values empirically and shifted the emphasis for preferred methods to using the more sophisticated equations of state approach such as those based on perturbation thermodynamics theory like the statistical associating fluid theory (SAFT) framework models [7]. However, in contrast to the cubic equations of state, these models over predict the mixture critical conditions, since they do not include in their pure component parameters, any critical point information.

Almehaideb et al. [6] present an accurate *k*-value correlation for the UAE crude oil components at high pressures using PVT laboratory data. Material balance techniques are used to extract the *k*-values of the crude oil and gas components from the constant volume depletion and differential liberation (DL) tests for the oil and gas samples, respectively. When plotting the log *k*-value vs. pressure, the curves should plot in a parallel-like trend. The upper curve should correspond to nitrogen, the lightest component, followed by the curves of methane and CO_2. Then, either ethane or hydrogen sulfide (depending on the fluid composition) followed by the rest of the components.

1.3 Research Objectives

The commercial service provider collected two bottom-hole samples A#22 and A#33 from Field A in UAE and provided the following information for both wells: reservoir initial static pressure, bottom-hole temperature, bubble point pressure, and compositional analyses of the reservoir fluids.

Since bottom-hole sampling is really difficult and costly and the volume collected by the down-hole fluid sampling is small compared to that of the surface-fluid sampling. The first objective of this work is to have surface samples from the stock-tank oil and gas leaving the first separator to perform recombination process using high-pressure PVT cell in order to obtain the same saturation pressure at the reservoir temperature and fluid composition close to the original reservoir composition. The second objective is to simulate the phase behavior in crude oil system at high pressure using the commercial Eclipse Simulator [1]. In particular, the effect of CO_2 injection on reservoir fluid will be investigated using two major cubic equation of state (Soave-Redlich-Kwong and Peng-Robinson). Further, swelling tests will be carried out to determine the volumes or moles of a specified gas composition added to the reservoir fluid in a number of stages. Prior to and after each addition, the fluid will be brought to its saturation pressure and the relative change in volume (swelling factor) is determined.

Chapter Two

Theory and Methodology

2.1 Phase Behavior of Hydrocarbon Fluids

In a petroleum mixture of known composition one can ask how the mixture components distribute themselves at some specified pressure and temperature conditions. In particular, is the fluid a gas, oil or a mixture of both?

Limiting our interest in hydrocarbon mixtures, up to 2-phases (gas and oil) present at surface conditions and are called vapor and liquid under reservoir and/or production conditions.

Wherever hydrocarbons are found, water is usually found. Hydrocarbons and water should be considered together when fluid properties are studied. However, their related solubility is commonly very low and for most purposes, water is independently considered. An important exception is gas-water mixtures in production systems. At low flow rates or shut-ins, the gas-water mixture is capable of forming gas hydrate at temperatures above 0 °C. Once the gas hydrate is formed, it is difficult to be cleared. The operators require adding an expensive fluid (e.g., methanol) in the flow line to overcome the hydrate formation [8].

Petroleum oils containing very heavy hydrocarbon molecules, called resins and Asphaltenes, can also be found. These materials cause most problems in the production system but they can also be a problem in the near well bore region where they can drop out as pressure falls and effectively reduce the porosity. Again, expensive chemical treatments may be needed to remove them if they occur [9].

Carbon dioxide injection is famous for many old oil fields. Large CO_2 reservoirs mean there is more supply of material for injection and under the right conditions it can significantly enhance oil production. At relatively low pressures and temperatures, say 150 °F (338.7 K) and 1500 psia (10.3 MPa); a four-phase system is seen consisting of an aqueous phase, a hydrocarbon vapor, a hydrocarbon liquid and a CO_2-rich liquid. Given the narrow range of conditions under which this effect occurs, it is generally not modeled in reservoir simulation although it is studied as a PVT problem [10].

Any analysis of reservoir behavior depends on the *PVT* relationships for the co-existing fluids. It is usually to represent the phase behavior of hydrocarbon reservoir fluids on the *P-T* plane showing the limits over which the fluid exists as a single phase and the proportions of the oil and gas in equilibrium over the two-phase *P-T* range.

2.1.1 Phase Behavior of Single-Component Systems

Single-component hydrocarbons are not found in nature; however it is beneficial to observe the behavior of a pure hydrocarbon substance under varying pressures and temperatures to gain insight into more complex hydrocarbon systems under similar conditions. To study the behavior of a pure hydrocarbon substance, the PVT cell is charged, for example, with ethane at 60 °F (288.7 K) and 1000 psia (6.89 MPa). Under these conditions, ethane is in liquid state. If the cell volume is increased, while holding the temperature constant at 60 °F throughout, it will be found that the pressure falls rapidly until the first bubble of the gas appears. This is called bubble point. Further increase of cylinder volume does not reduce the pressure provided, temperature is held at 60 °F although heat must be added to the system to maintain a constant temperature. The gas volume increases at this constant pressure until the point is reached where all of the liquid is vaporized. This is called the dew point. The ethane gas expands with further increase of cylinder volume at 60 °F as pressure decreases hyperbolically [11].

2.1.2 Phase Behavior of Multi-Component Systems

Consider the phase behavior of a 50:50 mixture of two pure hydrocarbon components on the P-T plane as shown in Figure 2.1. The vapor pressure and bubble point lines do not coincide but form an envelope enclosing a broad range of temperatures and pressures at which two phases (gas and oil) exist in equilibrium. The dew point and the bubble point curves meet at the critical point, which is defined as that temperature and pressure at which liquid and vapor phases have identical intensive fluid properties. The fluid above the bubble point is in the liquid state, the fluid below the dew point line is vapor, and the fluid in the space

enveloped between the two lines is a two-phase mixture (liquid and vapor) in equilibrium [12].

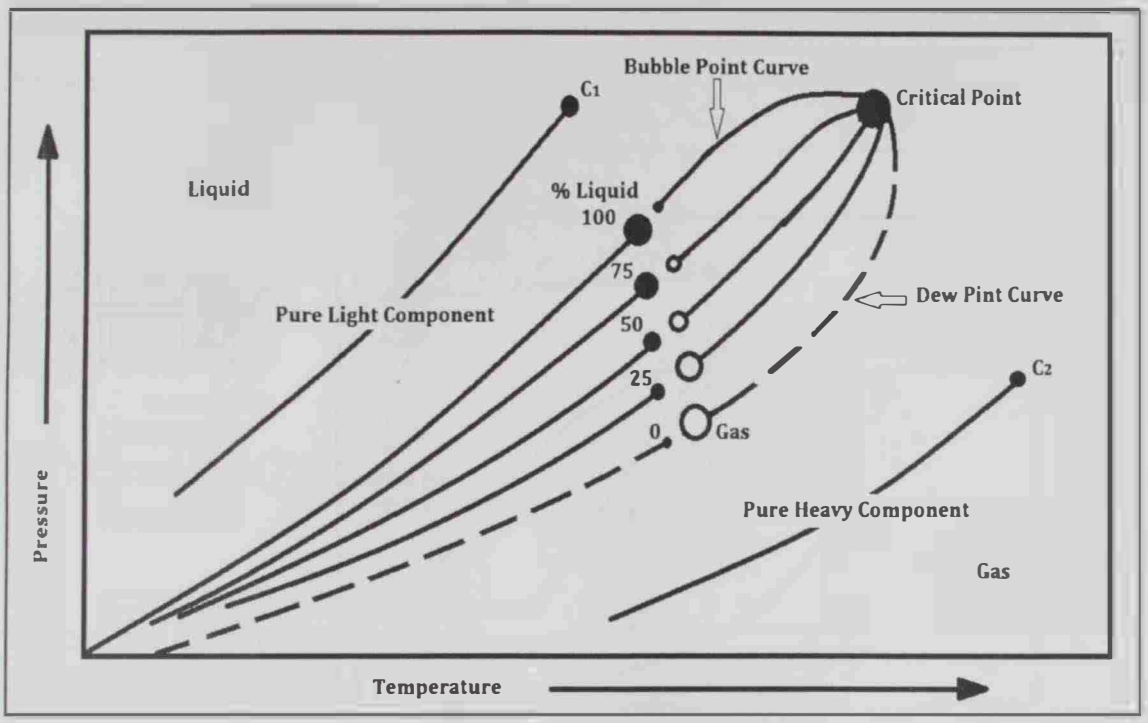

Figure 2.1: *P-T* curves for a binary equimolal mixture [12]

2.1.3 Phase Behavior of Low Shrinkage Reservoir Fluid

The chemical composition and amount of each constituent present determine the shape of the two-phase envelope and its position on the *P-T* diagram. Each reservoir fluid has a unique phase diagram. Figure 2.2 is a phase diagram typical of a low shrinkage oil of a reservoir. Fluid at reservoir temperature and pressure at point *A'* exists as under-saturated liquid. If a sample of this fluid is expanded in a PVT cell at a reservoir temperature T_{res}, the bubble point pressure will be reached at *A*. This is approximately the path that fluids follow in moving horizontally through the reservoir to the well bore [13].

2.1.4 Phase Behavior of Retrograde Condensate Reservoir Gas

The phase diagram shown in Figure 2.3 represents the behavior of a retrograde condensate gas of a reservoir. The fluid at point *A'* is above the critical temperature and is therefore classified as gas. On reduction of pressure at constant temperature

from point *A'*, the dew point line is crossed at *A* and liquid begins to condense from the reservoir gas. If the pressure and temperature are reduced from *A* along the dashed path to separator condition, the diagram shows that 25 % of liquid is recovered at this point. On further reduction to atmospheric pressure, only 2 % of the liquid will remain.

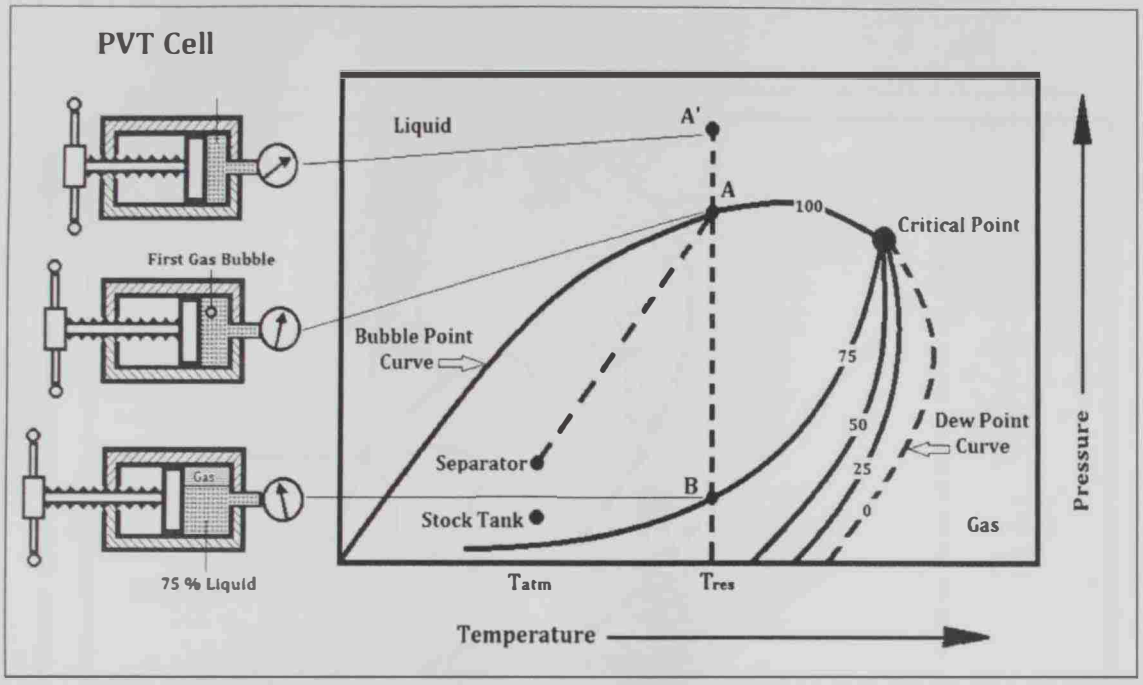

Figure 2.2: *P-T* phase diagram of low-shrinkage reservoir fluid [13]

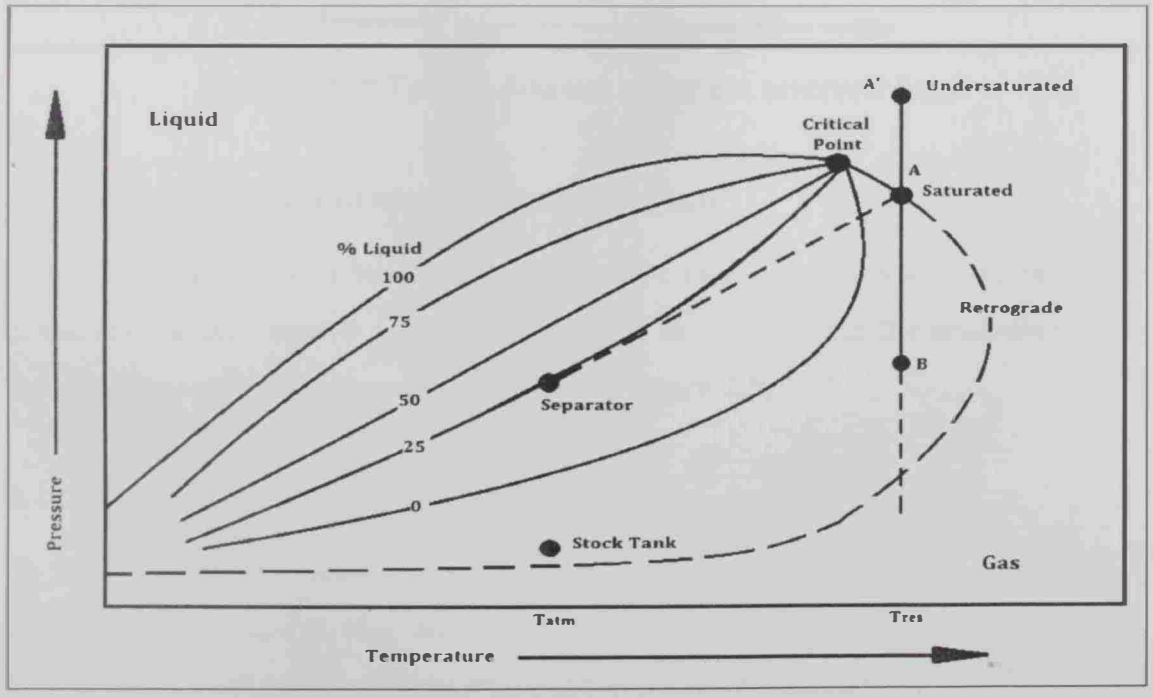

Figure 2.3: *P-T* phase diagram of retrograde condensate reservoir gas

2.1.5 Phase Behavior of Dry Gas Reservoir Fluid

The phase diagram on the *P-T* plane represents the behavior of a dry gas reservoir fluid. If the pressure and temperature are reduced from the original reservoir conditions at point to standard stock tank conditions (60 °F and 14.7 psia), there is no liquid recovery and the reservoir fluid remains completely in the gaseous phase during the process as shown in Figure 2.4.

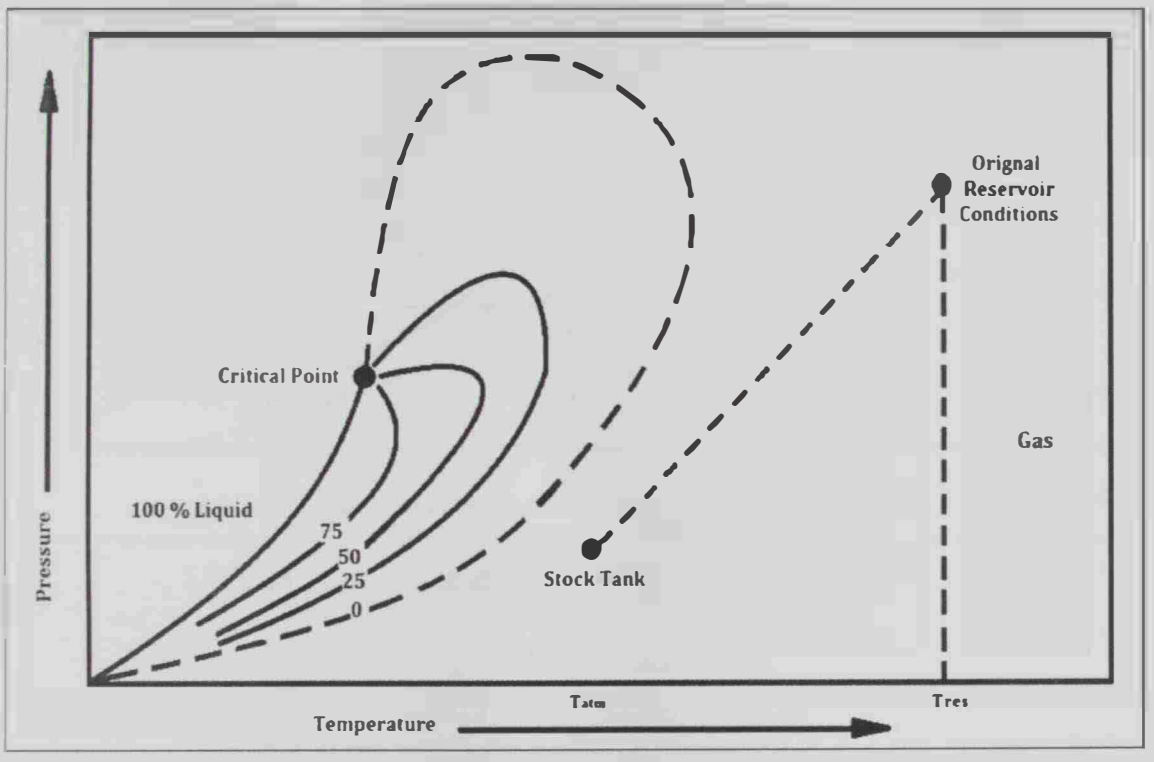

Figure 2.4: *P-T* phase diagram of dry gas reservoir fluid

2.1.6. Phase Behavior of Wet Gas Reservoir Fluid

A fluid that exists above its critical temperature as gas at reservoir conditions, but produces a small quantity of liquid condensate on reduction to the separator/stock tank conditions, may be termed wet gas (see Figure 2.5).

2.1.7 Phase Behavior of Crude Oil System

As the difference between the reservoir temperature and the critical temperature increases, with $T_{res} = T_c$, the lines of constant vapor fraction spread out. Therefore, as the pressure falls down from the bubble point, the amount of vapor liberated falls. In addition, the liquid content of the liberated vapor is reduced. If the

assumption that the liberated vapor can be treated as dry gas is acceptable, then the fluid can be treated as a crude oil.

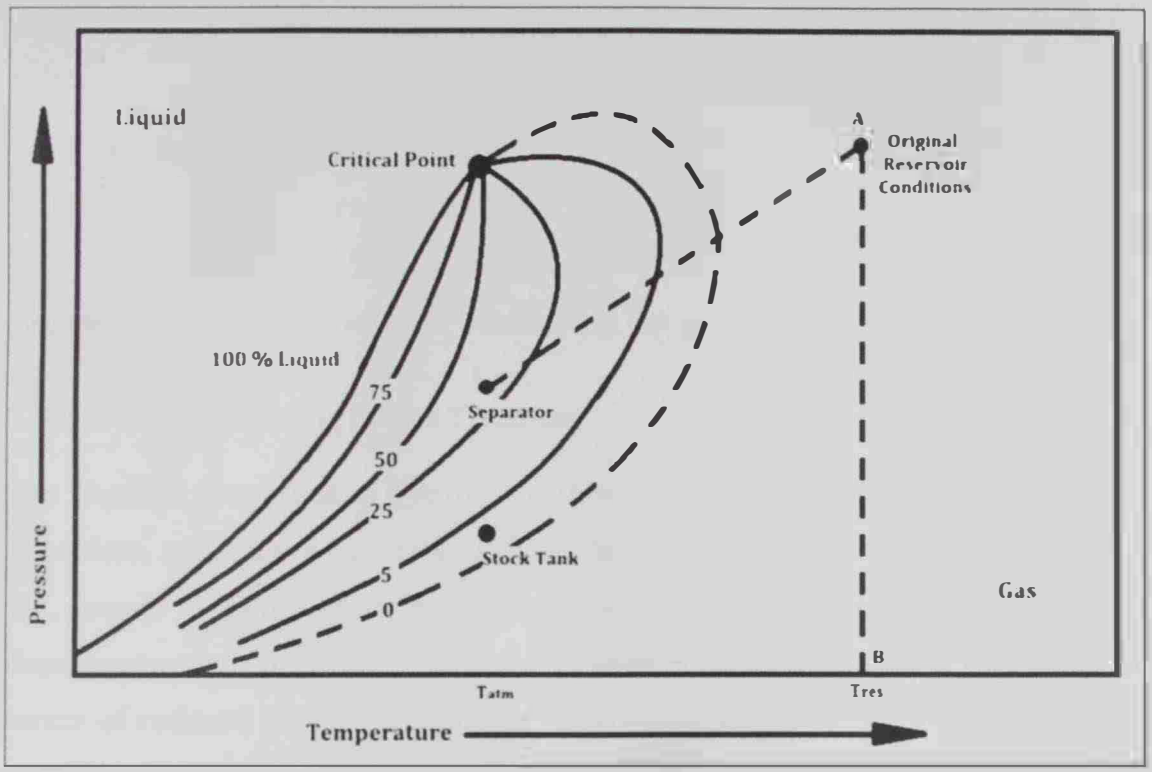

Figure 2.5: Phase diagram of wet gas reservoir fluid

At pressures in excess of the bubble point, the crude oil will be referred to as being under-saturated, that is, more vapor could be dissolved if it were present. At the bubble point, the crude is called saturated, i.e., it holds as much vapor as it can. Strictly, at all pressures less than the bubble point pressure the liquid will be saturated, as vapor will continue to grow.

The relative simplicity of the crude oil phase behavior has given rise to numerous correlations to describe their behavior. These consist of expressions to calculate:

- Bubble point pressure (P_b)
- Oil formation volume factor (FVF_o)
- Solution Gas-to-Oil Ratio (GOR) at any condition (R_s)
- Oil viscosity (μ_o)
- Gas viscosity (μ_g)

These correlations generally use the following set of parameters:

- Oil API gravity (γ_{API})
- Gas specific gravity (γ_g); $\gamma_{air} = 1.0$
- Solution GOR at initial conditions (R_{si})
- Reduced temperature, (T_r)

The correlations are therefore of the form

$$P_b = f(\gamma_{API}, \gamma_g, T_r) \tag{2.1}$$

The more commonly known correlations are due to Standing and Katz [14].

2.3 The Corresponding States Theorem

The physical properties of hydrocarbons vary with molecular weight and shape. Therefore, resulting properties such as density, viscosity, thermal conductivity, etc., cannot be easily comprehended for one species based on measurements of those properties for another species. However, it was observed that this works in terms of reduced properties such as reduced temperature, T_r, and pressure, P_r, defined by

$$P_r = P/P_c \quad \text{and} \quad T_r = T/T_c \tag{2.2}$$

In particular, the corresponding states theorem says all pure gases will have the same Z-factor at the same P_r and T_r.

Figure 2.6 (usually known as the Standing-Katz Z-factor chart [15]), shows the variation of the Z-factor with pseudo-reduced pressure, $P_{pr} = P/P_{pc}$ and pseudo-reduced temperature, $T_{pr} = T/T_{pc}$, both calculated at the pseudo-critical properties of the mixture. All hydrocarbon gases (up to C_6) and the inorganic gases N_2, CO_2 and H_2S obey this chart to within a few percent. Mixtures of these components can also have their Z-factors computed from this chart instead of the pure component critical pressure and temperature in Eq. (2.2).

In this work, the pseudo-critical pressure, P_{pc}, and pseudo-critical temperature, T_{pc}, are used as defined below:

$$P_{pc} = \sum_{i=1}^{N} y_i P_{ci}$$

$$T_{pc} = \sum_{i=1}^{N} y_i T_{ci} \tag{2.3}$$

where y_i is the mole fraction of the i^{th} component in the mixture. In the absence of compositional analysis, the pseudo-critical properties can be estimated from correlations based on gas specific gravity [16].

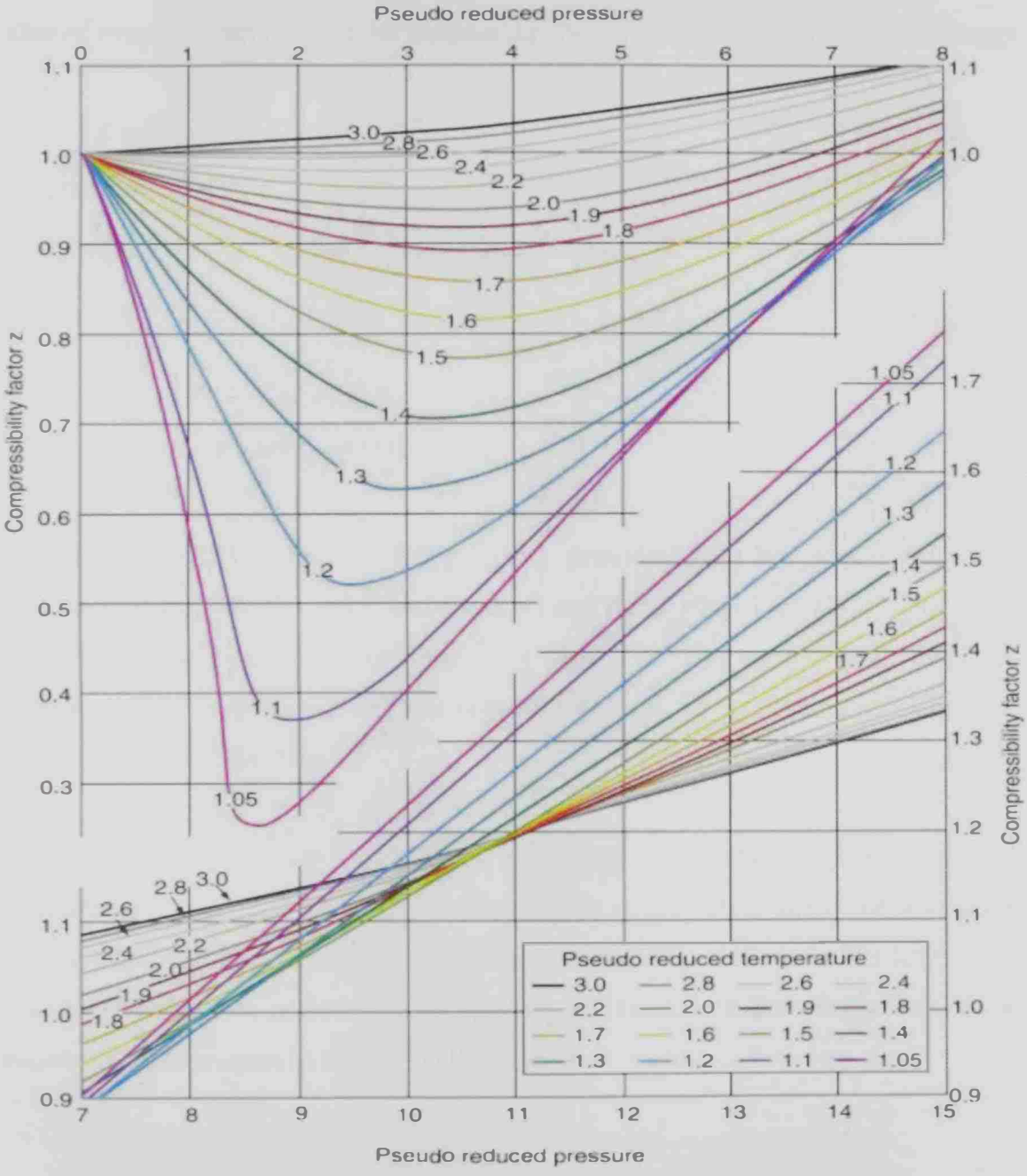

Figure 2.6: Compressibility of natural gases as a function of reduced pressure and temperature (Based on Standing and Katz, 1942).

In the equations of state models both pressure and temperature replaces the critical terms in Eq. (2.3) as reduced quantities. Other models apply the

corresponding states theorem for estimating viscosity and thermal conductivity of hydrocarbon mixtures [17].

2.4 Z-factor correlation

One of simplest correlations for estimating the Z-factors is due to Brill and Beggs [18]:

$$Z = A + (1 - A)e^{-B} + CP_{pr}^{D} \tag{2.4}$$

where

$$A = 1.39(T_{pr} - 0.92)^{0.5} - 0.36T_{pr} - 0.101$$

$$B = P_{pr}(0.62 - 0.23\,T_{pr}) + P_{pr}^{2}\left(\frac{0.066}{(T_{pr} - 0.86)} - 0.037\right) + 0.32\,P_{pr}^{6}.e^{[-20.723(T_{pr}-1)]}$$

$$C = 0.132 - 0.32 * \log T_{pr}$$

$$D = e^{(0.715 - 1.128\,T_{pr} + 0.42\,T_{pr}^{2})} \tag{2.5}$$

Correlation (2.5) is adequate (±2% error) provided that the temperature lies between 80 and 340 °F (299.8 and 444.2 K) and the pressure is below 10,000 psia (68.9 MPa). The main advantage of this correlation is being explicit in z. The phase behaviors and correlations discussed above can be used in assessing the experimental calculations.

In the next chapters we will discuss sampling and its types, conditions, and procedures as well as laboratory analyses (such as saturation pressure, separator and swelling test procedure) which will be conducted in this work. The Kay's rule, Z-factor correlations, and reduced properties will be used in the calculations of the recombination process in the PVT cell.

Chapter Three

Sampling and Laboratory Analysis

3.1 Sampling

Mathematical models encapsulated within software packages are increasingly used to predict the behavior of hydrocarbon reservoirs and their related production systems. These models require input, initialization and calibration data. For fluid property determination this requires to take samples of the fluids of interest, determine their composition, and finally, perform a set of standard tests to produce data to calibrate these models [19].

Before conducting any test, samples of the fluid of interest should be taken as part of the initial well testing program. There are usually conflicts in the well test program with the need to obtain reservoir parameters versus the collection of representative samples. Proper design and careful planning is the key to minimizing these conflicts [20].

3.1.1 Well Testing

The main problems in the well test design for sampling is concerned with the production interval and the tubing size. In large hydrocarbon columns, a significant variation in composition with depth is possible. In this case, it is preferable to sample only a limited interval by restricting the perforations. It suggested that the intervals be restricted to 30-ft column. This then requires several tests to be performed over large (over 300-ft) columns, and a minimum of three separate tests [21].

When considering well conditioning, the sample collection is best served by low flow rates (using small diameter tubing) since low rate production in large diameter tubing gives rise to an unstable flow regime called slugging. However, the rate must be high enough to ensure that liquids are produced to surface [22].

Technological advances in recent years have helped here since it may be possible to run small diameter coiled tubing during the sampling phase, returning back to the large diameter tubing for the other aspects of the well test.

3.1.2 Conditioning

There are two ways of sampling: (1) down-hole and (2) surface sampling as illustrated in Figure 3.1.

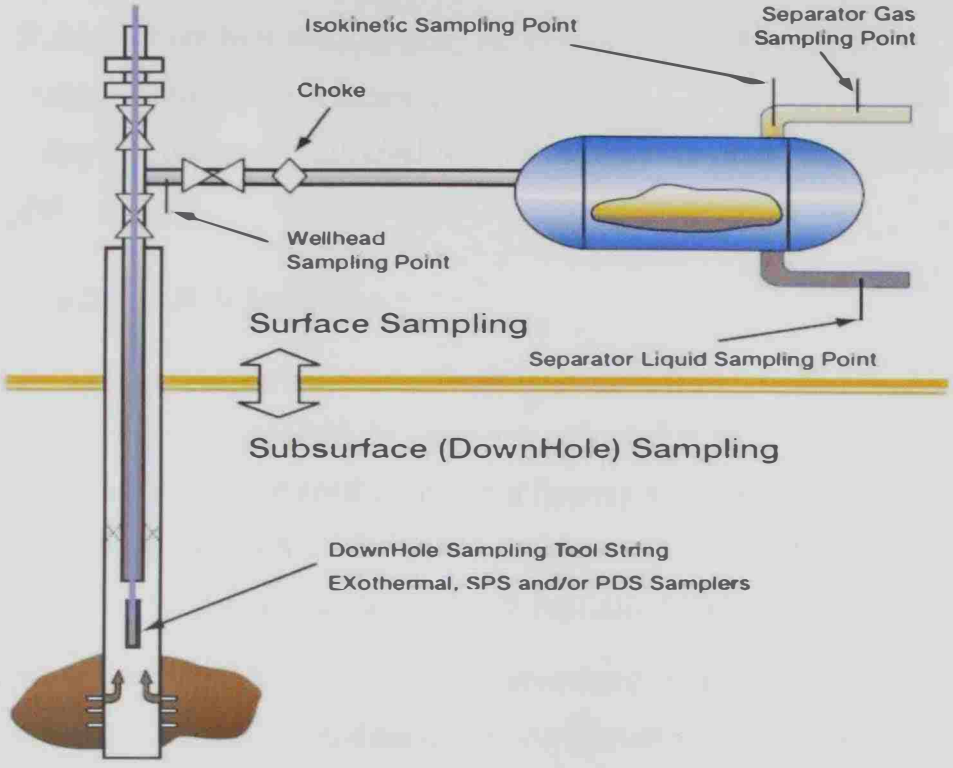

Figure 3.1: Reservoir fluid and sampling [23]

In both methods, proper conditioning of the well prior to taking the sample is necessary:

1. Sampling should be done as soon as possible after the well is completed.
2. The process of drilling and completion usually results in near-well bore damage and contamination, which must be cleaned-up before the sample can be taken. This is best achieved by a high flow rate. However, this may cause a large pressure draw down that might cause the bottom-hole pressure to fall below the saturation pressure. Then, depending on the relative permeability effects, the fluid flowing into the well may be unrepresentative of the reservoir fluid.

Once the balance is achieved between maximizing clean-up time and minimizing pressure draw down, the main aim of which is to achieve

- Uniform flow rate,
- Uniform gas-to-oil ratio, GOR,
- Stable top hole pressure (P_{TH})
- Stable bottom hole pressure (P_{BH})
- Stable bottom hole density, (ρ_{BH}) (to ensure no liquid build up)
- Stable wellhead temperature, (T_{WH})

The stability conditions are satisfied for at least 6 hours prior to the sample being taken [24].

3.1.3 The Down-Hole Sampling

In this technique, a bottle is lowered down hole on a wire line and placed as close as possible to the open interval. At some pre-arranged time or on a command from the surface, the bottle is opened to the fluid flowing around it upon which some of that fluid is allowed to enter the bottle. Unlike surface sampling, the volume of fluid that can be collected is relatively small, typically 1 liter or so.

The sample bottle is returned to the laboratory and the fluid is flashed to atmospheric conditions. The normalized mass fractions of the gas (w_{gi}) and the oil (w_{oi}) in the stock tank sample are found by gas chromatography. The molar weight (M_o) and density (ρ_o) of the oil sample are then measured.

The flash gas-to-oil ratio (GOR or R_s) in consistent units (ft^3/ft^3 or m^3/m^3) is given by

$$R_s = \frac{V_g}{V_o} = \frac{n_g V_{gm}}{n_o V_{om}} \tag{3.1}$$

where V_{gm} and V_{om} are respectively the gas and oil molar volumes (in field units, ft^3/lb-mol) and n_g and n_o are the corresponding number of moles. If the number of moles of the feed is assumed unity, then $n_o = 1.0 - n_g$. The molar volume of the oil, by definition, equals its molar weight divided by density, i.e.

$$V_{om} = \frac{M_o}{\rho_o} \tag{3.2}$$

Combining these results allows calculation of the number of moles of the gas as

$$n_g = \frac{(M_o/\rho_o)R_s}{V_{gm}+(M_o/\rho_o)R_s} \tag{3.3}$$

Meanwhile, the oil and gas mass fractions are converted to mole fractions (x_i and y_i) using the oil and gas molar weights, M_o and M_g):

$$x_i = \frac{(w_{oi}/M_{oi})}{\Sigma_{j \neq C_{7+}}[w_{oj}/M_{oj}] + (w_{C_{7+}}/M_{o_{C7+}})} \quad (3.4)$$

$$y_i = \frac{(w_{gi}/M_{gi})}{\Sigma_{j \neq C_{7+}}[w_{gj}/M_{gj}] + (w_{C_{7+}}/M_{g_{C7+}})} \quad (3.5)$$

Finally, with the gas and oil samples' mole fractions (x_i and y_i) and the number of moles of the gas, the feed composition, z_{Fi}, is calculated from

$$z_{Fi} = n_g y_i + (1 - n_g)x_i \quad (3.6)$$

The measurement of molar weights is extremely difficult and can be subject to an error (as large as ±10%); which will clearly affect the determination of the well stream molar composition [25].

3.1.4 The Surface Sampling

The well is permitted to flow to the surface where a fraction of the well stream fluid is re-directed to a test separator held at some pre-determined pressure and temperature. After ensuring the stability conditions being met, samples of the separator vapor and liquid are collected in a number of bottles, which are then sent to regional laboratories for analysis.

The main advantage of surface sampling over the down-hole sampling is the ability to collect large volumes of fluid. However, there are a number of issues to be considered:

- Lifting all the produced fluids,
- Ensuring a representative mix is taken from the flow line,
- Accurate metering with the consequent problem of recombining the vapor and liquid streams to reconstitute the well stream fluid.

Most surface samples are taken through a test separator. Ideally, the inlet of the test separator should be inserted into the main flow line from the well head manifold. The probe should be preceded by a baffle arrangement to ensure the fluid is well mixed.

A number of analysis techniques can be employed to ensure any recombined sample is representative. Firstly, when the liquid bottle is opened back in the laboratory, the bubble point pressure should be the same as the separator pressure at which it was sampled and should be corrected for temperature. Secondly, since all the components of the vapor and liquid phases are in equilibrium, then the *k*-values for each component in the mixture can be calculated.

$$k_i = y_i/x_i \tag{3.7}$$

Standing suggested that the measured *K* values should obey the following equation [26]

$$\log_{10}(k_i P_{sep}) = A_0 + A_1 F_i \tag{3.8}$$

where P_{sep} is the separator pressure (in psia) and F_i is given by

$$F_i = \left(\frac{1/T_{bi} - 1/T}{1/T_{bi} - 1/T_{ci}}\right) \log\left(\frac{P_{ci}}{P_{st}}\right) \tag{3.9}$$

Where T_{bi}, T_{ci}, and P_{ci} are respectively the normal boiling temperature, the critical temperature and the critical pressure of component *i* in the mixture. P_{st} is the standard pressure (in consistent units). The constants A_0 and A_1 are calculated from [26]:

$$A_0 = 1.2 + 4.5\text{x}10^{-4} P_{sep} + 15\text{x}10^{-8} P_{sep}^2 \tag{3.10}$$

$$A_1 = 0.890 - 1.7\text{x}10^{-4} P_{sep} - 3.5\text{x}10^{-8} P_{sep}^2 \tag{3.11}$$

Eq. (3.8) is generally assumed valid for hydrocarbon mixtures at pressures up to 1000 psia (68 bar) and temperatures up to 200 °F (366.4 K).

3.2 Laboratory Analysis

After obtaining one or more representative samples, the next task is to analyze them to find which components are present and in what proportions. Then a set of standard experiments should be performed to determine a set of important parameters. The parameters measured depend on the nature of the reservoir fluid, i.e. liquid and/or vapor.

3.2.1 Composition Determination

The workhorse in this area is the gas chromatograph (see Figure 3.2), which usually comes in one of two types, packed column or capillary column. The packed column consists of a glass or stainless steel coil, typically 1-5 m in length and 5 mm inner diameter. The capillary columns are thin fused silica, typically 10-100 m in length with an inner diameter of 250 μm [27].

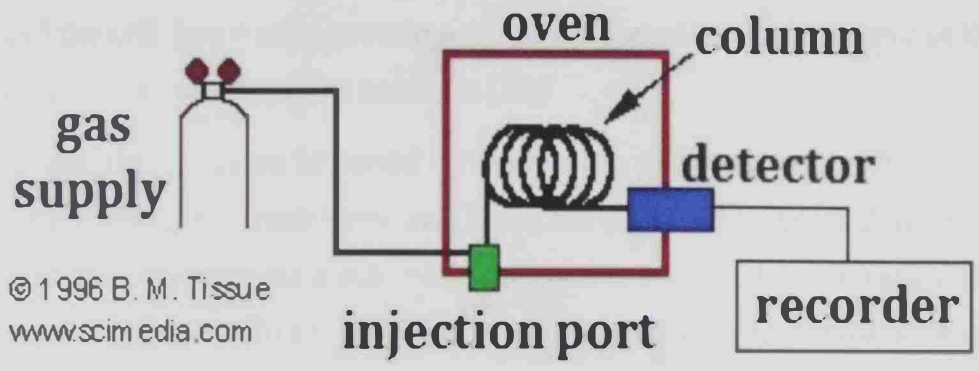

Figure 3.2: A schematic of a gas chromatographic system [28].

The sample is injected into the column, which is housed in a temperature-controlled oven. As the temperature is increased on some pre-programmed schedule, the components will boil depending on their volatility.

An inert carrier gas such as helium or argon then carries the components along the tube to a detector. The effluent from the GC mixes with an air/hydrogen mixture and passes through a flame. The resulting ions are collected between the electrodes to produce an electrical signal.

The most popular types of detectors are the Flame Ionization Detector (FID) and the Thermal Conductivity Detector (TCD). The FID is very sensitive but it destroys the sample. The TCD consists of an electrically-heated wire whose resistance is affected by the thermal conductivity of the surrounding gas. The change in resistance can be correlated to the nature of the surrounding gas. The TCD is not as accurate as the FID but it is non- destructive.

3.2.2 Saturation Pressure Determination

The bubble point pressure for a reservoir liquid or the dew point pressure for a reservoir vapor is one of the important measurements performed at saturation conditions. The exact mechanics of the measurement depend on the fluid type but in both cases it begins by loading a volume of the reservoir fluid into a PVT cell (discussed in Chapter 4). This cell is placed in a chamber whose temperature can be set as that of the reservoir temperature. Pistons can raise and lower the pressure and valves allow fluid to be injected and removed from the top and bottom of the cell. Some cells contain a window, located near the bottom of the cell to allow visual inspection of the contents [29].

For a liquid, the pressure is raised to some high pressure, generally slightly in excess of the initial reservoir pressure. Then, the pressure is reduced in a series of stages and the corresponding volume of the fluid is recorded at each stage [30]. In this case, the relative volume-pressure behavior presented in Figure 3.3 has been observed.

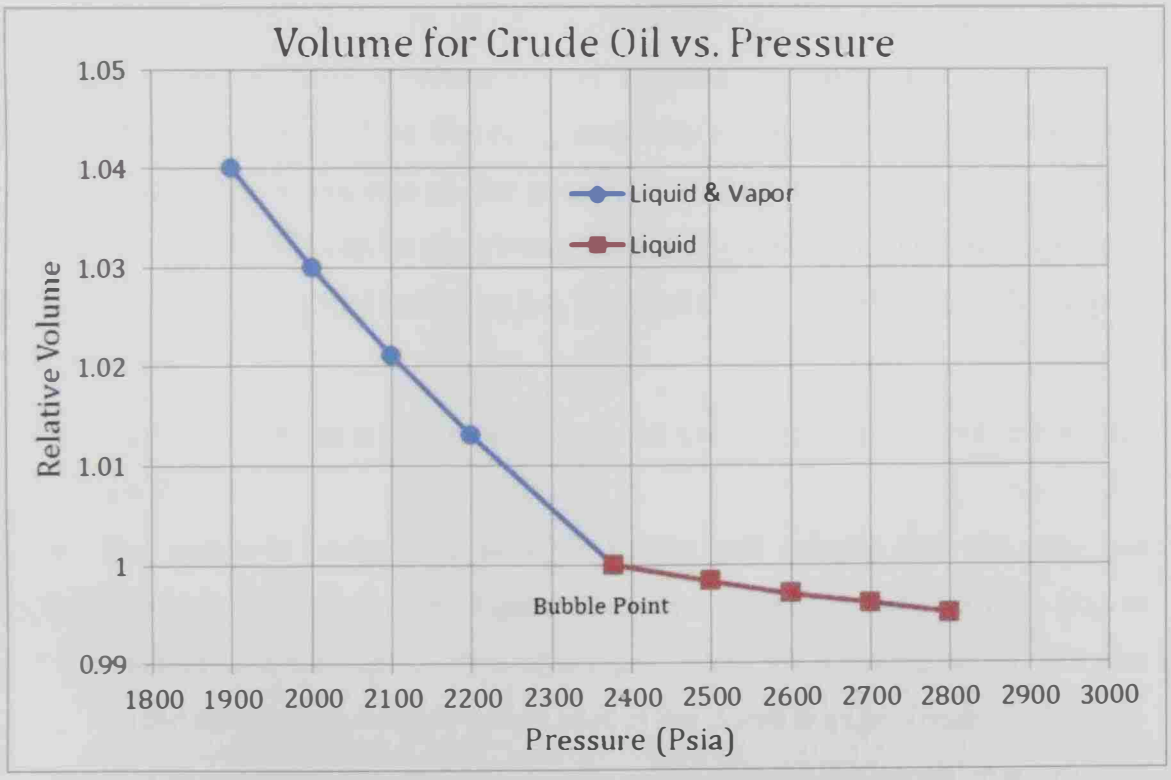

Figure 3.3: Expected V_{rel} - P curves of crude oil around the bubble point for well A#33.

3.2.3 The Constant Mass Study (CMS) Test

The CMS test is a test performed with a known quantity of representative reservoir fluid sample, which remains constant throughout the test. It is also known as Constant Composition Expansion (CCE) test or Constant Mass Expansion (CME) test. The CMS test is a flash liberation process, since the sample composition remains constant and as the gas is liberated from solution, it remains in contact with the liquid and equilibrium is attained with all components still present [31]. The following can be determined from the CMS test:

- Reservoir temperature at saturation pressure
- Ambient temperature at saturation pressure
- Relative volume–pressure relationship
- Compressibility factor
- Thermal Expansion

A fixed volume of the reservoir fluid is charged into a high pressure PVT cell well above the saturation pressure of the fluid. The cell volume is increased in small increments, with the pressure being recorded after each volume increment and after it reaches equilibrium. When the cell reaches the sample bubble point, the first bubble of the gas evolves. The compressibility of the two phases present in the cell drastically increases due to the gas compressibility being much larger than that of the liquid. This can be seen when the sample volume is plotted against the cell pressure as illustrated in Figure 3.4. The test can be described step by step as follows [32]:

- The cell starts at a pressure well above the bubble point pressure Figure 3.4-A.
- The pump is backed off to increase the cell volume and the new cell pressure is recorded. In Figure 3.4-B the bubble point pressure (P_b) is reached and the first bubble of the gas is formed. Looking at the *V-P* plot under each cell, the single-phase part of the curve is quite linear.
- In Figure 3.4-C the cell volume is further increased, such that the cell pressure is now P_3, which is less than P_b. More gas has come out of the

solution; as a result the sample compressibility changes significantly. This is illustrated in the *V-P* plot by the deviation from linearity.

- In Figure 3.4-D the cell volume is further expanded and the pressure continues to decrease, however, it decreases less with step increase in the sample volume.

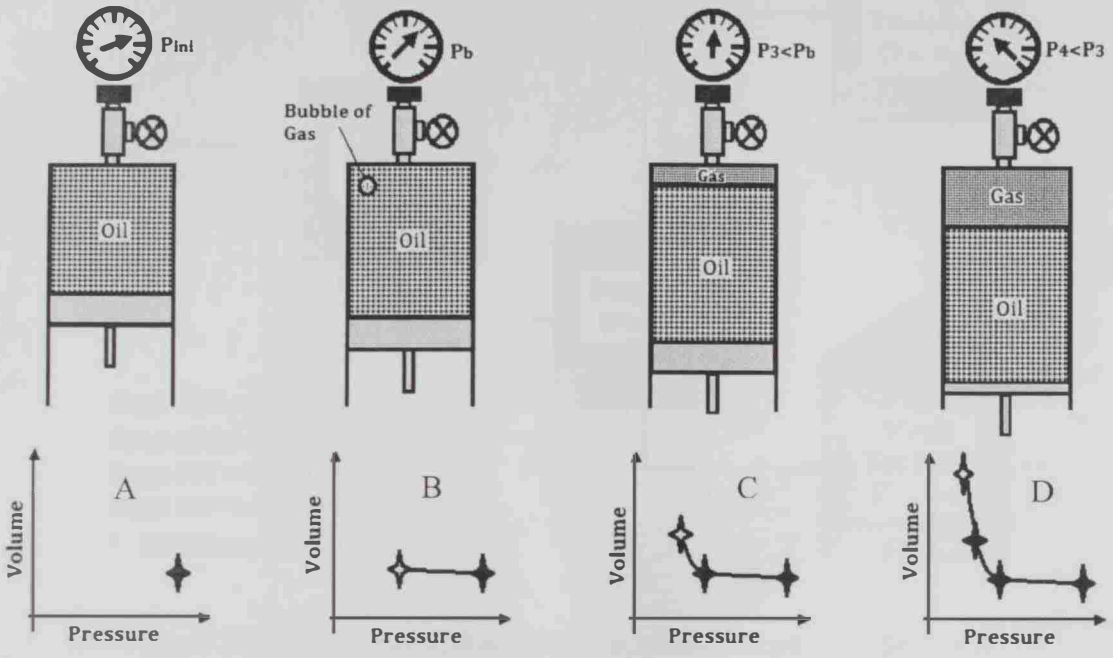

Figure 3.4: Schematic representation of the Constant Mass Study (CMS) test and the corresponding *V-P* curves [31].

3.2.4 The Separator Test (SEP)

The well stream fluid arriving at the surface is usually put through two or more stages of separation. A schematic of a 2-stage separator test is presented in Figure 3.5. A separator is effectively a large tank held at some pre-determined pressure and temperature, which allows the fluid to separate into vapor, liquid and optionally aqueous phases. Usually, the liquid from a first stage separator is taken as the feed for the second stage separator, and so on. Theoretically at least, the last stage is at standard conditions (P_{st} = 14.7 psia and T_{st} = 60 °F) and the liquid arriving here is the stock-tank oil. In practice, especially in an offshore environment, the liquid will be put into a sales line at some pressure in excess of the standard pressure. The vapor produced from each stage is collected together

and reported as if it had been taken to standard conditions. Again, in practice, the vapor will rarely be taken down to standard conditions although the volumes are corrected to these conditions [33].

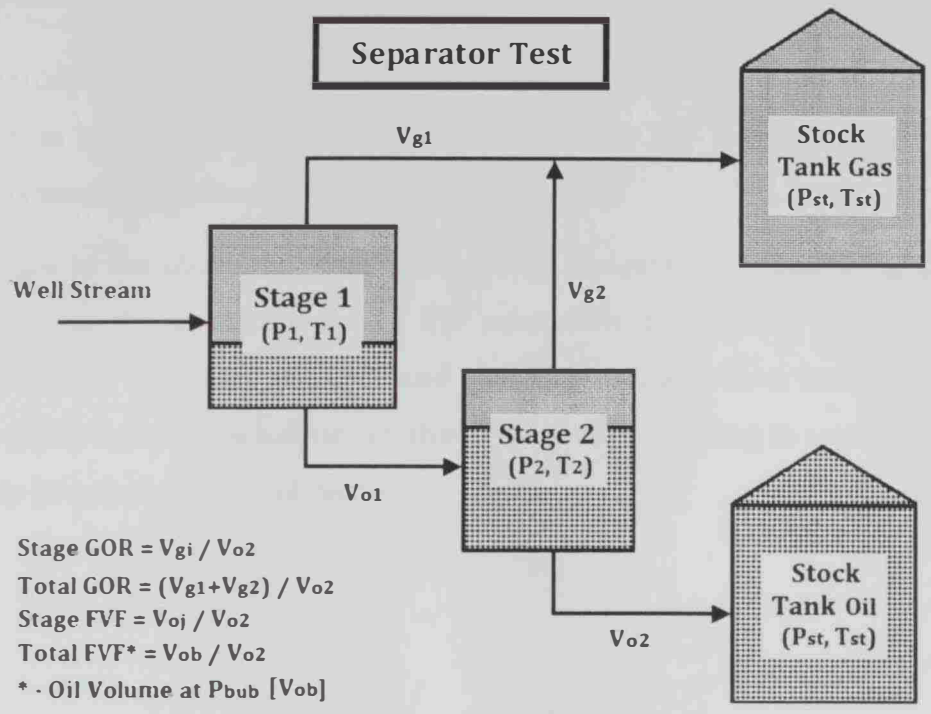

Figure 3.5: A schematic diagram of a 2-stage separator test [33].

The set of separator stages is sometimes referred to as separator sequence, which represents an approximation to the processing plant used in practice. The key parameters to determine are

- Gas-to-oil ratio (GOR) at each stage ($=V_{gi}/V_{o2}$) and hence the total GOR $=(V_{g1}+V_{g2})/V_{o2}$
- Oil formation volume factor (FVF_o) at each stage ($= V_{oi}/V_{o2}$), the total FVF_o ($= V_{ob}/V_{o2}$), where V_{ob} is the oil volume at saturation pressure (P_b)
- Densities of liberated fluids (oil and gas) at each stage.

The GOR is usually reported as the gas volume per oil volume both at stock tank standard conditions (P_{st}, T_{st}). The volume of the gas liberated at each stage, V_{gi} is at some elevated pressure and temperature (P_i, T_i) at which its Z-factor, Z_i, is measured. Then from the real gas law

$$PV = ZRT \tag{3.12}$$

One can compute the volume the gas will occupy at standard conditions from

$$V_{st} = \left[\frac{P_i V_i}{Z_i T_i}\right]\left[\frac{Z_{st} T_{st}}{P_{st}}\right] \tag{3.13}$$

By definition, the standard Z-factor at standard conditions, Z_{st} = 1.0. It is sometimes possible to adjust the pressure and temperature of the stages, usually the first-stage pressure, to maximize liquid production.

In addition to the above mentioned laboratory analysis and procedures, Chapter 4 is devoted to the determination of the saturation pressure by a recombination process at the reservoir pressure and temperature, and then swelling tests are conducted to investigate how much the CO_2 injection is going to swell the oil. This will help in enhancing the oil recovery.

Chapter Four

Experimental Setup and Procedures

4.1 Experimental Setup

The experimental setup used in this work consists of a high-pressure variable-volume PVT cell (made in Brazil), a syringe pump (ISCO 260D) and a heating device with magnetic stirrer (Stuart Magnetic Stirrer CC162/SC162) (see Figure 4.1). The view cell has two sapphire windows for visual observations, an absolute pressure transducer (Smar, LD 301) with a precision of ±0.31 bar, and a portable programmer (Smar, HT 201) for pressure data acquisition.

The equilibrium cell includes a movable piston, which permits the control of pressure inside the cell. Phase transitions are recorded through pressure manipulation using the syringe pump and a solvent (CO_2) as a pressurizing fluid. A set of valves used in the unit (see Figure 4.1) and their objectives are as outlined below:

V1: Needle valve (HIP, Model 15-12AF2). When opened allows the flow of CO_2 (or gas) from the first-stage separator to the chamber of the syringe pump.

V2: Two-way valve (HIP, Model 15-AF1). This valve is used to inject CO_2 or the gas from the first-stage separator through the syringe pump into the process line.

V3 and V5: Needle valves (Autoclave Engineers, Model MVE 1001). The function of these valves is to cut or allow the flow in a given line. V3 is used to isolate the unit from the pressure pump during assembly and disassembly of the equilibrium cell, and thus avoid gas or CO_2 loss. V5 function is to avoid any fluid flow to the piston during gas or CO_2 injection into the cell. When V5 is opened the pressurization or depressurization of the sample takes place through the piston displacement.

V4: Flush needle valve (HIP Model 1511AF1). Used for flushing the system and the cell depressurization. V4 is also used for gas removal during the two stage recombination process.

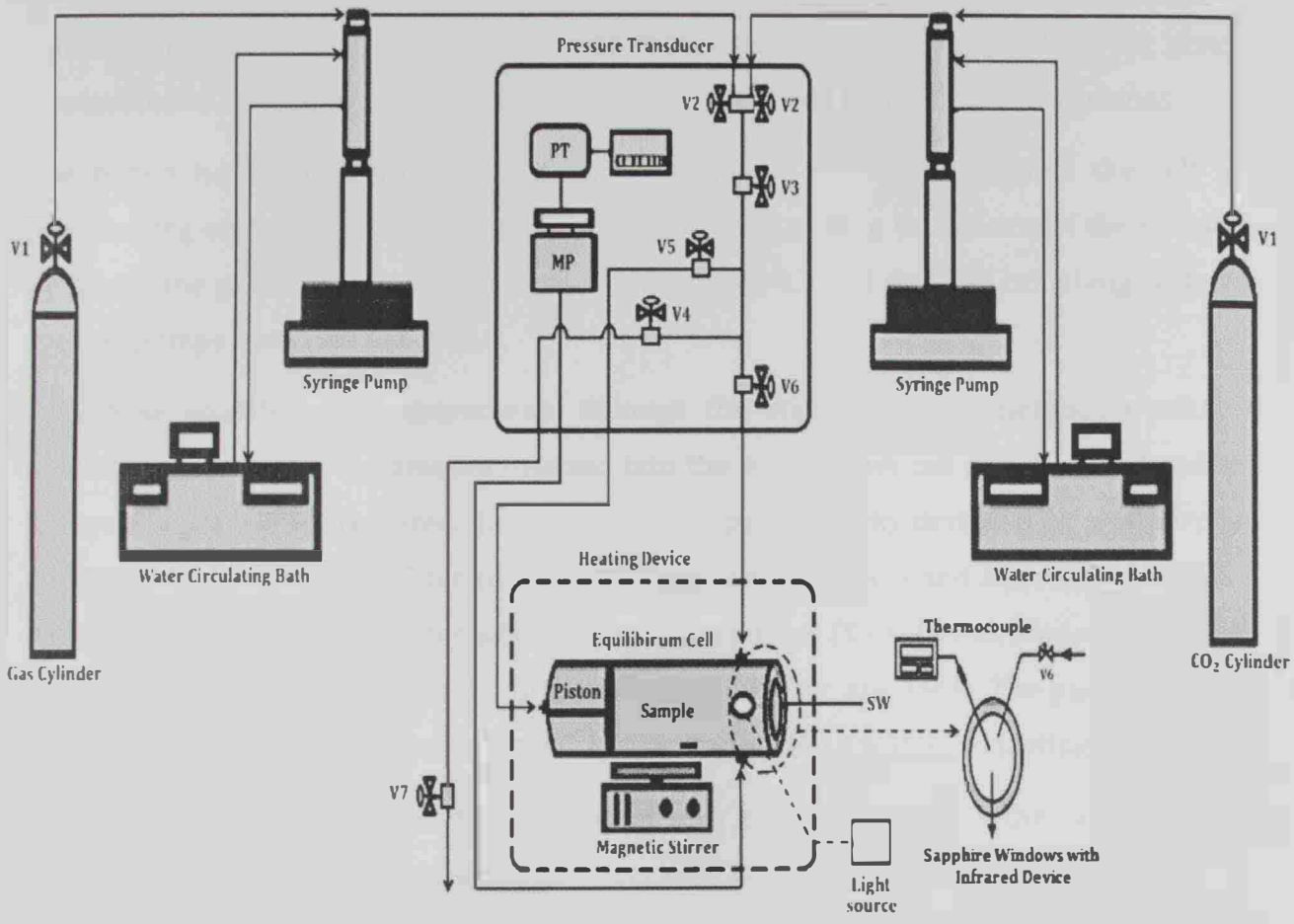

Figure 4.1: A schematic drawing of the experimental setup used in this work.

V6: Needle valve (Autoclave Engineers, Model MVE 1001). This valve is used as a feeding valve to inject a compressed fluid into the cell and is suitable for rigorous flow control of the fluid being injected.

V7: One-way valve (HIP Model 15-41AF1). This valve allows the flow in one direction and is used together with V4 to remove the gas from the pressurized system to ambient atmosphere during the recombination process.

The equilibrium PVT cell consists of a 316 stainless steel cylinder, with an internal diameter of 17.2 mm and a length of 176 mm. The cell is equipped with a piston for volume and system pressure variation.

Figure 4.2 presents the equilibrium cell which has three top holes: for thermocouple connection, for feed valve (V6) connection and for gas removal during the recombination process. The equilibrium cell has also a rear hole, lateral and front windows for piston displacement, light source and infrared device to detect and record phase transitions.

The piston has two BUNA N90 O-rings that allow a smooth slip inside the cell for pressurizing or depressurizing. The O-rings ensure the sealing (insulation of the sample). Details of the piston components are shown in Figure 4.3 and the PVT cell along with the syringe pumps shown in Figure 4.4.

For phase equilibrium measurements through the static-synthetic method, a suitable device for quantifying the amount injected into the equilibrium cell and also for handling the system pressure is required. Syringe-type pumps are ideally designed for this purpose and they have an inner cylinder connected to an automatic flow and a pressure indicator controller (COEL K484P). In this work, two syringe pumps (ISCO Brand, Model 260D) with an inner cylinder of 266 ml, and a pressure up to 500 bar are used. The pump chamber cylinder is jacketed, to keep its temperature constant using a water circulating bath.

The equilibrium assembly of the cell begins with the adjustment of the piston O-rings tightness. This step requires special care, because piston tightening should not be weak; this will allow fluid passage into the cell and changing the overall composition, and at the same time should not be too strong to avoid pressure drop between the sample and the process line.

Figure 4.2: The equilibrium cell used in this work.

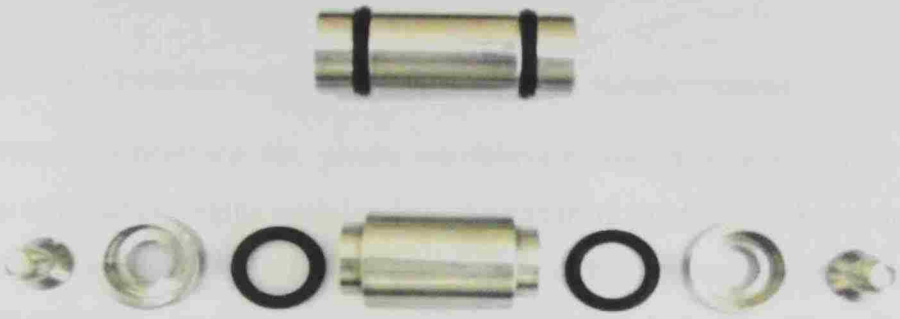

Figure 4.3: Details of the piston components

Figure 4.4: The PVT cell experimental setup used in this work

Once assembled, the equilibrium cell with the magnetic stirrer is placed into the heating device. A given amount of stock-tank oil is weighed and then injected into the cell using the syringe. The cell is then connected to the process line which has a temperature

controller and a pressure transducer for monitoring the sample temperature and pressure, respectively.

4.2 Experimental Procedure for Phase Equilibrium Measurement

The experimental procedure for phase equilibrium measurement, using this type of experimental apparatus, begins with loading the gas from the first-stage separator into the syringe pump chamber. Since the gas from the first stage separator is a mixture of hydrocarbons up to C_{7+}, its average vapor pressure is relatively low. Thus, the opening of the valve on the cylinder containing this gas might not be sufficient to move a reasonable amount of solvent (gas) into the syringe pump chamber. Usually, with the gas cylinder valve V1 opened for about thirty minutes and V2 closed, the temperature of the syringe pump chamber is kept at 283.15 K. This arrangement allows a natural flow from an ambient temperature zone (the gas cylinder) to a reduced temperature zone (the syringe pump chamber). While the syringe pump chamber is being filled, the equilibrium cell assembly can be started. A typical recombination process starts by insertion of a precise amount of stock-tank oil into the cell together with the magnetic stirrer on. The cell is then closed and connected to the process line, keeping valves V4, V5 and V6 closed, and valves V2 and V3 opened. With valve V1 closed, the entire line is kept pressurized using the syringe pump and stabilized at a pressure of 100 bar and 283.15 K. The stabilization of the system (zero pump flow) requires about 10 to 15 minutes, and should be done carefully because any trace of flow may lead to systematic errors in the volume of the gas injected. Once the system is stabilized the volume of the gas inside the syringe pump chamber is recorded and a given volume of the gas is injected into the cell through the micrometric valve V6. For a mass of stock-tank oil of 9 g, a 10 ml of gas is injected at 100 bar and 283.15 K. After the first gas injection the process is concluded, then the pressure of the system is lowered to (68 bar for well A#22 and 74 bar for well A#33) and valve V5 is opened (keeping valves V1, V4, and V6 closed and valves V2 and V3 opened). The recombination process is carried out at ambient temperature of 22.85 °C, so during this step no heating is required. For saturation pressure measurements, the light source from the lateral window of the equilibrium cell is turned on and an infrared device (which allows precise phase transition detection even at low or without visibility) is used to record the phase transitions. A sequence of procedures aiming to obtain a monophasic system is then started. By means of the magnetic stirrer, the system is continuously stirred

and the pressure inside the cell is gradually increased until the condition of a single-phase system is established. The pressure is then lowered to the saturation pressure of the well sample at 22.85 °C (i.e., 68 bar for well A#22 and 74 bar for well A#33) and the resulting vapor phase is removed by opening valves V6, V4 and V7.

The second stage for the recombination test is made by injecting fresh gas and repeating the above described procedure. Once the recombination process is completed, the saturation pressure of the recombined oil is measured at reservoir temperatures of wells A#22 and A#33 (235 °F and 257 °F, respectively), and the result is compared to the experimental data of the well sample. For this purpose the heating device is turned on and the pressure is monitored by the pressure indicator controller.

For CO_2 injection, the same procedure employed for the recombination process is used, replacing the gas from the first-stage separator by CO_2. In this case the CO_2 gas is injected at 224 bar and at reservoir temperature of 235 °F and 257 °F for wells A#22 & A#33 respectively.

4.3 Experimental Procedure for Swelling Measurement

A schematic of the swelling test apparatus is shown in Figure 4.5. For volume measurements of both live oil and CO_2/live oil mixture, the syringe pump along with the CO_2 material balance is used. The saturation pressure of the live oil is first measured then the pressure is lowered down to about 60 bar in order to leave the piston at its maximum position at the backside of the PVT cell. Valve V5 is then closed and the pressure of the syringe pump is increased up to the previously measured saturation pressure. The temperature of the syringe pump chamber is kept constant at 283.15 K (one has to wait up to complete stabilization of the system (zero flow in the syringe pump controller). The initial volume of the syringe pump, V_i, is recorded and while keeping the pressure constant, valve V5 is opened, to allow the movement of the piston. The final position of the piston keeps the live oil at saturation conditions (constant pressure and temperature). After stabilization the final saturation volume, V_f, is recorded. The displaced volume inside the syringe pump, V_s^0, is then computed as $V_s^0 = V_i - V_f$. Using the CO_2 chart [34], the density of CO_2 at the given temperature and pressure is calculated and the displaced CO_2 mass inside the syringe pump, m^0, is determined. This mass is the same as the mass displaced in the cell. Since the cell temperature is known (257 °F), the volume at the backside of the piston, V_c^0, can be computed. The volume of saturated live oil, V^0, can be

obtained by the difference between the overall available cell volume and the displaced volume inside the syringe pump, i.e. V^0 = 26.22 – V_s^0 ml. A given amount of CO_2 is then injected into the cell and the procedure described above is used to compute the displaced volume, V_s^{01}, the displaced CO_2 mass, m^{01}, inside the syringe pump, the volume at the backside of the piston, V_c^{01}, and the volume of the mixture, V^{01}.

The swelling factor is defined as the ratio between the volume of a saturated mixture of CO_2/live oil and the volume of saturated live oil at the reservoir temperature [34]. The amount of swelling experienced by a crude oil and the increase in the saturation pressure as a result of CO_2 injection is determined by the swelling factor which is the relative total volume or relative swollen volume, V^{sw} (= new saturation volume, V^{01}, at each incremental addition of CO_2, divided by the original saturation volume, V^0).

$$V^{sw} = \frac{V^{01}}{V^0} \tag{4.1}$$

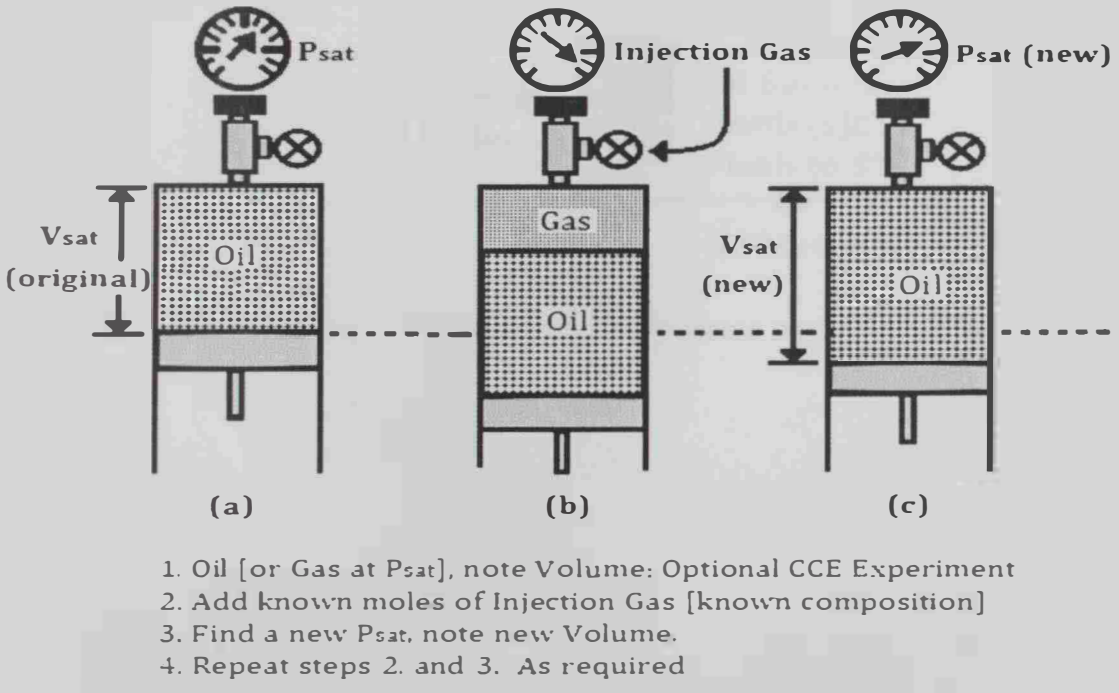

Figure 4.5: A schematic diagram of the swelling test procedure [31].

The results and discussion of the above experimental works will be shown in the next chapter.

4.4 Recombination of the Reservoir Fluid

Recombination of the stock-tank oil with the gas from the separator is the first and fundamental step for PVT study in petroleum systems. Since the gas composition from the first-stage separator is different from that obtained by flashing the monophasic well fluid directly to standard conditions, the recombination process using the gas from the first-stage separator can lead to live oil different from the well oil. The surface separation process can be illustrated in the schematic diagram shown in Figure 4.6.

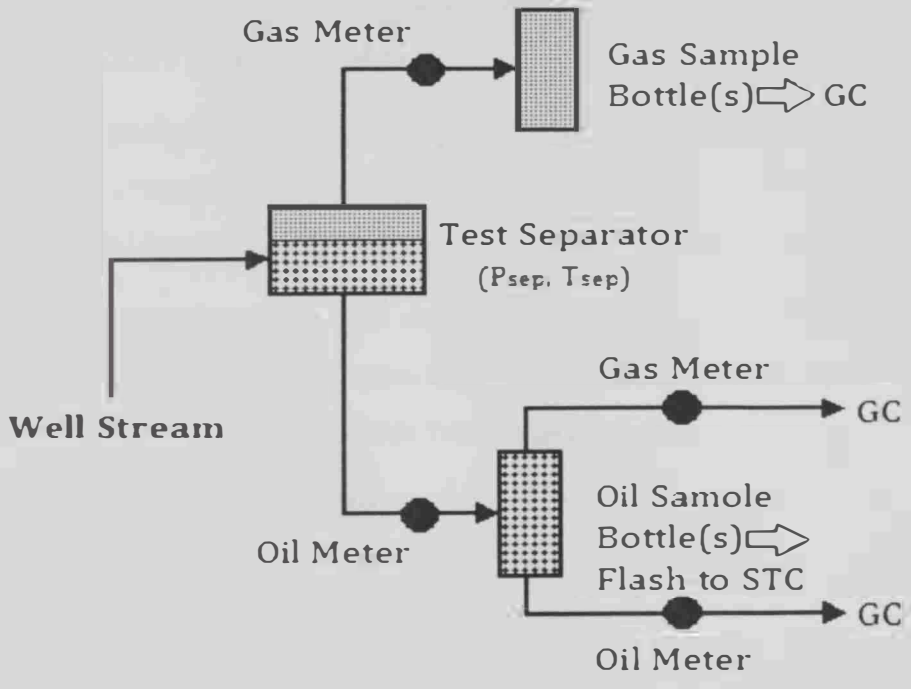

Figure 4.6: A schematic diagram of the surface separator metering and sampling [35].

Chapter Five
Field Data and Related Calculations

5.1 Field Data

Two bottom-hole samples were collected from Field A in UAE, denoted as wells A#22 & A#33. For well A#22, the reservoir initial static pressure was 4687 psia (32.32 MPa) and the bottom-hole temperature was 235 °F (385.9 K) while the bubble point pressure was 2277 psia (15.70 MPa). For well A#33, the reservoir initial static pressure was 2820 psia (19.4 MPa) and the bottom-hole temperature was 257 °F (398.15 K), while the bubble point pressure was 2377 psia (16.39 MPa).

The compositional analysis of the reservoir fluid was made through using a combination of distillation and chromatographic techniques. It should be noted that the Katz and Firoozabadi data [36] has been used during the calculation of the compositional analysis.

Exact values for the molar mass and densities of the heavier single carbon number fractions were obtained using Gas Chromatography-Mass Spectrometry (GC-MS) analysis and these can be used for optimized predictions using equations of state.

The available reservoir fluid compositions for flashed liquid, flashed gas and monophasic fluid from wells A#22 and A#33 are shown in Table 5.1 and the phase properties (molar mass and density) of $C_{20}+$ and fluid fractions are given in Table 5.2.

5.2 Compositional Analysis

Due to the difficulty and costs of bottom-hole samples measurements this work (project) is seeking to synthesize a reservoir fluids sample whose composition and bubble point is consistent with the available PVT data (wells A#22 and A#33) making these viable as representative of the reservoir oil. Thus, recombination is needed to reproduce as close as possible the reservoir fluid composition needed for the PVT studies using gas samples from the first-stage separator and stock-tank oil whose composition was performed by a commercial service provider.

The global composition of component i in the monophasic fluid is obtained through a global material balance:

$$z_i = \beta\, y_i + (1-\beta)\, x_i \qquad (5.1)$$

Table 5.1: Reservoir Fluid Compositions from Service Provider.

Compositions	Well A#22			Well A#33		
Components	Flashed Liquid (mol %)	Flashed Gas (mol %)	Monophasic Fluid (mol %)	Flashed Liquid (mol %)	Flashed Gas (mol %)	Monophasic Fluid (mol %)
N_2	0.00	0.23	0.119	0.00	0.18	0.101
CO_2	0.01	3.58	1.860	0.03	4.86	2.738
H_2S	0.00	0.00	0.000	0.00	0.00	0.000
CH_4	0.06	61.09	31.692	0.08	58.58	32.858
C_2H_6	0.15	11.80	6.188	0.25	11.73	6.682
C_3H_8	0.60	10.54	5.752	1.05	10.72	6.468
i-C_4H_{10}	0.37	2.24	1.339	0.57	2.39	1.590
n-C_4H_{10}	1.38	5.23	3.375	2.06	5.62	4.055
i-C_5H_{12}	1.36	1.65	1.510	1.73	1.88	1.814
n-C_5H_{12}	2.27	1.92	2.089	2.90	2.24	2.530
Pseudo C_6H_{14}	5.51	1.14	3.245	6.56	1.27	3.596
Pseudo C_7H_{16}	7.31	0.46	3.760	8.42	0.43	3.943
Pseudo C_8H_{18}	8.08	0.11	3.949	9.33	0.09	4.153
Pseudo C_9H_{20}	7.42	0.01	3.579	8.49	0.01	3.739
Pseudo $C_{10}H_{22}$	6.96	0.00	3.353	7.61	0.00	3.346
Pseudo $C_{11}H_{24}$	5.73	0.00	2.760	6.13	0.00	2.695
Pseudo $C_{12}H_{26}$	4.92	0.00	2.370	5.00	0.00	2.199
Pseudo $C_{13}H_{28}$	4.77	0.00	2.298	4.50	0.00	1.979
Pseudo $C_{14}H_{30}$	4.94	0.00	2.380	3.74	0.00	1.644
Pseudo $C_{15}H_{32}$	4.42	0.00	2.129	3.41	0.00	1.499
Pseudo $C_{16}H_{34}$	4.01	0.00	1.932	2.79	0.00	1.227
Pseudo $C_{17}H_{36}$	3.49	0.00	1.681	2.42	0.00	1.064
Pseudo $C_{18}H_{38}$	3.05	0.00	1.469	2.15	0.00	0.945
Pseudo $C_{19}H_{40}$	2.81	0.00	1.354	2.04	0.00	0.897
C_{20+}	20.38	0.00	9.817	18.75	0.00	8.244
Σ	100.00	100.00	100.00	100.01	100.00	100.00
Molar Ratio	0.4817	0.5183	1.00	0.4397	0.5603	1.00

Table 5.2: Phase properties of C_{20+} and fluid for flashed and monophasic fluids from wells A#22 and A#33.

	Well A#22			Well A#33		
Phase Properties	Flashed Liquid	Flashed Gas	Monophasic Fluid	Flashed Liquid	Flashed Gas	Monophasic Fluid
Molar mass	(g/mol)	(g/mol)	(g/mol)	(g/mol)	(g/mol)	(g/mol)
C_{20+}	403.78	--	403.78	424.48	--	424.48
Fluid	200.25	28.08	111.02	190.79	29.06	100.18
Density	(g/cm^3)	(g/cm^3)	(g/cm^3)	(g/cm^3)	(g/cm^3)	(g/cm^3)
C_{20+}	0.909	--	0.909	0.916	--	0.916
Fluid	0.832	0.001185	--	0.828	0.001227	--
Relative density (Air = 1)	--	0.970	--	--	1.003	--

Where β is the vapor molar ratio, y_i is the mole fraction of component i in the vapor phase, and x_i is the mole fraction of component i in the liquid phase. The values of β, y_i and x_i for wells A#22 and A#33 were obtained by flashing the monophasic fluid from the well condition to the standard conditions (60 °F and 14.7 psia). The resulting gas and liquid phases were then analyzed by gas chromatography. For the project chart, the values of y_i and x_i were obtained by chromatography analysis of the gas from the first-stage separator and the stock-tank oil.

With the objective to obtain a monophasic fluid with a composition close to that of the reservoir fluid, a simulation using PVTi module was performed at the saturation pressure of reservoir fluid on the recombined live oil obtained from the first-stage separator gas and the stock-tank oil. Noting that the field vapor molar ratios for wells A#22 and A#33 were 0.5183 and 0.5603, respectively.

By tuning the PVTi, the saturation pressure has been obtained for each well at the reservoir conditions but the PVTi did not succeed in getting the required vapor phase composition, especially for the methane, which has the highest percentage in the reservoir fluid, as shown in Figures 5.1 and 5.2. This might be attributed to the fact that we are using the gas available from the first-stage separator rather than a non-available late-stage separator gas. In order to solve such a problem, the monophasic fluid has been reproduced by recombining the resulting gas phase from the PVTi simulator with the stock-tank oil.

The average absolute errors in composition between the original and the reproduced monophasic fluids were 0.68% and 0.99% for wells A#22 and A#33, respectively. But still there was a high deviation error in the methane composition; 7.4% and 11% for wells A#22 and A#33, respectively. In order to minimize the deviation error in the methane composition, the vapor molar ratio was varied in this work until almost similar methane composition was obtained for each reservoir monophasic fluid. The final trial values of the vapor molar ratios were 0.4199 and 0.4196 for wells A#22 and A#33, respectively, as shown in Figures 5.1 and 5.2. The resulting average absolute errors in composition after these trial runs were 0.79% and 1.09% for wells A#22 and A#33, respectively.

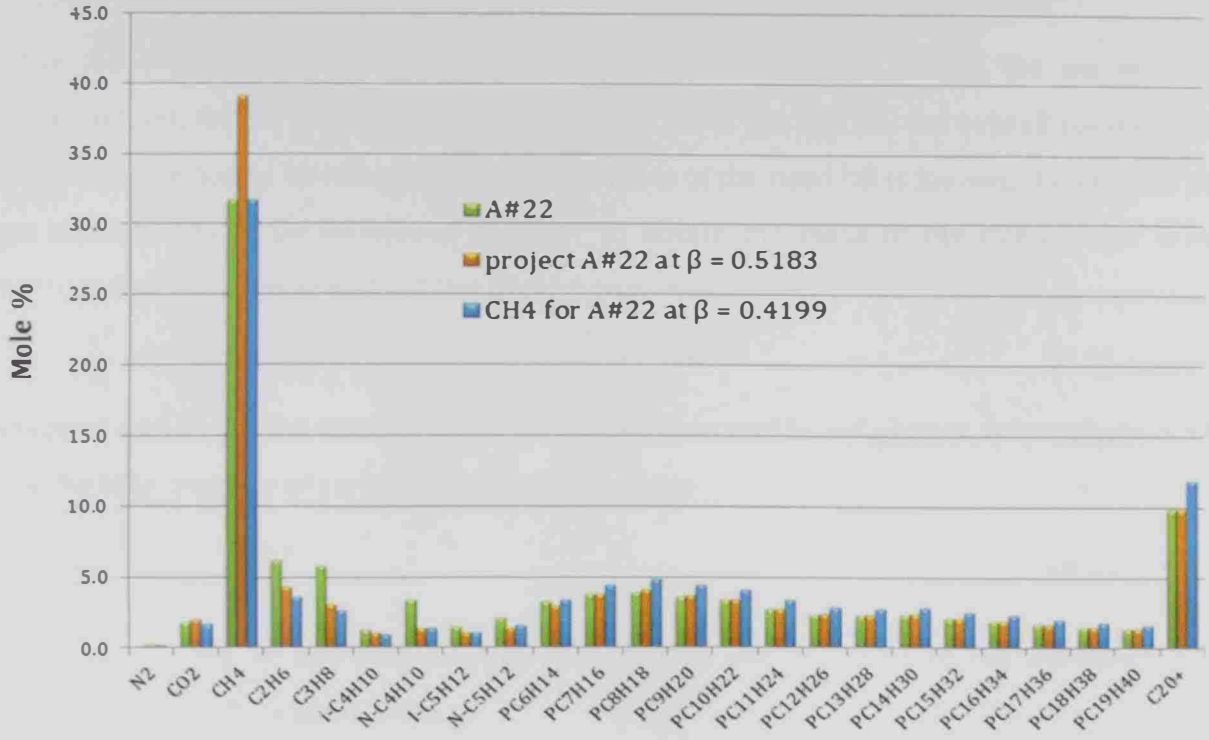

Figure 5.1: Compositional analysis of well A#22 fluid, recombined oil at β = 0.5183 and recombined oil at β = 0.4199 (0% deviation in methane composition).

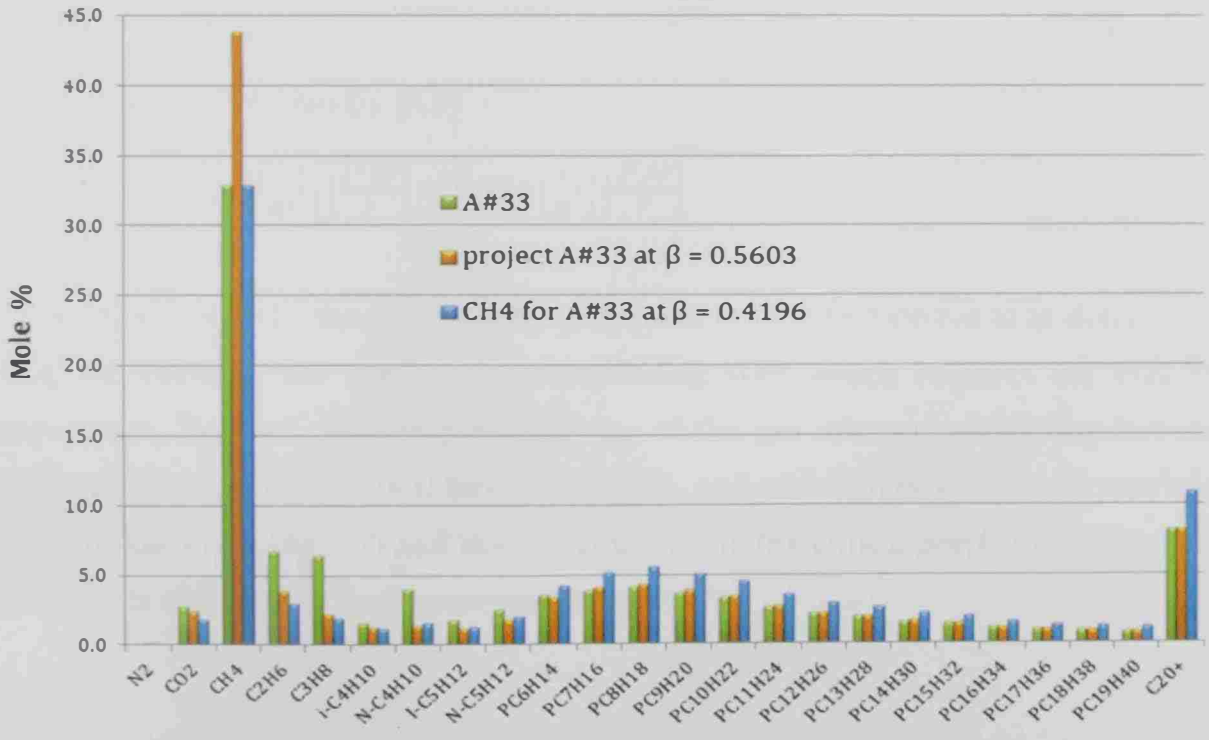

Figure 5.2: Compositional analysis of well A#33 fluid, recombined oil at β = 0.5603 and recombined oil at β = 0.4196 (0% deviation in methane composition).

5.3 Calculations for the Recombination Process

Since the two-stage recombination process is performed by injecting the gas into the stock-tank oil, for the phase behavior measurement of the live oil, the overall composition of the mixture has to be computed. Since the mass of the dead oil is known, the mass of the gas injected has to be estimated in order to obtain the mass of the live oil. For these purpose the same molar ratio of the project was used:

$$\frac{n^V}{n_t} = 0.42 \qquad \& \qquad \frac{n^L}{n_t} = 0.58 \tag{5.2}$$

where n^V and n^L are the number of moles in the vapor and liquid phases, respectively, and n_t is the total number of moles in both phases. Since

$$n^L = \frac{m^L}{M^L} = \frac{\rho^L V^L}{M^L} \tag{5.3}$$

where ρ^L, V^L and M^L are respectively, the density, the volume and the average molar weight of the stock-tank oil. Thus,

$$n_t = \frac{n^L}{0.42} \qquad \& \qquad n^V = 0.52\, n_t = 0.724 \frac{\rho^L V^L}{M^L} \tag{5.4}$$

For non-ideal gas,

$$V^V = n^V \left[\frac{Z^V RT}{P}\right] \tag{5.5}$$

Substituting Eq. (5.4) into Eq. (5.5)

$$V^V = 0.724 \left[\frac{\rho^L V^L}{M^L}\right]\left[\frac{Z^V RT}{P}\right] = 0.724 \left[\frac{m^L}{M^L}\right]\left[\frac{Z^V RT}{P}\right] \tag{5.6}$$

In order to calculate V^V, the compressibility factor of the gas mixture has to be determined using, for example, the theory of corresponding state which requires the reduced temperature, T_{rm}, and reduced pressure, P_{rm}, of the gas mixture; which requires the estimation of the mixture critical temperature, T_{cm}, and critical pressure, P_{cm}, for example, using the Kay's rule (Eq. 5.7) and the composition and the critical properties of the pure components of the gas mixture presented in Table 5.3.

$$T_{cm} = \sum_{i=1}^{n} y_i T_{ci}$$

$$P_{cm} = \sum_{i=1}^{n} y_i P_{ci} \tag{5.7}$$

Table 5.3: Critical properties and composition of the gas mixture of wells A#22 and A#33.

	Critical Properties		Mole fraction, y_i	
Component	**P_c, bar**	**T_c, K**	**A#22**	**A#33**
N_2	33.9	126.2	0.0049	0.0035
CO_2	73.9	304.7	0.0396	0.0426
C_1	46.0	190.6	0.7539	0.7820
C_2	48.8	305.4	0.0824	0.0672
C_3	42.5	369.8	0.0543	0.0318
i-C_4	36.5	408.1	0.0173	0.0193
n-C_4	38.0	425.2	0.0143	0.0089
i-C_5	33.9	460.4	0.0082	0.0070
n-C_5	33.7	469.6	0.0061	0.0090
C_6	30.1	507.5	0.0051	0.0087
C_7^+	16.8	733.7	0.0140	0.0199

In this work, the gas is injected at 283.15 K and 100 bar which correspond to the T_{rm} and P_{rm} values shown in Table 5.4 for wells A#22 A#33. Assuming the gas used to be a natural gas [16], then after estimation of the Z-factor as a function of the mixture reduced properties, Eq. (5.6) gives the volume of the gas, V^v, to be injected into the PVT cell.

Table 5.4: Calculated Z and V^v of the gas injected into the PVT cell for wells A#22 and A#33.

Property	**A#22**	**A#33**
Vapor molar ratio, β	0.42	0.42
P, bar	100	100
T, K	283.15	283.15
P_{cm}, bar	46.324	46.862
T_{cm}, K	231.66	223.25
P_{rm}	2.159	2.1339
T_{rm}	1.222	1.2683
Z^v (Using Eq. 2.4)	0.5804	0.5712
ρ^L, g/cc (Field data)	0.825	0.816
m^L, g (oil injected)	5.70	5.70
M^L, g/g-mol (Field data)	200.04	190.74
V^v, cc/g (Using Eq. 5.6)	0.6936	0.7161

For simulation purposes, a modified Peng-Robinson equation of state will be used to improve the accuracy of the calculated crude oil density.

5.4 The Modified Peng-Robinson Model

Suitable description of the PVT relationship and phase properties of real hydrocarbons is essential to get an accurate prediction of the reservoir performance, oil recovery and the performance of surface processing equipment.

In designing gas injection schemes and in many reservoir engineering situations, a reliable method to predict the crude oil density which is required for the calculation of the oil swelling and formation volume factors. This has led to many prediction methods and correlations which are generally applicable to specific cases and often require knowledge of molar volume and solubility of the gas in the live oil at the reservoir conditions. These correlations are empirical by their nature and thus can lead to large errors when extrapolated beyond the existing range of the variables.

Equations of state are used for generating the fluid model which helps in predicting the properties of the reservoir fluid at different pressures and compositions and also helps in material balance and flash calculations. The use of an EOS at certain temperature and pressure with known overall composition, allows to determine whether the fluid is a single or multi-phase and to estimate the density and composition of the existing phases.

Equation of state has been proven to be useful tools in the petroleum industry, allowing the improvement of the performance of equilibrium-based equipment, using a relatively small amount of input data. Calculation of phase behavior of multicomponent systems is the first and fundamental step in reservoir composition analysis.

Given a fluid of known composition at a certain temperature and pressure, the use of an equation of state allows to determine whether the fluid is a single phase and to estimate the density and composition of the existing phases. Density calculations can be performed using the approach of ideal solution, partial molar volume, corresponding state theory, and equations of state (EOS) [37].

Two cubic equations of state with three parameters (critical temperature, critical pressure and acentric factor) are widely used in the petroleum industry for phase properties calculations; the Soave-Redlich-Kwong (SRK) and the Peng-Robinson (PR) equations of state.

The SRK equation of state is given by

$$P = \frac{RT}{v-b} - \frac{a(T)}{v(v+b)} \tag{5.8}$$

where

$$a(T) = a_c \,.\, \alpha(T) \tag{5.9}$$

For pure components, a_c and b can be calculated using the $(\partial P/\partial V)$ and $(\partial^2 P/\partial V^2)$ at the critical point; and from which

$$a_c = 0.42748 \frac{R^2 T_c^2}{P_c} \tag{5.10}$$

$$b = 0.08664 \frac{RT_c}{P_c} \tag{5.11}$$

Soave [38] suggested that a_c is a function of the acentric factor (ω) and the reduced temperature (T_r) and calculated values of a at a series of temperatures for a large number of pure hydrocarbons, using the iso-fugacity criteria for equilibrium along the saturation pressure curve. Results show that $\alpha^{0.5}$ is a linear function of $T_r^{0.5}$ with a negative slope, thus

$$\alpha^{0.5} = 1 + m\,(1 - T_r^{0.5}) \tag{5.12}$$

where m is fitting function of the acentric factor (ω) of various compounds,

$$m = 0.480 + 1.574\omega - 0.176\omega^2 \tag{5.13}$$

and the acentric factor can be obtained using the Pitzer et al. [39] definition:

$$\omega = -1 - \log\left(\frac{P^{sat}}{P_c}\right)_{T_r=0.7} \tag{5.14}$$

The major failure of the SRK equation of state is the high predicted critical compressibility factor (Z_c = 0.333) and consequently a poor prediction of the liquid density.

A modification of the SRK equation of state was done by Peng and Robinson [40], where Eq. (5.8) through Eq. (5.14) are re-formulated as follows:

$$P = \frac{RT}{v-b} - \frac{a}{v(v+b)+b(v-b)} \tag{5.15}$$

where

$$b = 0.07780 \frac{RT_c}{P_c} \tag{5.16}$$

$$a_c = \left(\frac{0.45724 R^2 T_c^2}{P_c}\right) \tag{5.17}$$

For components with $\omega \leq 0.49$, the following function is used:

$$m = 0.379642 + 1.5422\omega - 0.2699\omega^2 \quad (5.18)$$

and for components with $\omega > 0.49$, the following function is used [40]:

$$m = 0.379642 + 1.48502\omega - 0.164423\omega^2 - 0.016666\omega^3 \quad (5.19)$$

The predicted critical compressibility factor from the PR EOS ($Z_c = 0.307$) is a significant improvement over that of the SRK equation of state, and consequently, the PR EOS predicts the liquid density better than the SRK EOS. However, the experimental values of Z_c for hydrocarbons are generally less than 0.29.

Modification of the equations of state using a volume shift correction leads to reduction of the Z-factor and is used to improve density estimation, especially that for liquids. Thus a fourth parameter usually referred to as volume-shift parameter, c_i, is introduced through the following relation [41]:

$$v^{(3)} = v^{(2)} - \sum_{i=1}^{N} z_i c_i \quad (5.20)$$

$v^{(3)}$ is called the corrected third-parameter molar volume, $v^{(2)}$ is the molar volume predicted by the two-parameter equation of state, and z_i is the liquid or vapor mole fraction (x_i or y_i) of component i. The values of c_i ($i = 1, N$), are commonly calculated by comparing the observed liquid molar volume (v^{OBS}) at standard conditions (T_{st} and P_{st}) with that obtained by the three-parameter equation of state (v^{EOS}) at the same conditions [42]. The difference between them determines the value of c_i for that specified component.

$$c_i = v^{EOS}(P_{st}, T_{st}) - v^{OBS}(P_{st}, T_{st}) \quad (5.21)$$

The shift parameters are usually defined as a ratio between the values of c_i and b_i

$$s_i = \frac{c_i}{b_i} \quad (5.22)$$

where b_i is the pure component volume parameter defined by the equation state, e.g., Eq. (5.16) for the PR EOS.

The volume-shift correction has no effect on the iso-fugacity condition and thus the other predicted values like the saturation pressure and k-values still unchanged [42].
Application of equations of state for fluid mixtures requires the use of mixing rules to obtain the mixture parameters from the pure components ones. For hydrocarbon system the modified van der Waals mixing rules are commonly used [43].

$$a = \sum_{i=1}^{n} \sum_{i=1}^{n} x_i x_j a_{ij} \quad (5.23)$$

$$a_{ij} = \left[(a_i a_j)^{0.5} \right] (1 - k_{ij}) \quad (5.24)$$

$$b = \sum_{i=1}^{n} x_i b_i \quad (5.25)$$

The k_{ij} parameters are usually referred to as binary interaction parameters and usually calculated by tuning the equation of state with experimental K values [34]. The k_{ij} for hydrocarbon systems are commonly set to zero, except for interaction between non-hydrocarbons and hydrocarbons and between light and heavy hydrocarbons, for k_{ij} between methane and heavy hydrocarbons the Katz-Firoozabadi equation is widely used [36]:

$$k_{ij} = 0.14\gamma_j - 0.06 \quad (5.26)$$

where γ_j is the specific gravity of component j.

Estimation of k_{ij} for non-polar pairs usually involves critical volumes. For example, the relationship of Chueh and Prausnitz [44] has been reconfirmed for non-polar pairs which is apparently reliable to within ±0.02 [45]. An alternative method for evaluating k_{ij} had been proposed [45].

$$k_{ij} = 1 - 8 \left[\frac{(v_{ci} v_{cj})^{1/6}}{(v_{ci}^{1/3} + v_{cj}^{1/3})} \right]^3 \quad (5.27)$$

where v_{ci} is the critical molar volume of component i. The physical meaning of the Chueh and Prausnitz correlation is based on the fact that the cubic root of the volume is the radius and therefore the k_{ij}'s are functions of a weighted average of the proximity within which two unequal species can come in contact.

In this work the k_{ij} values were calculated by the Chueh and Prausnitz correlation for the HC-HC components by tuning the Peng-Robinson equation of state with the available experimental saturation pressure data from the field wells A#22 and A#33. The results obtained from the SRK and PR equations of state have been obtained through the PVTi Eclipse Simulator and the results are presented in the next chapter.

Chapter Six

Results and Discussion

6.1 Simulation Results

The Schlumberger phase behavior (PVTi) package, along with the Soave-Redlich-Kwong and Peng-Robinson equations of state were used. The comparison between SRK & PR equations of state at saturation pressure of both wells A#22 and A#33 are shown in Table 6.1. The procedure of the PVTi simulator and the simulation results for the saturation pressure, CCE, DL, *P-T* flash, and separator tests are presented in Appendix A.

Table 6.1: Comparison between SRK and PR EOS predictions (using the PVTi Simulator) for (a) well A#22 and (b) well A#33.

(a) Well A#22 at 235 °F and converged P^{sat} = 2277 psia					
		3-parameter SRK EOS		3-parameter PR EOS	
Calculated Properties	**Field Data**	Value	Relative Error (%)	Value	Relative Error (%)
Vapor MW, g/mol	28.080	22.797	18.814	22.629	19.412
Liquid Viscosity, cP	0.460	0.366	20.435	0.352	23.478
Liquid MW, g/mol	111.020	110.940	0.072	110.940	0.072
Liquid Density, lb/ft³	41.880	43.460	3.773	43.200	3.152

(b) Well A#33 at 257 °F and converged P^{sat} = 2377 psia					
		3-parameter SRK EOS		3-parameter PR EOS	
Calculated Properties	**Field Data**	Value	Relative Error (%)	Value	Relative Error (%)
Vapor MW, g/mol	29.060	24.996	13.984	24.840	14.522
Liquid MW, g/mol	100.180	100.140	0.040	100.140	0.040
Liquid Viscosity, cP	0.320	0.255	20.313	0.247	22.813
Liquid Density, lb/ft³	40.827	40.979	0.372	40.830	0.007

The PR EOS generally gives better results than the SRK EOS when compared with the field data, as shown in Table 6.1. The PR EOS is selected to be used in experimental work using the PVTi Simulator.

In both the 2-parameter EOS (a & b) and the 3-parameter EOS (a, b and ω) the volume shift and binary interaction coefficients were used as correction parameters. Table 6.2 shows a comparison between 2- and 3-parameter PR EOS along with/without corrections for wells A#22 and A#33.

Table 6.2: Comparison between 2- & 3-parameter PR EOS (using PVTi Simulator) for (a) well A#22 and (b) well A#33.

(a) Well A#22 at 235 °F and converged P^{sat} = 2277 psia					
Calculated Properties	Field Data	2-parameter PR EOS		3-parameter PR EOS	
		Before Correction	*After correction*	*Before correction*	*After Correction*
Vapor MW, g/mol	28.08	22.6806	22.6815	22.6806	22.6286
Liquid MW, g/mol	111.02	110.9404	110.9404	110.9404	110.9404
Liquid Viscosity, cP	0.46	0.0750	0.1900	0.3464	0.3517
Liquid Density, lb/ft^3	41.889	31.0023	39.3745	43.2239	43.2033

(b) Well A#33 at 257 °F and converged P^{sat} = 2377 psia					
Calculated Properties	Field Data	2-parameter PR EOS		3-parameter PR EOS	
		Before Correction	*After correction*	*Before Correction*	*After Correction*
Vapor MW, g/mol	29.06	24.8371	24.8398	24.9164	24.8398
Liquid MW, g/mol	100.18	100.1410	100.1410	100.1410	100.1410
Liquid Viscosity, cP	0.32	0.1445	0.1487	0.2446	0.2474
Liquid Density, lb/ft^3	40.828	37.0567	36.1108	40.8283	40.8309

The PVTpro (Oilphase-DBR) is also works as PVTi in calculating the PVT properties of the reservoir fluids. Results of both simulators were used to be compared with field data and to know the accuracy of each simulator. The procedure of the PVTpro simulator is presented in the Appendix B which contains the results of simulation tests such as saturation pressure, CCE, DL, P-T Flash, Swelling and Separator Tests. The comparison results of both wells A#22 and A#33 fluids properties using PVTi and PVTpro are shown in Table 6.3 and 6.4 respectively. The vapor molar volume were seams good but the both simulators gave inaccurate results for saturated liquid molar volume for both wells, so, Rackett equation as explained below in detail, was used to calculate saturated liquid molar volume as shown in Tables 6.6 and 6.7.

The recombination flash simulation was performed at the reservoir temperature of 235 °F for well A#22 and 257 °F for well A#33 and saturation pressure of 2277 psia for well A#22 and 2377 psia for well A#33 using the monophasic fluid. The resulting gas phase was then removed through differential liberation. This step constitutes the first-stage of the recombination process.

The second-stage of the recombination flash simulation was performed at the reservoir conditions using numerically recombined monophasic fluid by using the liquid phase from the first-stage recombination process (stock-tank oil) and fresh gas from the first-stage separator and repeating the procedure used in the first stage. The resulting liquid phase was taken to represent the original reservoir live oil. The individual component

compositions from the simulated two-stage recombined fluid, simulated 1st- and 2nd-stage flash vs. field individual component compositions are shown in Figures 6.1 and 6.2 for wells A#22 and A#33, respectively.

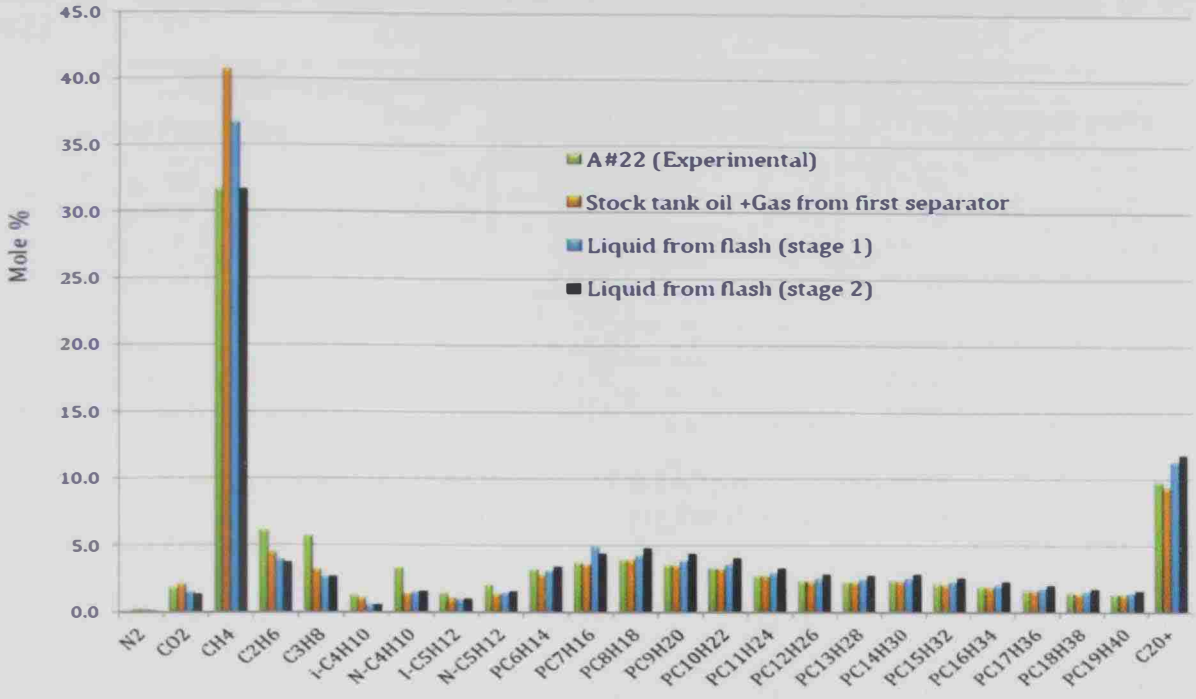

Figure 6.1: Simulated 2-stage recombined fluid, 1-stage flash, and 2-stage flash vs. field individual component compositions for well A#22.

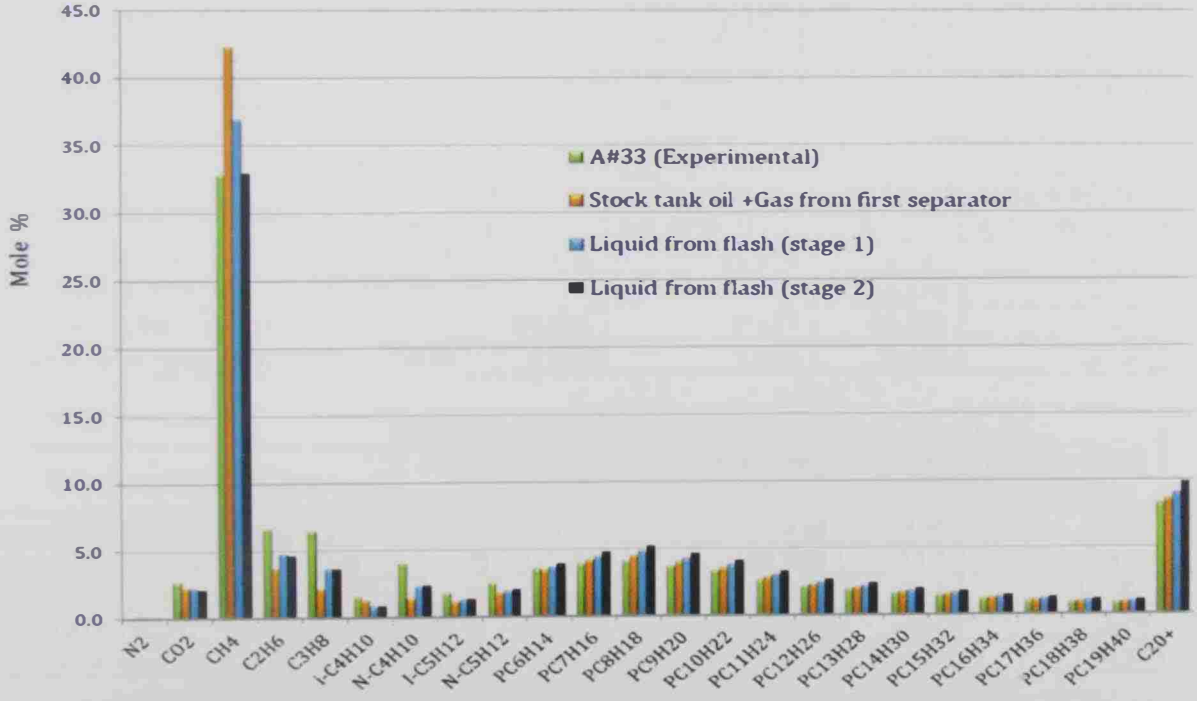

Figure 6.2: Simulated 2-stage recombined fluid, 1-stage flash, and 2-stage flash vs. field individual component compositions for well A#33.

It is clear that the two-stage recombination process can lead to a crude oil with a composition close enough to that of the reservoir fluid when compared to the one-stage recombination process.

Table 6.3: Comparison between PVTi & PVTpro in calculating fluid properties of well A#22.

Saturation pressure test at 235 °F and converged P^{sat} = 2277 psia					
Calculated Properties	Field Data	PVTi (Eclipse Simulator)		PVTpro (Oilphase-DBR)	
		Value	Rel. Error (%)	Value	Rel. Error (%)
Liquid MW, g/mol	111.02	110.94	0.072	110.96	0.054
Vapor MW, g/mol	28.08	22.63	19.42	23.03	17.98
Liquid Density, lb/ft³	41.89	43.20	3.127	44.29	5.729
Vapor Density, lb/ft³	---	7.923	---	8.100	---
Liquid Z-factor	---	0.7843	---	0.7652	---
Vapor Z-factor	---	0.7843	---	0.8685	---
Liquid Molar Vol, ft³/lb-mol	---	2.570	---	2.510	---
Vapor Molar Vol, ft3/lb-mol	---	2.856	---	2.840	---

Flash to standard conditions (60 °F & 14.7 psia) for Well A#22					
Calculated Properties	Field Data	PVTi (Eclipse Simulator)		PVTpro (Oilphase-DBR)	
		Value	Rel. Error (%)	Value	Rel. Error (%)
Flashed Liquid MW, g/mol	200.250	193.610	3.316	---	---
Flashed Vapor MW, g/mol	28.080	26.730	4.808	---	---
Flashed Liquid Density, lb/ft³	51.940	51.860	0.154	53.200	2.426
Flashed Vapor Density, lb/ft³	0.074	0.0708	4.324	0.0710	4.054

Constant Composition Expansion Test for Well A#22					
Calculated Properties	Field Data	PVTi (Eclipse Simulator)		PVTpro (Oilphase-DBR)	
		Value	Rel. Error (%)	Value	Rel. Error (%)
Compressibility P_i, psia^{-1}	1.10E-05	---		1.09E-05	0.909
Reservoir Oil Density, lb/ft³	43.262	43.203	0.137	45.800	5.865
Oil Viscosity at P_i, cP	0.520	0.475	8.654	0.465	10.577
Oil Viscosity at P_b, cP	0.460	0.371	19.348	0.378	17.826

Differential Liberation Test for Well A#22					
Calculated Properties	Field Data	PVTi (Eclipse Simulator)		PVTpro (Oilphase-DBR)	
		Value	Rel. Error (%)	Value	Rel. Error (%)
Oil Volume Factor	1.502	1.336	11.079	1.480	1.465
Solution GOR, ft³/bbl	671.000	---	---	710.300	5.857
Reservoir Oil Density, lb/ft³	43.262	43.203	0.137	44.300	2.398
Residual Oil Relative Density	0.840	0.781	7.012	0.867	3.167

Separator Test for Well A#22					
Calculated Properties	Field Data	PVTi (Eclipse Simulator)		PVTpro (Oilphase-DBR)	
		Value	Rel. Error (%)	Value	Rel. Error (%)
Separator GOR @ 265 psia, ft³/bbl	395	373.479	5.448	400	1.266
Separator GOR @ 60 psia, ft³/bbl	69	155.599	125.506	71.7	3.913
Separator GOR @ 15 psia, ft³/bbl	36	101.162	181.006	22.9	36.389
Oil Volume Factor	1.361	1.075	21.014	1.311	3.674
Stock-tank oil density, lb/ft³	51.503	51.438	0.126	52.602	2.133

Table 6.4: Comparison between PVTi & PVTpro in calculating fluid properties of well A#33.

Saturation pressure test at 257 °F and converged P_{sat} = 2377 psia					
Calculated Properties	Field Data	PVTi (Eclipse Simulator)		PVTpro (Oilphase-DBR)	
		Value	Rel. Error (%)	Value	Rel. Error (%)
Liquid MW, g/mol	100.18	100.141	0.0389	102.93	2.745
Vapor MW, g/mol	29.06	24.839	14.525	25.430	12.491
Liquid Density, lb/ft³	40.83	40.832	0.005	42.810	4.849
Vapor Density, lb/ft³	---	8.907	---	9.122	---
Liquid Z-factor	---	0.758	---	0.755	---
Vapor Z-factor	---	0.758	---	0.859	---
Liquid Molar Volume, ft³/lb-mol	---	2.45	---	2.44	---
Vapor Molar Volume, ft3/lb-mol	---	2.79	---	2.78	---

Flash to standard conditions (60 °F & 14.7 psia) for Well A#33					
Calculated Properties	Field Data	PVTi (Eclipse Simulator)		PVTpro (Oilphase-DBR)	
		Value	Rel. Error (%)	Value	Rel. Error (%)
Flashed Liquid MW, g/mol	190.790	185.677	2.680	---	---
Flashed Vapor MW, g/mol	29.060	28.133	3.190	---	---
Flashed Liquid Density, lb/ft³	51.692	51.428	0.511	52.800	2.143
Flashed Vapor Density, lb/ft³	0.077	0.0745	2.742	0.0750	2.089

Constant Composition Expansion Test for Well A#33					
Calculated Properties	Field Data	PVTi (Eclipse Simulator)		PVTpro (Oilphase-DBR)	
		Value	Rel. Error (%)	Value	Rel. Error (%)
Compressibility at P_i, psia^{-1}	1.82E-05	---	---	1.88E-05	3.242
Reservoir oil density, lb/ft³	41.202	41.283	0.195	43.199	4.847
Oil Viscosity at P_i, cP	0.340	0.267	21.382	0.333	2.059
Oil Viscosity at P_b, cP	0.320	0.247	22.688	0.319	0.313

Differential Liberation Test for Well A#33					
Calculated Properties	Field Data	PVTi (Eclipse Simulator)		PVTpro (Oilphase-DBR)	
		Value	Rel. Error (%)	Value	Rel. Error (%)
Oil Volume Factor	1.645	1.458	11.368	1.670	1.520
Solution GOR, ft³/bbl	893.000	---	---	914.100	2.363
Reservoir Oil Density, lb/ft³	40.828	40.831	0.008	42.800	4.830
Residual Oil Relative Density	0.841	0.857	1.902	0.870	3.448

Separator Test for Well A#33					
Calculated Properties	Field Data	PVTi (Eclipse Simulator)		PVTpro (Oilphase-DBR)	
		Value	Rel. Error (%)	Value	Rel. Error (%)
Separator GOR @ 265 psia, ft³/bbl	487.00	450.290	7.538	437.500	10.164
Separator GOR @ 60 psia, ft³/bbl	90.000	173.770	93.078	80.200	10.889
Separator GOR @ 15 psia, ft³/bbl	50.000	126.520	153.040	27.500	45.000
Oil Volume Factor	1.422	1.019	28.340	1.364	4.079
Stock-tank oil density, lb/ft³	50.941	50.873	0.134	52.100	2.275

The fluid of each well was also recombined using the PVTpro simulator. The inputs to the simulator were the first-stage separator gas and the stack-tank oil, which were recombined based on the reservoir saturation temperature and pressure. The compositions of the reservoir fluid and the resulting recombined fluid (as obtained by PVTpro) are shown in Figures 6.3 and 6.4 for wells A#22 and A#33, respectively.

These results are also shown in Table 6.5 along with the relative errors for each component with an average relative error of 0.17% for well A#22 and 3.11% for well A#33, respectively.

Table 6.5: Experimental composition (reservoir fluid) vs. predicted (recombined fluid using PVTpro) composition for wells A#22 and A#33.

Well A#22			
Comp.	Reservoir Fluid, mol%	Recombined Fluid (PVTpro), mol%	Relative Error, %
N_2	0.1192	0.1190	0.1753
CO_2	1.8603	1.8568	0.1898
C1	31.6918	31.6313	0.1911
C2	6.1882	6.1766	0.1874
C3	5.7519	5.7420	0.1722
iC4	1.3392	1.3375	0.1285
nC4	3.3755	3.3717	0.1112
iC5	1.5103	1.5101	0.0137
nC5	2.0886	2.0889	0.0146
C6	3.2450	3.2494	0.1347
C7	3.7596	3.7664	0.1797
C8	3.9491	3.9571	0.2013
C9	3.5794	3.5867	0.2040
C10	3.3526	3.3595	0.2049
C11	2.7601	2.7658	0.2050
C12	2.3700	2.3748	0.2041
C13	2.2977	2.3024	0.2042
C14	2.3796	2.3845	0.2060
C15	2.1291	2.1335	0.2060
C16	1.9316	1.9356	0.2062
C17	1.6811	1.6846	0.2062
C18	1.4692	1.4722	0.2052
C19	1.3536	1.3564	0.2086
C20+	9.8170	9.8372	0.2053
		Average ARE =	0.1735

Well A#33			
Comp.	Reservoir Fluid, mol%	Recombined Fluid (PVTpro), mol%	Relative Error, %
N_2	0.1000	0.0977	2.2602
CO_2	2.7397	2.6523	3.1901
C1	32.8567	31.8413	3.0904
C2	6.6793	6.4828	2.9419
C3	6.4694	6.3001	2.6169
iC4	1.5898	1.5581	1.9940
nC4	4.0496	3.9927	1.4051
iC5	1.8098	1.8114	0.0884
nC5	2.5297	2.5415	0.4665
C6	3.5996	3.6876	2.4447
C7	3.9396	4.0816	3.6044
C8	4.1496	4.3129	3.9353
C9	3.7396	3.8856	3.9042
C10	3.3497	3.4780	3.8302
C11	2.6997	2.8016	3.7745
C12	2.1998	2.2851	3.8776
C13	1.9798	2.0566	3.8792
C14	1.6398	1.7093	4.2383
C15	1.4999	1.5585	3.9069
C16	1.2299	1.2751	3.6751
C17	1.0599	1.1060	4.3495
C18	0.9499	0.9826	3.4425
C19	0.8999	0.9323	3.6004
C20+	8.2392	8.5692	4.0052
		Average ARE =	3.1051

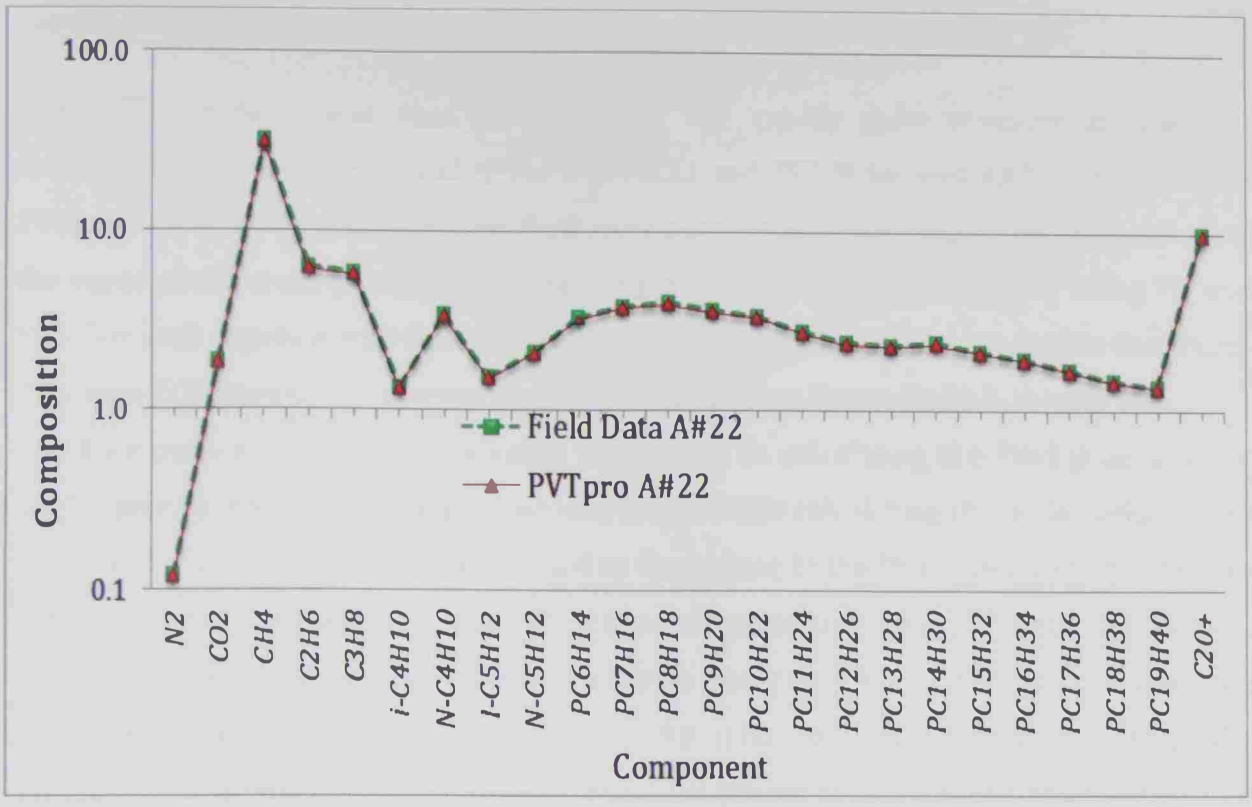

Figure 6.3: Experimental (reservoir fluid) vs. predicted (recombined fluid using PVTpro) compositions for well A#22.

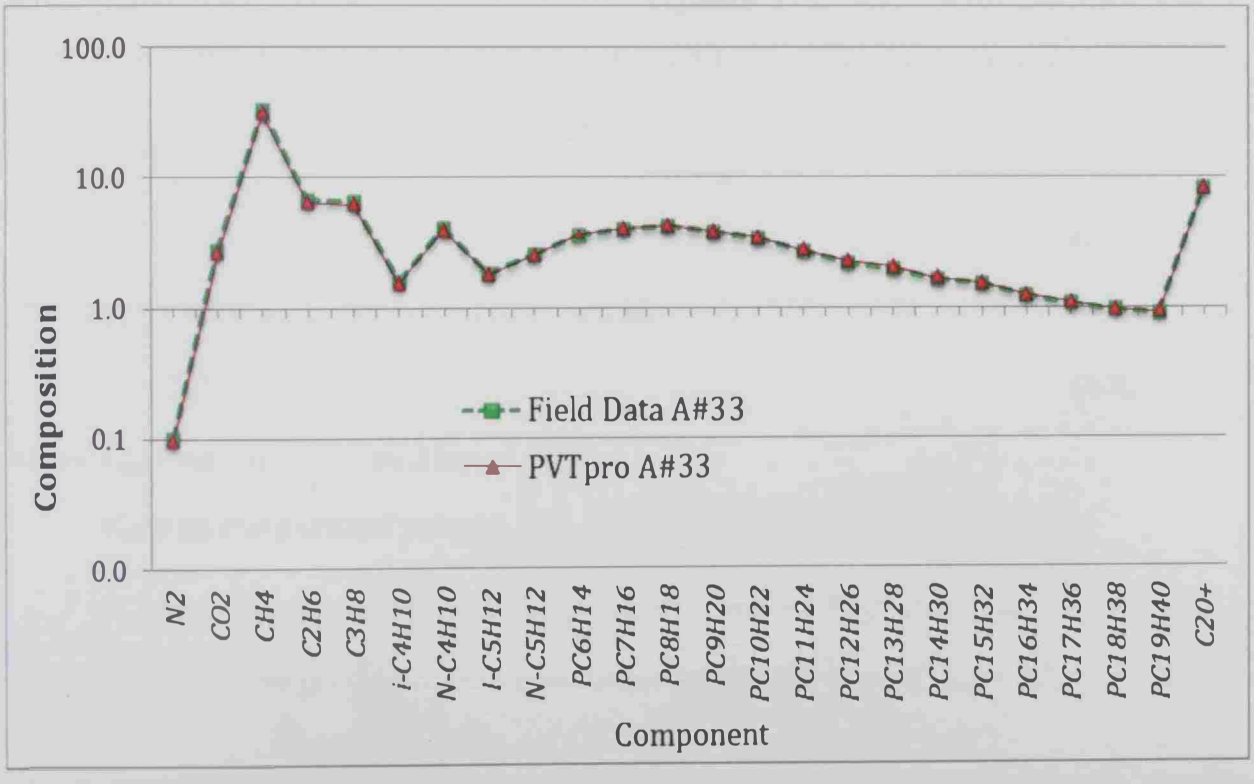

Figure 6.4: Experimental (reservoir fluid) vs. predicted (recombined fluid using PVTpro) compositions for well A#33.

Liquid Density

The PVTi simulator was used in calculating the bubble point pressure at reservoir temperatures of both wells (235 °F for well A#22 and 257 °F for well A#33), the inputs in PVTi simulator was the monophasic fluid mole percent as feed for liquid phase to calculate the vapor phase mole percent. So, comparing the results of PVTi simulator using PR and SRK EOS with experimental field data as shown in "Appendix A", one can realize that Peng-Robinson EOS gave more accurate and better results than Soave-Redlich-Kwong EOS.

The PR equation of state was selected to be used in calculating the fluid properties at bubble point pressure, but some error was found while calculating the molar volume and Z-factor for the liquid phase which is used as feed phase in the PVTi simulator, the error in the liquid molar volume was about 32% when compared to the experimental field data. It was then decided to use the following Rackett equation [45, p. 4.35] to calculate the saturated liquid volume as a function of the mixture pseudo-conditions. Thus the assumption in applying corresponding states to mixtures is that the *PVT* behavior will be the same as that of a pure component whose T_c and P_c are equal to the pseudo-critical temperature, T_{cm}, and pseudo-critical pressure of the mixture, P_{cm}, and other corresponding states principle (CSP) parameters such as acentric factor can also be made composition dependent adequately for reliable estimation purposes [45, p. 5.5].

$$V_s = V_c Z_c^{(1-T/T_c)^{(2/7)}} = \frac{RT_c}{P_c} Z_c^{\left[1+(1-T/T_c)^{(2/7)}\right]} \tag{6.1}$$

$$Z_c = 0.29056 - 0.08775\,\omega \tag{6.2}$$

The mixture acentric factor is approximated by

$$\omega = \sum_{i=1}^{N} x_i w_i \tag{6.3}$$

where V_{sm} = mixture saturated liquid volume,

V_{cm} = mixture critical volume, $\left(V_{cm} = \frac{Z_{cm} R T_{cm}}{P_{cm}}\right)$,

T_{cm} = mixture pseudo-critical temperature using the Kay's rule ($T_{cm} = \sum_{i=1}^{n} x_i T_{ci}$)

P_{cm} = mixture pseudo-critical pressure using the Kay's rule ($P_{cm} = \sum_{i=1}^{n} x_i P_{ci}$,).

The mixture critical compressibility factor, Z_{cm}, was then determined using the pseudo-reduced properties (P_{rm} and T_{rm}) and the Standing-Katz chart.

The input data used in the above calculations and the results obtained from the Rackett equation are summarized in Tables 6.5 and 6.6 for wells A#22 and A#33, respectively. Thus using the Rackett equation in calculating the saturated liquid volume, V_{sm}, the relative error was reduced to about 6.25% for well A#22 and 6.74% for well A#33 when compared to the reservoir fluid values.

Table 6.6: Calculated saturated liquid volume and density using the Rackett equation for well A#22 at 2277 psia and 235 °F. (See Table A.1 for pure component properties)

Component	x_i	$x_i P_{ci}$	$x_i T_{ci}$	$x_i M_i$	$\omega_i x_i$	V_{sL}, ft³/lb-mol	V_{sL}, ft³/lb	ρ_L, lb/ft³	ρ_L, kg/m³
N_2	0.0000	0.00	0.00	0.00	0.0000	-	-	-	-
CO_2	0.0001	0.11	0.05	0.00	0.0000	-	-	-	-
C1	0.0006	0.40	0.21	0.01	0.0000	-	-	-	-
C2	0.0015	1.06	0.83	0.05	0.0001	-	-	-	-
C3	0.0060	3.70	4.00	0.26	0.0009	-	-	-	-
iC4	0.0037	1.96	2.72	0.22	0.0007	2.33	0.040	24.928	399.31
nC4	0.0138	7.60	10.58	0.80	0.0028	2.11	0.036	27.556	441.41
iC5	0.0136	6.67	11.29	0.98	0.0031	2.26	0.031	31.962	511.99
nC5	0.0227	11.10	19.22	1.64	0.0057	2.23	0.031	32.322	517.76
C6	0.0551	27.32	50.81	4.68	0.0143	2.21	0.026	38.435	615.68
C7	0.0731	32.61	72.04	7.02	0.0204	2.48	0.026	38.739	620.55
C8	0.0808	32.89	84.02	8.61	0.0249	2.73	0.026	39.037	625.33
C9	0.0742	27.84	80.71	8.89	0.0253	2.97	0.025	40.372	646.70
C10	0.0696	24.26	78.70	9.31	0.0262	3.19	0.024	41.924	671.58
C11	0.0573	18.67	67.04	8.49	0.0236	3.40	0.023	43.547	697.57
C12	0.0492	15.06	59.35	8.00	0.0221	3.60	0.022	45.161	723.42
C13	0.0477	13.77	59.14	8.40	0.0231	3.79	0.022	46.379	742.94
C14	0.0494	13.50	62.79	9.48	0.0257	3.98	0.021	48.205	772.19
C15	0.0442	11.47	57.48	9.12	0.0245	4.16	0.020	49.601	794.54
C16	0.0401	9.91	53.25	8.84	0.0235	4.33	0.020	50.904	815.41
C17	0.0349	8.23	47.25	8.19	0.0215	4.50	0.019	52.112	834.76
C18	0.0305	6.882	42.043	7.574	0.0197	4.666	0.019	53.227	852.632
C19	0.0281	6.077	39.387	7.359	0.0190	4.827	0.018	54.253	869.061
C20+	0.2038	23.900	419.685	82.131	0.2032	9.273	0.023	43.459	696.165
Mixture	1.00	305.00	1322.61	200.04	0.5303	3.632	0.0180	55.082	882.35
Field data							0.0192	52.000	833.00
Av. AR.E. (%)							6.25	5.926	5.924

Pressure	2277	*Psia*
Temperature	695	*°R*
P_{cm}	305	*Psia*
T_{cm}	1322.61	*°R*
P_{rm}	7.47	
T_{rm}	0.525	

Table 6.7: Calculated saturated liquid volume and density using the Rackett equation for well A#33 at 2377 psia and 257 °F. (See Table A.1 for pure component properties)

Component	x_i	$x_i P_{ci}$	$x_i T_{ci}$	$x_i M_i$	$\omega_i x_i$	V_{sL}, ft³/lb-mol	V_{sL}, ft³/lb	ρ_L, lb/ft³	ρ_L, kg/m³
N_2	0.0000	0.00	0.00	0.00	0.000	-	-	-	-
CO_2	0.0003	0.36	0.19	0.01	0.000	-	-	-	-
C1	0.0008	0.53	0.28	0.01	0.000	-	-	-	-
C2	0.0025	1.77	1.38	0.08	0.000	-	-	-	-
C3	0.0105	6.47	7.00	0.46	0.002	-	-	-	-
iC4	0.0057	3.02	4.20	0.33	0.001	2.60	0.045	22.344	357.93
nC4	0.0206	11.34	15.79	1.20	0.004	2.25	0.039	25.832	413.80
iC5	0.0173	8.48	14.36	1.25	0.004	2.34	0.032	30.773	492.95
nC5	0.0290	14.17	24.56	2.09	0.007	2.31	0.032	31.221	500.13
C6	0.0656	32.53	60.50	5.57	0.017	2.27	0.027	37.489	600.52
C7	0.0842	37.56	82.98	8.08	0.024	2.53	0.026	37.954	607.98
C8	0.0933	37.98	97.02	9.94	0.029	2.78	0.026	38.346	614.25
C9	0.0849	31.86	92.35	10.17	0.029	3.02	0.025	39.724	636.33
C10	0.0761	26.53	86.05	10.18	0.029	3.24	0.024	41.302	661.61
C11	0.0613	19.97	71.73	9.08	0.025	3.45	0.023	42.941	687.86
C12	0.0500	15.31	60.31	8.13	0.022	3.65	0.022	44.564	713.86
C13	0.0450	12.99	55.79	7.92	0.022	3.84	0.022	45.794	733.56
C14	0.0374	10.22	47.54	7.18	0.019	4.03	0.021	47.620	762.81
C15	0.0341	8.85	44.34	7.03	0.019	4.21	0.020	49.018	785.21
C16	0.0279	6.90	37.05	6.15	0.016	4.38	0.020	50.323	806.12
C17	0.0242	5.71	32.77	5.68	0.015	4.55	0.019	51.533	825.50
C18	0.0215	4.85	29.64	5.34	0.014	4.72	0.019	52.650	843.39
C19	0.0204	4.41	28.59	5.34	0.014	4.88	0.019	53.677	859.84
C20+	0.1875	21.99	386.12	79.50	0.187	9.33	0.022	45.429	727.72
Mixture	1.00	323.81	1280.52	190.74	0.499	3.46	0.0180	55.102	882.66
Field data							0.0193	51.690	828.00
Av. AR.E. (%)							6.735	6.600	6.6014

Pressure	2377	*Psia*
Temperature	716.67	*°R*
P_{cm}	323.81	*Psia*
T_{cm}	1280.52	*°R*
P_{rm}	7.34	
T_{rm}	0.56	

6.2 Experimental Results

Typical results of the synthetic static method are bubble point and dew point curves. It is important to emphasize that for a system with known global composition, at a given temperature and pressure, this technique can only determine whether the system is composed by one, two or three phases. These respective phase composition are still unknown (dead oil) as in Figure 6.5 and 6.6, respectively, show the photography of single and initial phase formation in live oil system, while Figure 6.7 and 6.8, respectively, show the monophasic fluid and phase transition for the system CO_2/Live oil system with 50% of CO_2 in mass.

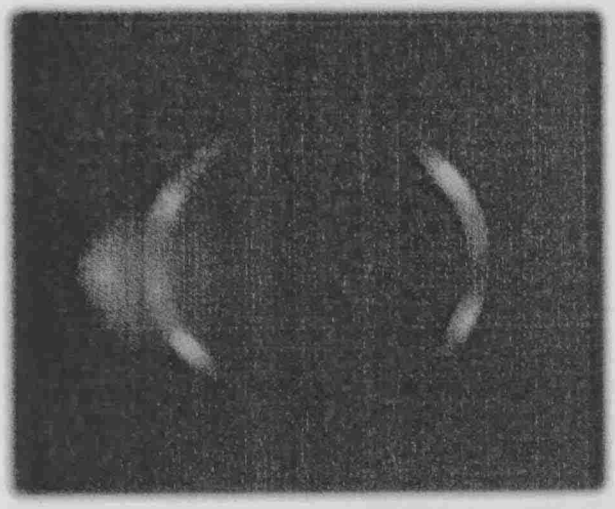

Figure 6.5: Monophasic live oil at 257 °F for well A#33.

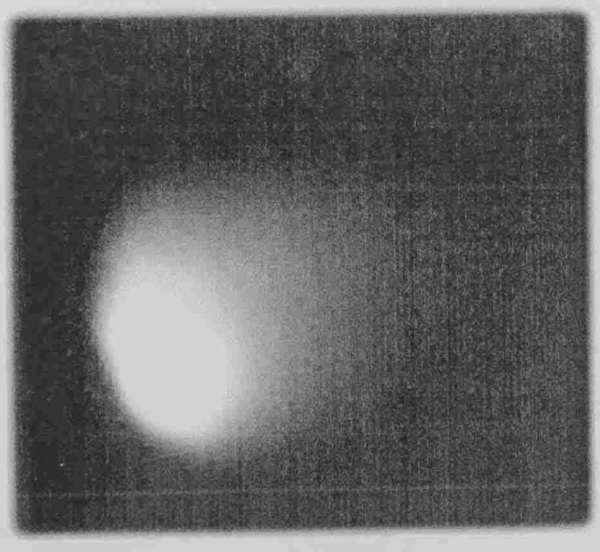

Figure 6.6: Initial phase formation in live oil at 257 °F for well A#33.

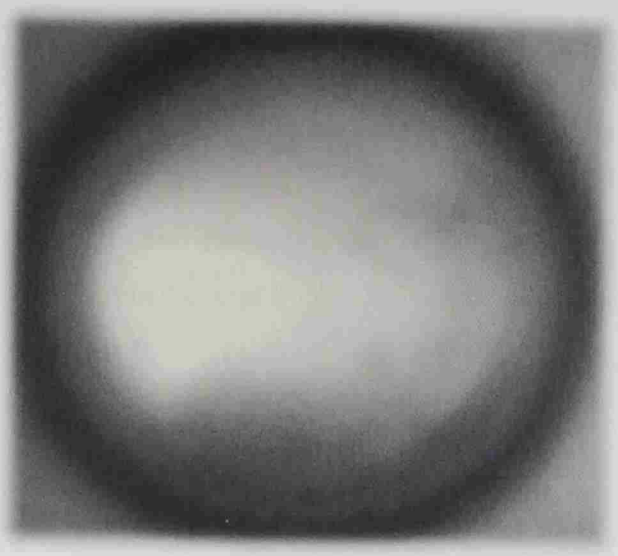

Figure 6.7: Monophasic fluid of the system CO_2/live oil at 257 °F for well A#33.

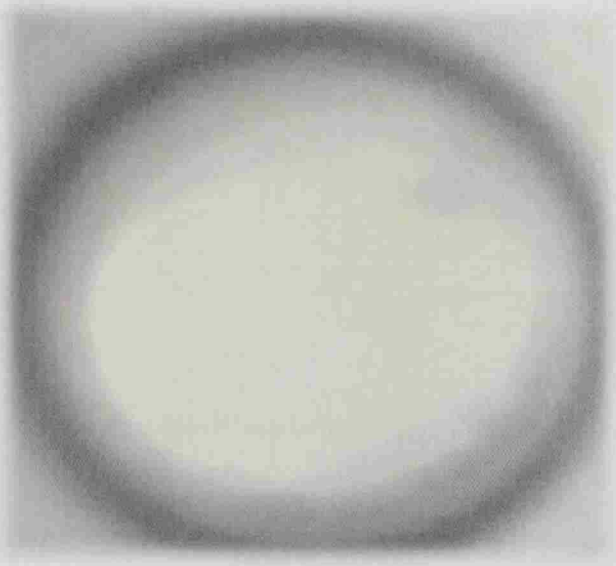

Figure 6.8: Phase transition in the CO_2/live oil system at 257 °F for well A#33.

Injection of CO_2 into the oil reservoir results in reduced interfacial tension and viscosity which improves mobility. Also CO_2 can dissolve in the oil leading to oil swelling. Swelling tests were performed to determine the relationship between saturation pressure, swelling factor and CO_2 mass fraction injected. Tables 6.8 & 6.9 present all experimental results of this work for both wells A#22 and A#33 respectively. There were more than 20 runs for experimental work all were performed at the reservoir temperature, T (235 °F for well A#22 and 257 °F for well A#33). At the first stage the recombination process (gas from first stage separator and oil from stock tank) were performed, obtaining the same

saturation pressure at which it was sampled, P^{sat0} (bar). Then the initial volume for the swelling test, V^0 (ml) was observed by stabilizing the syringe pump. The CO_2 was then injected into the live oil (recombined oil) to observe a two-phase system $P^{sat}_{(LV)}$, and sometimes in a narrow range the observation was a three-phase system $P^{sat}_{(LLV)}$, depending on the pressure and the mass fraction of CO_2. Then the final volume for the swelling test, V^{01} (ml) was noted by stabilizing the syringe pump. The relative swelling volume, V^{sw}, was defined earlier by Eq. (4.1) as $V^{sw} = V^{01}/V^0$.

Table 6.8: Saturation pressure and swelling data for the CO_2/live oil system for well A#22 at 235 °F.

Run	P^{sat0} (bar)	V^0 (ml)	w_{CO2}	$P^{sat}_{(LV)}$ (bar)	$P^{sat}_{(LLV)}$ (bar)	V^{01} (ml)	$V^{sw} = V^{01}/V^0$
1	157.3	6.31	0.05	167.2	-	6.43	1.02
2	157.8	6.97	0.10	192.6	-	7.90	1.13
3	157.4	7.91	0.15	205.9	-	9.03	1.14
4	158.0	6.60	0.20	230.4	-	8.30	1.26
5	157.9	7.13	0.25	242.6	-	9.29	1.30
6	157.2	6.73	0.30	253.4	255.9	9.61	1.43
7	156.9	7.74	0.35	267.0	270.9	11.50	1.49
8	157.6	7.32	0.40	287.3	292.0	12.30	1.68
9	157.1	7.58	0.50	317.1	323.3	13.10	1.73
10	157.5	-	0.60	357.4	-	-	-

Table 6.9: Saturation pressure and swelling data for the CO_2/live oil system for well A#33 at 257 °F.

Run	P^{sat0} (bar)	V^0 (ml)	w_{CO2}	$P^{sat}_{(LV)}$ (bar)	$P^{sat}_{(LLV)}$ (bar)	V^{01} (ml)	$V^{sw} = V^{01}/V^0$
1	165.2	7.36	0.05	178.0	-	8.68	1.00
2	164.7	8.40	0.10	195.5	-	8.82	1.05
3	164.5	9.44	0.15	212.0	-	10.86	1.15
4	163.8	8.30	0.20	235.2	-	10.04	1.21
5	164.6	8.56	0.25	248.3	-	10.79	1.26
6	163.9	8.14	0.30	261.1	265.1	11.07	1.36
7	164.2	9.20	0.35	277.3	280.5	12.97	1.41
8	163.4	9.22	0.40	289.1	293.2	14.48	1.57
9	165.0	8.07	0.50	324.0	330.0	15.14	1.74
10	164.1	-	0.60	400.0	-	-	-

Swelling tests were conducted on the reservoir fluid with CO_2 gas. It was found that the CO_2 caused the saturation pressure to increase. Figures 6.9 and 6.10 show the swelling

factor (relative volume) for the CO_2/live oil system as function of saturation pressure at 235 °F for well A#22 and at 257 °F for well A#33.

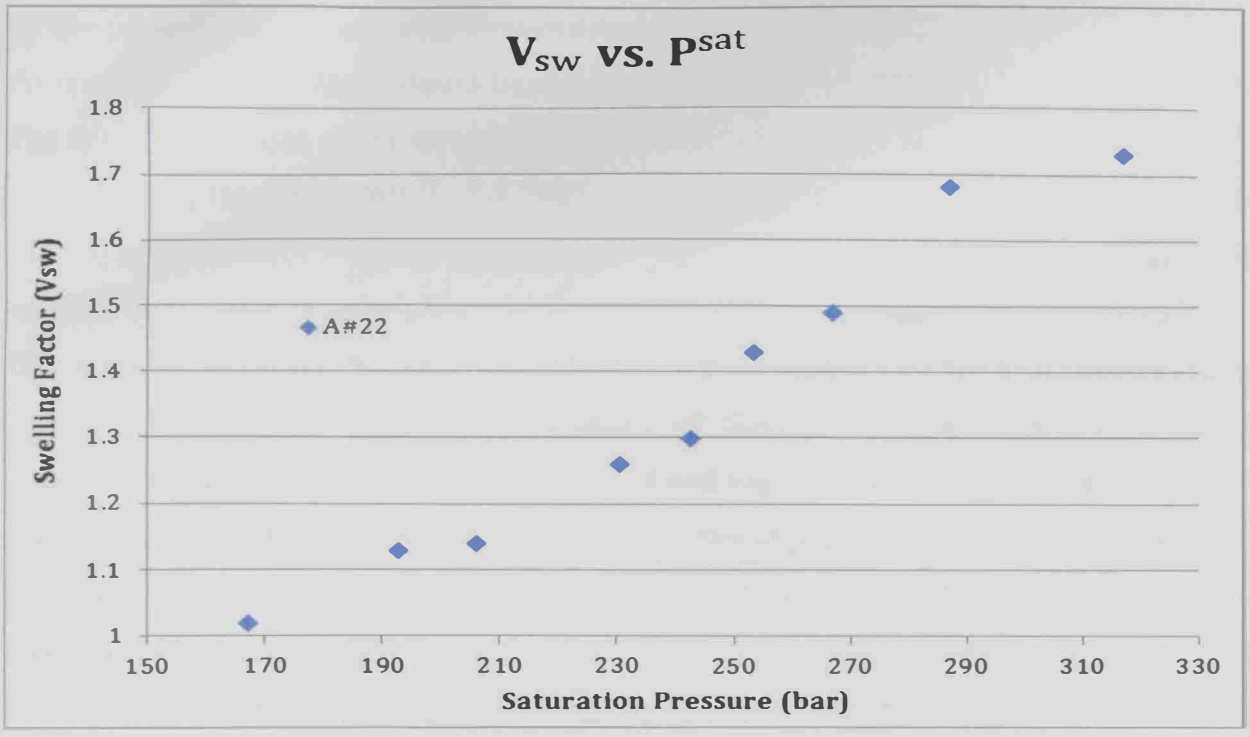

Figure 6.9: Swelling factor of CO_2/live oil system as function of saturation pressure at 235 °F for well A#22.

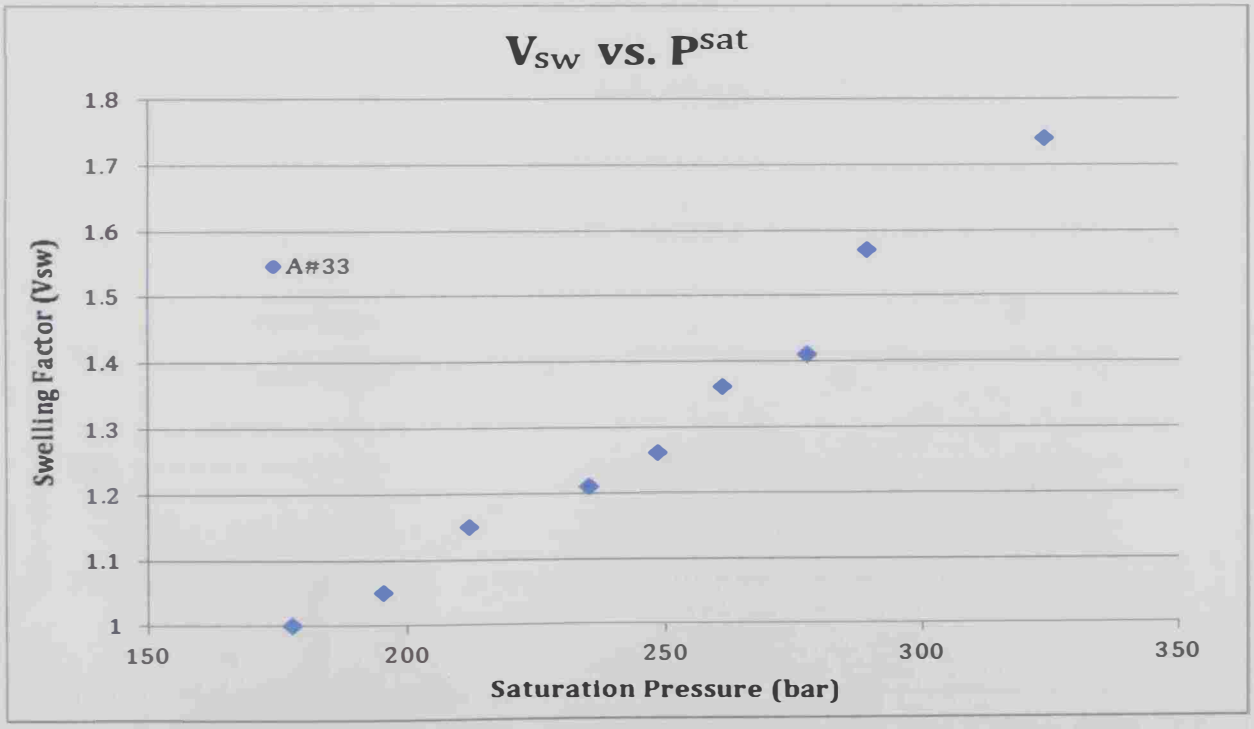

Figure 6.10: Swelling factor of CO_2/live oil system as function of saturation pressure at 257 °F for well A#33.

Figures 6.11 and 6.12 show the effect of CO_2 mass fraction on the saturation pressure for wells A#22 and A#33, at the corresponding reservoir temperatures. At CO_2 mass fractions lower than 0.3, the interaction between the hydrocarbon molecules is not affected enough by the presence of CO_2 and only conventional vapor-liquid transition is observed while a three-phase system (vapor-liquid-liquid) exists at CO_2 mass fractions higher than 0.30. The real observations of the three-phase system are shown in Figure 6.13 where the live oil is divided into three phase fractions: the light phase (gas), the intermediate phase (liquid) and the heavy oil phase (liquid). A proposed mechanism of the phase formation at low CO_2 mass fractions as a function of saturation pressure is presented in Figure 6.14.

The behavior of binary mixtures of CO_2 and crude oil depends on the CO_2 concentration and the pressure. For instance, the original oil (before injecting CO_2) is a liquid at pressures above 164 bar, but splits into liquid and vapor below that pressure. A mixture containing 30% CO_2 mass fraction forms a single liquid phase above 340 bar and a liquid and a vapor at lower pressures. At high CO_2 concentrations, the phase behavior is more complex. At low pressures liquid and vapor phases form. As the pressure is increased, the vapor phase, which contains CO_2 and the light hydrocarbon gases, condenses into a second liquid phase. There is a narrow pressure range over which two liquids (a CO_2-rich liquid and an oil-rich liquid) and a vapor coexists.

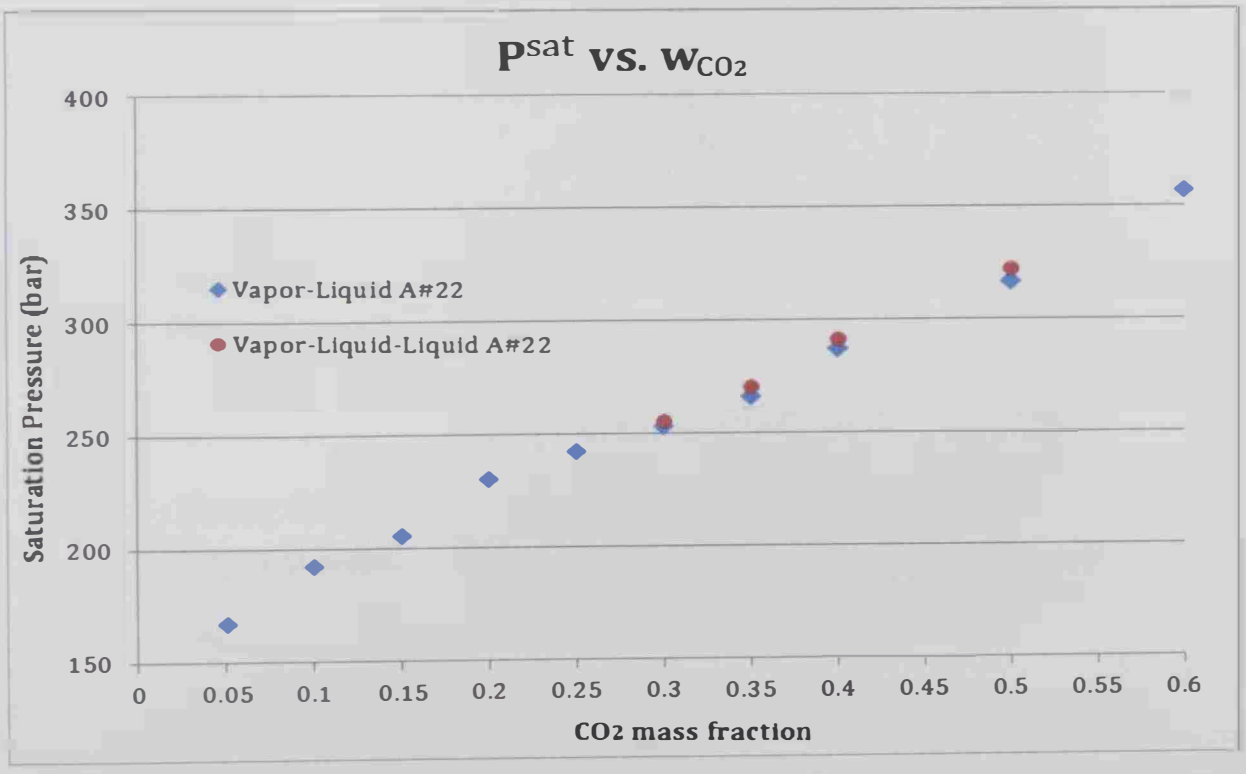

Figure 6.11: Measured saturation pressure vs. CO_2 mass fraction at 235 °F for well A#22.

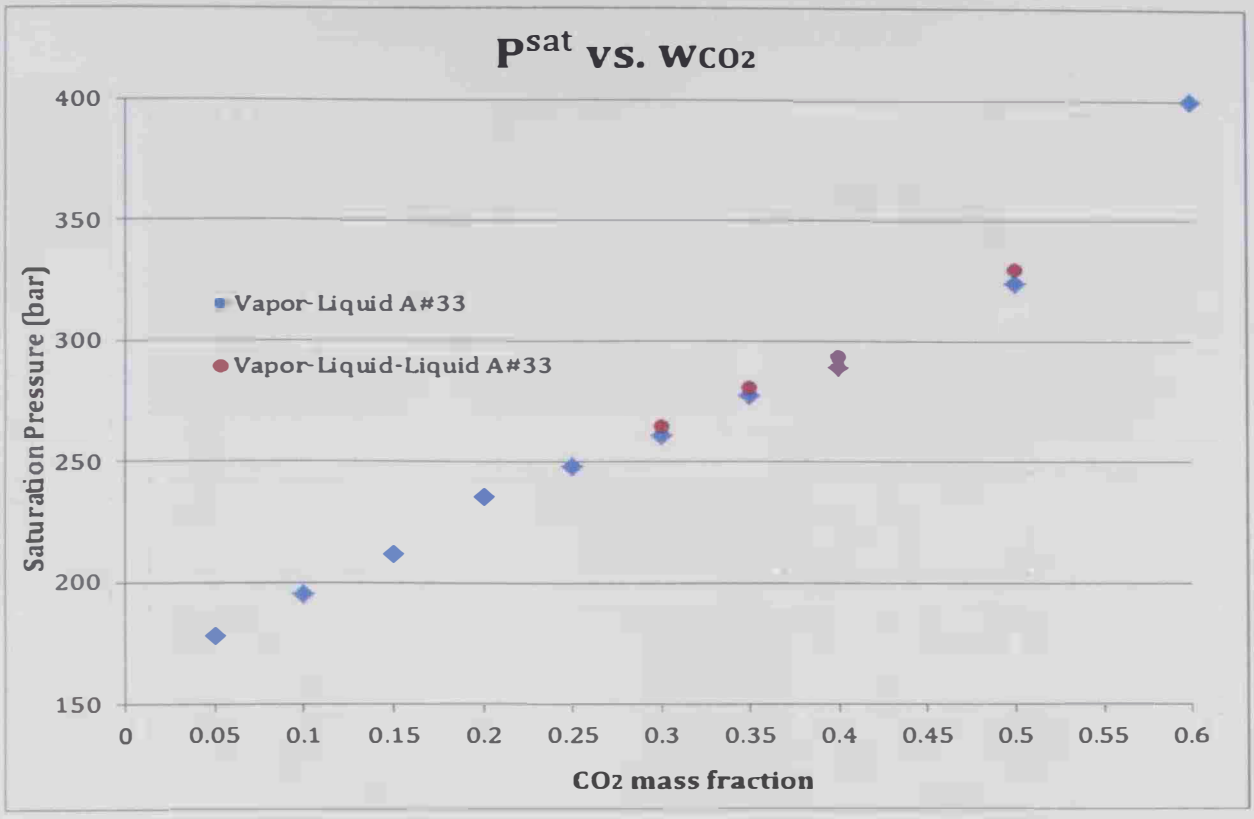

Figure 6.12: Measured saturation pressure vs. CO_2 mass fraction at 257 °F for well A#33.

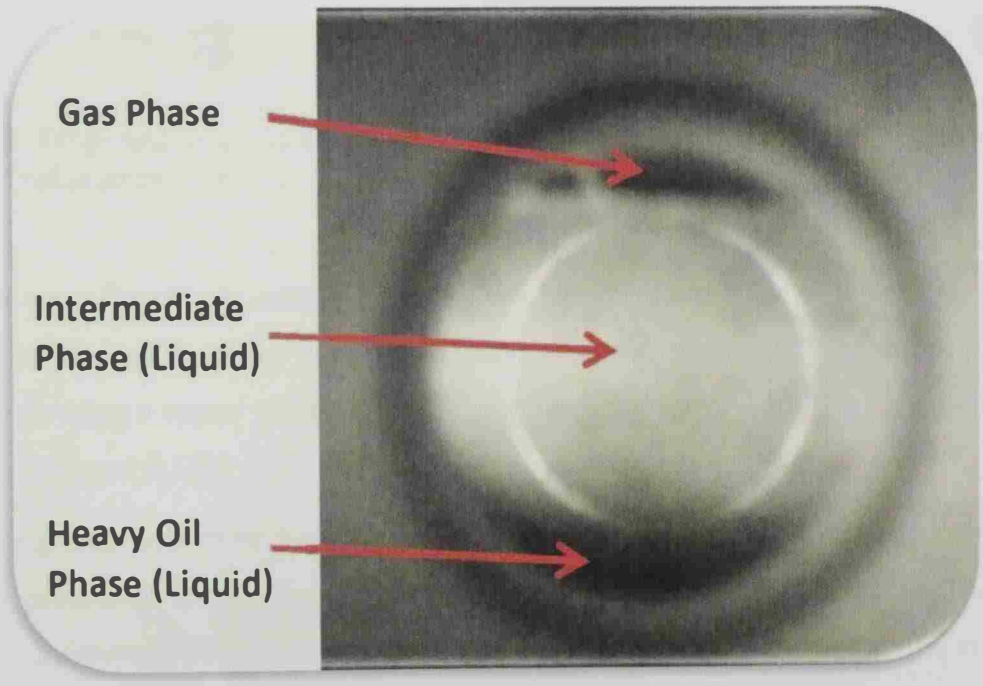

Figure 6.13: Experimentally observed vapor-liquid-liquid transition at 257 °F for well A#33.

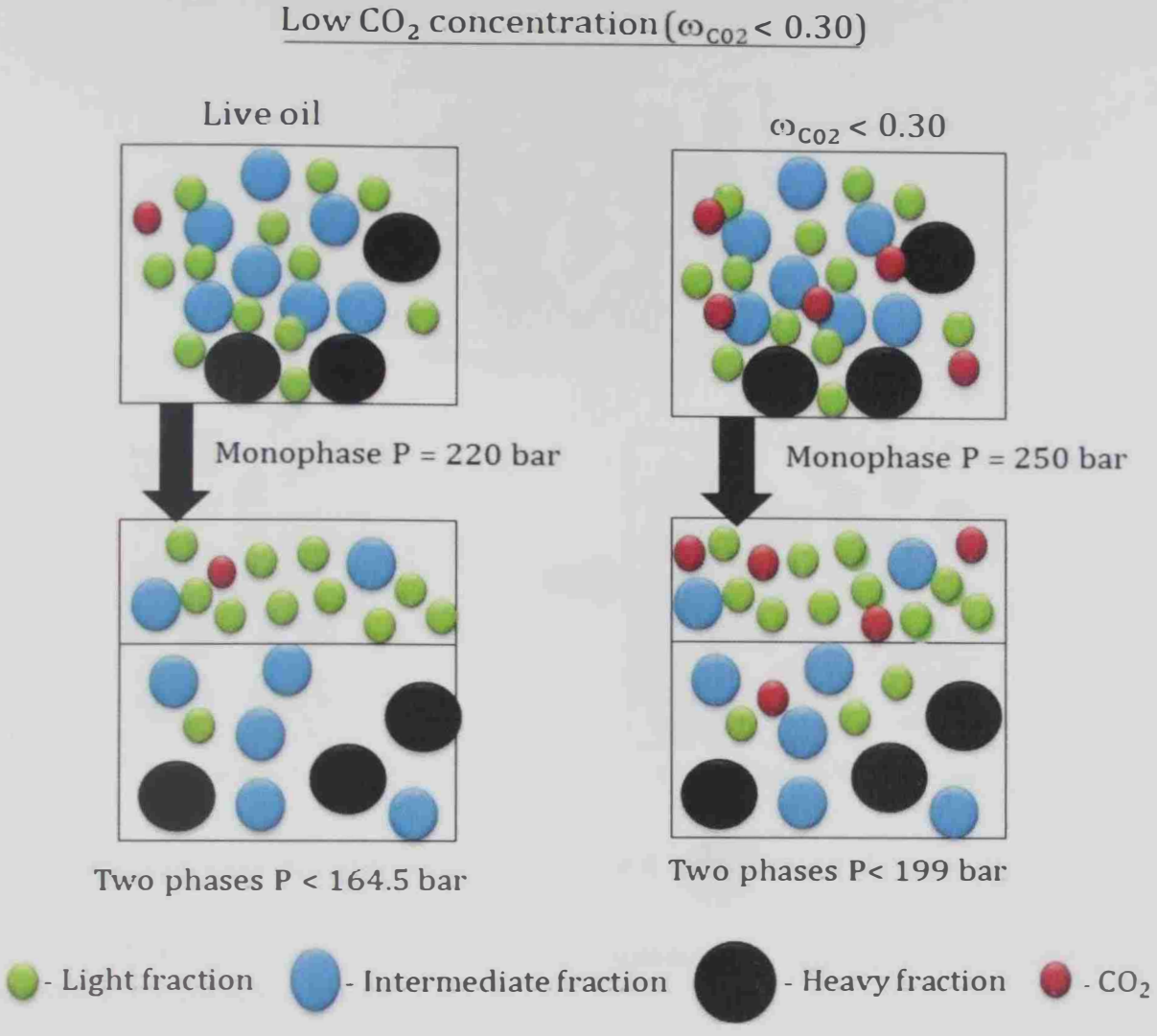

Figure 6.14: Proposed mechanism of phase formation at low CO_2 mass fractions as a function of saturation pressure.

As the CO_2 mass fraction is increased above 0.3, the interaction between the hydrocarbon molecules is affected in such a way that a heavy phase is segregated when the pressure is lowered, following a vapor phase formation, essentially formed by the light hydrocarbon fraction (see Figure 6.15)

The swelling test was then performed using the PVTpro simulator and the calculated saturation pressures were compared with those obtained experimentally. The average relative errors were 8.44% and 6.33% for wells A#22 and A#33, respectively, as shown in Table 6.10 and Figures 6.16 and 6.17.

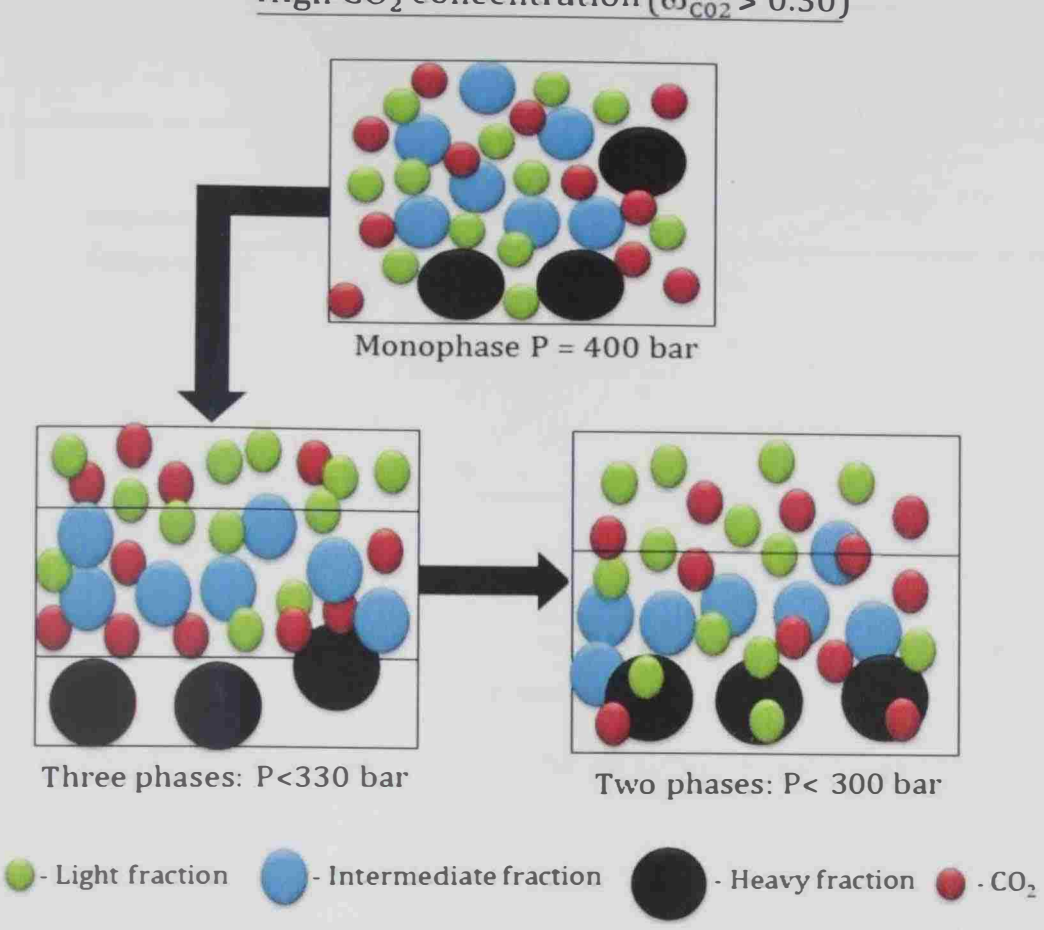

Figure 6.15: Proposed mechanism of phase formation at high CO_2 mass fractions as a function of saturation pressure.

Table 6.10: Comparison between experimental and simulated (using PVTpro) swelling test results for wells A#22 and A#33.

Well A#22			
w_{CO2}	P^{sat}, (Exp.), bar	P^{sat} (PVTpro), bar	ARE, %
0.05	167.2	165.2	1.196
0.10	192.6	177.0	8.100
0.15	205.9	186.7	9.325
0.20	230.4	198.4	13.889
0.25	242.6	211.4	12.861
0.30	253.4	226.0	10.813
0.35	267.0	242.8	9.064
0.40	287.3	262.8	8.528
0.50	317.1	316.0	0.347
0.60	357.4	394.0	10.241
		Average ARE =	8.436

Well A#33			
w_{CO2}	P^{sat}, (Exp.), bar	P^{sat} (PVTpro), bar	ARE, %
0.05	178.0	174	2.247
0.10	195.5	185	5.371
0.15	212.0	196	7.547
0.20	235.2	209	11.139
0.25	248.3	224	9.948
0.30	261.1	240	8.081
0.35	277.3	259	6.599
0.40	289.1	282	2.456
0.50	324.0	340	4.938
0.60	400.0	420	5.000
		Average ARE =	6.333

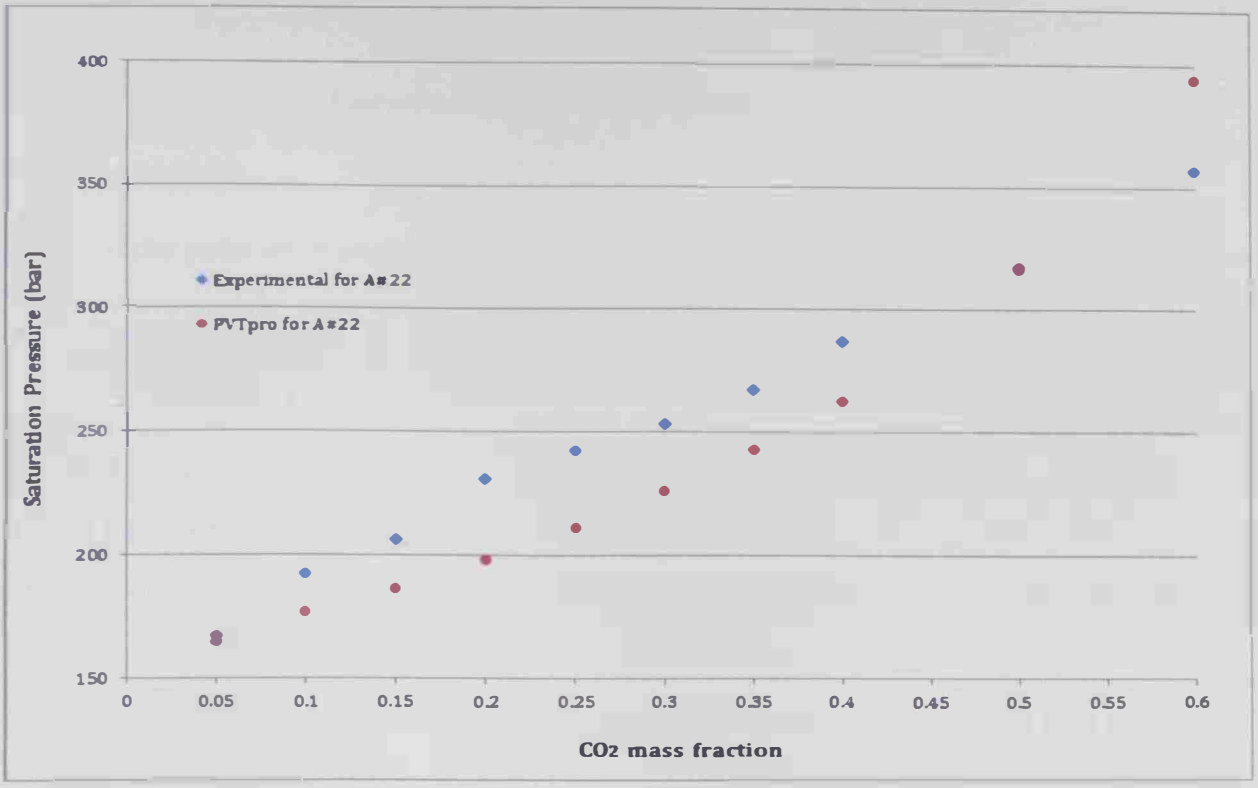

Figure 6.16: Experimental vs. simulated (using PVTpro) swelling test results for well A#22.

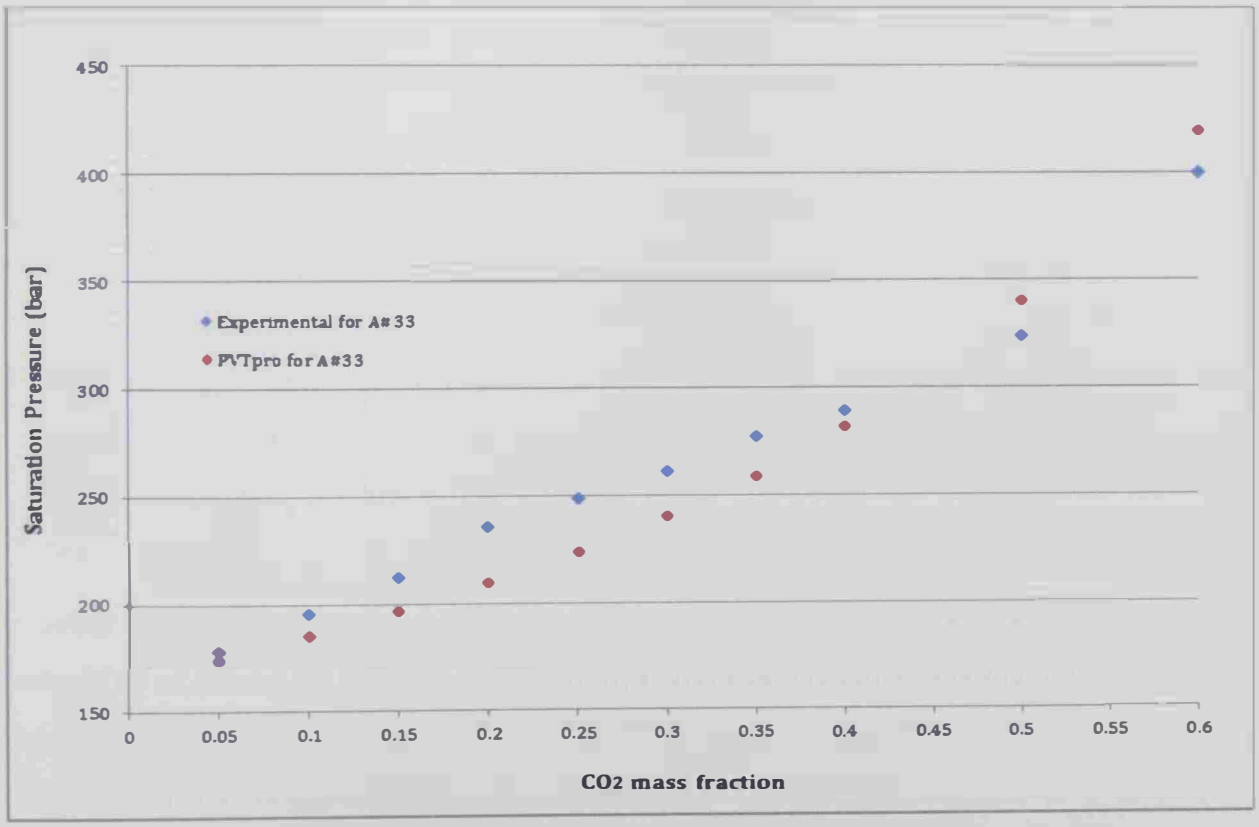

Figure 6.17: Experimental vs. simulated (using PVTpro) swelling test results for well A#33.

Chapter Seven

Conclusions and Recommendations

7.1 Conclusions

Much of the petroleum engineering work involved in the development and exploitation of oil reservoirs world-wide depends on the representative fluid samples which are required in the measurement of PVT properties and/or assessment of enhanced oil recovery (EOR) strategies. Also it is known that surface sampling is advantageous over down-hole sampling in the ability to collect large volumes of fluid and avoiding the cost and time of losing production. The recombination process of the surface fluid samples is considered successful if the same bubble pressure (at which the down-hole fluid sample was taken) is obtained at reservoir temperature.

The recombination of the surface fluid samples (first-stage separator gas and stock-tank oil) performed in this work to regenerate the original oil composition shows that the composition of the recombined fluid does not match the reservoir fluid composition. The vapor molar ratio was varied in steps until the fluids with compositions similar to those of wells A#22 and A#33 fluids, with an average deviation error 0.77% and 1.09%, respectively, were obtained. The trial (corrected to optimize the error of methane) vapor molar ratio was found to be about 0.42 for both wells.

The swelling test performed to determine the relationship between saturation pressure, swelling factor and the mass fraction of the CO_2 injected indicated that the saturation pressure tends to increase with the addition of CO_2 to the crude oil. At a critical CO_2 mass fraction of 0.3 a liquid-liquid-vapor transition was observed. The swelling factor has changed from 1 to 1.74 upon the increase of the injected CO_2 from 0.0 to 0.6 mass fractions. In general, the higher the swelling factor the better the enhanced oil recovery (EOR).

In order to get meaningful and accurate estimates of fluid properties and phase behavior, some kind of tuning on the C_{20}^+ critical temperature or pressure was made to reproduce the original field VLE data using SRK EOS or PR EOS built in the PVTi Simulator. Generally, the PR EOS predicts Z_c and liquid density better than the SRK EOS, but neither of these EOS predicted accurate liquid densities.

It was noticed that the PVTi simulator gives almost the same value of the Z-factor and the molar volume for the liquid and vapor phases at saturation conditions. The PVTpro simulator gives a little better answer than the PVTi for the Z-factor. However, neither of the two of simulators succeeded in predicting accurate saturated liquid molar volumes; the relative error was 29.1% for well A#22 and 28.9% for well A#33. When the Rackett equation was used for prediction of the saturated liquid molar volume the error was 6.2% for well A#22 and 6.7% for well A#33, when compared with the corresponding field values.

On the other hand, when the reservoir fluid of either well was recombined using the PVTpro simulator, the error in predicted composition was 0.3% for well A#22 and 1.7% for well A#33 compared to that of the corresponding reservoir fluid.

Swelling test using PVTpro simulator the average ARE in the predicted saturation pressures were 8.4% for well A#22 and 6.3% for well A#33 compared to those values obtained from the swelling test experiments.

7.2 Recommendations

It is recommended to perform the two-stage recombination process for the different reservoir fluids at their reservoir temperatures. The fluids were used in this work are free of water and future work requires considering water with hydrocarbons together when the fluid properties are studied. Also further work is needed to be done to achieve minimum miscibility pressure test (MMP) using slim tube experiments.

References

1. Schlumberger Eclipse Software, PVTi, Pressure-Volume-Temperature Analysis Software, version 2010.1.
2. PVTpro (OilPhase-DBR), Schlumberger Canada Ltd., version 5.10.
3. Sim., S. S. K., Pressure-Volume-Temperature correlations for crude oil from the illinois basin, illinois petroleum 140, 1993, Illnoise 61820-6964, p 1.
4. Bon, J.G., Sarma, H.K., Rodrigues, J.T., Bon, J., Reservoir-Fluid Sampling Revisited- A Practical Perspective, SPE Reservoir Evaluation & Engineering, Vol. 10 (6), 2007: 589-596.
5. Sattar, A., Iqbal G.M., Buchwalter J.L., Practical Enhanced Reservoir Engineering: Assisted with Simulation Software, 2008: PennWell Books, ISBN 10: 1593700563, p.102.
6. Almehaideb R.A., Ashour I. and El-Fattah K.A., Improved *k*-value correlation for UAE crude oil components at high pressures using PVT laboratory data. Fuel, 2003, 82(9): 1057-1065.
7. de Hemptinne, J. C.; Mougin, P.; Barreau, A.; Ruffine, L.; Tamouza, S. and Inchekel, R. Oil & Gas Science and Technology-Rev. Ifp., 2006, 61(3): 363-386.
8. Carroll, J.J, Natural Gas Hydrates: A Guide for Engineers, Chemical, Petrochemical & Process, 2009: Gulf Professional Publishing, ISBN 0-75068490-9, pp. 276.
9. Chilingarian, G.V. (Co-editor and Co-author: T.F. Yen), Bitumens, Asphalts and Tar Sands, Volume 7 (Developments in Petroleum Science) 1978: Elsevier Science, ISBN 0444416196, pp.331, p.37.
10. Polishuk I., Wisniak J. and Segura H., Estimation of Liquid–Liquid–Vapor Equilibria Using Predictive EOS Models. 1. Carbon Dioxide–n-Alkanes. The Journal of Physical Chemistry B, 2003, 107(8): 1864-1874.
11. Hydrocarbon Phase Behavior (http://ipims.com/data/fe31/E3109.asp?UserID=&Code=3281).
12. Schlumberger, Introduction to well Testing, Bath, England, 1998, p.27.
13. Mignot, R., Reservoir Fluids Properties, IFP Training, 2003, p.35. (http://geology.adonlead.com/PETROLEUM%20GEOLOGY/Tuyen%20Tap%201/books%20about%20oil/Reservoir fluids properties book.pdf).
14. Standing, M.B. and Katz, D. L., Density of Natural Gases, *Trans. AIME,* Vol. 146, 1942, pp. 140-149.

15. Danesh A., PVT and Phase Behaviour of Petroleum Reservoir Fluids, 1998: Elsevier Science, ISBN 0-44482196-1, 47, pp. 67.
16. Rojey. A., Natural Gas: Production, Processing, Transport, 1997: Editions OPHRYS, Technology & Engineering, ISBN: 2710806932, pp.429, p.88
17. McCain W.D., Spivey, J.P. and Lenn, C.P., The Properties of Petroleum Fluids, 1990: PennWell Books, pp. 240.
18. Pedersen, K.S., Fredenslund A. and Thomassen P., Properties of Oils and Natural Gases, 1989: Gulf Pub. Co., Book Division, p. 8.
19. Guo, B., Lyons, W.C. and Ghalambor, A., Petroleum Production Engineering: A Computer-Assisted Approach, 2007: Gulf Professional, p. 24.
20. Nagarajan, N.R., Honarpour, M.M., and Sampath K., ExxonMobil Upstream Research Co., Distinguished Author Series: Reservoir-Fluid Sampling and Characterization-Key to Efficient Reservoir Management, JPT 2007, p. 82.
21. New Solutions in Fluid Sampling (http://www.slb.com/~/media/Files/resources/mear/num6/fluid_sampling.ashx).
22. American Petroleum Institute, Recommended Practice for Sampling Petroleum Reservoir Fluids, 1966: API, Dallas, Texas, p. 44.
23. Turner R.G., Hubbard M. G. and Dukler A.E., Analysis and Prediction of Minimum Flow Rate for Continuous Removal of Liquids from Gas Wells, 1969: Journal of Petroleum Technology (JPT), 11: p. 1475-1482.
24. Fluids sampling and analysis (http://www.exprogroup.com).
25. McCain, Jr., W.D and Alexander, R.A: Sampling Gas condensate wells, SPE Res. Eng., 1992, pp. 358-362.
26. Ahmed T., Working Guide to Vapor-Liquid Phase Equilibria Calculations, 2009: Elsevier Science, ISBN: 1856178269, p. 14.
27. Berezkin V.G., Alishoev R.A. and Nemirovskaya I.B., Basic principles of gas chromatography, Chapter 1 in Journal of Chromatography Library, 1977: Elsevier Science & Technology, 10: p. 1-31.
28. Gas Chromatography (GC), (http://elchem.kaist.ac.kr/vt/chem-ed/sep/gc/gc.htm).
29. Gozalpour, F., Danesh A., Todd A.C. and Tohidi B., Vapor–liquid equilibrium compositional data for a model fluid at elevated temperatures and pressures, Fluid Phase Equilibria, 2003, 208(1–2): 303-313.

30. Chung, T.H., Feasibility study for the application of gas EOR processes in DOE's NPR-3 reservoirs, NIPER-625, Distribution Category UC-122, 1992, pp.14, p. 5.
31. Bon, J., Laboratory and modelling studies on the effects of injection gas composition on CO_2-rich flooding in Cooper basin, 2009: PhD Thesis, The University of Adelaide, Australia, p. 227.
32. Ahmed, T.H., Hydrocarbon Phase Behavior, 1989: Gulf Publishing Co., Vol. 7, pp. 172.
33. Lyons, W.C. and Plisga, G.J., Standard Handbook of Petroleum and Natural Gas Engineering, 2005: Elsevier Science, p. 12.
34. Angus, S., Armstrong, B., de Reuck, K.M., Altunin, V.V., Gadetskii, O.G., Chapela, G.A., and Rowlinson, J.S. International Union of Pure and Applied Chemistry (IUPAC). Carbon Dioxide: International Thermodynamic Tables of the Fluid State, 1976: Pergamon Press, Oxford, UK, Vol. 3, 1522-2640.
35. Falcone, G., Hewitt, G.F, Alimonti, C., Multiphase Flow Metering: Principles and Applications, Vol. 54, 2009: Elsevier, ISBN: 0444529918, p. 210.
36. Katz, D.L. and Firoozabadi, A., Predicting phase behavior of condensate/crude oil systems using methane interaction coefficients, JPT, 1978, 30 (11): p. 1649-1655.
37. Lielmezs, J., Howell, S.K. and Campbell, H.D., Modified Redlich-Kwong equation of state for saturated vapor-liquid equilibrium, Chemical Engineering Science, 1983, 38(8): 1293-1301.
38. Soave, G., Equilibrium constants from a modified Redlich-Kwong equation of state, Chemical Engineering Science, 1972, 27(6): 1197-1203.
39. Pitzer, K.S., Lippman, D.Z., Curl, Jr. R.F., Huggins, C.M., and Petersen, D.E., The volumetric and thermodynamic properties of fluids, II- Compressibility factor, vapor pressure, and entropy of vaporization. J. Am. Chem. Soc., 1955, 77: 3433-3440.
40. Melhem, G.A., Saini, R. and Goodwin, B.M., A modified Peng-Robinson equation of state. Fluid Phase Equilibria, 1989, 47(2-3): 189-237.
41. Peneloux, A., Rauzy, E. and Freze, R., A consistent correction for Redlich-Kwong-Soave volumes. J. Fluid Phase Equilibria, 1982, 8: 7-23.
42. Nasrifar, K. and Moshfeghian, M., Application of an improved equation of state to reservoir fluids: computation of minimum miscibility pressure. Journal of Petroleum Science and Engineering, 2004, 42(2-4): 223-234.

43. Kwak, T.Y. and Mansoori, G.A., van der Waals mixing rules for cubic equation of state, applications for supercritical fluid extraction modeling, Chemical Engineering science, 1985, 41(5): 1303-1309.
44. Chueh, P.L. and Prausnitz, J.M. Calculation of high-pressure vapor-liquid equilibria, Ind. Eng. Chem., 60 (3), 34–52, 1968.
45. Poling B.E., Prausnitz J. M., O'Connell J.P., The properties of gases and liquids. 5th ed., 2001, McGraw-Hill, ISBN: 0070116822, p. 5.10.
46. Ahmed, T.H. Reservoir Engineering: Handbook, Gulf Professional Publishing, 2006 - 1360 pages

Appendix A

The PVTi Simulator

The PVT_i simulator is a compositional *PVT* equation-of-state based program used for characterizing a set of fluid samples for use in the Schlumberger ECLIPSE simulators. The PVT_i is needed because it is vital to have a realistic physical model of the reservoir fluid sample(s) before trying to use it in a reservoir simulation. PVT_i can be used to simulate experiments that have been performed in the lab on a set of fluid samples and then theoretical predictions can be made of any observations that were performed during a lab experiment, in order to test the accuracy of the fluid model.

Any differences between the measured and calculated data are minimized using a regression facility which adjusts various equation-of-state parameters. This 'tuned' model is then exported in a form suitable for one of the ECLIPSE simulators.

To open a new project start the Schlumberger Simulator launcher, run the PVT_i and choose a filename to save your data (as shown in Figures A-1, A-2 and A-3).

Figure A-1: Schlumberger Simulation Launcher on a PC

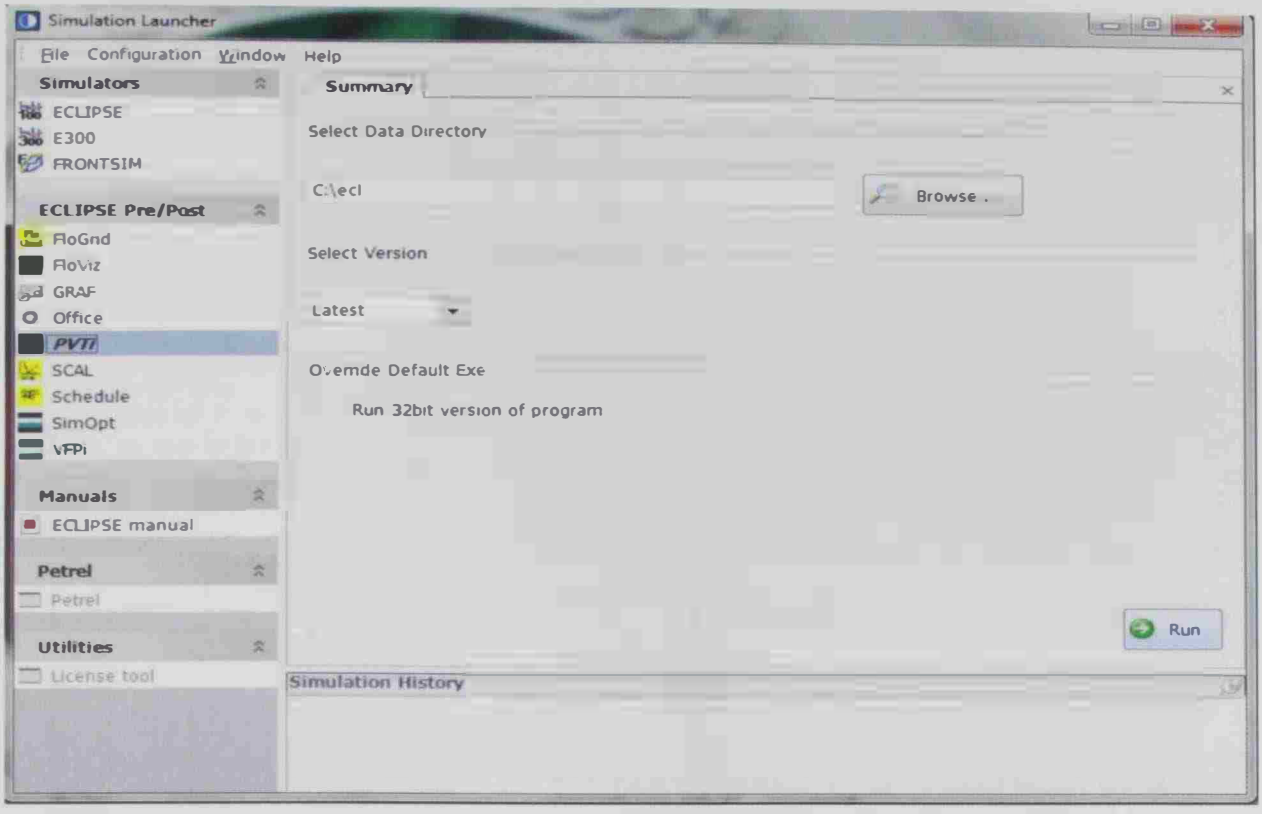

Figure A-2: Select PVT$_i$ and click on RUN.

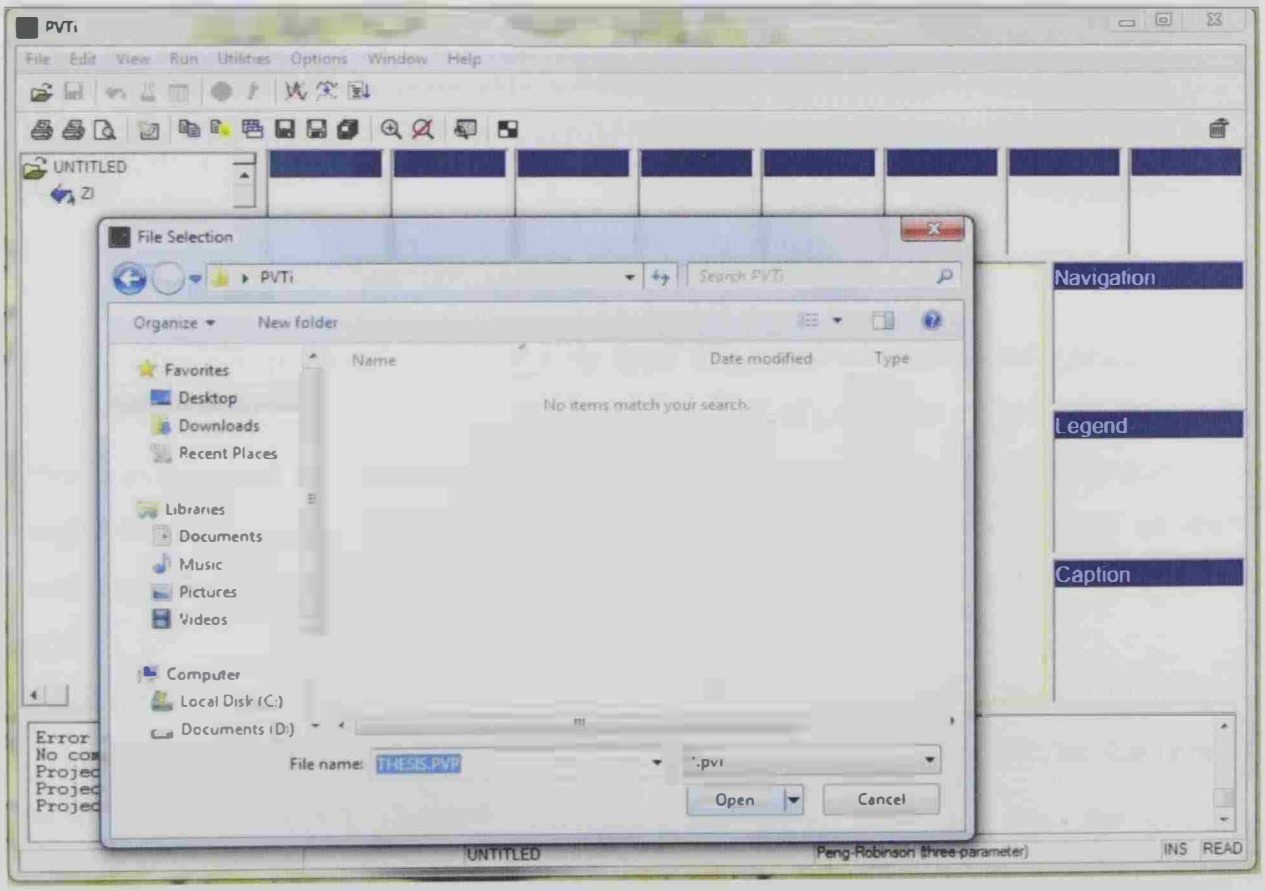

Figure A-3: Create a project filename in any directory

PVTi starts; recognizes that it has a new project and immediately opens the Fundamentals Panel (shown in Figure A-4). This panel has been specifically designed to make setting up a new project as easy as possible. Simply fill in the components and ZI columns with the components' names and mole fractions, respectively, which is the minimum requirement to have a project within PVTi.

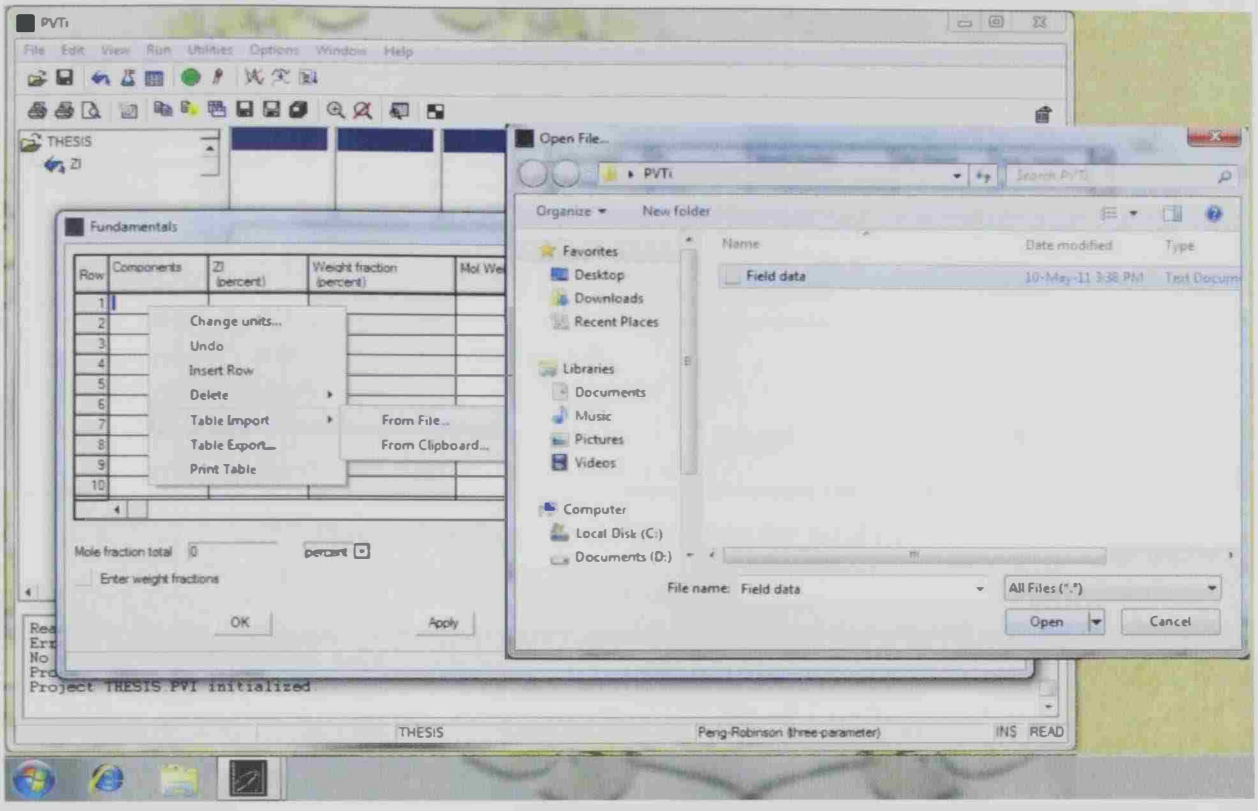

Figure A-4: Fundamentals Panel.

To fill in the components' names simply type the standard shorthand names for the components in your fluid, for example, C_1, N_2, CO_2, H_2S, iC_5, etc. The mole fractions can be entered as fractions or percentages by selecting the appropriate option on the panel. Also, weight fractions/percentages can be entered for the components instead of mole fractions/percentages (as shown in Figure A-5 for well A#22 and Figure A-6 for well A#33).

Once the Fundamentals Panel is completed you will see a sample called ZI on the tree view on the left-hand side of the main window. This is the fundamental sample for the project and the name ZI *cannot* be changed.

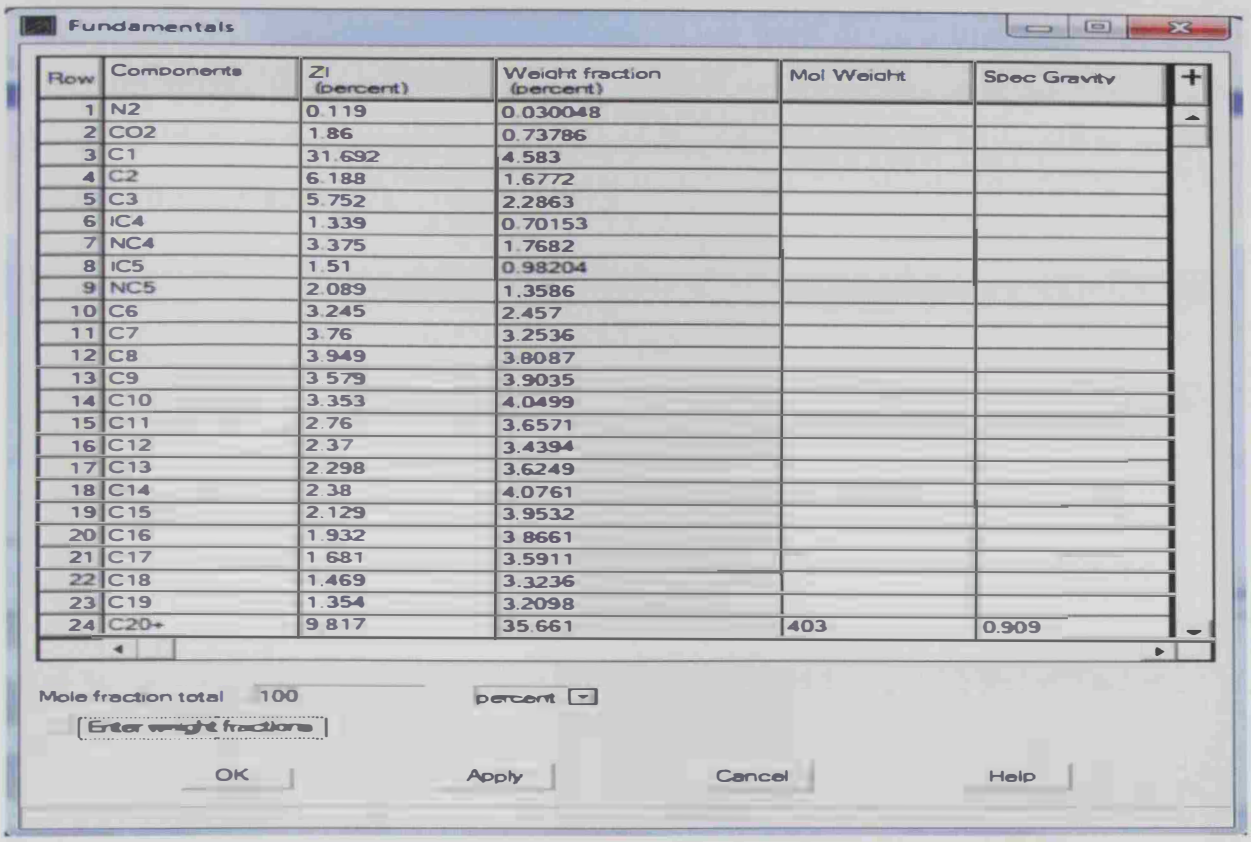

Figure A-5: Imported Field Data for well A#22

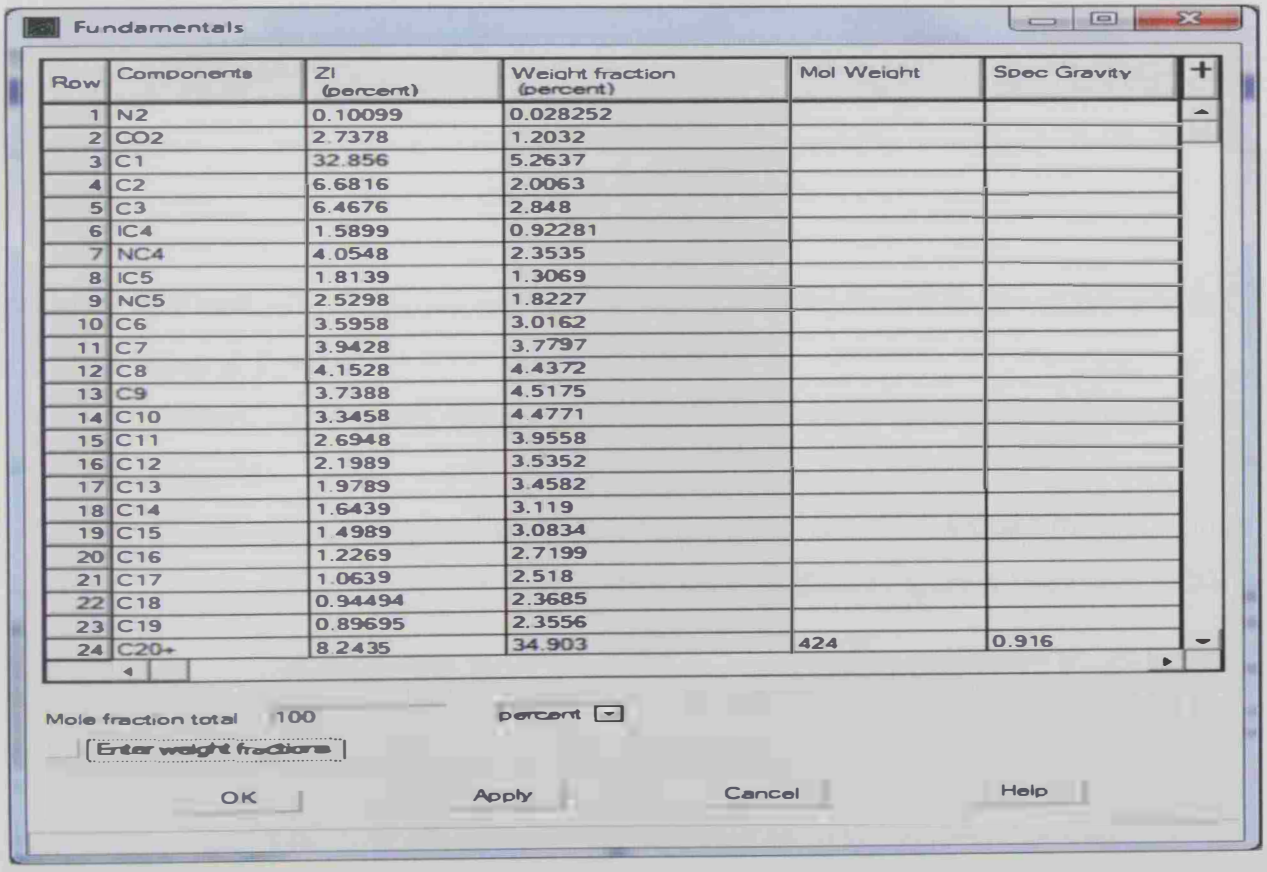

Figure A-6: Imported Field Data for well A#33

Once at least one fluid sample (the ZI sample) has been defined then any experiment supported within PVT_i can be simulated as well as operations such as phase plots, fingerprint plots and splitting. But before running any experiment one need to set PVT_i unit definitions (Figure A-7).

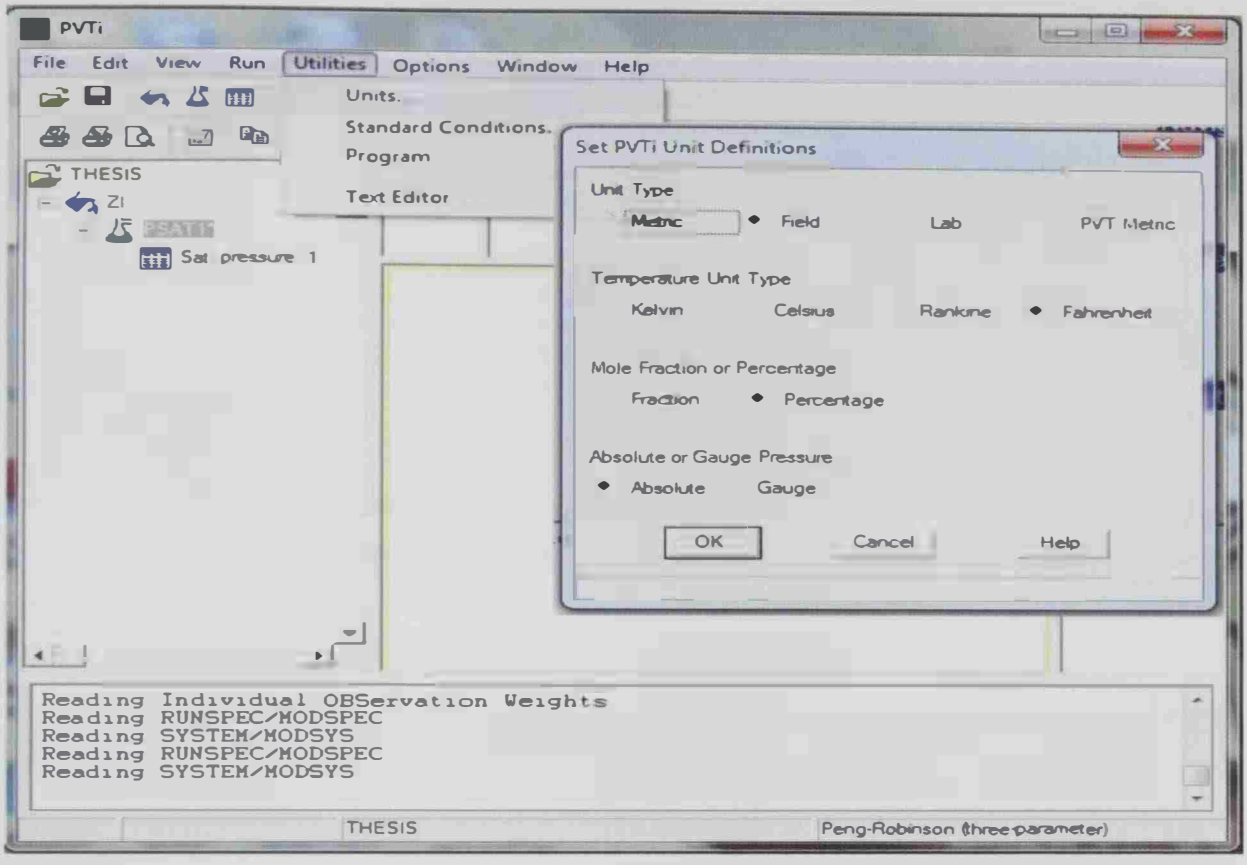

Figure A-7: Set PVT_i units

Multiple fluid samples can be defined by specifying the components as one of three types:

1. User defined.
2. Library components require only that the appropriate component mnemonic be entered.
3. Characterized components defined properties of plus fractions from a limited set of information as in Figure A-8 for well A#22 and Figure A-9 for well A#33.

Finally all the properties of a component can be defined; a facility which can be used selectively to edit the properties of existing components.

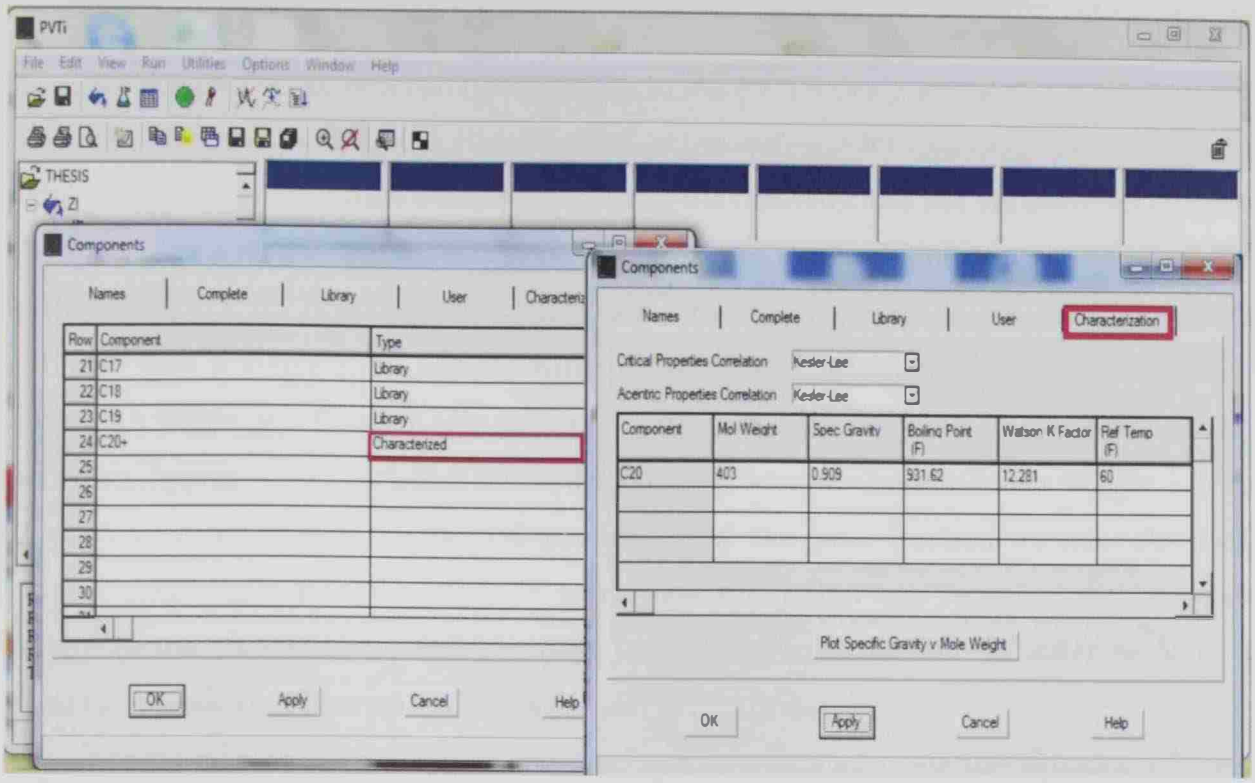

Figure A-8: Characterize the component in the mixture using various correlations for well A#22

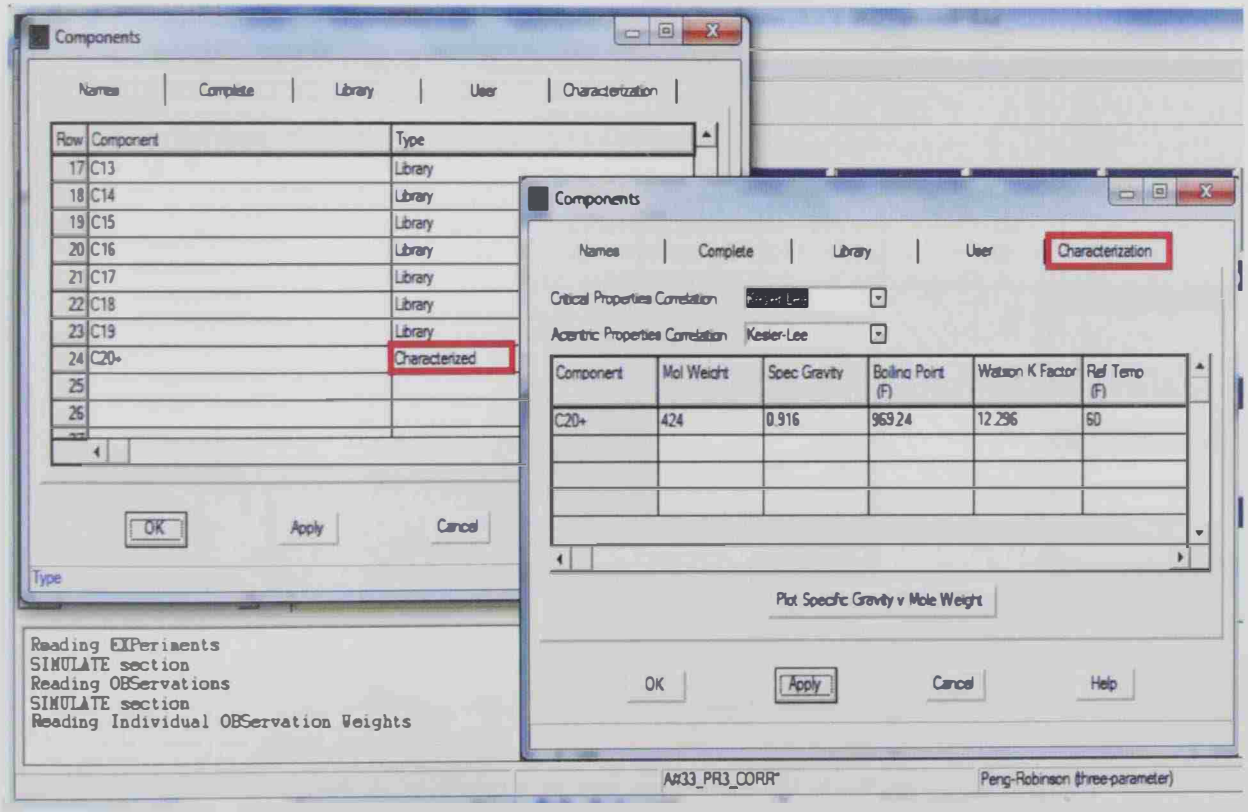

Figure A-9: Characterize the component in the mixture using various correlations for well A#33

The Fluid Properties Estimation (FPE) facility in the PVT$_i$ is designed so that it can be used when you have minimal data at your disposal, at the well-site for example. In this scenario, a full lab analysis of multiple fluid samples from the reservoir has not yet been performed. Typically, just a single sample would be available and minimal fluid behavior known, for example, saturation pressure at a particular temperature. Specifically, the FPE facility assumes that a single fluid sample with compositional information is available which includes a single plus fraction (for example C_7^+) component for which the weight fraction is known. Typically, this weight fraction data is fairly accurate but the molar weight, which is used to characterize the critical properties of the plus fraction, is not. The FPE functionality allows you to perform a quick look simulation that regresses on the mole weight of the plus fraction, and keep the weight fraction constant, in order to fit to a saturation pressure observation at a particular temperature.

Experiments may be performed on the fluid systems defined using the equation of state model (Figure A-10 for well A#22 and Figure A-11 for well A#33). Possibilities are:

- Saturation pressures
- Pressure depletion
- Flash calculations
- Multi-stage separator simulations.

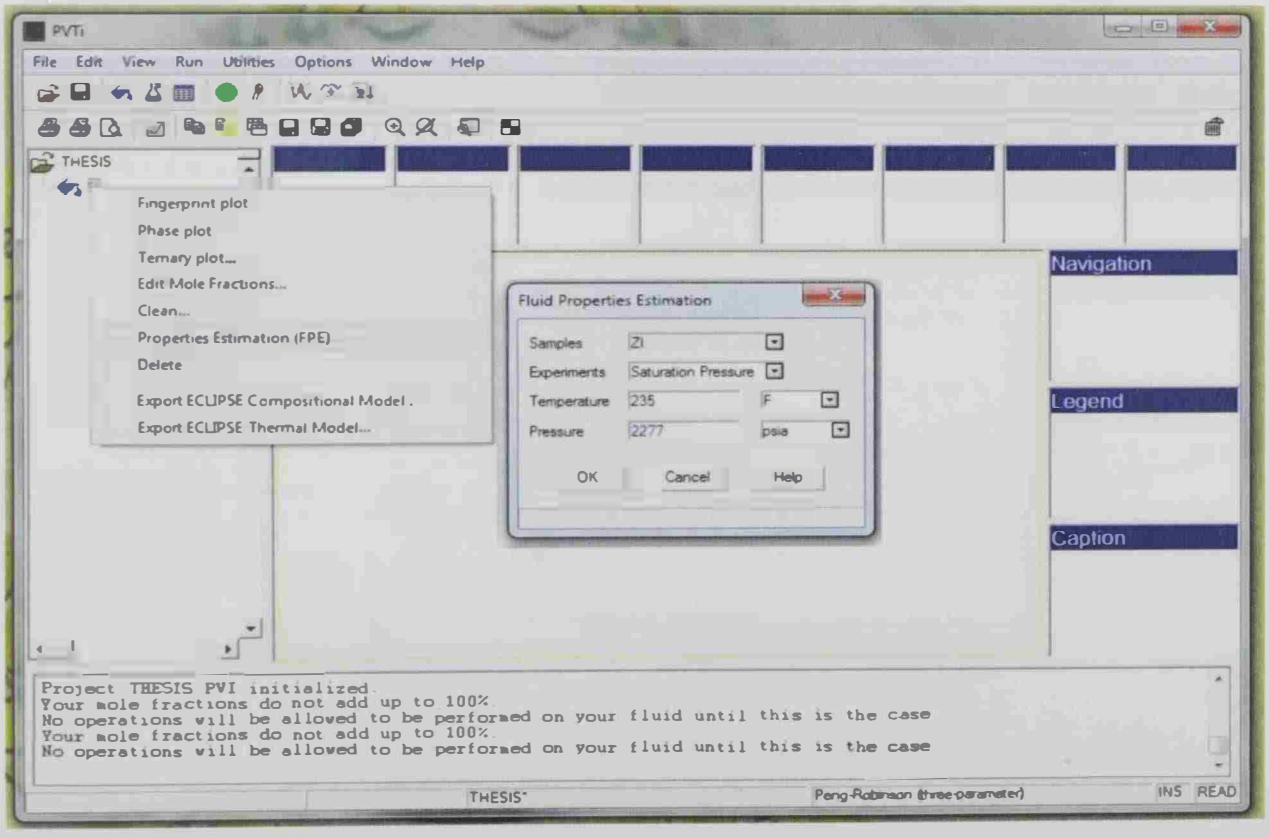

Figure A-10: Adding fluid properties estimation for well A#22

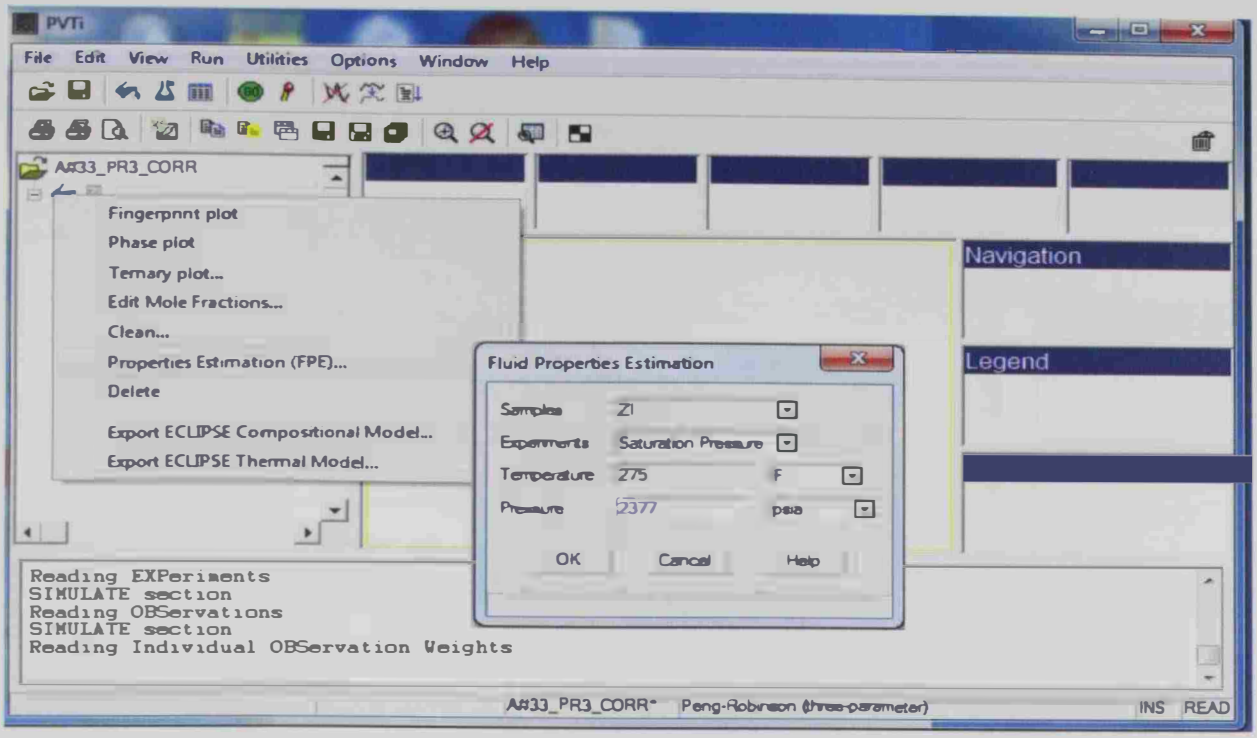

Figure A-11: Adding fluid properties estimation for well A#33

A simulation report is shown in Figure A-12 for well A#22 and Figure A-13 for well A#33 indicating that the observed saturation pressure is not the same as that calculated by the PVT$_i$ simulator. The PVTi continues regression until the observed saturation pressure is obtained.

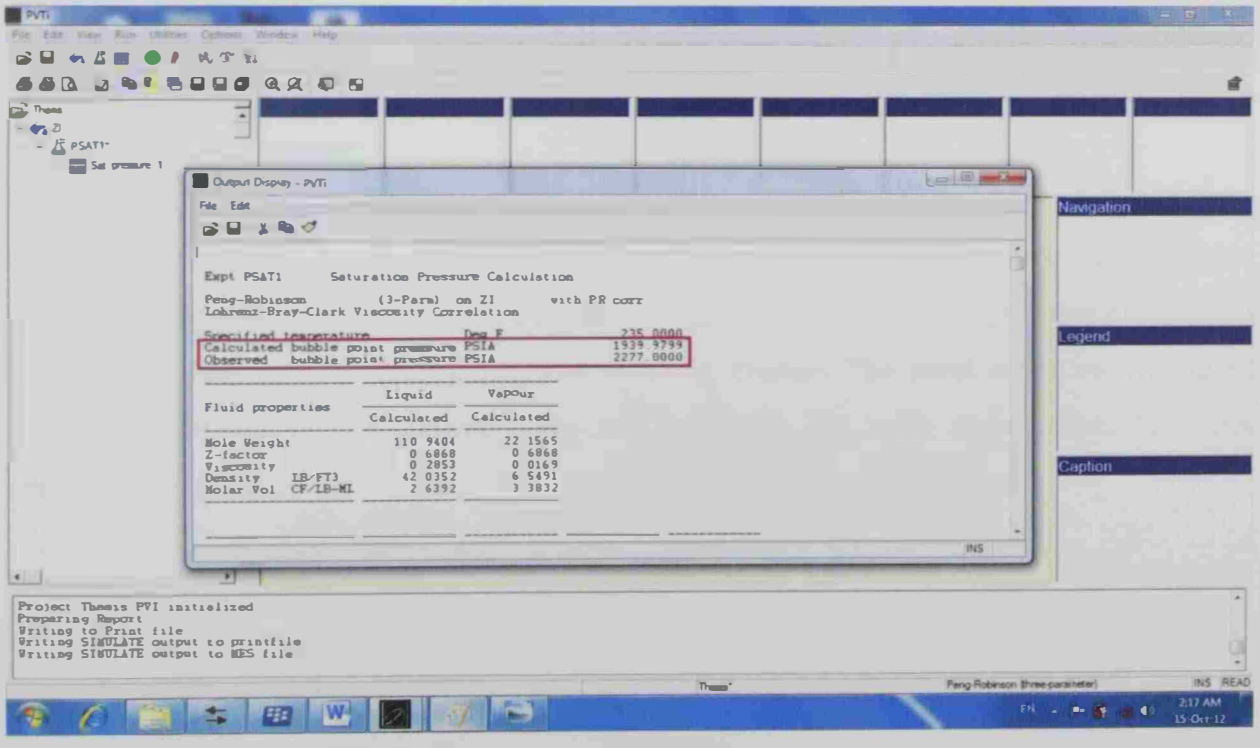

Figure A-12: Simulation result for well A#22

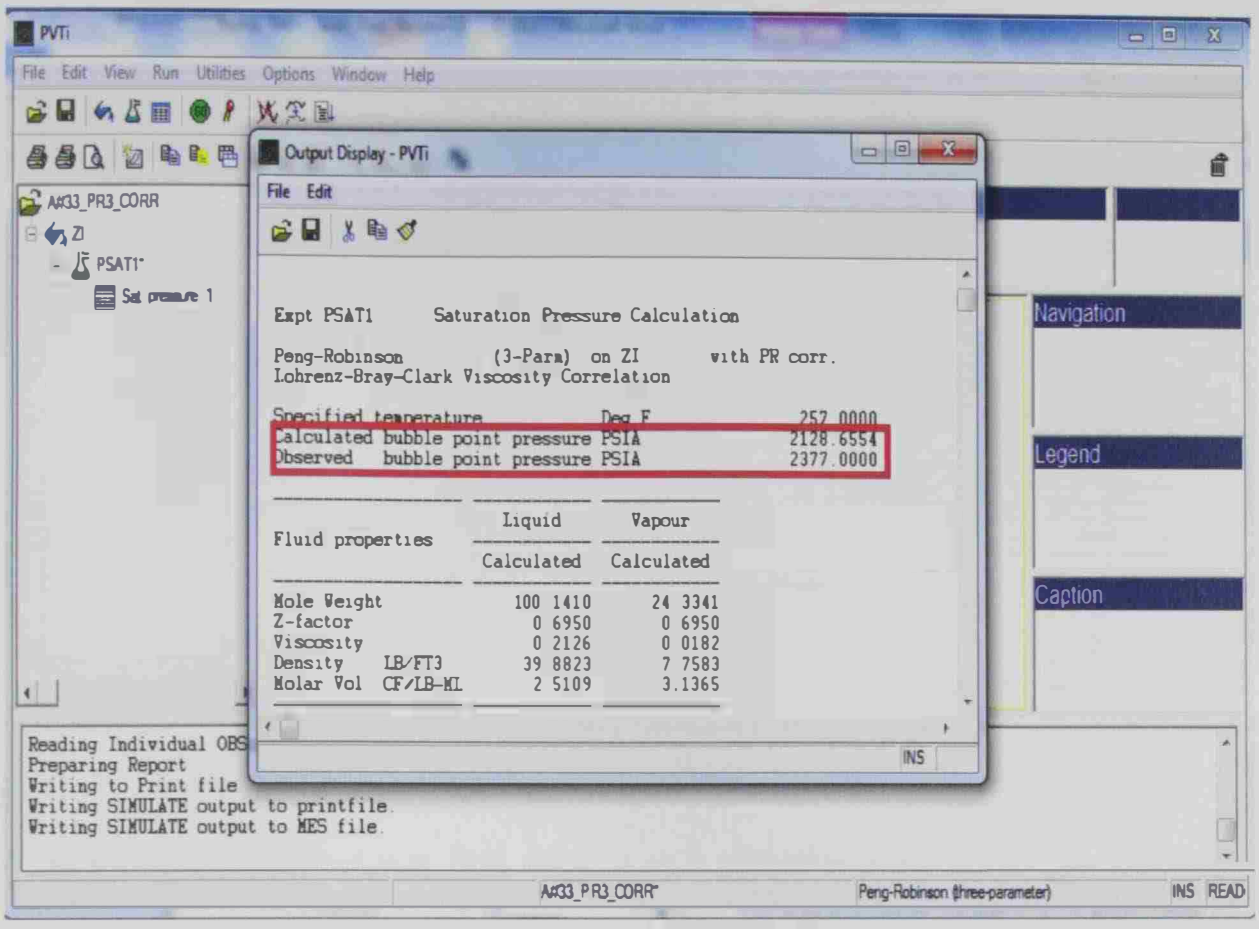

Figure A-13: Simulation result for well A#33

The fluid samples that the PVT$_i$ performs regression on every experiments even if there are multiple fluid samples, each with their own experiments. The reason for this is that, the equation of state is fitted to the observation data to produce a better representation of the fluid.

A Sensitivity analysis is used to establish which fluid properties most affect the difference between the observed and simulated values and to determine which attributes of the fluid components improve the solution by the smallest change. The most sensitive attributes are calculated for critical temperature and pressure for each experiment, for both regression variables.

Finally the most sensitive properties will be selected for use in the regression to improve the equation of state model of the fluid (Figure A-14).

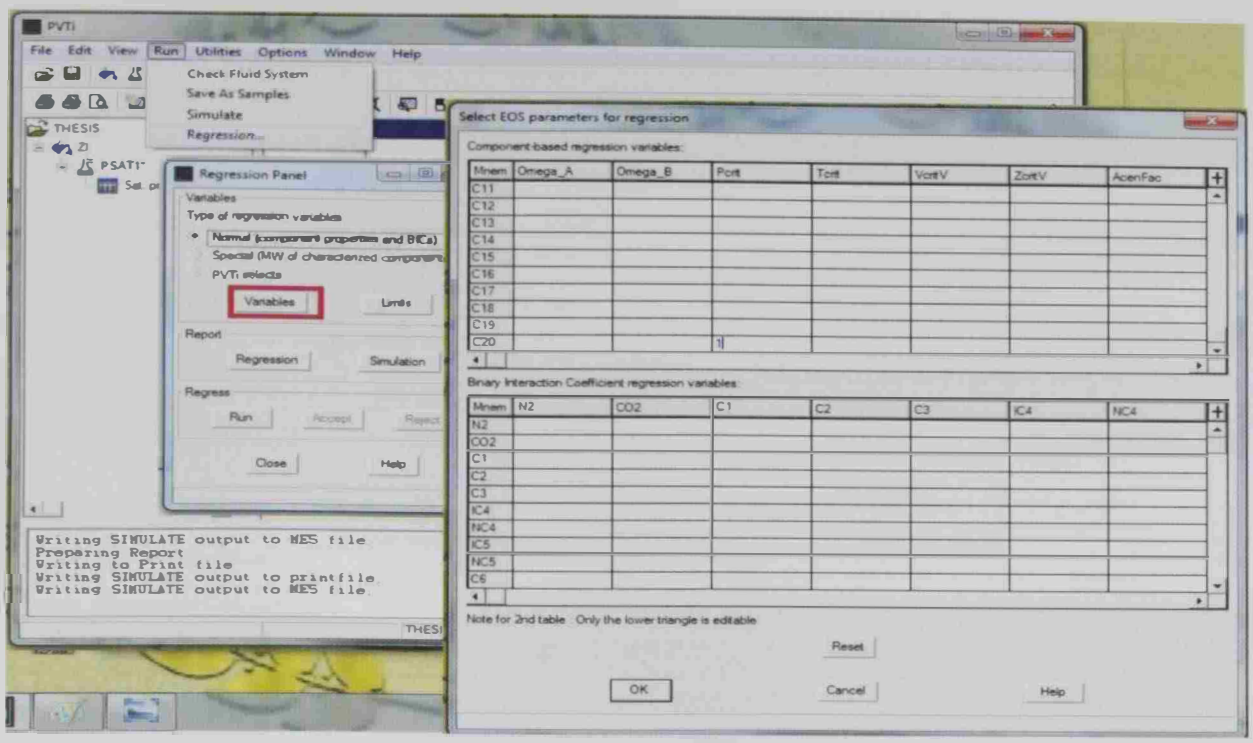

Figure A-14: Select EOS parameters for regression.

In this work, T_c for C_{20}^+ was first selected as a sensitive attribute but the calculated saturation pressure was not accurate then P_c for C_{20}^+ was selected to accurately fit the required saturation pressure (see Figure A-15 for well A#22 and Figure A-16 for well A#33)

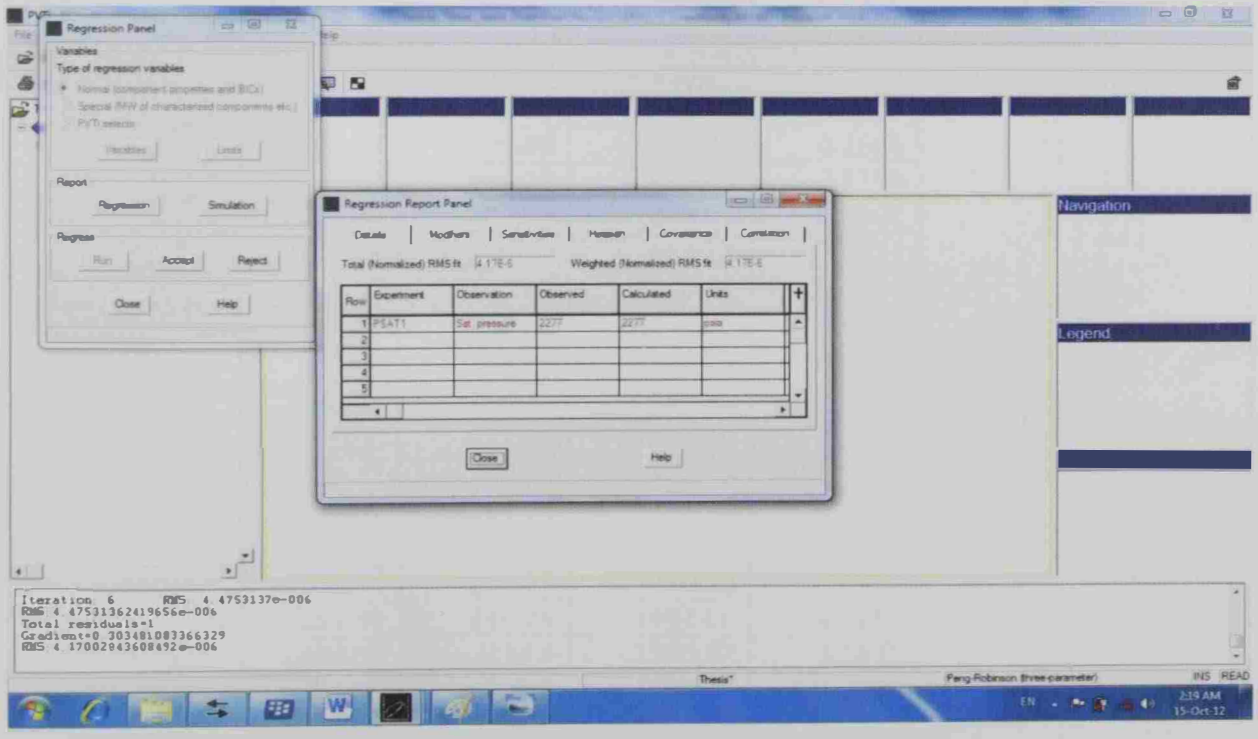

Figure A-15: Regression observed vs. calculated saturation pressure for well A#22

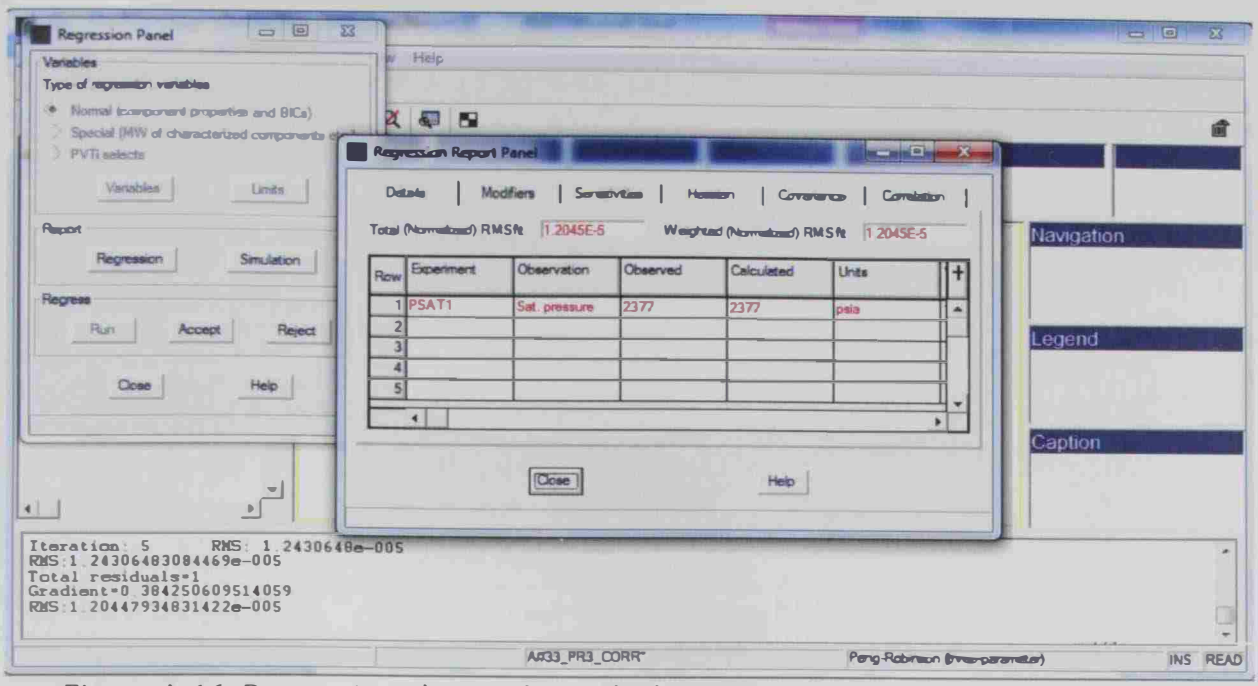

Figure A-16: Regression observed vs. calculated saturation pressure for well A#33

Table A.1 Molecular weights and critical properties of the components used in this study.

Component	MW	P_c, psia	T_c, °R	ω
N_2	28.01	492.26	228.31	0.0403
CO_2	44.01	1070.67	548.87	0.2276
C_1	16.04	667.03	344.34	0.0115
C_2	30.07	706.62	550.91	0.0995
C_3	44.10	616.12	667.02	0.1523
i-C_4	58.12	529.10	735.98	0.1770
n-C_4	58.12	550.56	766.55	0.2002
i-C_5	72.15	490.37	830.10	0.2275
n-C_5	72.15	488.78	846.79	0.2515
C_6	84.98	495.88	922.20	0.2586
C_7	96.00	446.13	985.53	0.2794
C_8	106.59	407.05	1039.83	0.3081
C_9	119.79	375.22	1087.72	0.3411
C_{10}	133.75	348.59	1130.79	0.3764
C_{11}	148.12	325.85	1170.07	0.4126
C_{12}	162.69	306.12	1206.24	0.4489
C_{13}	176.00	288.77	1239.80	0.4847
C_{14}	191.85	273.37	1271.10	0.5196
C_{15}	206.27	259.58	1300.43	0.5534
C_{16}	220.52	247.15	1327.99	0.5860
C_{17}	234.55	235.88	1353.96	0.6172
C_{18}	248.34	225.63	1378.48	0.6469
C_{19}	261.89	216.25	1401.66	0.6752
C_{20}+ for A#22	403.00	234.4	1555.37	1.1675
C_{20}+ for A#33	424.00	229.0	1584.87	1.1882

The final report after regression shows the fitting of the observed and calculated saturation pressures (Figure A-12 for well A#22). The results of PVTi experiments such flash, CCE, DL and Separator tests for well A#22 shown below

Expt PSAT1 : Saturation Pressure Calculation

Peng-Robinson (3-Parm) on ZI with PR corr.
Lohrenz-Bray-Clark Viscosity Correlation

Specified temperature	Deg F	235.0000
Calculated bubble point pressure	PSIA	2276.9906
Observed bubble point pressure	PSIA	2277.0000

Fluid properties		Liquid Calculated	Vapour Calculated
Mole Weight		110.9404	22.6286
Z-factor		0.7843	0.7843
Viscosity		0.3517	0.0183
Density	LB/FT3	43.2033	7.9228
Molar Vol	CF/LB-ML	2.5679	2.8561

Molar Distributions		Total, Z	Liquid,X	Vapour,Y	K-Values
Components					
Mnemonic	Number	Measured	Calculated	Calculated	Calculated
N2	1	0.1190	0.1190	0.4852	4.0773
CO2	2	1.8600	1.8600	2.9645	1.5938
C1	3	31.6920	31.6920	79.5409	2.5098
C2	4	6.1880	6.1880	7.3397	1.1861
C3	5	5.7520	5.7520	4.3027	0.7480
IC4	6	1.3390	1.3390	0.7006	0.5232
NC4	7	3.3750	3.3750	1.5148	0.4488
IC5	8	1.5100	1.5100	0.4898	0.3244
NC5	9	2.0890	2.0890	0.6122	0.2931
C6	10	3.2450	3.2450	0.6116	0.1885
C7	11	3.7600	3.7600	0.4607	0.1225
C8	12	3.9490	3.9490	0.3541	0.0897
C9	13	3.5790	3.5790	0.2209	0.0617
C10	14	3.3530	3.3530	0.1480	0.0441
C11	15	2.7600	2.7600	0.0876	0.0317
C12	16	2.3700	2.3700	0.0544	0.0230
C13	17	2.2980	2.2980	0.0386	0.0168
C14	18	2.3800	2.3800	0.0281	0.0118
C15	19	2.1290	2.1290	0.0177	0.0083
C16	20	1.9320	1.9320	0.0117	0.0061
C17	21	1.6810	1.6810	0.0074	0.0044
C18	22	1.4690	1.4690	0.0050	0.0034
C19	23	1.3540	1.3540	0.0035	0.0026
C20+	24	9.8170	9.8170	6.5272E-05	6.6489E-06
Composition Total		100.0000	100.0000	100.0000	

Figure A-12: Saturation pressure calculation report after regression for well A#22.

Expt FLASH1 : Flash Calculation

Peng-Robinson (3-Parm) on ZI with PR corr.
Lohrenz-Bray-Clark Viscosity Correlation
Two phase state

Specified temperature	Deg F	60.0000
Specified pressure	PSIA	14.6700
Mole Percentage in vapour		49.5380
Calculated GOR	MSCF/BBL	0.5602

Fluid properties		Liquid Calculated	Vapour Calculated
Mole Weight		193.6051	26.7339
Z-factor		0.0098	0.9938
Viscosity		1.4194	0.0100
Density	LB/FT3	51.8587	0.0708
Molar Vol	CF/LB-ML	3.7333	377.7917

Molar Distributions / Components		Total, Z	Liquid,X	Vapour,Y	K-Values
Mnemonic	Number	Measured	Calculated	Calculated	Calculated
N2	1	0.1190	0.0004	0.2399	674.0273
CO2	2	1.8600	0.0609	3.6926	60.5903
C1	3	31.6920	0.3066	63.6629	207.6716
C2	4	6.1880	0.4263	12.0572	28.2859
C3	5	5.7520	1.3766	10.2091	7.4164
IC4	6	1.3390	0.7507	1.9383	2.5819
NC4	7	3.3750	2.4587	4.3084	1.7523
IC5	8	1.5100	1.8152	1.1991	0.6606
NC5	9	2.0890	2.8057	1.3589	0.4843
C6	10	3.2450	5.6614	0.7836	0.1384
C7	11	3.7600	7.1291	0.3281	0.0460
C8	12	3.9490	7.6737	0.1549	0.0202
C9	13	3.5790	7.0475	0.0458	0.0065
C10	14	3.3530	6.6299	0.0150	0.0023
C11	15	2.7600	5.4652	0.0043	0.0008
C12	16	2.3700	4.6953	0.0013	0.0003
C13	17	2.2980	4.5535	0.0005	0.0001
C14	18	2.3800	4.7163	0.0002	3.4950E-05
C15	19	2.1290	4.2190	4.8914E-05	1.1594E-05
C16	20	1.9320	3.8286	1.5609E-05	4.0768E-06
C17	21	1.6810	3.3312	4.8464E-06	1.4548E-06
C18	22	1.4690	2.9111	1.8031E-06	6.1938E-07
C19	23	1.3540	2.6832	7.3100E-07	2.7243E-07
C20+	24	9.8170	19.4542	1.0471E-13	5.3825E-15
Composition Total		100.0000	100.0000	100.0000	

Figure A-13: Flash calculation report for well A#22

Expt SEPS1 : Separators

Peng-Robinson (3-Parm) on ZI with PR corr.
Lohrenz-Bray-Clark Viscosity Correlation

Stage number 1

Specified pressure PSIA	239.9696
Specified temperature Deg F	96.0000

GOR calc. is Gas Vol at STC/Stage Oil Vol

Feed is wellstream only

Output is 100.0% of liquid to	stage 2	number moles	0.6353
100.0% of vapour to	cumulative	number moles	0.3647

Total number moles output to liquid stream	0.6353
Total number moles output to vapour stream	0.3647
Total liquid volume output BBL	0.3687
Total vapour volume output MSCF	0.1384
Stage Gas-oil ratio (Calculated) MSCF/BBL	0.3753
Vapour mole fraction (Calculated)	36.4676
Stage Oil FVF (Calculated) RB/STB	1.0650

Fluid properties		Liquid		Vapour	
		Observed	Calculated	Observed	Calculated
Mole Weight			162.3773		21.3291
Z-factor			0.1311		0.9492
Viscosity			1.0438		0.0114
Density	LB/FT3		49.8341		0.9043
Molar Vol	CF/LB-ML		3.2584		23.5865

Molar Distributions		Fluid, Z	K-Values	Liquid,X	Vapour,Y
Components					
Mnemonic	Number	Calculated	Calculated	Calculated	Calculated
N2	1	0.1190	41.3185	0.0076	0.3131
CO2	2	1.8600	5.2495	0.7295	3.8295
C1	3	31.6920	14.7335	5.2747	77.7152
C2	4	6.1880	2.6946	3.8246	10.3055
C3	5	5.7520	0.8661	6.0472	5.2377
IC4	6	1.3390	0.3558	1.7501	0.6227
NC4	7	3.3750	0.2552	4.6336	1.1823
IC5	8	1.5100	0.1118	2.2334	0.2497
NC5	9	2.0890	0.0863	3.1329	0.2704
C6	10	3.2450	0.0300	5.0212	0.1505
C7	11	3.7600	0.0116	5.8791	0.0681
C8	12	3.9490	0.0057	6.1954	0.0354
C9	13	3.5790	0.0022	5.6262	0.0124
C10	14	3.3530	0.0009	5.2749	0.0048
C11	15	2.7600	0.0004	4.3433	0.0016
C12	16	2.3700	0.0002	3.7300	0.0006
C13	17	2.2980	6.9224E-05	3.6169	0.0003
C14	18	2.3800	2.7537E-05	3.7461	0.0001
C15	19	2.1290	1.0933E-05	3.3510	3.6637E-05
C16	20	1.9320	4.5730E-06	3.0410	1.3906E-05
C17	21	1.6810	1.9305E-06	2.6459	5.1079E-06
C18	22	1.4690	9.4609E-07	2.3122	2.1875E-06
C19	23	1.3540	4.7623E-07	2.1312	1.0149E-06
C20+	24	9.8170	1.6288E-13	15.4519	2.5169E-12
Composition Total		100.0000		100.0000	100.0000

Figure A-14: Fist Stage Separator test report for well A#22.

Expt SEPS1 : Separators

Peng-Robinson (3-Parm) on ZI with PR corr.
Lohrenz-Bray-Clark Viscosity Correlation

Stage number 2

Specified pressure PSIA	14.6959
Specified temperature Deg F	60.0000

GOR calc. is Gas Vol at STC/Stage Oil Vol

Feed is 100.0% of liquid from stage 1		number moles	0.6353
Output is 100.0% of liquid to	cumulative	number moles	0.5425
100.0% of vapour to	cumulative	number moles	0.0928

Total number moles output to liquid stream	0.5425
Total number moles output to vapour stream	0.0928
Total liquid volume output BBL	0.3462
Total vapour volume output MSCF	0.0352
Stage Gas-oil ratio (Calculated) MSCF/BBL	0.1017
Vapour mole fraction (Calculated)	14.6105
Stage Oil FVF (Calculated) RB/STB	1.0000

Fluid properties	Liquid		Vapour	
	Observed	Calculated	Observed	Calculated
Mole Weight		184.2981		34.2627
Z-factor		0.0094		0.9897
Viscosity		1.3449		0.0093
Density LB/FT3		51.4379		0.0912
Molar Vol CF/LB-ML		3.5829		375.5743

Molar Distributions Components		Fluid, Z	K-Values	Liquid,X	Vapour,Y
Mnemonic	Number	Calculated	Calculated	Calculated	Calculated
N2	1	0.0076	667.8109	7.6994E-05	0.0514
CO2	2	0.7295	60.2844	0.0755	4.5517
C1	3	5.2747	205.3733	0.1709	35.1034
C2	4	3.8246	28.1372	0.7703	21.6747
C3	5	6.0472	7.3887	3.1277	23.1099
IC4	6	1.7501	2.5804	1.4218	3.6689
NC4	7	4.6336	1.7525	4.1747	7.3160
IC5	8	2.2334	0.6616	2.3496	1.5545
NC5	9	3.1329	0.4853	3.3876	1.6440
C6	10	5.0212	0.1391	5.7437	0.7987
C7	11	5.8791	0.0463	6.8309	0.3164
C8	12	6.1954	0.0203	7.2303	0.1471
C9	13	5.6262	0.0066	6.5815	0.0432
C10	14	5.2749	0.0023	6.1750	0.0141
C11	15	4.3433	0.0008	5.0858	0.0041
C12	16	3.7300	0.0003	4.3680	0.0012
C13	17	3.6169	0.0001	4.2357	0.0005
C14	18	3.7461	3.5561E-05	4.3870	0.0002
C15	19	3.3510	1.1816E-05	3.9244	4.6370E-05
C16	20	3.0410	4.1612E-06	3.5613	1.4819E-05
C17	21	2.6459	1.4872E-06	3.0986	4.6083E-06
C18	22	2.3122	6.3396E-07	2.7078	1.7167E-06
C19	23	2.1312	2.7918E-07	2.4958	6.9680E-07
C20+	24	15.4519	5.6802E-15	18.0958	1.0279E-13
Composition Total		100.0000		100.0000	100.0000

Figure A-15: Second Stage Separator test report for well A#22

Expt SEPS1 : Separators

Peng-Robinson (3-Parm) on ZI with PR corr.
Lohrenz-Bray-Clark Viscosity Correlation

Cumulatives for Separator Train

Standard pressure PSIA	14.6959
Standard temperature Deg F	60.0000
Cumulative liquid mole fraction	0.5425
Cumulative vapour mole fraction	0.4575
Cumulative Surface volume oil BBL	0.3462
Cumulative Surface volume gas MSCF	0.1736
Cumulative GOR (Calculated) MSCF/BBL	0.5015

Fluid properties		Liquid Calculated	Vapour Calculated
Mole Weight		184.2981	23.9532
Z-factor		0.0094	0.9950
Viscosity		1.3449	0.0103
Density	LB/FT3	51.4379	0.0634
Molar Vol	CF/LB-ML	3.5829	377.5968

Molar Distributions		Total, Z	Liquid,X	Vapour,Y	K-Values
Components Mnemonic	Number	Measured	Calculated	Calculated	Calculated
N2	1	0.1190	7.6994E-05	0.2600	3377.1173
CO2	2	1.8600	0.0755	3.9760	52.6599
C1	3	31.6920	0.1709	69.0695	404.0931
C2	4	6.1880	0.7703	12.6123	16.3727
C3	5	5.7520	3.1277	8.8638	2.8340
IC4	6	1.3390	1.4218	1.2408	0.8727
NC4	7	3.3750	4.1747	2.4268	0.5813
IC5	8	1.5100	2.3496	0.5145	0.2190
NC5	9	2.0890	3.3876	0.5491	0.1621
C6	10	3.2450	5.7437	0.2820	0.0491
C7	11	3.7600	6.8309	0.1185	0.0173
C8	12	3.9490	7.2303	0.0581	0.0080
C9	13	3.5790	6.5815	0.0186	0.0028
C10	14	3.3530	6.1750	0.0067	0.0011
C11	15	2.7600	5.0858	0.0021	0.0004
C12	16	2.3700	4.3680	0.0007	0.0002
C13	17	2.2980	4.2357	0.0003	6.8736E-05
C14	18	2.3800	4.3870	0.0001	2.5959E-05
C15	19	2.1290	3.9244	3.8612E-05	9.8390E-06
C16	20	1.9320	3.5613	1.4091E-05	3.9569E-06
C17	21	1.6810	3.0986	5.0065E-06	1.6157E-06
C18	22	1.4690	2.7078	2.0920E-06	7.7258E-07
C19	23	1.3540	2.4958	9.5039E-07	3.8079E-07
C20+	24	9.8170	18.0958	2.0271E-12	1.1202E-13
Composition Total		100.0000	100.0000	100.0000	

Figure A-15: Cumulative for Separator train report for well A#22

Expt CCE1 : Constant Composition Expansion

Peng-Robinson (3-Parm) on ZI with PR corr.
Lohrenz-Bray-Clark Viscosity Correlation
Density units are LB/FT3
Specific volume units are CF/LB-ML
Viscosity units are CPOISE
Surface Tension units are DYNES/CM

Specified temperature Deg F 235.0000

Liq Sat calc. is Vol oil/Vol Fluid at Sat. Vol

Pressure PSIA	Inserted Point	Rel Volume Calculated	Vap Mole Frn Calculated	Liq Density Calculated	Vap Density Calculated
4687.000		0.9641		44.8109	
4445.999		0.9670		44.6776	
4204.998		0.9700		44.5393	
3963.997		0.9731		44.3956	
3722.996		0.9764		44.2463	
3481.995		0.9799		44.0908	
3240.994		0.9835		43.9288	
2999.993		0.9873		43.7597	
2758.992		0.9913		43.5828	
2517.991		0.9955		43.3976	
2276.990	- Psat	1.0000		43.2033	7.9228
2050.761		1.0424	0.0510	43.6592	7.0887
1824.531		1.0992	0.1002	44.1220	6.2698
1598.302		1.1769	0.1480	44.5944	5.4666
1372.072		1.2868	0.1949	45.0802	4.6790
1145.843		1.4496	0.2413	45.5854	3.9070
919.613		1.7070	0.2882	46.1200	3.1497
693.384		2.1584	0.3368	46.7030	2.4047
467.154		3.1073	0.3902	47.3769	1.6664
240.925		6.0771	0.4571	48.2717	0.9198

Pressure PSIA	Inserted Point	Liq Z-Fac Calculated	Vap Z-Fac Calculated	Surf Tension Calculated	Liq Sat Calculated
4687.000		1.5566			1.0000
4445.999		1.4809			1.0000
4204.998		1.4050			1.0000
3963.997		1.3288			1.0000
3722.996		1.2522			1.0000
3481.995		1.1753			1.0000
3240.994		1.0980			1.0000
2999.993		1.0202			1.0000
2758.992		0.9421			1.0000
2517.991		0.8635			1.0000
2276.990	- Psat	0.7843	0.8724	4.6582	1.0000
2050.761		0.7290	0.8738	5.5534	0.9793
1824.531		0.6701	0.8770	6.5691	0.9593
1598.302		0.6073	0.8820	7.7143	0.9397
1372.072		0.5402	0.8889	8.9985	0.9203
1145.843		0.4686	0.8978	10.4331	0.9007
919.613		0.3917	0.9088	12.0338	0.8803
693.384		0.3090	0.9221	13.8278	0.8581
467.154		0.2195	0.9384	15.8720	0.8319
240.925		0.1214	0.9592	18.3247	0.7943

Figure A-16: Constant composition expansion test report for well A#22 (continue....)

Expt CCE1 : Constant Composition Expansion

Peng-Robinson (3-Parm) on ZI with PR corr.
Lohrenz-Bray-Clark Viscosity Correlation
Density units are LB/FT3
Specific volume units are CF/LB-ML
Viscosity units are CPOISE
Surface Tension units are DYNES/CM

Specified temperature Deg F 235.0000

Liq Sat calc. is Vol oil/Vol Fluid at Sat. Vol

Pressure PSIA	Inserted Point	Liq Visc Calculated	Vap Visc Calculated	Liq Mole Wt Calculated	Vap Mole Wt Calculated
4687.000		0.4745		110.9404	
4445.999		0.4624		110.9404	
4204.998		0.4504		110.9404	
3963.997		0.4382		110.9404	
3722.996		0.4260		110.9404	
3481.995		0.4138		110.9404	
3240.994		0.4015		110.9404	
2999.993		0.3891		110.9404	
2758.992		0.3767		110.9404	
2517.991		0.3642		110.9404	
2276.990	- Psat	0.3517	0.0183	110.9404	22.6286
2050.761		0.3738	0.0174	115.6952	22.5165
1824.531		0.3977	0.0166	120.7967	22.4668
1598.302		0.4238	0.0159	126.3096	22.4889
1372.072		0.4526	0.0153	132.3230	22.5979
1145.843		0.4846	0.0147	138.9686	22.8201
919.613		0.5209	0.0143	146.4581	23.2027
693.384		0.5634	0.0138	155.1761	23.8398
467.154		0.6165	0.0134	165.9591	24.9544
240.925		0.6944	0.0128	181.3574	27.2983

Pressure PSIA	Inserted Point	Liq Mol Vol Calculated	Vap Mol Vol Calculated
4687.000		2.4757	
4445.999		2.4831	
4204.998		2.4908	
3963.997		2.4989	
3722.996		2.5073	
3481.995		2.5162	
3240.994		2.5255	
2999.993		2.5352	
2758.992		2.5455	
2517.991		2.5564	
2276.990	- Psat	2.5679	2.8561
2050.761		2.6500	3.1764
1824.531		2.7378	3.5833
1598.302		2.8324	4.1139
1372.072		2.9353	4.8296
1145.843		3.0485	5.8408
919.613		3.1756	7.3667
693.384		3.3226	9.9137
467.154		3.5030	14.9747
240.925		3.7570	29.6784

Figure A-17: Constant composition expansion test report for well A#22.

Expt DL1 : Differential Liberation

Peng-Robinson (3-Parm) on ZI with PR corr.
Lohrenz-Bray-Clark Viscosity Correlation

Density units are	LB/FT3
Specific volume units are	CF/LB-ML
Viscosity units are	CPOISE
Surface Tension units are	DYNES/CM
Gas-Oil Ratio units are	MSCF/STB
Relative Volume units are	RB/STB
Gas FVF units are	RB/MSCF
Extracted Gas Volume units are	FT3
Oil Relative Volume units are	BBL/STB

Specified temperature Deg F 235.0000

Relative Oil Saturated Volume (Bo(Pbub)) 1.3356

GOR calc. is Gas Vol at STC/Stock Tank Oil Vol
Oil Rel Vol calc. is Stage Vol oil/Stock Tank Oil Vol

Pressure PSIA	Inserted Point	GOR Calculated	Total RelVol Calculated	Oil RelVol Calculated	Liq Dens Calculated
4687.000		0.5178	1.2877	1.2877	44.8109
4445.999		0.5178	1.2915	1.2915	44.6776
4204.998		0.5178	1.2955	1.2955	44.5393
3963.997		0.5178	1.2997	1.2997	44.3956
3722.996		0.5178	1.3041	1.3041	44.2463
3481.995		0.5178	1.3087	1.3087	44.0908
3240.994		0.5178	1.3135	1.3135	43.9288
2999.993		0.5178	1.3186	1.3186	43.7597
2758.992		0.5178	1.3239	1.3239	43.5828
2517.991		0.5178	1.3296	1.3296	43.3976
2276.990	- Psat	0.5178	1.3356	1.3356	43.2033
2050.761		0.4612	1.3922	1.3079	43.6592
1824.531		0.4069	1.4678	1.2813	44.1199
1598.302		0.3545	1.5706	1.2555	44.5859
1372.072		0.3039	1.7147	1.2304	45.0582
1145.843		0.2547	1.9255	1.2058	45.5387
919.613		0.2066	2.2536	1.1813	46.0303
693.384		0.1589	2.8171	1.1566	46.5398
467.154		0.1102	3.9694	1.1305	47.0842
240.925	@ Tres	0.0548	7.4531	1.0982	47.7343
14.695	@ Tstd	6.2319E-17	92.2322	1.0000	51.5211

Pressure PSIA	Inserted Point	Vap Dens Calculated	Gas Grav Calculated	Vap Z-Fac Calculated	Liq Z-Fac Calculated
4687.000					1.5566
4445.999					1.4809
4204.998					1.4050
3963.997					1.3288
3722.996					1.2522
3481.995					1.1753
3240.994					1.0980
2999.993					1.0202
2758.992					0.9421
2517.991					0.8635
2276.990	- Psat	7.9228	0.7811	0.8724	0.7843
2050.761		7.0887	0.7772	0.8738	0.7290
1824.531		6.2725	0.7757	0.8769	0.6700
1598.302		5.4750	0.7771	0.8816	0.6070
1372.072		4.6970	0.7823	0.8880	0.5395
1145.843		3.9391	0.7927	0.8961	0.4673
919.613		3.2011	0.8113	0.9057	0.3896
693.384		2.4816	0.8445	0.9170	0.3059
467.154		1.7753	0.9094	0.9300	0.2155
240.925	@ Tres	1.0610	1.0710	0.9451	0.1172
14.695	@ Tstd	0.0932	1.2074	0.9893	0.0095

Figure A-18: Differential Liberation test report for well A#22 (Continued...)

Expt DL1 : Differential Liberation

Peng-Robinson (3-Parm) on ZI with PR corr.
Lohrenz-Bray-Clark Viscosity Correlation

Density units are	LB/FT3
Specific volume units are	CF/LB-ML
Viscosity units are	CPOISE
Surface Tension units are	DYNES/CM
Gas-Oil Ratio units are	MSCF/STB
Relative Volume units are	RB/STB
Gas FVF units are	RB/MSCF
Extracted Gas Volume units are	FT3
Oil Relative Volume units are	BBL/STB

Specified temperature Deg F 235.0000

Relative Oil Saturated Volume (Bo(Pbub)) 1.3356

GOR calc. is Gas Vol at STC/Stock Tank Oil Vol
Oil Rel Vol calc. is Stage Vol oil/Stock Tank Oil Vol

Pressure PSIA	Inserted Point	Surf Tension Calculated	Gas FVF Calculated	Liq Visc Calculated	Vap Visc Calculated
4687.000			0.7322	0.4745	
4445.999			0.7591	0.4624	
4204.998			0.7896	0.4504	
3963.997			0.8247	0.4382	
3722.996			0.8652	0.4260	
3481.995			0.9126	0.4138	
3240.994			0.9686	0.4015	
2999.993			1.0354	0.3891	
2758.992			1.1164	0.3767	
2517.991			1.2160	0.3642	
2276.990	- Psat	4.6582	1.3405	0.3517	0.0183
2050.761		5.5534	1.4908	0.3738	0.0174
1824.531		6.5657	1.6816	0.3975	0.0166
1598.302		7.7015	1.9300	0.4232	0.0159
1372.072		8.9663	2.2646	0.4510	0.0153
1145.843		10.3652	2.7362	0.4812	0.0148
919.613		11.9042	3.4461	0.5139	0.0143
693.384		13.5935	4.6274	0.5498	0.0138
467.154		15.4589	6.9652	0.5905	0.0133
240.925	@ Tres	17.6070	13.7258	0.6421	0.0126
14.695	@ Tstd	26.1696	176.1975	1.3641	0.0093

Pressure PSIA	Inserted Point	Moles Extrac Calculated	GasVol Extrc Calculated	Liquid Sat Calculated	Vapour Sat Calculated
4687.000				1.0000	
4445.999				1.0000	
4204.998				1.0000	
3963.997				1.0000	
3722.996				1.0000	
3481.995				1.0000	
3240.994				1.0000	
2999.993				1.0000	
2758.992				1.0000	
2517.991				1.0000	
2276.990	- Psat			1.0000	
2050.761		0.0510	42.6905	0.9394	0.0606
1824.531		0.1001	83.7152	0.9334	0.0666
1598.302		0.1473	123.2490	0.9255	0.0745
1372.072		0.1930	161.4733	0.9148	0.0852
1145.843		0.2374	198.5992	0.8996	0.1004
919.613		0.2808	234.9152	0.8769	0.1231
693.384		0.3238	270.9119	0.8398	0.1602
467.154		0.3678	307.7111	0.7690	0.2310
240.925	@ Tres	0.4178	349.5417	0.5908	0.4092
14.695	@ Tstd	0.4673	390.9052	0.0939	0.9061

Figure A-19: Differential Liberation test report for well A#22 (Continued...)

Expt DL1 : Differential Liberation

Peng-Robinson (3-Parm) on ZI with PR corr.
Lohrenz-Bray-Clark Viscosity Correlation

Density units are	LB/FT3
Specific volume units are	CF/LB-ML
Viscosity units are	CPOISE
Surface Tension units are	DYNES/CM
Gas-Oil Ratio units are	MSCF/STB
Relative Volume units are	RB/STB
Gas FVF units are	RB/MSCF
Extracted Gas Volume units are	FT3
Oil Relative Volume units are	BBL/STB

Specified temperature Deg F 235.0000

Relative Oil Saturated Volume (Bo(Pbub)) 1.3356

GOR calc. is Gas Vol at STC/Stock Tank Oil Vol
Oil Rel Vol calc. is Stage Vol oil/Stock Tank Oil Vol

Pressure PSIA	Inserted Point	Liq Mol Wt Calculated	Vap Mol Wt Calculated	Liq Visc Calculated	Vap Visc Calculated
4687.000		110.9404		0.4745	
4445.999		110.9404		0.4624	
4204.998		110.9404		0.4504	
3963.997		110.9404		0.4382	
3722.996		110.9404		0.4260	
3481.995		110.9404		0.4138	
3240.994		110.9404		0.4015	
2999.993		110.9404		0.3891	
2758.992		110.9404		0.3767	
2517.991		110.9404		0.3642	
2276.990	- Psat	110.9404	22.6286	0.3517	0.0183
2050.761		115.6952	22.5165	0.3738	0.0174
1824.531		120.7748	22.4735	0.3975	0.0166
1598.302		126.2204	22.5140	0.4232	0.0159
1372.072		132.0836	22.6627	0.4510	0.0153
1145.843		138.4334	22.9640	0.4812	0.0148
919.613		145.3702	23.5032	0.5139	0.0143
693.384		153.0637	24.4661	0.5498	0.0138
467.154		161.8806	26.3452	0.5905	0.0133
240.925	@ Tres	173.1188	31.0266	0.6421	0.0126
14.695	@ Tstd	185.9390	34.9791	1.3641	0.0093

Pressure PSIA	Inserted Point	Liq Mol Vol Calculated	Vap Mol Vol Calculated
4687.000		2.4757	
4445.999		2.4831	
4204.998		2.4908	
3963.997		2.4989	
3722.996		2.5073	
3481.995		2.5162	
3240.994		2.5255	
2999.993		2.5352	
2758.992		2.5455	
2517.991		2.5564	
2276.990	- Psat	2.5679	2.8561
2050.761		2.6500	3.1764
1824.531		2.7374	3.5829
1598.302		2.8310	4.1121
1372.072		2.9314	4.8249
1145.843		3.0399	5.8298
919.613		3.1581	7.3423
693.384		3.2889	9.8591
467.154		3.4381	14.8400
240.925	@ Tres	3.6267	29.2441
14.695	@ Tstd	3.6090	375.4070

Figure A-20: Differential Liberation test report for well A#22.

The experiment results for well A#33 as shown below:

Expt PSAT1 : Saturation Pressure Calculation

Peng-Robinson (3-Parm) on ZI with PR corr.
Lohrenz-Bray-Clark Viscosity Correlation

Specified temperature	Deg F	257.0000
Calculated bubble point pressure	PSIA	2377.0063
Observed bubble point pressure	PSIA	2377.0000

Fluid properties		Liquid Calculated	Vapour Calculated
Mole Weight		100.1410	25.6020
Z-factor		0.7602	0.7602
Viscosity		0.2428	0.0199
Density	LB/FT3	40.7130	9.3040
Molar Vol	CF/LB-ML	2.4597	2.7517

Molar Distributions Components		Total, Z	Liquid,X	Vapour,Y	K-Values
Mnemonic	Number	Measured	Calculated	Calculated	Calculated
N2	1	0.1010	0.1010	0.3354	3.3211
CO2	2	2.7378	2.7378	4.1798	1.5267
C1	3	32.8560	32.8560	72.9394	2.2200
C2	4	6.6816	6.6816	8.4940	1.2713
C3	5	6.4676	6.4676	5.5188	0.8533
IC4	6	1.5899	1.5899	1.0208	0.6421
NC4	7	4.0548	4.0548	2.3103	0.5698
IC5	8	1.8139	1.8139	0.7726	0.4259
NC5	9	2.5298	2.5298	0.9918	0.3920
C6	10	3.5958	3.5958	0.9922	0.2759
C7	11	3.9428	3.9428	0.7529	0.1910
C8	12	4.1528	4.1528	0.6048	0.1456
C9	13	3.7388	3.7388	0.3933	0.1052
C10	14	3.3458	3.3458	0.2622	0.0784
C11	15	2.6948	2.6948	0.1579	0.0586
C12	16	2.1989	2.1989	0.0970	0.0441
C13	17	1.9789	1.9789	0.0664	0.0335
C14	18	1.6439	1.6439	0.0406	0.0247
C15	19	1.4989	1.4989	0.0274	0.0183
C16	20	1.2269	1.2269	0.0170	0.0139
C17	21	1.0639	1.0639	0.0112	0.0105
C18	22	0.9449	0.9449	0.0079	0.0084
C19	23	0.8969	0.8969	0.0060	0.0067
C20-	24	8.2435	8.2435	0.0003	3.4985E-05

Figure A-21: Saturation pressure calculation report after regression for well A#33.

Other experimental works also performed using PVTi such: Flash calculation, Separator test, Constant composition expansion and Differential liberation. The results report for well A#33 is shown below:

Expt FLASH1 : Flash Calculation

Peng-Robinson (3-Parm) on ZI with PR corr.
Lohrenz-Bray-Clark Viscosity Correlation
Two phase state

Specified temperature	Deg F	60.0000
Specified pressure	PSIA	15.0000
Mole Percentage in vapour		54.1908
Calculated GOR	MSCF/BBL	0.6989

Fluid properties		Liquid Calculated	Vapour Calculated
Mole Weight		185.4026	28.0667
Z-factor		0.0097	0.9931
Viscosity		1.3696	0.0099
Density	LB/FT3	51.4145	0.0760
Molar Vol	CF/LB-ML	3.6060	369.2354

Molar Distributions Components		Total, Z	Liquid,X	Vapour,Y	K-Values
Mnemonic	Number	Measured	Calculated	Calculated	Calculated
N2	1	0.1010	0.0003	0.1861	602.6512
CO2	2	2.7378	0.0860	4.9795	57.9111
C1	3	32.8560	0.3157	60.3634	191.2117
C2	4	6.6816	0.4441	11.9544	26.9176
C3	5	6.4676	1.4981	10.6685	7.1216
IC4	6	1.5899	0.8818	2.1885	2.4819
NC4	7	4.0548	2.9353	5.0010	1.7037
IC5	8	1.8139	2.2507	1.4446	0.6419
NC5	9	2.5298	3.5415	1.6747	0.4729
C6	10	3.5958	6.7669	0.9152	0.1352
C7	11	3.9428	8.1679	0.3712	0.0454
C8	12	4.1528	8.8549	0.1779	0.0201
C9	13	3.7388	8.0999	0.0522	0.0064
C10	14	3.3458	7.2845	0.0163	0.0022
C11	15	2.6948	5.8774	0.0046	0.0008
C12	16	2.1989	4.7985	0.0013	0.0003
C13	17	1.9789	4.3193	0.0004	0.0001
C14	18	1.6439	3.5884	0.0001	3.3584E-05
C15	19	1.4989	3.2720	3.6200E-05	1.1064E-05
C16	20	1.2269	2.6783	1.0296E-05	3.8441E-06
C17	21	1.0639	2.3225	3.1682E-06	1.3641E-06
C18	22	0.9449	2.0628	1.1890E-06	5.7639E-07
C19	23	0.8969	1.9580	4.9352E-07	2.5205E-07
C20+	24	8.2435	17.9953	8.4182E-15	4.6780E-16
Composition Total		100.0000	100.0000	100.0000	

Figure A-22: Flash calculation report for well A#33

Expt SEPS1 : Separators

Peng-Robinson (3-Parm) on ZI with PR corr.
Lohrenz-Bray-Clark Viscosity Correlation

Stage number 1

Specified pressure PSIA	239.9696
Specified temperature Deg F	96.0000

GOR calc. is Gas Vol at STC/Stage Oil Vol
Feed is wellstream only

Output is 100.0% of liquid to	stage 2	number moles	0.6040
100.0% of vapour to	cumulative	number moles	0.3960

Total number moles output to liquid stream	0.6040
Total number moles output to vapour stream	0.3960
Total liquid volume output BBL	0.3321
Total vapour volume output MSCF	0.1503
Stage Gas-oil ratio (Calculated) MSCF/BBL	0.4525
Vapour mole fraction (Calculated)	39.5988
Stage Oil FVF (Calculated) RB/STB	1.0828

Fluid properties	Liquid		Vapour	
	Observed	Calculated	Observed	Calculated
Mole Weight		151.2133		22.2390
Z-factor		0.1242		0.9458
Viscosity		0.9308		0.0114
Density LB/FT3		48.9803		0.9462
Molar Vol CF/LB-ML		3.0872		23.5032

Molar Distributions		Fluid, Z	K-Values	Liquid,X	Vapour,Y
Components Mnemonic	Number	Calculated	Calculated	Calculated	Calculated
N2	1	0.1010	37.8133	0.0065	0.2452
CO2	2	2.7378	5.1098	1.0420	5.3245
C1	3	32.8560	13.8414	5.3995	74.7363
C2	4	6.6816	2.6184	4.0720	10.6622
C3	5	6.4676	0.8506	6.8743	5.8473
IC4	6	1.5899	0.3509	2.1399	0.7509
NC4	7	4.0548	0.2543	5.7538	1.4632
IC5	8	1.8139	0.1116	2.7983	0.3124
NC5	9	2.5298	0.0866	3.9635	0.3431
C6	10	3.5958	0.0302	5.8376	0.1763
C7	11	3.9428	0.0118	6.4775	0.0765
C8	12	4.1528	0.0059	6.8489	0.0403
C9	13	3.7388	0.0023	6.1807	0.0140
C10	14	3.3458	0.0009	5.5359	0.0052
C11	15	2.6948	0.0004	4.4604	0.0017
C12	16	2.1989	0.0002	3.6401	0.0006
C13	17	1.9789	7.0250E-05	3.2761	0.0002
C14	18	1.6439	2.7940E-05	2.7216	7.6040E-05
C15	19	1.4989	1.1058E-05	2.4816	2.7441E-05
C16	20	1.2269	4.5903E-06	2.0313	9.3243E-06
C17	21	1.0639	1.9335E-06	1.7614	3.4057E-06
C18	22	0.9449	9.4349E-07	1.5644	1.4760E-06
C19	23	0.8969	4.7353E-07	1.4850	7.0319E-07
C20+	24	8.2435	2.5498E-14	13.6479	3.4799E-13
Composition Total		100.0000		100.0000	100.0000

Figure A-23: Fist Stage Separator test report for well A#33

Expt SEPS1 : Separators

Peng-Robinson (3-Parm) on ZI with PR corr.
Lohrenz-Bray-Clark Viscosity Correlation

Stage number 2

Specified pressure PSIA				14.6959
Specified temperature Deg F				60.0000
GOR calc. is Gas Vol at STC/Stage Oil Vol				
Feed is 100.0% of liquid from stage 1			number moles	0.6040
Output is 100.0% of liquid to	cumulative		number moles	0.5014
100.0% of vapour to	cumulative		number moles	0.1026
Total number moles output to liquid stream				0.5014
Total number moles output to vapour stream				0.1026
Total liquid volume output BBL				0.3067
Total vapour volume output MSCF				0.0390
Stage Gas-oil ratio (Calculated) MSCF/BBL				0.1270
Vapour mole fraction (Calculated)				16.9943
Stage Oil FVF (Calculated) RB/STB				1.0000

Fluid properties		Liquid		Vapour	
		Observed	Calculated	Observed	Calculated
Mole Weight			174.7479		36.2624
Z-factor			0.0091		0.9886
Viscosity			1.2696		0.0093
Density	LB/FT3		50.8733		0.0967
Molar Vol	CF/LB-ML		3.4350		375.1694

Molar Distributions		Fluid, Z	K-Values	Liquid,X	Vapour,Y
Components					
Mnemonic	Number	Calculated	Calculated	Calculated	Calculated
N2	1	0.0065	611.0446	6.1939E-05	0.0378
CO2	2	1.0420	58.8963	0.0961	5.6620
C1	3	5.3995	193.2329	0.1604	30.9889
C2	4	4.0720	27.3659	0.7430	20.3319
C3	5	6.8743	7.2499	3.3336	24.1683
IC4	6	2.1399	2.5358	1.6970	4.3033
NC4	7	5.7538	1.7416	5.1098	8.8992
IC5	8	2.7983	0.6571	2.9714	1.9524
NC5	9	3.9635	0.4843	4.3442	2.1038
C6	10	5.8376	0.1389	6.8383	0.9498
C7	11	6.4775	0.0467	7.7296	0.3614
C8	12	6.8489	0.0207	8.2163	0.1700
C9	13	6.1807	0.0067	7.4360	0.0495
C10	14	5.5359	0.0023	6.6661	0.0154
C11	15	4.4604	0.0008	5.3728	0.0043
C12	16	3.6401	0.0003	4.3850	0.0012
C13	17	3.2761	0.0001	3.9467	0.0004
C14	18	2.7216	3.4967E-05	3.2788	0.0001
C15	19	2.4816	1.1541E-05	2.9896	3.4503E-05
C16	20	2.0313	4.0172E-06	2.4472	9.8309E-06
C17	21	1.7614	1.4281E-06	2.1221	3.0305E-06
C18	22	1.5644	6.0430E-07	1.8847	1.1390E-06
C19	23	1.4850	2.6463E-07	1.7890	4.7342E-07
C20+	24	13.6479	5.0745E-16	16.4421	8.3435E-15
Composition Total		100.0000		100.0000	100.0000

Figure A-24: Second Stage Separator test report for well A#33

Expt SEPS1 : Separators

Peng-Robinson (3-Parm) on ZI with PR corr.
Lohrenz-Bray-Clark Viscosity Correlation

Cumulatives for Separator Train

Standard pressure PSIA	14.6959
Standard temperature Deg F	60.0000
Cumulative liquid mole fraction	0.5014
Cumulative vapour mole fraction	0.4986
Cumulative Surface volume oil BBL	0.3067
Cumulative Surface volume gas MSCF	0.1892
Cumulative GOR (Calculated) MSCF/BBL	0.6169

Fluid properties		Liquid Calculated	Vapour Calculated
Mole Weight		174.7479	25.1258
Z-factor		0.0091	0.9947
Viscosity		1.2696	0.0103
Density	LB/FT3	50.8733	0.0666
Molar Vol	CF/LB-ML	3.4350	377.4525

Molar Distributions Components Mnemonic	Number	Total, Z Measured	Liquid,X Calculated	Vapour,Y Calculated	K-Values Calculated
N2	1	0.1010	6.1939E-05	0.2025	3269.0209
CO2	2	2.7378	0.0961	5.3940	56.1084
C1	3	32.8560	0.1604	65.7306	409.8664
C2	4	6.6816	0.7430	12.6527	17.0301
C3	5	6.4676	3.3336	9.6188	2.8854
IC4	6	1.5899	1.6970	1.4822	0.8734
NC4	7	4.0548	5.1098	2.9940	0.5859
IC5	8	1.8139	2.9714	0.6500	0.2188
NC5	9	2.5298	4.3442	0.7056	0.1624
C6	10	3.5958	6.8383	0.3355	0.0491
C7	11	3.9428	7.7296	0.1352	0.0175
C8	12	4.1528	8.2163	0.0670	0.0082
C9	13	3.7388	7.4360	0.0213	0.0029
C10	14	3.3458	6.6661	0.0073	0.0011
C11	15	2.6948	5.3728	0.0023	0.0004
C12	16	2.1989	4.3850	0.0007	0.0002
C13	17	1.9789	3.9467	0.0003	6.7946E-05
C14	18	1.6439	3.2788	8.3988E-05	2.5616E-05
C15	19	1.4989	2.9896	2.8895E-05	9.6649E-06
C16	20	1.2269	2.4472	9.4286E-06	3.8528E-06
C17	21	1.0639	2.1221	3.3285E-06	1.5685E-06
C18	22	0.9449	1.8847	1.4067E-06	7.4634E-07
C19	23	0.8969	1.7890	6.5589E-07	3.6662E-07
C20+	24	8.2435	16.4421	2.7807E-13	1.6912E-14
Composition Total		100.0000	100.0000	100.0000	

Figure A-25: Cumulative for Separator train report for well A#33

Expt CCE1 : Constant Composition Expansion

Peng-Robinson (3-Parm) on ZI with PR corr.
Lohrenz-Bray-Clark Viscosity Correlation
Density units are LB/FT3
Specific volume units are CF/LB-ML
Viscosity units are CPOISE
Surface Tension units are DYNES/CM

Specified temperature Deg F 257.0000

Liq Sat calc. is Vol oil/Vol Fluid at Sat. Vol

Pressure PSIA	Inserted Point	Rel Volume Calculated	Vap Mole Frn Calculated	Liq Density Calculated	Vap Density Calculated
2820.000		0.9890		41.2851	
2775.697		0.9900		41.2417	
2731.394		0.9911		41.1978	
2687.091		0.9922		41.1536	
2642.788		0.9932		41.1089	
2598.485		0.9943		41.0637	
2554.182		0.9954		41.0181	
2509.880		0.9966		40.9720	
2465.577		0.9977		40.9255	
2421.274		0.9988		40.8785	
2376.971	- Psat	1.0000		40.8309	8.9070
2140.743		1.0486	0.0608	41.3941	7.9468
1904.516		1.1137	0.1184	41.9633	7.0124
1668.288		1.2029	0.1733	42.5431	6.1027
1432.061		1.3295	0.2264	43.1394	5.2165
1195.833		1.5171	0.2786	43.7610	4.3524
959.606		1.8146	0.3308	44.4227	3.5082
723.378		2.3380	0.3849	45.1519	2.6800
487.151		3.4433	0.4446	46.0099	1.8600
250.923		6.9301	0.5204	47.1843	1.0296

Pressure PSIA	Inserted Point	Liq Z-Fac Calculated	Vap Z-Fac Calculated	Surf Tension Calculated	Liq Sat Calculated
2820.000		0.8894			1.0000
2775.697		0.8763			1.0000
2731.394		0.8633			1.0000
2687.091		0.8502			1.0000
2642.788		0.8371			1.0000
2598.485		0.8240			1.0000
2554.182		0.8108			1.0000
2509.880		0.7976			1.0000
2465.577		0.7844			1.0000
2421.274		0.7712			1.0000
2376.971	- Psat	0.7580	0.8619	3.2875	1.0000
2140.743		0.7063	0.8632	4.0894	0.9716
1904.516		0.6509	0.8665	5.0217	0.9448
1668.288		0.5914	0.8716	6.0965	0.9190
1432.061		0.5277	0.8787	7.3275	0.8938
1195.833		0.4591	0.8879	8.7313	0.8685
959.606		0.3852	0.8993	10.3316	0.8424
723.378		0.3052	0.9134	12.1683	0.8138
487.151		0.2181	0.9308	14.3230	0.7798
250.923		0.1218	0.9533	17.0176	0.7301

Figure A-26: Constant composition expansion test report for well A#33 (continue....)

Expt CCE1 : Constant Composition Expansion

Peng-Robinson (3-Parm) on ZI with PR corr.
Lohrenz-Bray-Clark Viscosity Correlation
Density units are LB/FT3
Specific volume units are CF/LB-ML
Viscosity units are CPOISE
Surface Tension units are DYNES/CM

Specified temperature Deg F 257.0000

Liq Sat calc. is Vol oil/Vol Fluid at Sat. Vol

Pressure PSIA	Inserted Point	Liq Visc Calculated	Vap Visc Calculated	Liq Mole Wt Calculated	Vap Mole Wt Calculated
2820.000		0.2664		100.1410	
2775.697		0.2645		100.1410	
2731.394		0.2626		100.1410	
2687.091		0.2607		100.1410	
2642.788		0.2588		100.1410	
2598.485		0.2569		100.1410	
2554.182		0.2550		100.1410	
2509.880		0.2531		100.1410	
2465.577		0.2512		100.1410	
2421.274		0.2493		100.1410	
2376.971	- Psat	0.2474	0.0195	100.1410	24.8398
2140.743		0.2659	0.0184	105.0325	24.6455
1904.516		0.2863	0.0174	110.2909	24.5359
1668.288		0.3090	0.0166	115.9937	24.5207
1432.061		0.3345	0.0159	122.2476	24.6167
1195.833		0.3638	0.0152	129.2117	24.8538
959.606		0.3980	0.0147	137.1453	25.2868
723.378		0.4398	0.0142	146.5263	26.0257
487.151		0.4951	0.0136	158.4157	27.3320
250.923		0.5834	0.0130	176.1579	30.0848

Pressure PSIA	Inserted Point	Liq Mol Vol Calculated	Vap Mol Vol Calculated
2820.000		2.4256	
2775.697		2.4282	
2731.394		2.4307	
2687.091		2.4333	
2642.788		2.4360	
2598.485		2.4387	
2554.182		2.4414	
2509.880		2.4441	
2465.577		2.4469	
2421.274		2.4497	
2376.971	- Psat	2.4526	2.7888
2140.743		2.5374	3.1013
1904.516		2.6283	3.4989
1668.288		2.7265	4.0180
1432.061		2.8338	4.7190
1195.833		2.9527	5.7103
959.606		3.0873	7.2078
723.378		3.2452	9.7110
487.151		3.4431	14.6942
250.923		3.7334	29.2199

Figure A-27: Constant composition expansion test report for well A#33.

Expt DL1 : Differential Liberation

Peng-Robinson (3-Parm) on ZI with PR corr.
Lohrenz-Bray-Clark Viscosity Correlation

Density units are	LB/FT3
Specific volume units are	CF/LB-ML
Viscosity units are	CPOISE
Surface Tension units are	DYNES/CM
Gas-Oil Ratio units are	MSCF/STB
Relative Volume units are	RB/STB
Gas FVF units are	RB/MSCF
Extracted Gas Volume units are	FT3
Oil Relative Volume units are	BBL/STB

Specified temperature Deg F 257.0000

Relative Oil Saturated Volume (Bo(Pbub)) 1.4580

GOR calc. is Gas Vol at STC/Stock Tank Oil Vol
Oil Rel Vol calc. is Stage Vol oil/Stock Tank Oil Vol

Pressure PSIA	Inserted Point	GOR Calculated	Total RelVol Calculated	Oil RelVol Calculated	Liq Dens Calculated
2820.000		0.6561	1.4420	1.4420	41.2851
2775.697		0.6561	1.4435	1.4435	41.2417
2731.394		0.6561	1.4450	1.4450	41.1978
2687.091		0.6561	1.4466	1.4466	41.1536
2642.788		0.6561	1.4482	1.4482	41.1089
2598.485		0.6561	1.4498	1.4498	41.0637
2554.182		0.6561	1.4514	1.4514	41.0181
2509.880		0.6561	1.4530	1.4530	40.9720
2465.577		0.6561	1.4547	1.4547	40.9255
2421.274		0.6561	1.4563	1.4563	40.8785
2376.971	- Psat	0.6561	1.4580	1.4580	40.8309
2140.743		0.5790	1.5288	1.4166	41.3941
1904.516		0.5063	1.6234	1.3776	41.9609
1668.288		0.4375	1.7524	1.3404	42.5323
1432.061		0.3719	1.9333	1.3048	43.1101
1195.833		0.3092	2.1978	1.2704	43.6967
959.606		0.2485	2.6094	1.2367	44.2967
723.378		0.1889	3.3163	1.2028	44.9197
487.151		0.1282	4.7635	1.1669	45.5911
250.923	@ Tres	0.0583	9.1608	1.1216	46.4155
14.695	@ Tstd		116.5083	1.0000	51.0623

Pressure PSIA	Inserted Point	Vap Dens Calculated	Gas Grav Calculated	Vap Z-Fac Calculated	Liq Z-Fac Calculated
2820.000					0.8894
2775.697					0.8763
2731.394					0.8633
2687.091					0.8502
2642.788					0.8371
2598.485					0.8240
2554.182					0.8108
2509.880					0.7976
2465.577					0.7844
2421.274					0.7712
2376.971	- Psat	8.9070	0.8574	0.8619	0.7580
2140.743		7.9468	0.8507	0.8632	0.7063
1904.516		7.0162	0.8473	0.8663	0.6508
1668.288		6.1150	0.8476	0.8711	0.5911
1432.061		5.2425	0.8529	0.8776	0.5269
1195.833		4.3982	0.8647	0.8856	0.4576
959.606		3.5803	0.8868	0.8953	0.3827
723.378		2.7856	0.9269	0.9066	0.3015
487.151		2.0057	1.0051	0.9195	0.2132
250.923	@ Tres	1.2111	1.1979	0.9349	0.1166
14.695	@ Tstd	0.0973	1.2599	0.9885	0.0092

Figure A-28: Differential Liberation test report for well A#33 (Continued...)

Expt DL1 : Differential Liberation

Peng-Robinson (3-Parm) on ZI with PR corr.
Lohrenz-Bray-Clark Viscosity Correlation

Density units are	LB/FT3
Specific volume units are	CF/LB-ML
Viscosity units are	CPOISE
Surface Tension units are	DYNES/CM
Gas-Oil Ratio units are	MSCF/STB
Relative Volume units are	RB/STB
Gas FVF units are	RB/MSCF
Extracted Gas Volume units are	FT3
Oil Relative Volume units are	BBL/STB

Specified temperature Deg F 257.0000

Relative Oil Saturated Volume (Bo(Pbub)) 1.4580

GOR calc. is Gas Vol at STC/Stock Tank Oil Vol
Oil Rel Vol calc. is Stage Vol oil/Stock Tank Oil Vol

Pressure PSIA	Inserted Point	Surf Tension Calculated	Gas FVF Calculated	Liq Visc Calculated	Vap Visc Calculated
2820.000			1.1157	0.2664	
2775.697			1.1318	0.2645	
2731.394			1.1485	0.2626	
2687.091			1.1658	0.2607	
2642.788			1.1838	0.2588	
2598.485			1.2026	0.2569	
2554.182			1.2221	0.2550	
2509.880			1.2425	0.2531	
2465.577			1.2637	0.2512	
2421.274			1.2858	0.2493	
2376.971	- Psat	3.2875	1.3089	0.2474	0.0195
2140.743		4.0894	1.4556	0.2659	0.0184
1904.516		5.0180	1.6420	0.2862	0.0174
1668.288		6.0818	1.8848	0.3085	0.0166
1432.061		7.2886	2.2120	0.3331	0.0159
1195.833		8.6464	2.6734	0.3603	0.0152
959.606		10.1651	3.3679	0.3905	0.0147
723.378		11.8609	4.5241	0.4247	0.0142
487.151		13.7728	6.8137	0.4648	0.0136
250.923	@ Tres	16.0550	13.4489	0.5193	0.0128
14.695	@ Tstd	26.1461	176.0586	1.3113	0.0093

Pressure PSIA	Inserted Point	Moles Extrac Calculated	GasVol Extrc Calculated	Liquid Sat Calculated	Vapour Sat Calculated
2820.000				1.0000	
2775.697				1.0000	
2731.394				1.0000	
2687.091				1.0000	
2642.788				1.0000	
2598.485				1.0000	
2554.182				1.0000	
2509.880				1.0000	
2465.577				1.0000	
2421.274				1.0000	
2376.971	- Psat			1.0000	
2140.743		0.0608	50.9061	0.9266	0.0734
1904.516		0.1182	98.9108	0.9203	0.0797
1668.288		0.1726	144.3834	0.9117	0.0883
1432.061		0.2243	187.6703	0.9000	0.1000
1195.833		0.2739	229.1313	0.8833	0.1167
959.606		0.3218	269.2041	0.8582	0.1418
723.378		0.3688	308.5620	0.8169	0.1831
487.151		0.4167	348.6514	0.7383	0.2617
250.923	@ Tres	0.4719	394.8231	0.5440	0.4560
14.695	@ Tstd	0.5180	433.3435	0.0887	0.9113

Figure A-29: Differential Liberation test report for well A#33 (Continued...)

Expt DL1 : Differential Liberation

Peng-Robinson (3-Parm) on ZI with PR corr.
Lohrenz-Bray-Clark Viscosity Correlation

Density units are	LB/FT3	
Specific volume units are	CF/LB-ML	
Viscosity units are	CPOISE	
Surface Tension units are	DYNES/CM	
Gas-Oil Ratio units are	MSCF/STB	
Relative Volume units are	RB/STB	
Gas FVF units are	RB/MSCF	
Extracted Gas Volume units are	FT3	
Oil Relative Volume units are	BBL/STB	
Specified temperature	Deg F	257.0000
Relative Oil Saturated Volume (Bo(Pbub))		1.4580

GCR calc. is Gas Vol at STC/Stock Tank Oil Vol
Oil Rel Vol calc. is Stage Vol oil/Stock Tank Oil Vol

Pressure PSIA	Inserted Point	Liq Mol Wt Calculated	Vap Mol Wt Calculated	Liq Visc Calculated	Vap Visc Calculated
2820.000		100.1410		0.2664	
2775.697		100.1410		0.2645	
2731.394		100.1410		0.2626	
2687.091		100.1410		0.2607	
2642.788		100.1410		0.2588	
2598.485		100.1410		0.2569	
2554.182		100.1410		0.2550	
2509.880		100.1410		0.2531	
2465.577		100.1410		0.2512	
2421.274		100.1410		0.2493	
2376.971	- Psat	100.1410	24.8398	0.2474	0.0195
2140.743		105.0325	24.6455	0.2659	0.0184
1904.516		110.2701	24.5454	0.2862	0.0174
1668.288		115.9007	24.5562	0.3085	0.0166
1432.061		121.9838	24.7073	0.3331	0.0159
1195.833		128.5996	25.0514	0.3603	0.0152
959.606		135.8675	25.6916	0.3905	0.0147
723.378		143.9931	26.8510	0.4247	0.0142
487.151		153.4312	29.1174	0.4648	0.0136
250.923	@ Tres	165.8399	34.7017	0.5193	0.0128
14.695	@ Tstd	178.1948	36.5003	1.3113	0.0093

Pressure PSIA	Inserted Point	Liq Mol Vol Calculated	Vap Mol Vol Calculated
2820.000		2.4256	
2775.697		2.4282	
2731.394		2.4307	
2687.091		2.4333	
2642.788		2.4360	
2598.485		2.4387	
2554.182		2.4414	
2509.880		2.4441	
2465.577		2.4469	
2421.274		2.4497	
2376.971	- Psat	2.4526	2.7888
2140.743		2.5374	3.1013
1904.516		2.6279	3.4984
1668.288		2.7250	4.0158
1432.061		2.8296	4.7128
1195.833		2.9430	5.6959
959.606		3.0672	7.1757
723.378		3.2056	9.6391
487.151		3.3654	14.5172
250.923	@ Tres	3.5729	28.6542
14.695	@ Tstd	3.4898	375.1109

Figure A-30: Differential Liberation test report for well A#33.

Appendix B

The PVTpro Simulator

Bottom-hole fluid samples from wells A#22 and A#33 were collected and analyzed by the Commercial Service Provider. Provided surface fluid samples were flashed and recombined at reservoir conditions. A final mole GOR of 1.0716 (Gas : Oil = 51.73 : 48.27) for well A#22 and 1.14 (Gas : Oil = 53.27 : 46.73) for well A#33 were obtained using the PVTpro simulator [2] as shown in Figures B.1 and B.2, respectively.

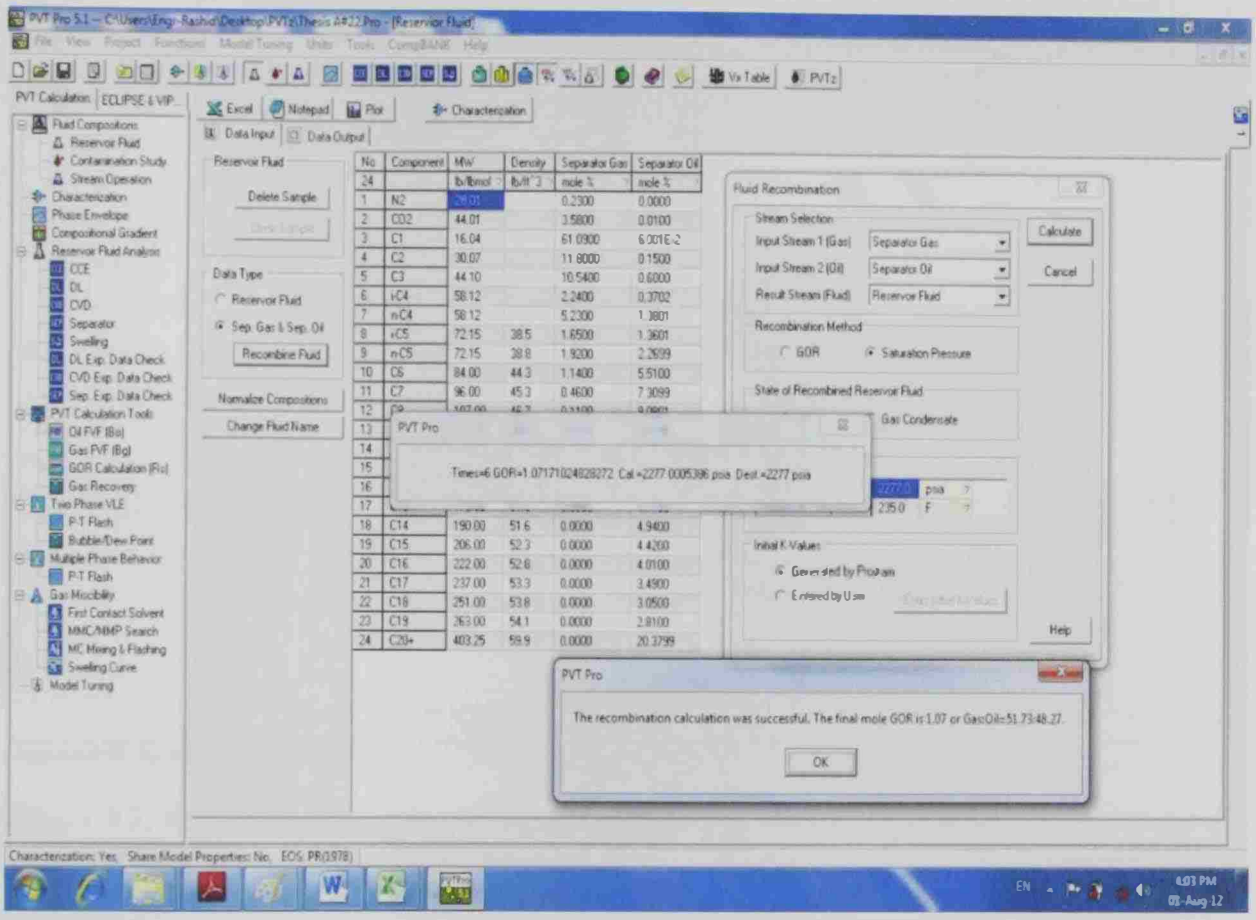

Figure B.1: Recombination calculation and final mole GOR for well A#22

The PVTpro simulator also generates the well stream compositions which consist of 24 components with C_{20}+ as the characterized component.

Tables B.1 and B.2 show the well stream fluid composition for well A#22 and A#33, respectively. For generation of the fluid thermodynamic and equilibrium properties (fluid model) an equation of state was used.

In this work the fluid model was generated using a 3-parameter Peng-Robinson Equation of State (PR EOS). The volume-shift parameters were calculated using temperature-dependent correlations.

The liquid and vapor viscosities were predicted using the Lohrenz-Bray-Clark (LBC) correlation. The binary interaction coefficients (k_{ij}) were regressed to obtain a good match between experimental and calculated data.

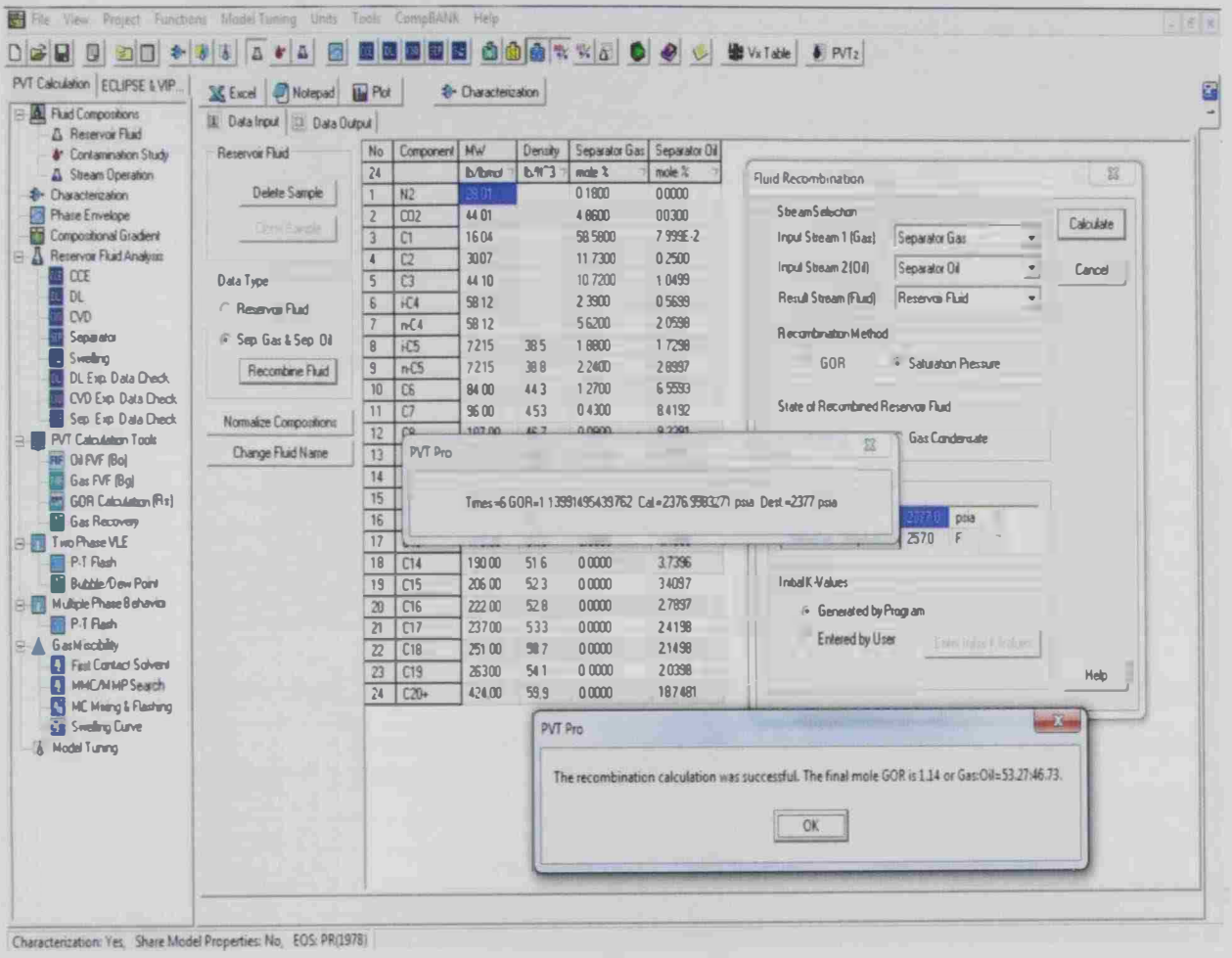

Figure B.2: Recombination calculation and final mole GOR for well A#33

The Oilphase-DBR module of the PVTpro simulator was used to generate the phase envelop of the reservoir fluids (Figures B.3 and for wells A#22 and A#33, respectively). These are *P-T* plots with gas fraction as a parameter. The bubble and dew point curves are shown at gas fractions of 0.0 and 1.0, respectively.

Table B.1: Reservoir fluid vs. stream compositions of the recombined fluid for well A#22.

Component	MW, g/mol	Reservoir Fluid, mole %	Separator Gas, mole %	Separator Oil, mole %	Recombined Fluid, mole %
N_2	28.014	0.1200	0.23	0	0.1190
CO_2	44.01	1.8597	3.58	0.01	1.8568
C1	16.043	31.687	61.09	6.00E-02	31.6313
C2	30.07	6.1895	11.8	0.15	6.1766
C3	44.096	5.7495	10.54	0.6	5.742
i-C4	58.123	1.3398	2.24	0.3702	1.3375
n-C4	58.123	3.3797	5.23	1.3801	3.3717
i-C5	72.15	1.5098	1.65	1.3601	1.5101
n-C5	72.15	2.0898	1.92	2.2699	2.0889
C6	84	3.2496	1.14	5.51	3.2494
C7	96	3.7596	0.46	7.3099	3.7664
C8	107	3.9496	0.11	8.0801	3.9571
C9	121	3.5796	0.01	7.4199	3.5867
C10	134	3.3497	0	6.9599	3.3595
C11	147	2.7597	0	5.73	2.7658
C12	161	2.3698	0	4.92	2.3748
C13	175	2.2998	0	4.77	2.3024
C14	190	2.3798	0	4.94	2.3845
C15	206	2.1298	0	4.42	2.1335
C16	222	1.9298	0	4.01	1.9356
C17	237	1.6798	0	3.49	1.6846
C18	251	1.4699	0	3.05	1.4722
C19	263	1.3499	0	2.81	1.3564
C20+	403.25	9.8190	0	20.3799	9.8372

Table B.2: Reservoir fluid vs. stream compositions of the recombined fluid for well A#33.

Component	MW, g/mol	Reservoir Fluid, mole %	Separator Gas, mole %	Separator Oil, mole %	Recombined Fluid, mole %
N_2	28.014	0.09940	0.18	0	0.0959
CO_2	44.01	2.6984	4.86	0.0300	2.6030
C1	16.043	32.3987	58.58	0.0800	31.2441
C2	30.07	6.5922	11.73	0.25	6.3656
C3	44.096	6.3922	10.72	1.0499	6.2014
i-C4	58.123	1.5754	2.39	0.5699	1.5395
n-C4	58.123	4.0267	5.62	2.0598	3.9563
i-C5	72.15	1.8128	1.88	1.7298	1.8098
n-C5	72.15	2.5352	2.24	2.8997	2.5483
C6	84	3.6372	1.27	6.5593	3.7416
C7	96	4.0055	0.43	8.4192	4.1632
C8	107	4.2249	0.09	9.3291	4.4072
C9	121	3.8048	0.01	8.4892	3.9722
C10	134	3.4055	0	7.6092	3.5556
C11	147	2.7432	0	6.1294	2.8641
C12	161	2.2375	0	4.9995	2.3361
C13	175	2.0137	0	4.4996	2.1025
C14	190	1.6736	0	3.7396	1.7474
C15	206	1.526	0	3.4097	1.5933
C16	222	1.2485	0	2.7897	1.3036
C17	237	1.0829	0	2.4198	1.1307
C18	251	0.9621	0	2.1498	1.0046
C19	263	0.9129	0	2.0398	0.9532
C20+	424	8.3906	0	18.7481	8.7606

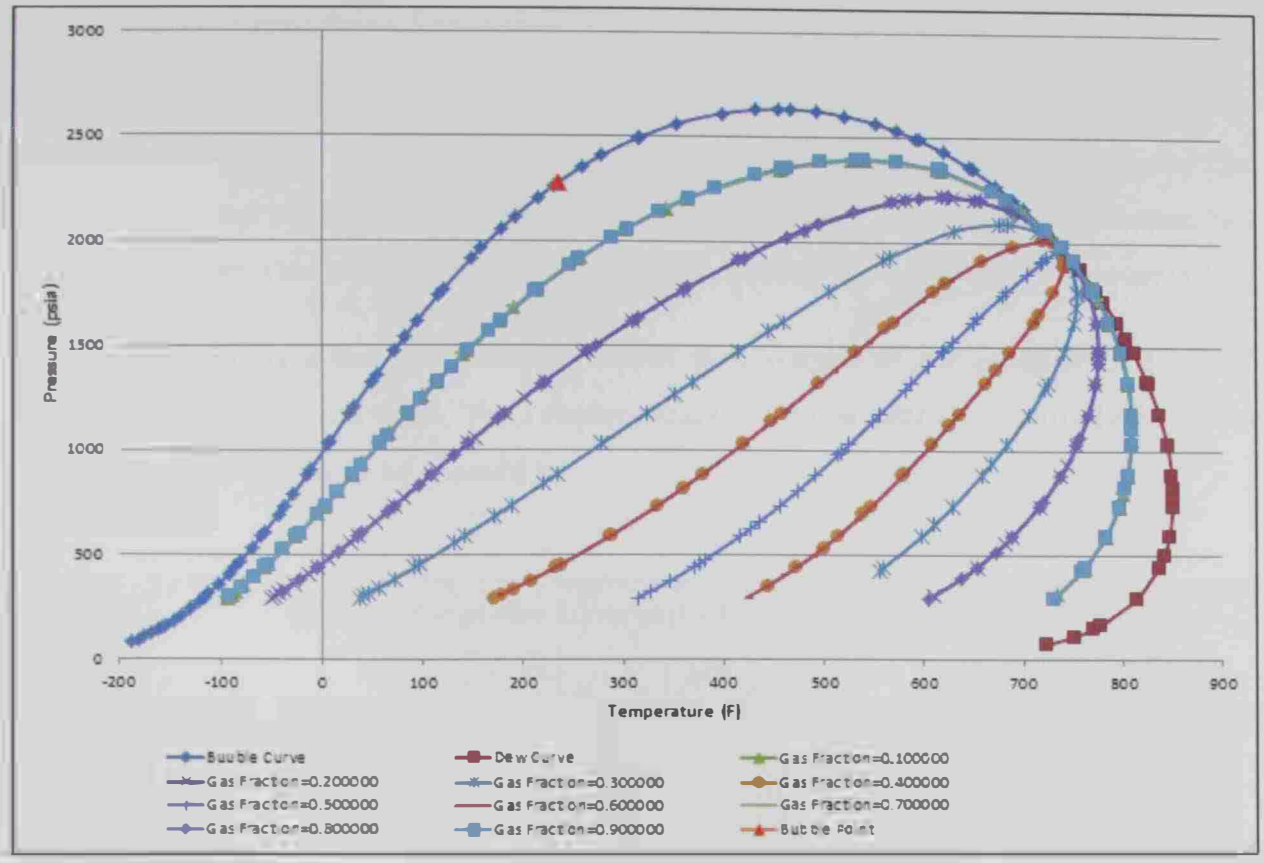

Figure B.3 The *P-T* phase envelope for well A#22

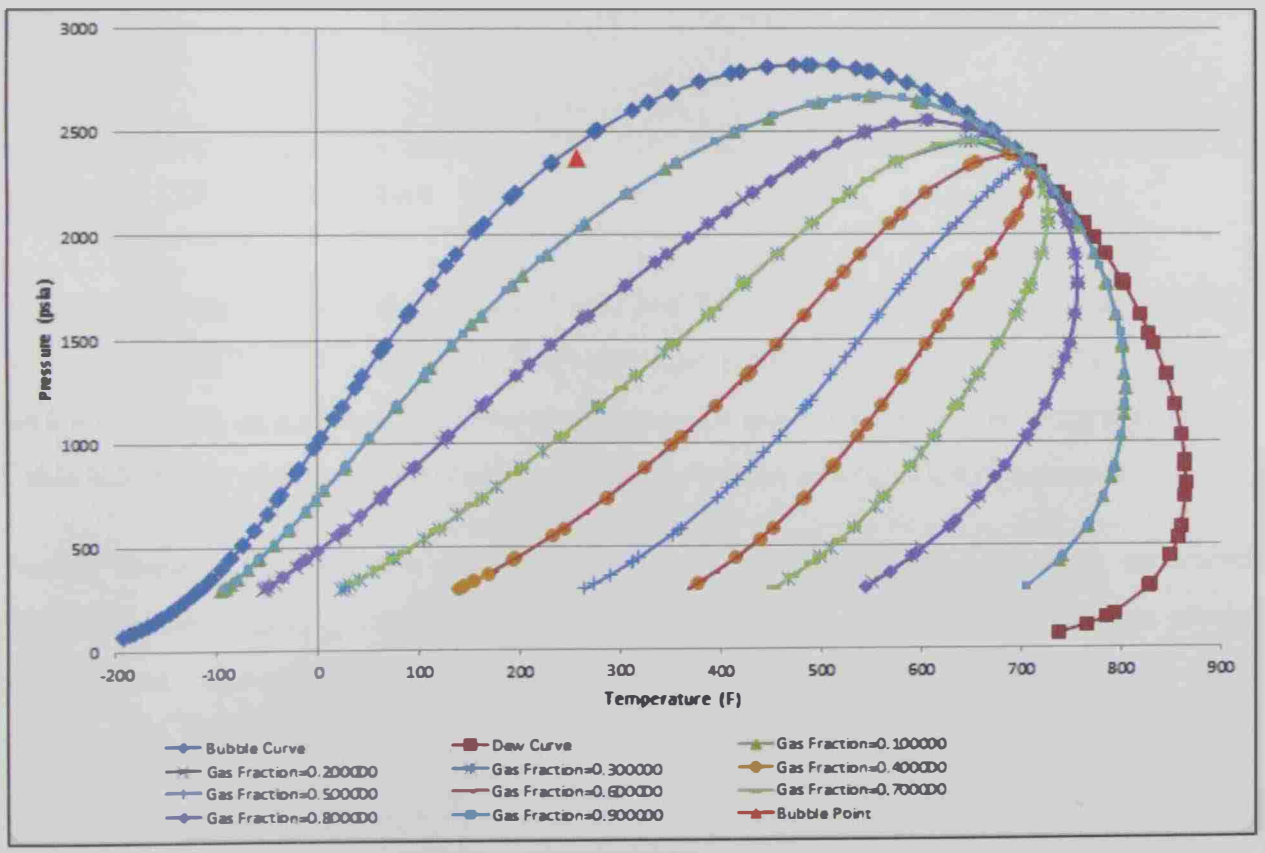

Figure B.4 The *P-T* phase envelope for well A#33

The Constant Composition Expansion (CCE) Test

The main aim of the CCE is test (Figure B.5) is to determine the initial fluid saturation pressure. The fluid is initially held in a cell in a single phase. At pressures above the saturation pressure only the single-phase volume is measured. The pressure reduction has to be made in several steps and at each step the liquid and vapor volumes are measured.

The relative volume is calculated as the ratio of fluid volume at any pressure to the fluid volume at saturation pressure. The relative volume is then plotted against pressure to yield the volume-pressure relationship.

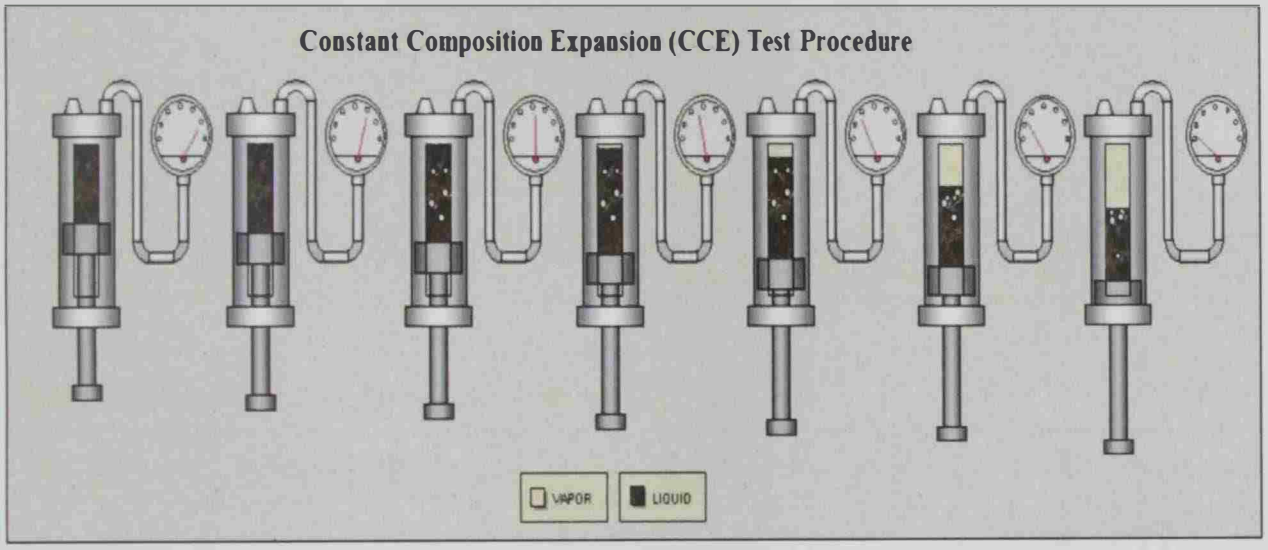

Figure B.5: CCE Test Procedure

The CCE test was performed at P = 2277 psia and T = 235 °F for well A#22 and at P = 2377 psia and T = 257 °F for well A#33. The calculated properties are shown in Table B.3 for well A#22 fluid, as an example. Several plots can be generated from the results shown in Table B.3 for the various properties of the reservoir fluid as a function of pressure.

Among these properties are: relative total liquid volume (V_{liq}/V_{tot}), relative saturated liquid volume (V_{liq}/V_{sat}), relative volume (V_{rel}), liquid density, liquid viscosity, gas molar weight, gas specific gravity, gas viscosity, Z-factor, Y-function, compressibility, bulk density, IFT, and gas density.

Table B.3: Results of the CCE test for well A#22 fluid

Pressure	Total Liq. Vol. %	Sat. Liq. Vol. %	Rel. Vol.	Liq. Density	Liq. Viscosity	Gas MW	Gas Specific Gravity	Gas Viscosity	Z-Factor	Y Function	Compressibility	Bulk Density	Interfacial Tension, IFT	Gas Density
Psia	V_{liq}/V_{tot}	V_{liq}/V_{sat}	V_{tot}/V_{sat}	g/cm³	cP	g/mol	Air=1	cP	*PV/RT*		10/psia	g/cm³	dyne/cm	g/cm³
6515	100	95.1	0.95	746.01	0.528						8.44E-06	746.007		
5975	100	95.6	0.96	742.49	0.510						9.06E-06	742.492		
5396	100	96.1	0.96	738.45	0.490						9.83E-06	738.448		
4687	100	96.8	0.97	733.04	0.465						1.09E-05	733.043		
4341	100	97.2	0.97	730.20	0.453						1.15E-05	730.200		
3833	100	97.8	0.98	725.74	0.435						1.26E-05	725.744		
3369	100	98.4	0.98	721.34	0.418						1.37E-05	721.342		
2922	100	99.0	0.99	716.76	0.402						1.49E-05	716.757		
2481	100	100	1.00	711.85	0.386						1.63E-05	711.851		
2277	100	100	1.00	709.44	0.378	23.04	0.7952	0.0195	0.8685		1.70E-05	709.435	0.005	129.757
2255	99.4	99.8	1.00	710.23	0.380	23.02	0.0194	0.0194	0.8686	2.554		706.733	0.005	128.388
2224	98.5	99.5	1.01	711.36	0.383	22.99	0.0193	0.0193	0.8688	2.542		702.844	0.005	126.465
2167	97.0	98.9	1.02	713.42	0.389	22.95	0.0191	0.0191	0.8692	2.519		695.419	0.005	122.948
2071	94.2	98.0	1.04	716.90	0.399	22.89	0.0187	0.0187	0.8702	2.481		682.085	0.005	117.074
1910	89.4	96.5	1.08	722.74	0.417	22.82	0.0181	0.0181	0.8725	2.417		657.185	0.006	107.358
1688	82.1	94.4	1.15	730.85	0.444	22.79	0.0173	0.0173	0.8771	2.328		616.970	0.007	94.233
1386	71.0	91.7	1.29	742.07	0.485	22.88	0.0164	0.0164	0.8862	2.206		549.361	0.008	76.866
1041	56.2	88.6	1.58	755.46	0.546	23.23	0.0156	0.0156	0.9009	2.061		450.138	0.010	57.677
728	40.6	85.6	2.11	768.72	0.589	23.96	0.0148	0.0148	0.9186	1.917		336.264	0.012	40.794
265	14.1	79.4	5.65	794.81	0.709	27.16	0.0137	0.0137	0.9560	1.633		125.582	0.016	16.176
100	4.62	74.2	16.2	812.84	0.837	31.48	0.0130	0.0130	0.9763	1.445		44.156	0.018	6.927
60	2.54	71.4	28.1	821.23	0.917	34.22	0.0127	0.0127	0.9829	1.364		25.252	0.018	4.488
14.7	0.47	62.5	132.1	844.17	1.236	43.51	0.0120	0.0120	0.9931	1.174		5.3692	0.020	1.384

Table B.4 Results of the CCE test for well A#33 fluid

Pressure	Total Liq. Vol. %	Sat. Liq. Vol. %	Rel. Vol.	Liq. Density	Liq. Viscosity	Gas MW	Gas Specific Gravity	Gas Viscosity	Z-Factor	Y Function	Compressibility	Bulk Density	Interfacial Tension, IFT	Gas Density
psia	V_{liq}/V_{tot}	V_{liq}/V_{sat}	V_{tot}/V_{sat}	g/cm³	cP	g/mol	Air=1	cP	*PV/RT*		1/Psia	g/cm³	dyne/cm	g/cm³
6515	100	94.3	0.94	727.20	0.443						9.90E-06	727.196		
5515	100	95.3	0.95	719.50	0.414						1.14E-05	719.501		
4515	100	96.5	0.97	710.63	0.385						1.35E-05	710.632		
3515	100	97.9	0.98	700.22	0.355						1.62E-05	700.218		
2820	100	99.1	0.99	691.78	0.333						1.88E-05	691.781		
2515	100	99.7	1.00	687.69	0.323						2.02E-05	687.685		
2415	100	99.9	1.00	686.28	0.32						2.07E-05	686.284		
2386	100	100	1.00	685.87	0.319						2.08E-05	685.870		
2377	100	100	1.00	685.74	0.319	25.36	0.8755	0.0209	0.8592		2.09E-05	685.742	0.004	146.122
2372	99.9	99.9	1.00	685.94	0.319	25.35	0.0209	0.0209	0.8592	2.441		685.153	0.004	145.771
2370	99.8	99.9	1.00	686.02	0.319	25.35	0.0209	0.0209	0.8592	2.441		684.916	0.004	145.631
2359	99.5	99.8	1.00	686.44	0.32	25.34	0.0208	0.0208	0.8593	2.436		683.604	0.004	144.859
2346	99.1	99.6	1.01	686.95	0.322	25.32	0.0208	0.0208	0.8594	2.431		682.037	0.004	143.949
2323	98.4	99.4	1.01	687.84	0.324	25.29	0.0207	0.0207	0.8595	2.422		679.226	0.004	142.345
2277	97.1	98.8	1.02	689.63	0.328	25.23	0.0204	0.0204	0.8599	2.404		673.443	0.004	139.155
2100	91.7	96.9	1.06	696.48	0.344	25.05	0.0196	0.0196	0.8619	2.336		649.090	0.004	127.122
2039	89.8	96.2	1.07	698.84	0.349	25.00	0.0193	0.0193	0.8628	2.312		639.873	0.005	123.057
1400	67.1	89.7	1.34	723.92	0.419	24.93	0.0170	0.0170	0.8795	2.066		512.618	0.007	82.666
793	39.7	83.4	2.10	750.29	0.518	26.01	0.0153	0.0153	0.9089	1.812		326.219	0.011	47.271
265	11.9	75.1	6.32	783.73	0.639	30.21	0.0139	0.0139	0.9513	1.499		108.546	0.015	17.525
100	3.70	68.3	18.43	806.62	0.776	35.58	0.0131	0.0131	0.9728	1.306		37.200	0.017	7.617
60	1.98	64.4	32.60	818.05	0.872	38.97	0.0128	0.0128	0.9801	1.222		21.035	0.018	4.969
14.7	0.34	52.6	156.0	850.72	1.344	49.64	0.0119	0.0119	0.9919	1.037		4.394	0.020	1.532

Total Liquid Volume, (V_{liq}/V_{tot}) %

Figure B.6 shows the ratio between liquid volume (at P and T_{res}) to the fluid (i.e., liquid ad gas) total volume (at P and T_{res}) presented as (V_{liq}/V_{tot}) % vs. pressure. The liquid volume remains almost constant at pressures well above the bubble pressure (P_b) due to the presence of a single liquid phase (incompressible) until the pressure reaches P_b where the gas starts to escape from the liquid causing a reduction in the liquid volume as the pressure goes below P_b.

Saturated Liquid Volume, (V_{liq}/V_{sat}) %

Figure B.7 shows the ratio between liquid volume (at P and T_{res}) to saturated liquid volume (at P_b and T_{res}) presented as (V_{liq}/V_{sat}) % vs. pressure. At pressures above the bubble point, the liquid volume increases as pressure decreases due to liquid expansion until the pressure reaches the bubble point where the gas starts to escape from the liquid causing reduction in liquid volume as the pressure goes down below the bubble point.

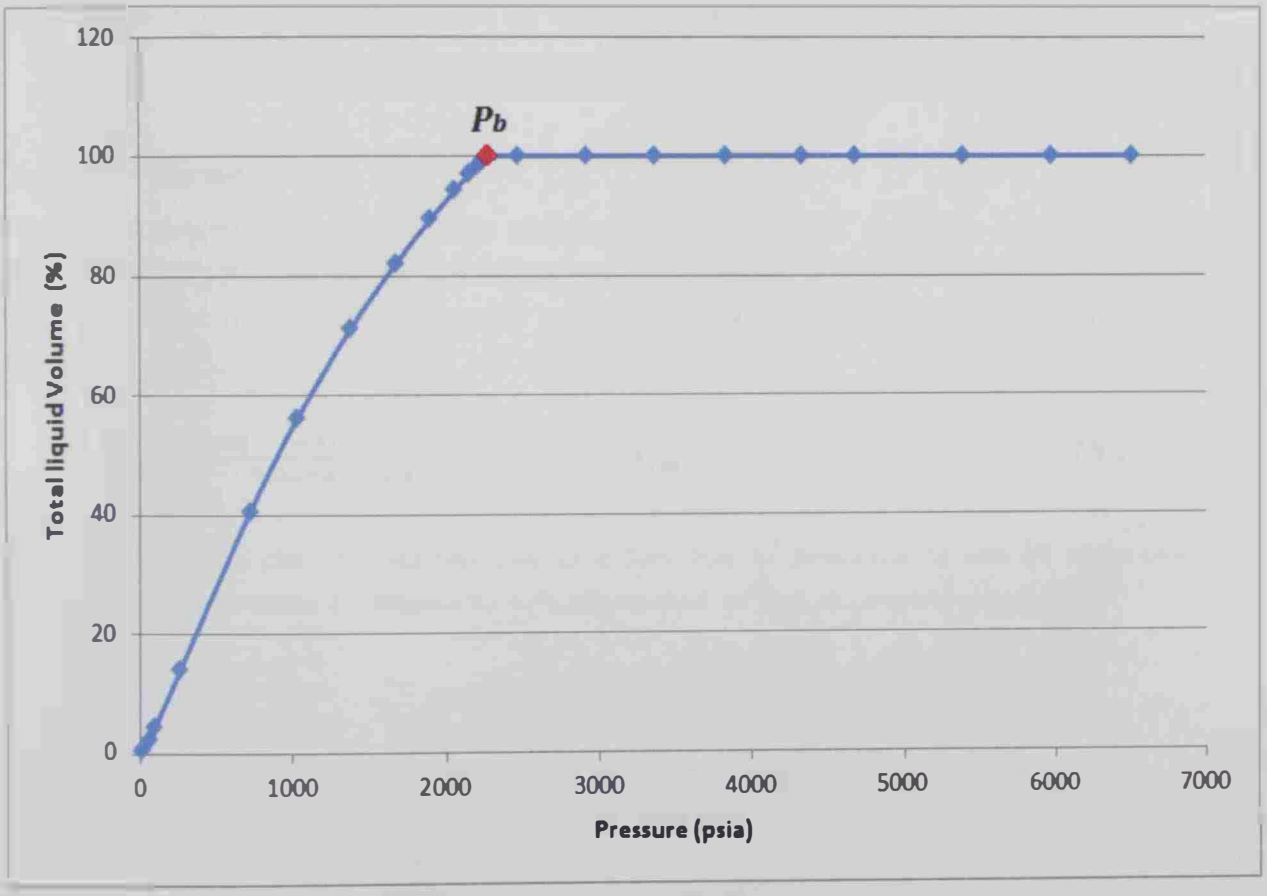

Figure B.6: (V_{liq}/V_{tot}) % vs. pressure for well A#22 at 235 °F (from the CCE test).

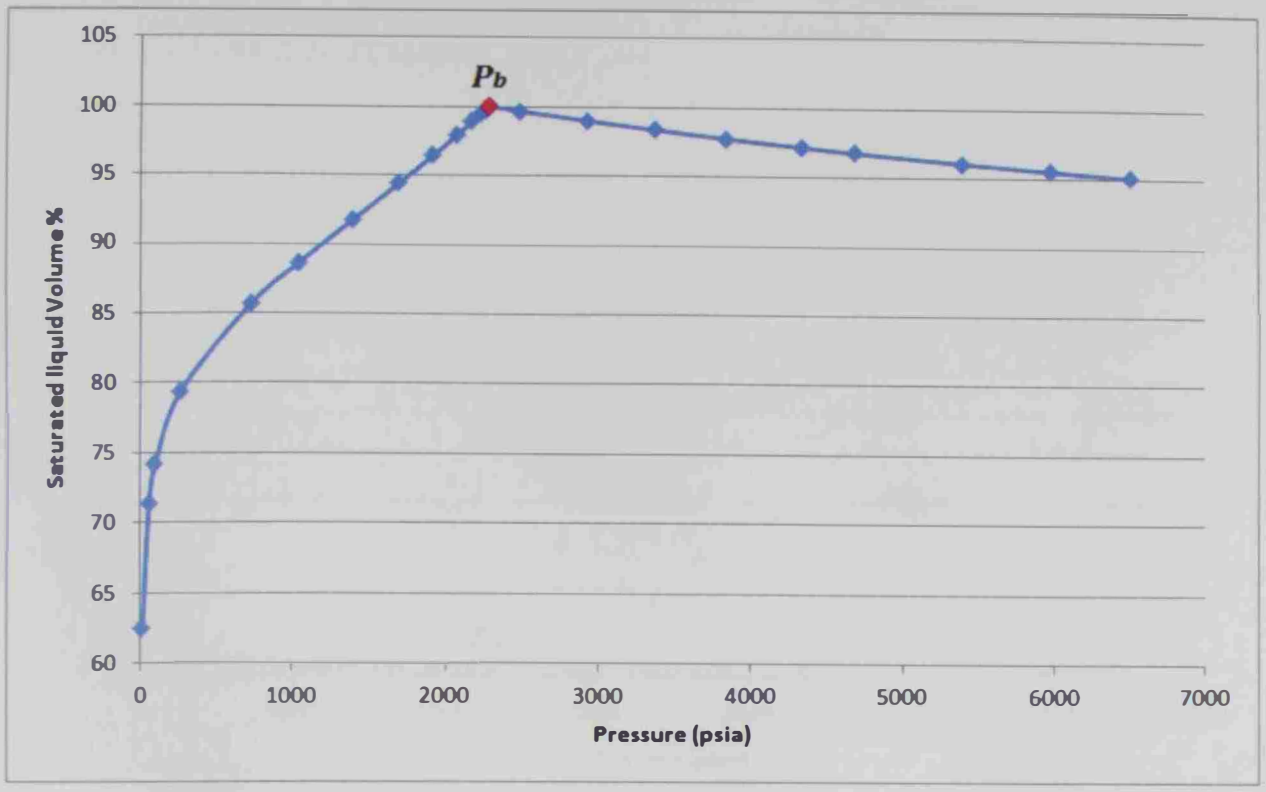

Figure B.7: (V_{liq}/V_{sat}) % vs. pressure for well A#22 at 235 °F (from the CCE test).

Relative Volume, (V_{rel}):

The volume-pressure relationship obtained from the CCE test can be studied at the reservoir temperature, or at any other specified temperature, starting from a pressure well above the initial static reservoir pressure, P_i, down to a relative volume (V_{rel}) of at least 2:

$$V_{rel} = \frac{\text{Total volume @ given } P \text{ \& } T_{res}}{\text{Volume @ } P_b \text{ \& } T_{res}} = V_{tot}/V_{sat} \qquad \text{(B.1)}$$

Figure B.8 shows the relative volume as a function of pressure. It can be seen that V_{rel} substantially increases at pressures < P_b, compared to that at pressures > P_b.

Liquid Density

Figure B.9 shows that the liquid density slowly decreases as the pressure is decreased until it reaches P_b (slow expansion of a compressed liquid) then starts to increase sharply as the pressure falls below P_b down to near atmospheric pressure (where the light fraction escapes from the liquid phase mixture leaving the heavy fraction behind).

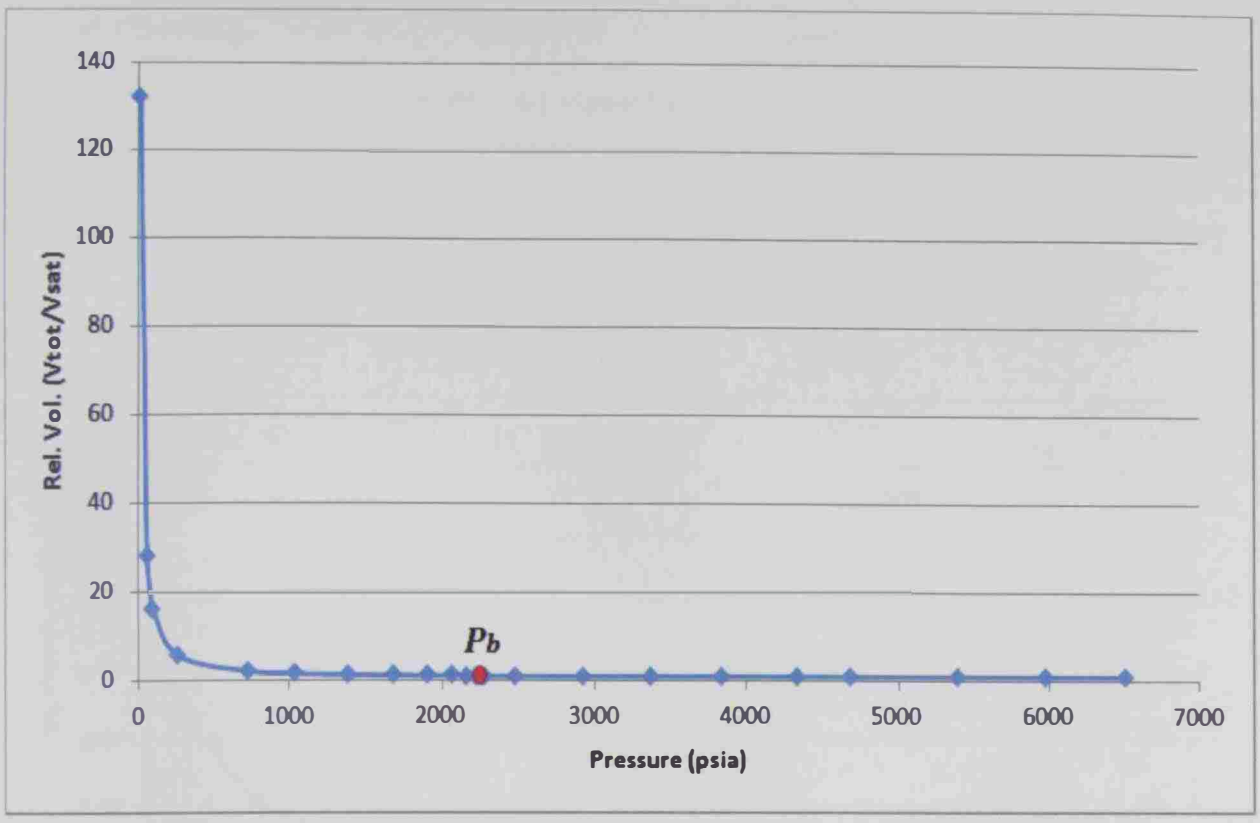

Figure B.8: Relative volume vs. pressure for well A#22 at 235 °F (from the CCE test).

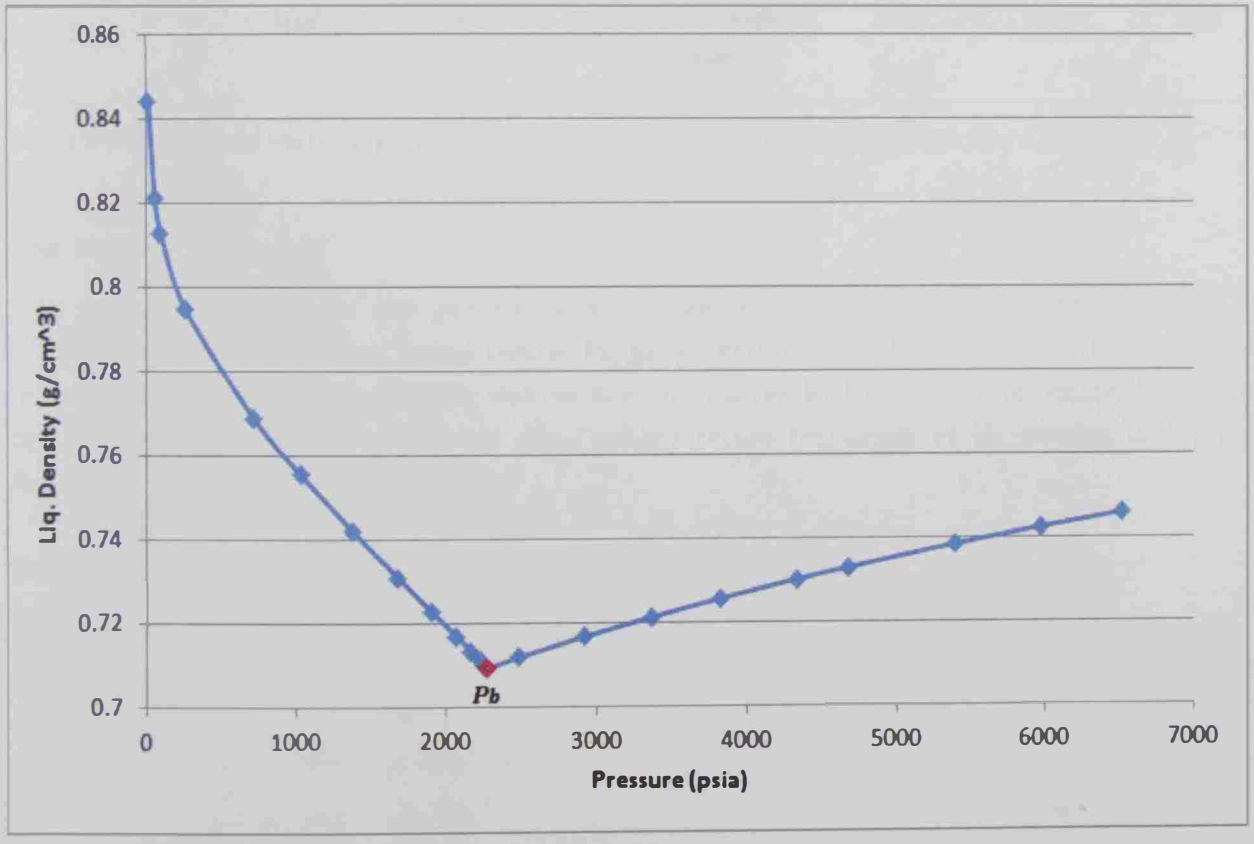

Figure B.9: Liquid density vs. pressure for well A#22 at 235 °F (from the CCE test).

Liquid Viscosity

Figure B.10 shows that the liquid (oil) viscosity decreases with the decrease of pressure from P to P_b (due to the slight decrease in the density of the liquid) while the oil viscosity starts to increase sharply when the pressure falls below P_b down to atmospheric (due to the release of light fractions with lower viscosities (and densities) from the liquid phase).

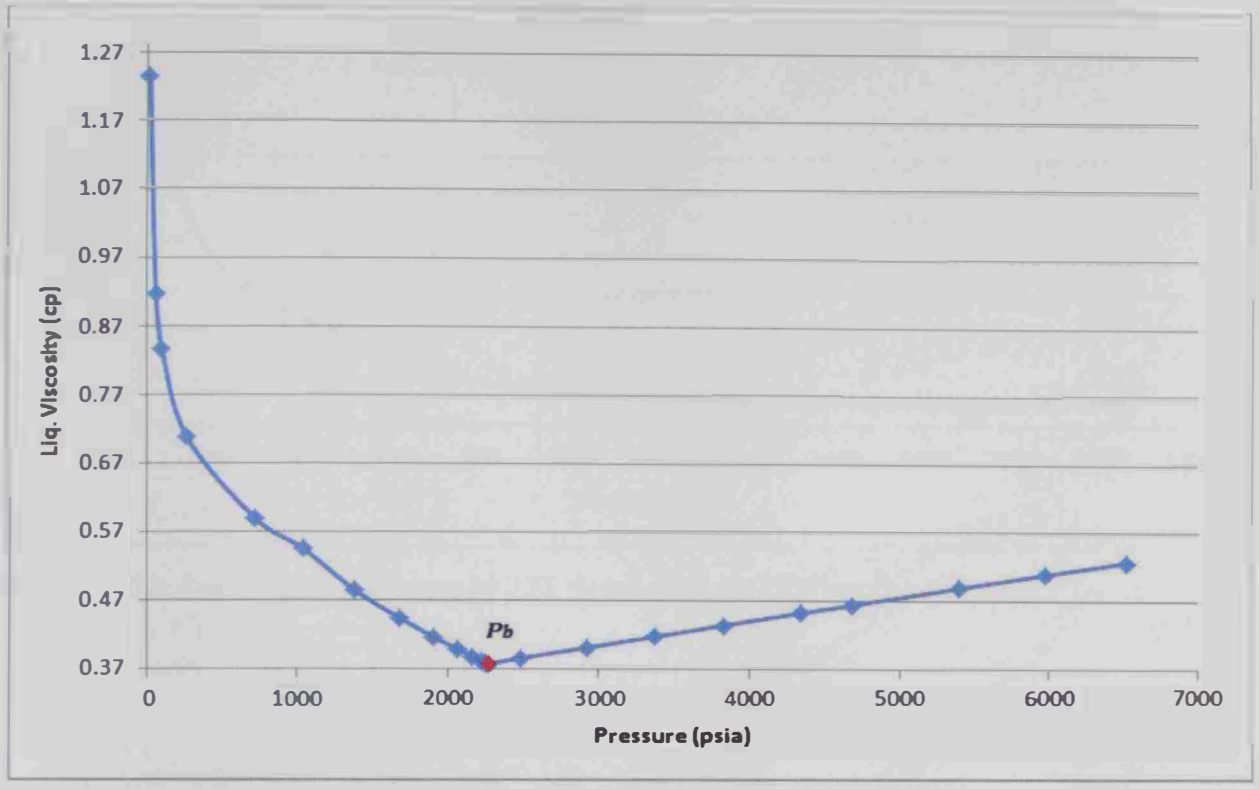

Figure B.10: liquid viscosity vs. pressure at 235 °F for well A#22 from the CCE test.

Gas Molecular Weight

The molecular weight of the gas mixture is inversely proportional to pressure ($MW = RT/PV$). As pressure is decreased below P_b, gases and light hydrocarbons start to escape from the liquid phase followed by conversion of heavier hydrocarbons to vapor. Thus the molecular weight of the generated gas (vapor) phase increases as illustrated in Figure B.11.

Gas specific gravity

The specific gravity of the gas is defined as the ratio between the density of the actual gas and the density of air at standard conditions. At a given temperature (here 235 °F for well A#22), the density (and the gas specific gravity) of the gas decreases as pressure is decreased from P_b down to near atmospheric pressure. Such behavior is illustrated in Figure B.12.

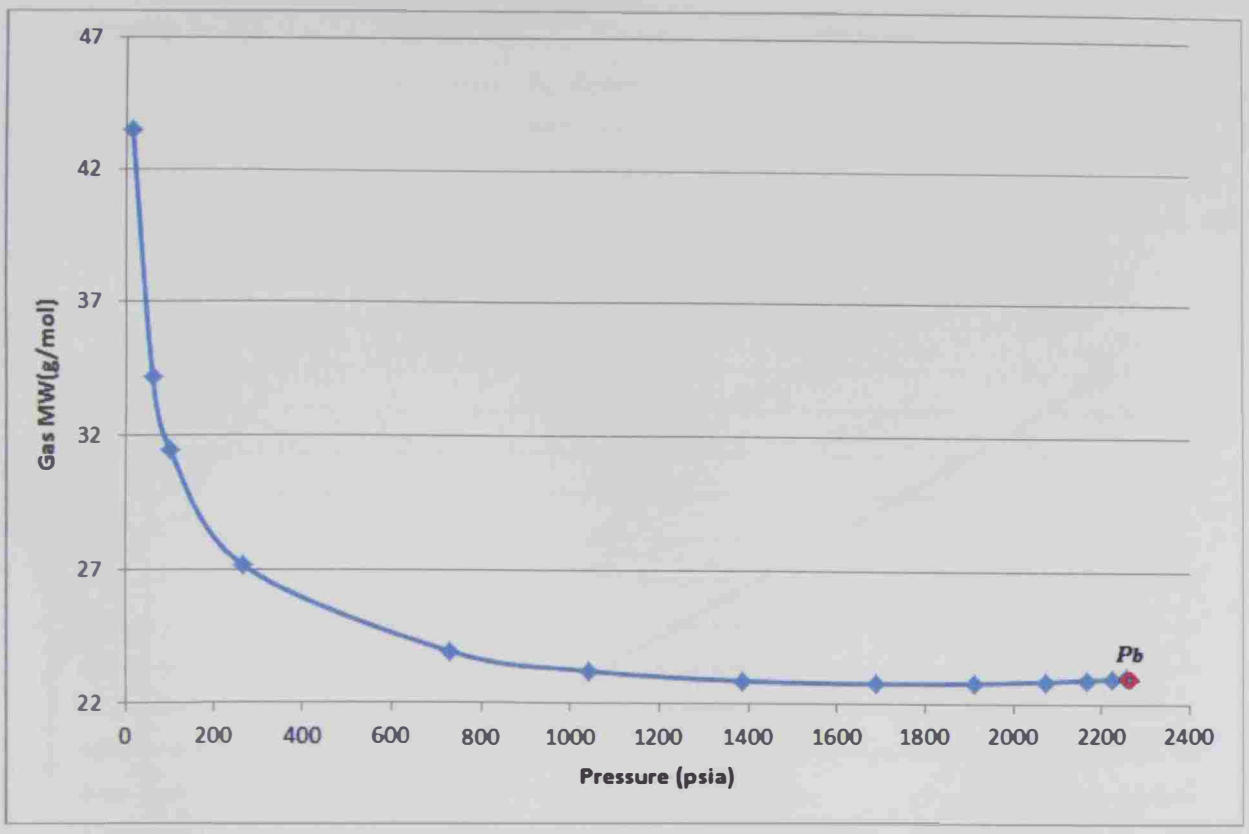

Figure B.11: Gas MW vs. pressure at 235 °F for well A#22 from the CCE test.

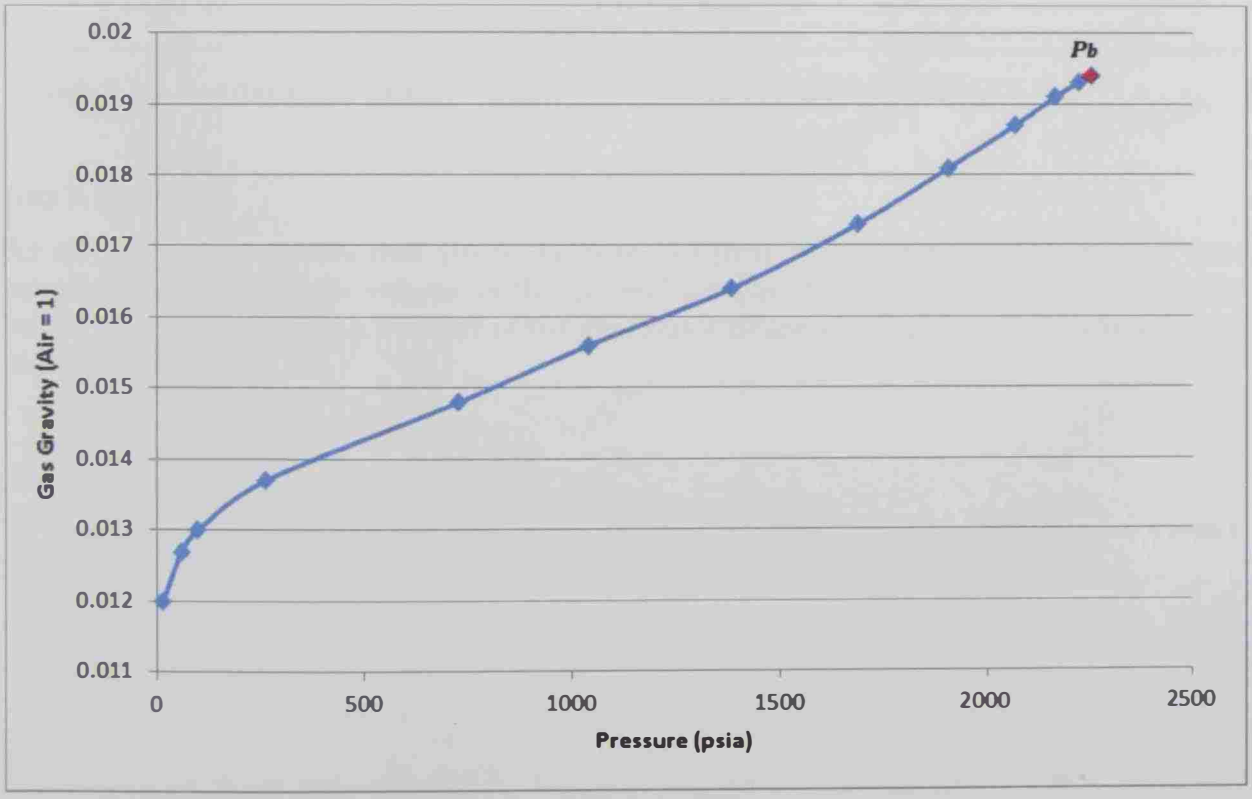

Figure B.12: Gas specific gravity vs. pressure at T= 235 °F from the CCE test for well A#22.

Gas Density

As the pressure is decreased from P_b down to near atmospheric pressure (at a fixed temperature), more gas/vapor is generated from the liquid phase mixture, the actual specific volume of the gas ($v = V/m$) will increase, and the resulting density of the gas ($\rho = 1/v = P/RT$) will decrease. Figure B.13 shows the resulting gas density vs. pressure. For well A#22.

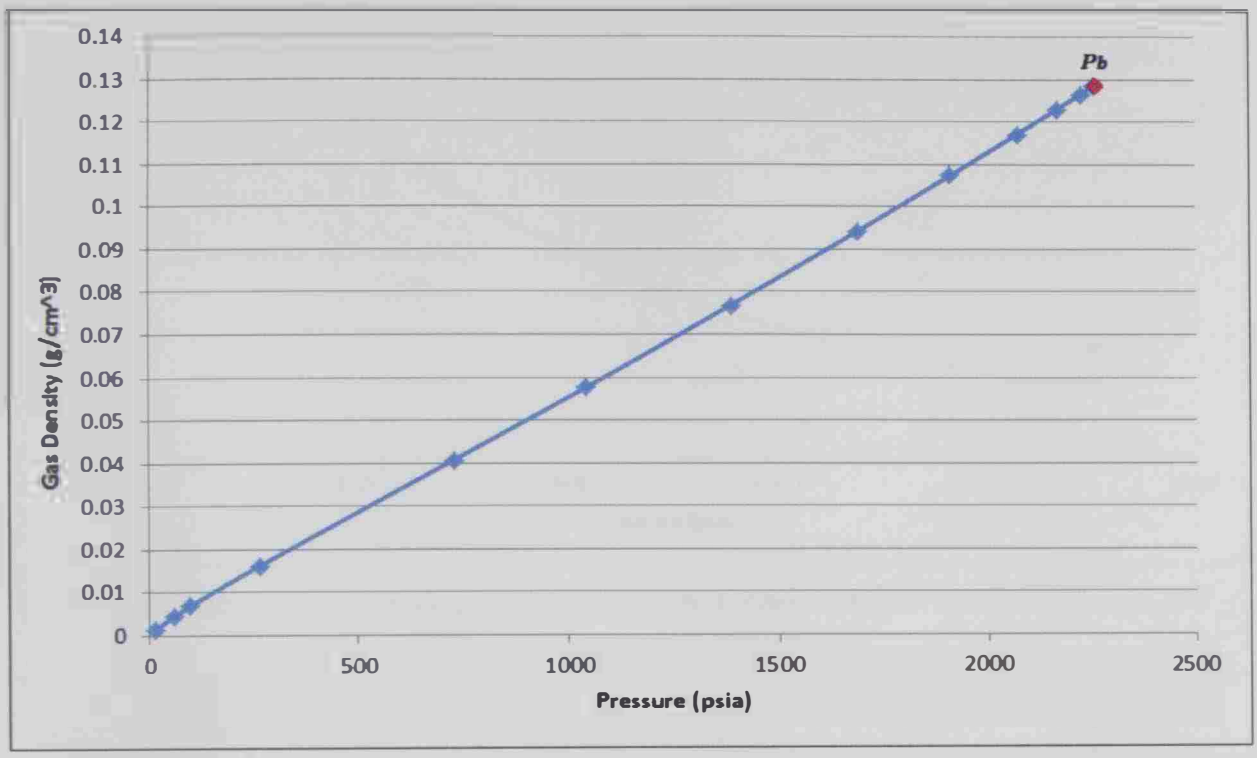

Figure B.13: Gas density vs. pressure at 235 °F for well A#22 from the CCE test.

Gas Z-factor

As the pressure is decreased (from P_b down to near atmospheric pressure at a fixed temperature) the specific volume of the gas will increase (as indicated above) and the net result is an increase in the Z-factor of the gas/vapor phase ($Z = P\,v/RT$) as shown in Figure B.14.

The Y-function

The value of the Y-function, defined by Eq. (B.2), is made to smoothen the relative volume data below the saturation pressure:

$$Y - \text{Function} = \frac{\left(\frac{P_b}{P} - 1\right)}{\left(\frac{V}{V_b} - 1\right)} \qquad \text{(B.2)}$$

When plotted, the Y-function usually forms a straight line or has only a small curvature. Figure B.15 illustrates the erratic behavior of the well A#22 data near the bubble-point

pressure down to near atmospheric pressure; as the pressure is decreased the Y-function will decrease as well.

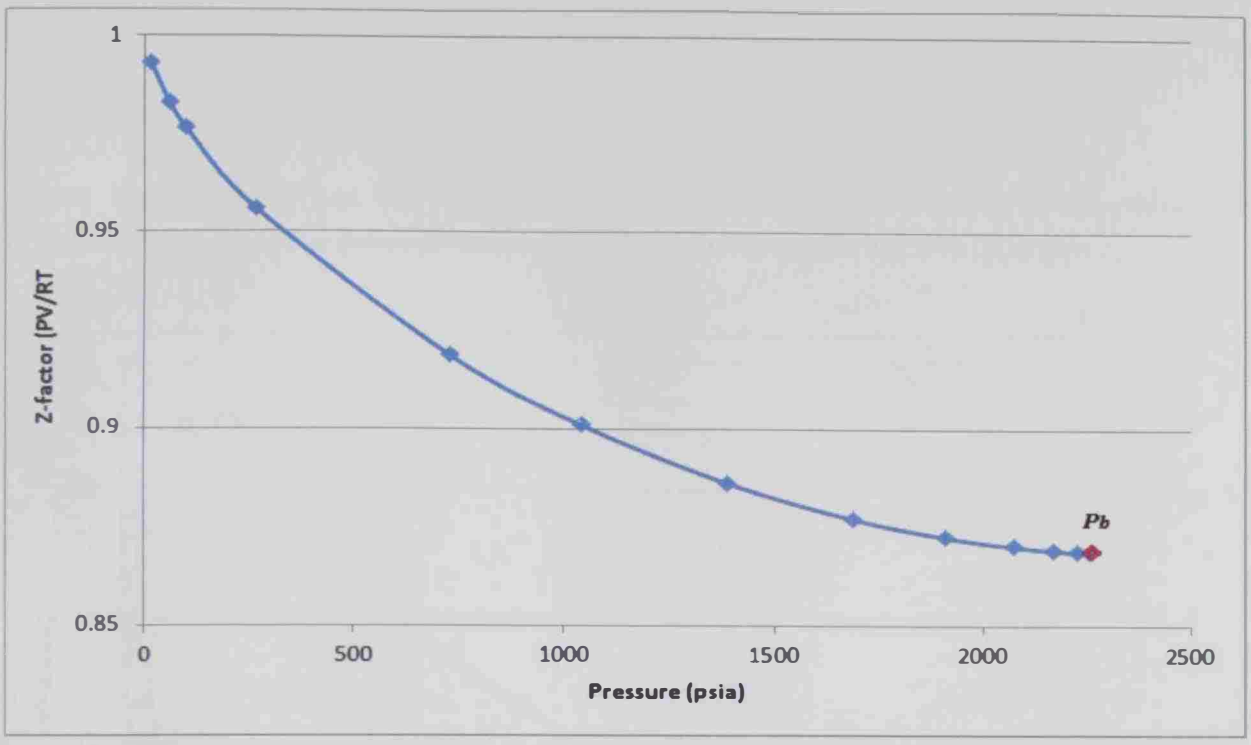

Figure B.14: The gas Z-factor vs. pressure at 235 °F for well A#22 from the CCE test.

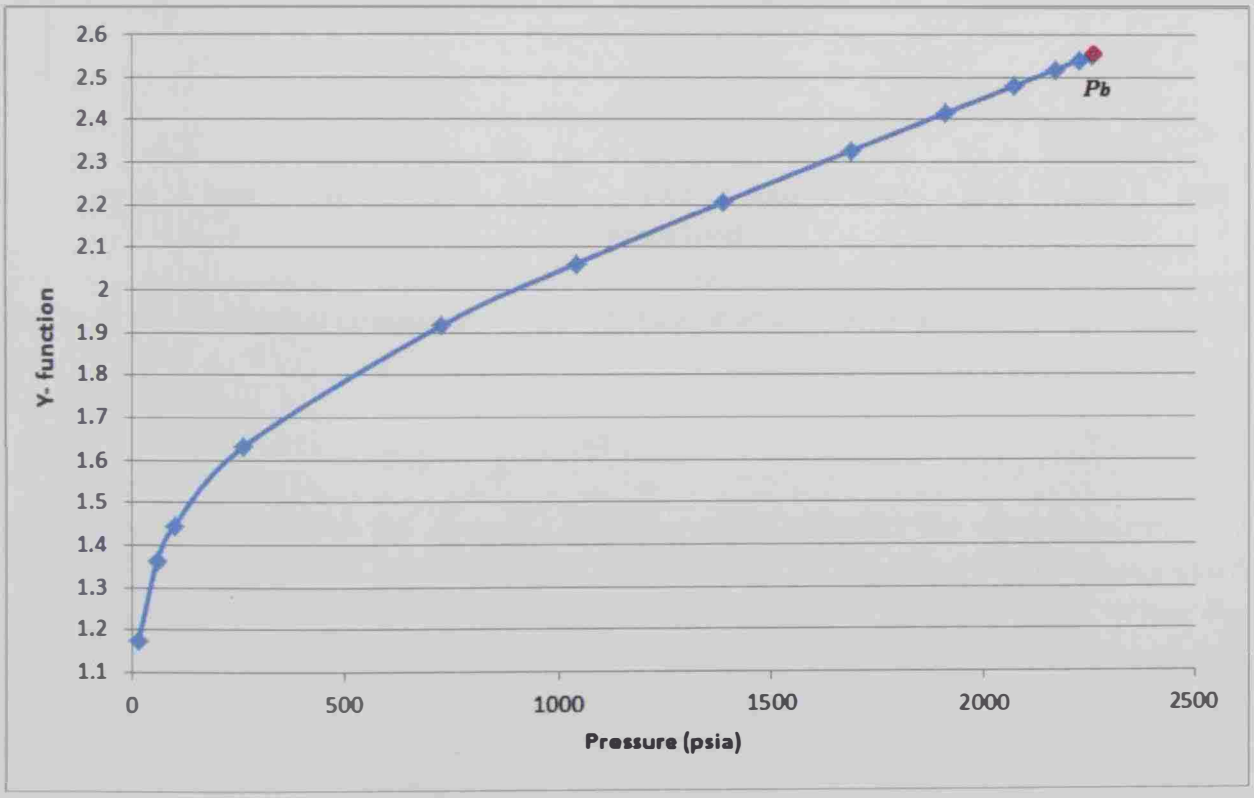

Figure B.15: The Y-function vs. pressure at 235 °F for well A#22 from the CCE test.

Isothermal compressibility of Liquid Phase

The liquid phase isothermal compressibility, defined by Eq. (B.3), is applicable only at pressures above the bubble point pressure, P_b:

$$C_o = \frac{1}{V_{rel}} \frac{\partial V_{rel}}{\partial P} \tag{B.3}$$

Figure B.16 shows that the isothermal compressibility is inversely proportional to pressure; as pressure is decreased the isothermal compressibility will increase.

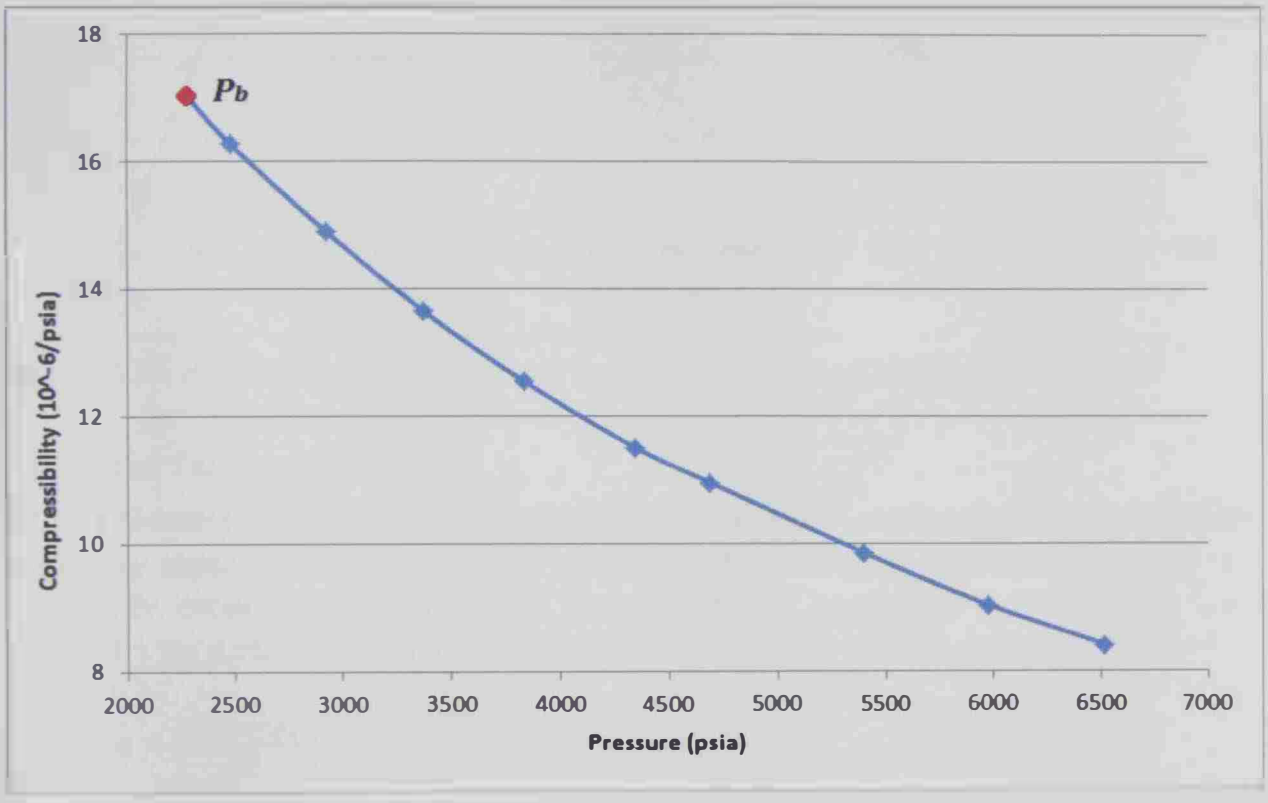

Figure B.16: Isothermal compressibility vs. pressure at 235 °F for well A#22 from the CCE test.

Bulk Density

Bulk density is defined as the mass of a bulk material divided by the volume occupied by that material. As shown in Figure B.17, the bulk density of the reservoir fluid (compressed liquid) slightly decreases as the pressure is decreased from P down to P_b. When the pressure falls below P_b down to near atmospheric pressure, the gas (and hydrocarbons) starts to be released from the liquid phase causing a substantial reduction in bulk density of the fluid.

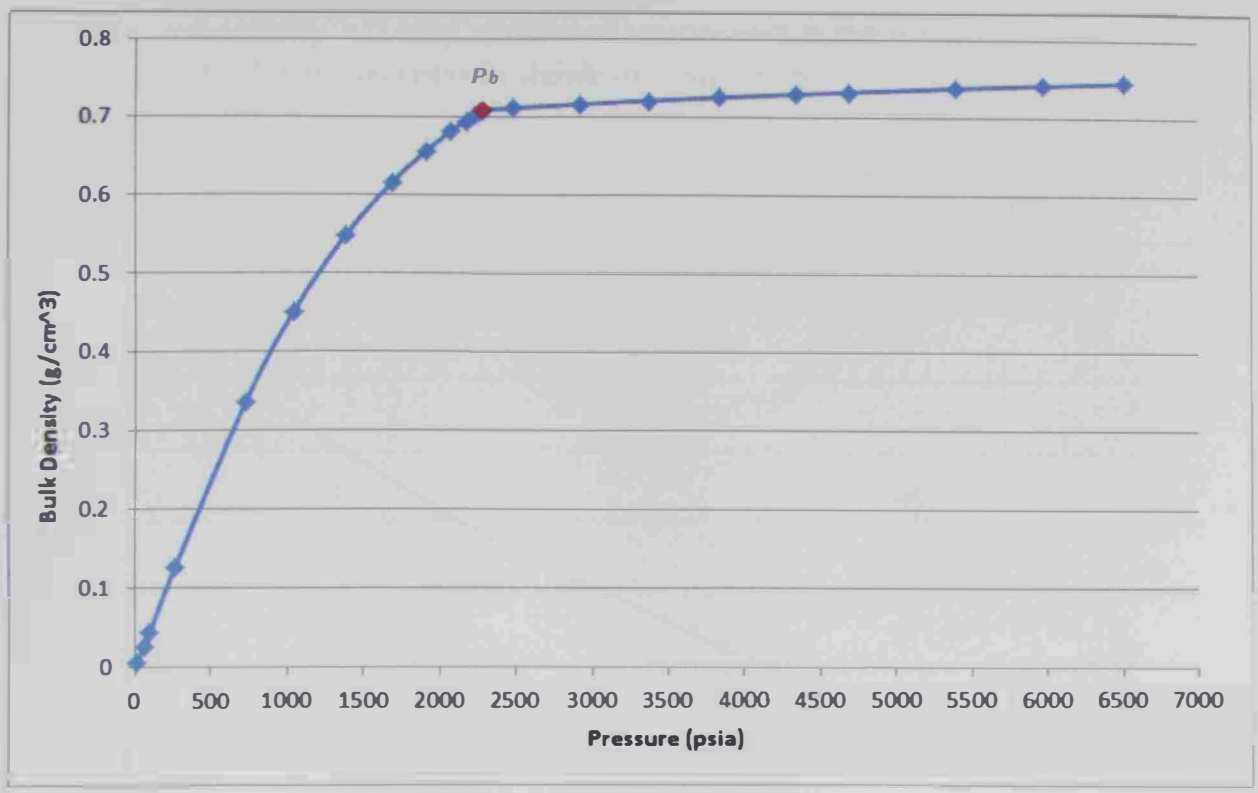

Figure B.17: Bulk Density vs. Pressure at T= 235 °F for well A#22 from the CCE test.

Interfacial Tension, (IFT):

IFT is a measure of the imbalance of molecular forces at the interface between two phases caused by physical attraction between molecules. IFT is function of density while density is directly proportional to pressure. Sugden (1924), suggested a relationship that correlates the surface tension of a pure liquid in equilibrium with its own vapor [46].

$$\sigma = \left[\frac{P_{ch}(\rho_l - \rho_v)}{M}\right]^4 \qquad \text{(B.4)}$$

where σ is the surface tension, M is molecular weight of pure component and P_{ch} is a temperature-independent parameter and is called the "Parachor". Katz et al. (1943) employed the Sugden correlation (1924) for mixtures by introducing the compositions of the two phases as follows [46]:

$$\sigma^{1/4} = \sum_{i=1}^{n} [(P_{ch})_i (Ax_i - By_i)] \qquad \text{(B.5)}$$

$$A = \frac{\rho_o}{62.4\, M_o} \quad \& \quad B = \frac{\rho_g}{62.4 M_g}$$

where ρ and M are the density and apparent molecular weight of the oil phase (o) and gas phase (g), respectively. x_i and y_i are the mole fractions of component i in the oil phase and

gas phase, respectively. n is total number of components in the system. So as the pressure is decreased, the IFT will increase as shown in Figure B.18.

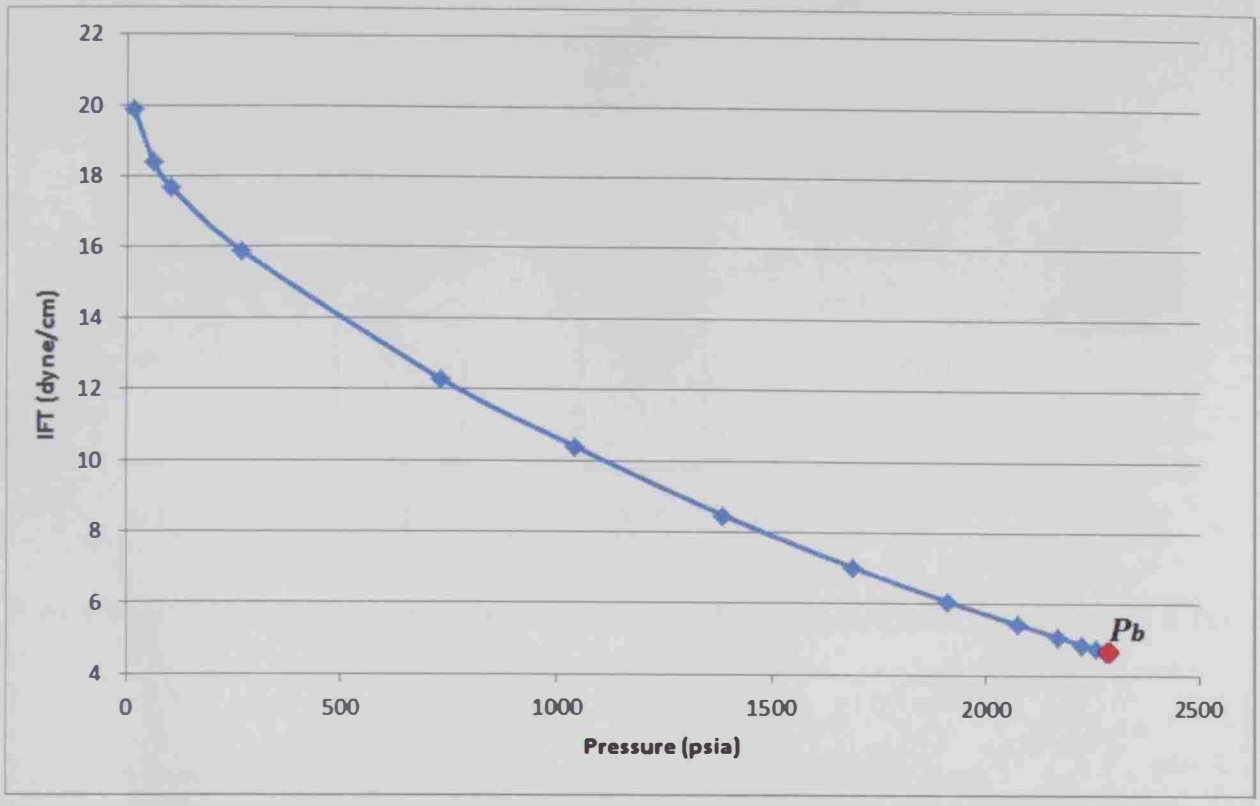

Figure B.18: IFT vs. pressure at 235 °F for well A#22 from the CCE test.

The Differential Liberation (DL) Test

The differential liberation test, schematically shown in Figure B.19, is considered better in describing the separation process taking place in the reservoir and simulating the flow behavior of hydrocarbon systems above the critical gas saturation conditions. During this test, the reservoir fluid is depleted by 6 to 16 steps from the saturation pressure to atmospheric pressure and the solution gas liberated at each step is continuously removed from contact with its equilibrium oil.

When the pressure of the cell is reduced to a value below Pb, the formed gas cap is pushed out from the cell to a gasometer. The remaining liquid is subsequently depleted down to the next pressure step. The liberated gas is analyzed by gas chromatography for molecular composition. The gas specific gravity and viscosity are calculated based on the measured composition. Tables B.5 and B.6 show the calculated properties of the gas and liquid phases of the DL test for wells A#22 and A#33, respectively as a function of pressure. These properties include liquid volume, liquid density, liquid viscosity, oil formation volume factor (FVFo), solution gas-to-oil ratio (GORS), liberated gas-to-oil ratio (GORL), gas molar mass, gas viscosity, gas Z-factor, gas formation volume factor (FVFg), gas gravity, and gas density as well as interfacial tension (IFT).

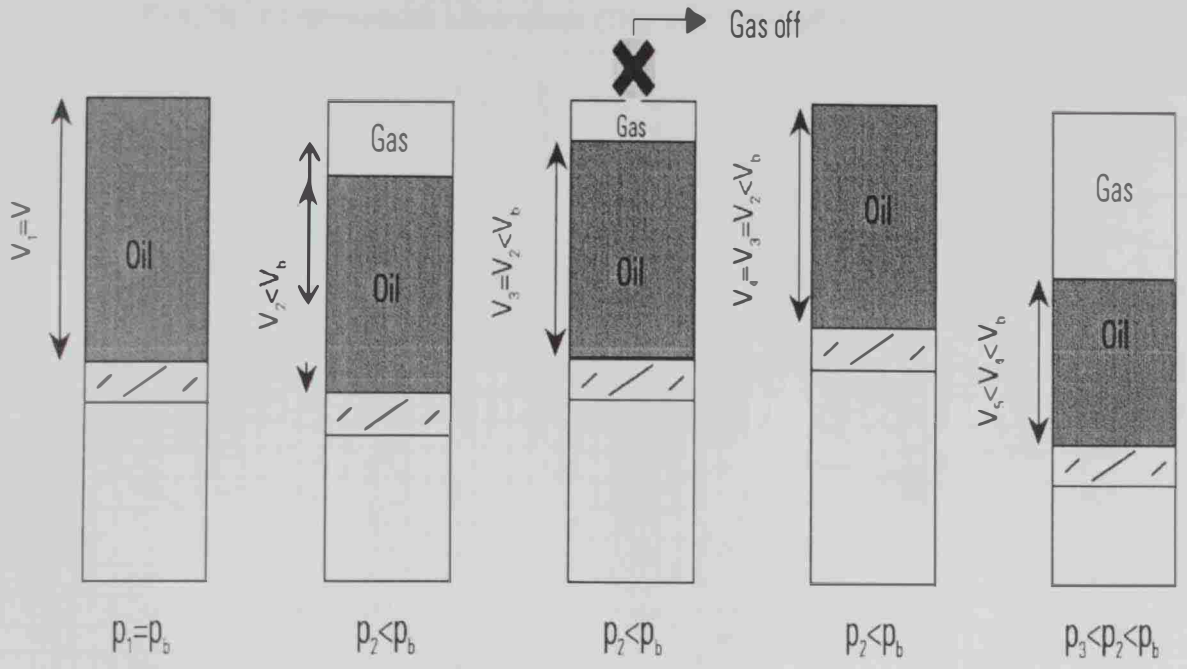

Figure B.19: Schematic diagram of the differential liberation (DL) test (Note: $V_1 = V_b$ at P_b)

Table B.5 Results of Differential Liberation (DL) test for well A#22 fluid.

Pressure	Liq. Density	Liq. Viscosity	Oil FVF	Soln. Gas GOR	Lib. Gas GOR	Gas MW	Gas Viscosity	Gas Z-Factor	Gas FVF	Gas Gravity	IFT	Liq. Vol. %	Gas Density
Psia	g/cm^3	cP	bbl/STB	ft^3/bbl	ft^3/bbl	g/mol	cP	PV/RT	bbl/mm scf	Air =1	dyne/cm	V_{liq}/V_{sat}	g/cm^3
2277.0	0.709	0.378	1.480	710.3	0.0	23.03	0.020	0.869	1341.0	0.795	4.70	100.00	0.130
1991.7	0.720	0.408	1.439	627.1	83.2	22.86	0.018	0.871	1537.8	0.789	5.75	97.22	0.112
1846.2	0.725	0.424	1.419	586.6	123.7	22.81	0.018	0.874	1663.3	0.788	6.34	95.86	0.104
1700.6	0.730	0.442	1.400	547.3	163.0	22.80	0.017	0.877	1811.9	0.787	6.97	94.55	0.095
1555.1	0.736	0.460	1.381	509.0	201.2	22.84	0.017	0.880	1989.6	0.788	7.63	93.27	0.087
1409.6	0.741	0.480	1.362	471.8	238.5	22.92	0.017	0.885	2206.0	0.791	8.33	92.02	0.079
1264.1	0.746	0.506	1.344	435.4	274.9	23.06	0.016	0.890	2473.9	0.796	9.07	90.79	0.070
1118.6	0.751	0.533	1.326	399.8	310.5	23.29	0.016	0.895	2813.6	0.804	9.84	89.59	0.063
973.1	0.757	0.549	1.309	364.7	345.5	23.61	0.015	0.901	3257.6	0.815	10.66	88.39	0.055
827.6	0.762	0.565	1.291	330.2	380.1	24.09	0.015	0.908	3860.5	0.832	11.51	87.21	0.047
682.1	0.768	0.583	1.273	295.8	414.5	24.80	0.015	0.916	4724.5	0.856	12.40	86.01	0.040
536.5	0.774	0.603	1.255	261.2	449.1	25.90	0.014	0.924	6063.5	0.894	13.35	84.78	0.032
391.0	0.780	0.627	1.236	225.3	485.0	27.75	0.014	0.933	8406.7	0.958	14.35	83.47	0.025
245.5	0.787	0.658	1.213	185.5	524.8	31.38	0.013	0.943	13553.5	1.083	15.45	81.92	0.018
100.0	0.798	0.721	1.173	126.1	584.1	41.41	0.012	0.956	33965.5	1.430	16.86	79.20	0.009
14.7	0.824	0.941	1.052	0.0	710.3	69.61	0.010	0.981	244172.5	2.403	18.79	71.05	0.002

Table B.6 Results of Differential Liberation (DL) test for well A#33 fluid

Pressure	Liq. Density	Liq. Viscosity	Oil FVF	Soln. Gas GOR	Lib. Gas GOR	Gas MW	Gas Viscosity	Gas Z-Factor	Gas FVF	Gas Gravity	IFT	Liq. Vol. %	Gas Density
Psia	g/cm^3	cP	bbl/STB	ft^3/bbl	ft^3/bbl	g/mol	cP	PV/RT	bbl/mm scf	Air = 1	dyne/cm	V_{liq}/V_{sat}	g/cm^3
2377.0	0.681	0.303	1.698	949.9	0.0	25.43	0.021	0.856	1307.1	0.878	3.38	100.00	0.147
2073.4	0.694	0.330	1.636	835.0	114.9	25.09	0.020	0.859	1504.3	0.866	4.37	96.35	0.126
1921.6	0.700	0.344	1.607	781.2	168.8	24.99	0.019	0.862	1628.1	0.863	4.92	94.65	0.116
1769.8	0.706	0.359	1.579	729.4	220.5	24.95	0.018	0.865	1774.3	0.861	5.52	93.01	0.106
1618.0	0.712	0.375	1.552	679.5	270.4	24.95	0.018	0.869	1949.6	0.861	6.15	91.43	0.097
1466.2	0.718	0.392	1.526	631.3	318.6	25.03	0.017	0.874	2162.9	0.864	6.81	89.90	0.088
1314.4	0.724	0.410	1.501	584.6	365.3	25.18	0.017	0.879	2427.1	0.869	7.52	88.42	0.078
1162.6	0.730	0.429	1.476	539.1	410.8	25.43	0.016	0.885	2762.4	0.878	8.27	86.97	0.070
1010.8	0.737	0.449	1.452	494.8	455.1	25.81	0.016	0.891	3201.0	0.891	9.06	85.55	0.061
859.0	0.743	0.471	1.428	451.2	498.7	26.39	0.016	0.898	3797.3	0.911	9.90	84.14	0.053
707.2	0.750	0.499	1.404	408.0	541.9	27.24	0.015	0.906	4653.2	0.941	10.78	82.72	0.044
555.4	0.756	0.517	1.380	364.5	585.4	28.58	0.015	0.914	5982.3	0.987	11.71	81.26	0.036
403.6	0.763	0.537	1.353	319.2	630.7	30.84	0.014	0.923	8320.7	1.065	12.72	79.69	0.028
251.8	0.772	0.564	1.320	267.9	682.0	35.28	0.013	0.932	13509.8	1.218	13.85	77.77	0.020
100.0	0.787	0.625	1.258	185.2	764.7	47.39	0.012	0.947	34873.8	1.636	15.39	74.08	0.010
14.7	0.824	0.879	1.059	0.0	949.9	78.96	0.010	0.978	254421.2	2.726	17.76	62.40	0.002

Oil Formation Volume Factor (FVF_o)

The oil formation factor is defined as

$$FVF_o = \frac{Volume\ of\ oil\ at\ P\ \&\ T_{res}}{Volume\ of\ residual\ oil\ at\ standard\ conditions} \tag{B.6}$$

FVF_o (bbl/STB) is generally greater than 1.0 at standard pressure (14.7 psia) because the reservoir temperature (T_{res}) is greater than the standard reference temperature (60 °F); oil expands with temperature increase at constant pressure. As shown in Figure B.20, FVF_o decreases with pressure decrease as a result of the decrease in the gas solubility and its release from the fluid (i.e., the volume of the oil phase decreases).

Gas-to-Oil Ratio (GOR or R_s) of Liberated Gas

The gas-to-oil ratio of the solution is defined as

$$R_s = \frac{Volume\ of\ liberted\ gas\ at\ standard\ conditions}{Volume\ of\ residual\ oil\ at\ standard\ conditions} \tag{B.7}$$

The volume of the dissolved gas in the oil decreases from an initial solution GOR, R_{si}, at the bubble point pressure P_b, to zero at atmospheric pressure as shown in Figure B.21. At pressures above P_b the gas in the solution remains constant at R_{si}.

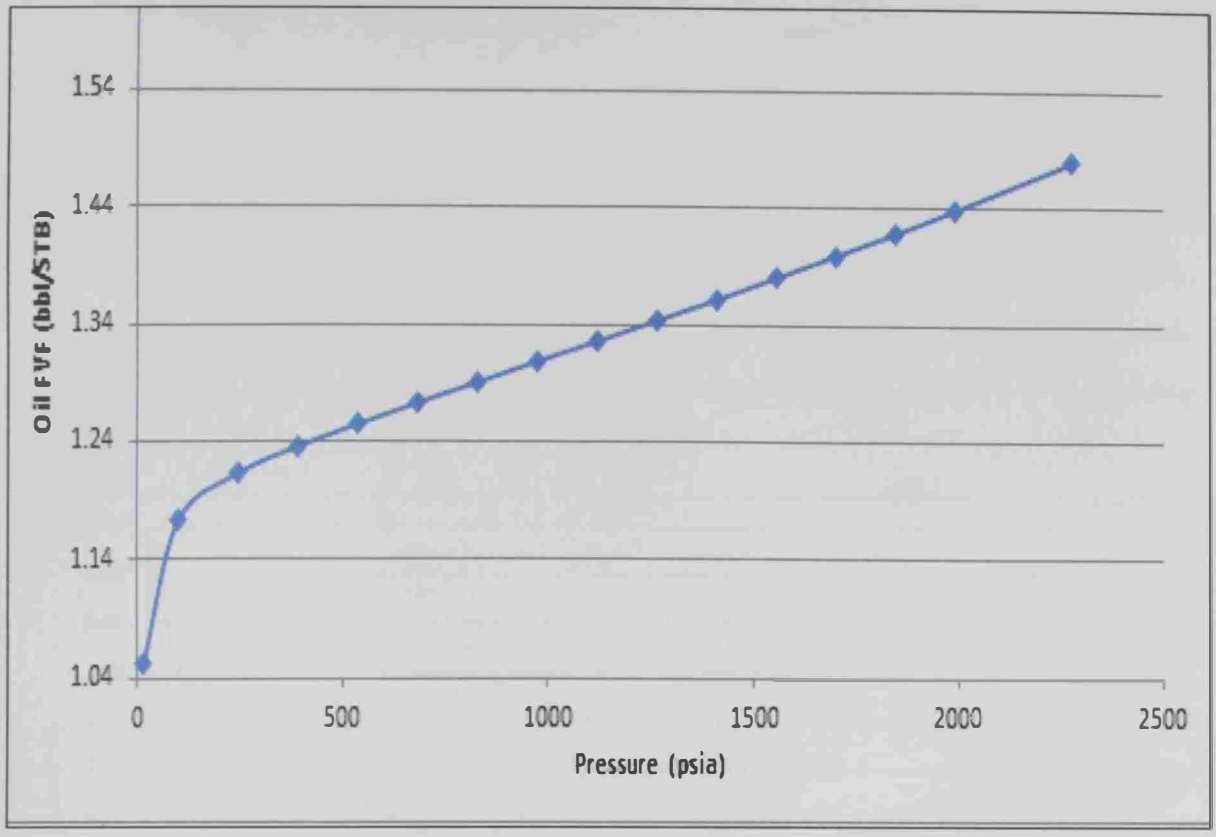

Figure B.20: Oil FVF vs. pressure at 235 °F for well A#22 from the DL test.

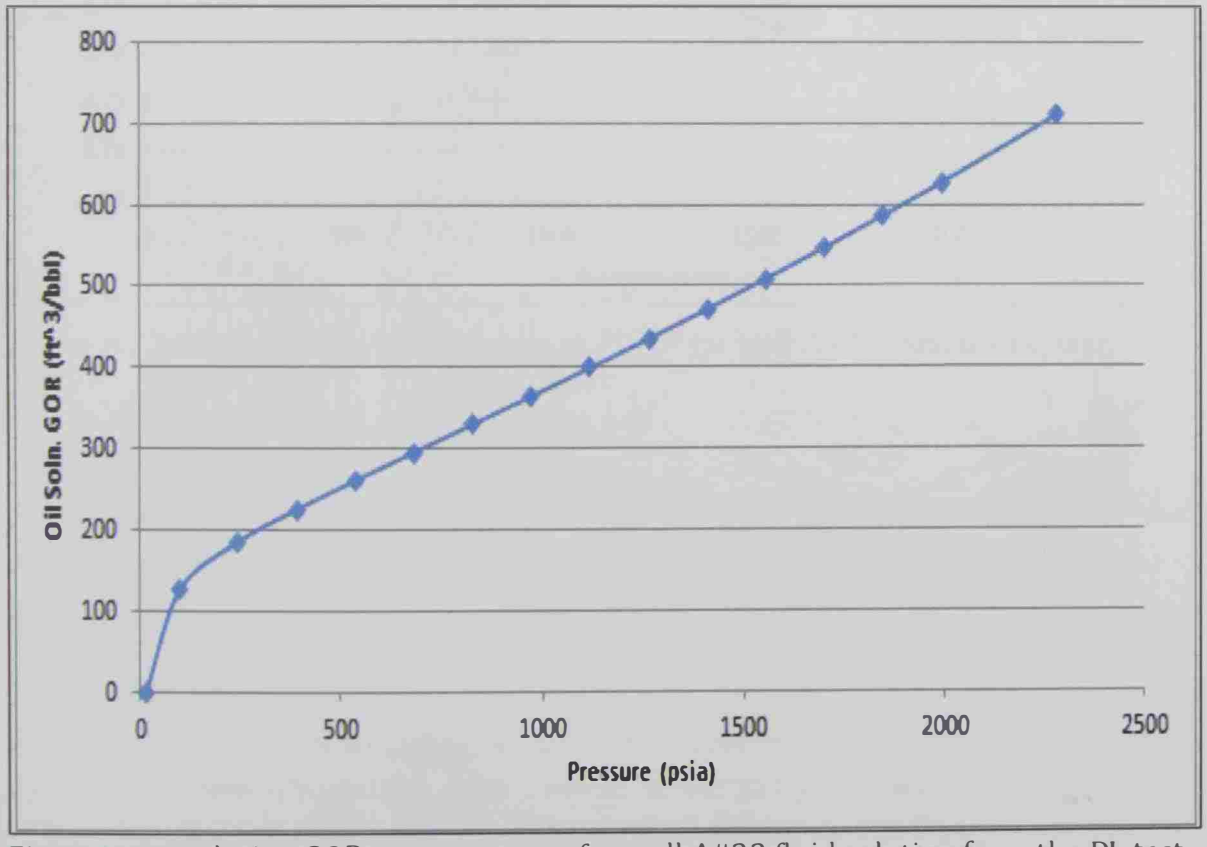

Figure B.21: Solution GOR vs. pressure at for well A#22 fluid solution from the DL test.

Liquid Density

Starting from the saturation pressure, P_b, the density increases as the pressure is decreased due to the liberation of the solution gas. This behavior is clearly noticed in the differential liberation test and is shown in Figure B.22. This kind of behavior is due to the shrinkage of the volume associated with the liberation of the solution gas with the decrease of the reservoir pressure or the swelling of the oil with re-pressurizing the reservoir fluid and re-dissolving the solution gas.

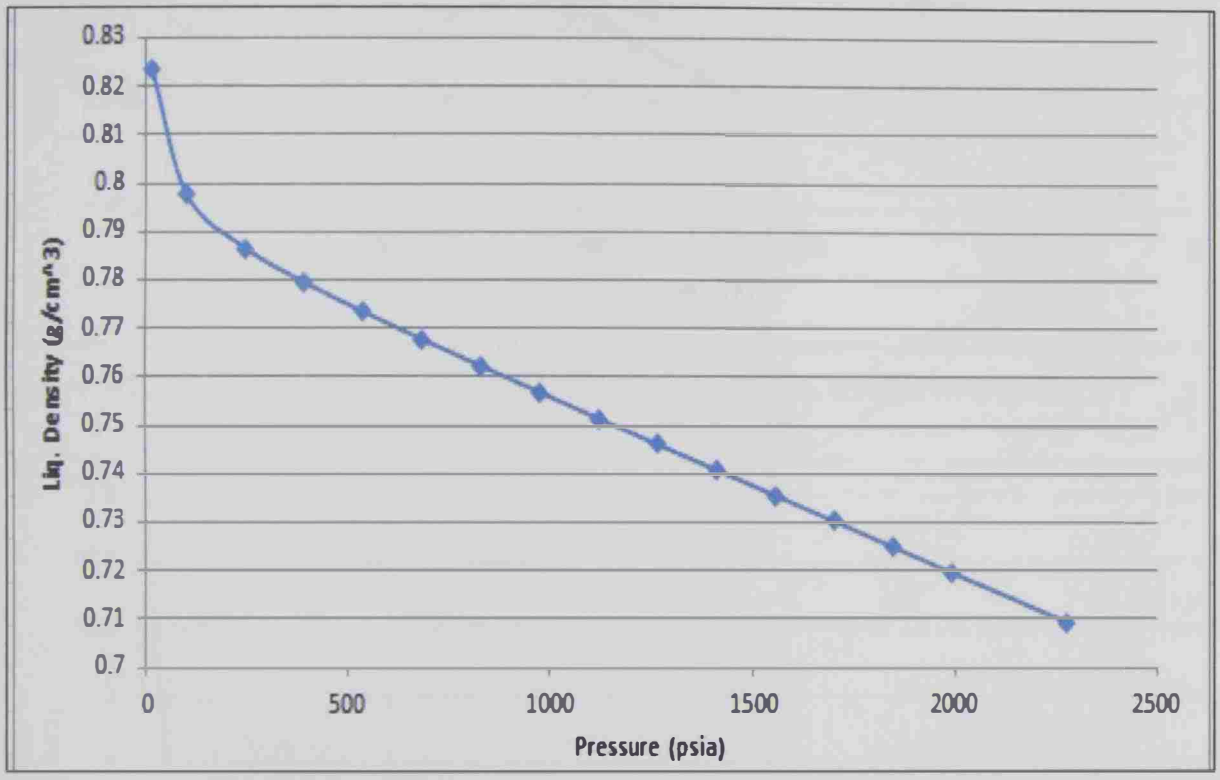

Figure B.22: Liquid density vs. pressure at 235 °F for well A#22 from the DL test.

Gas Z-Factor:

As pressure is decreased, the fluid approaches ideal gas behavior and the Z-factor reaches unity as shown in Figure B.23.

Gas Specific Gravity

As the pressure is decreased, the light gases are liberated from the reservoir fluid followed by heavier hydrocarbons thus their content in the gas phase will increase. This will be reflected in an increase in the gas specific gravity as illustrated in Figure B.24.

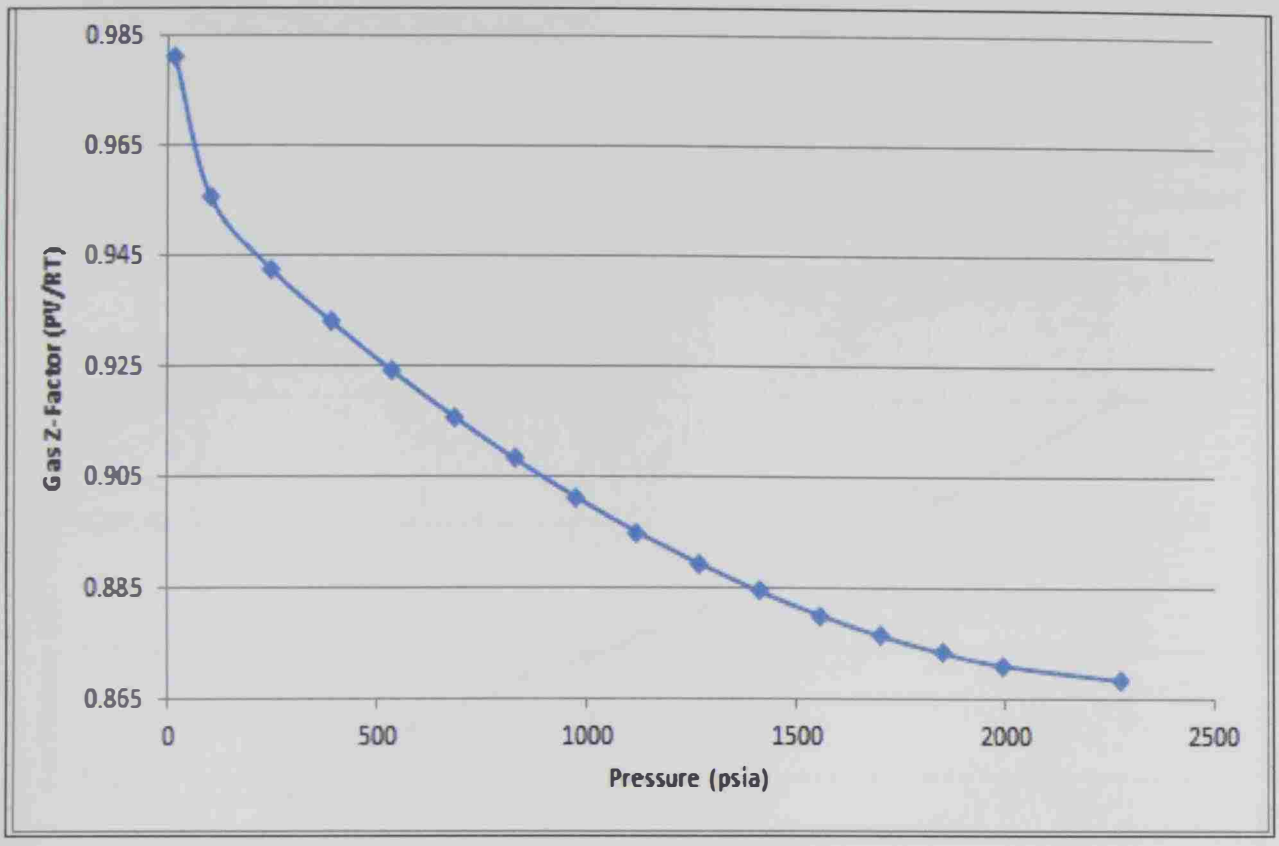

Figure B.23: Gas Z-factor vs. pressure at 235 °F from the DL test for well A#22.

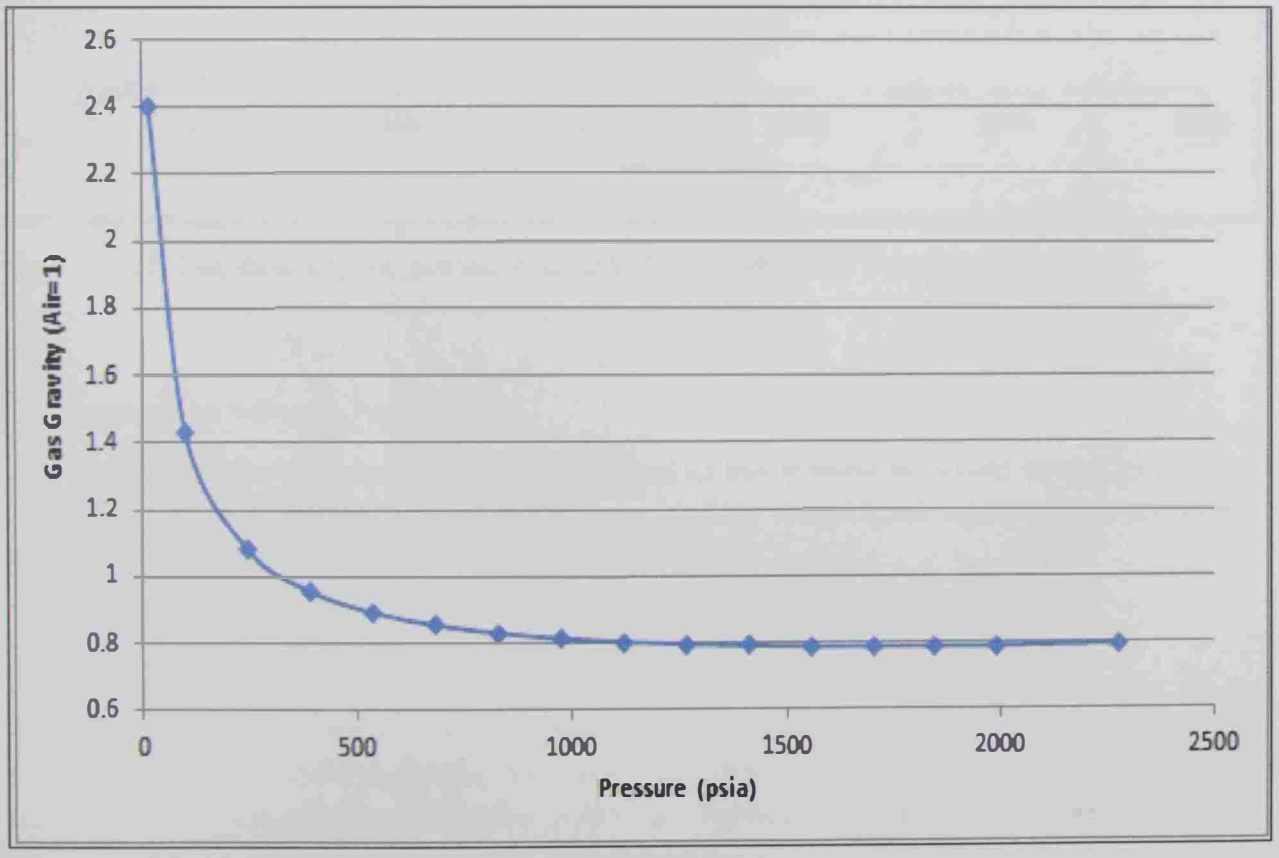

Figure B.24: Gas specific gravity vs. pressure at 235 °F for well A#22 from the DL test.

Gas Viscosity

The gas viscosity is usually calculated by correlations or by the corresponding states theory. The gas viscosity decreases as the reservoir pressure is decreased (at constant temperature); the molecules are simply farther apart and move more easily past each other at lower pressures. This effect of pressure on the gas viscosity is shown in Figure B.25.

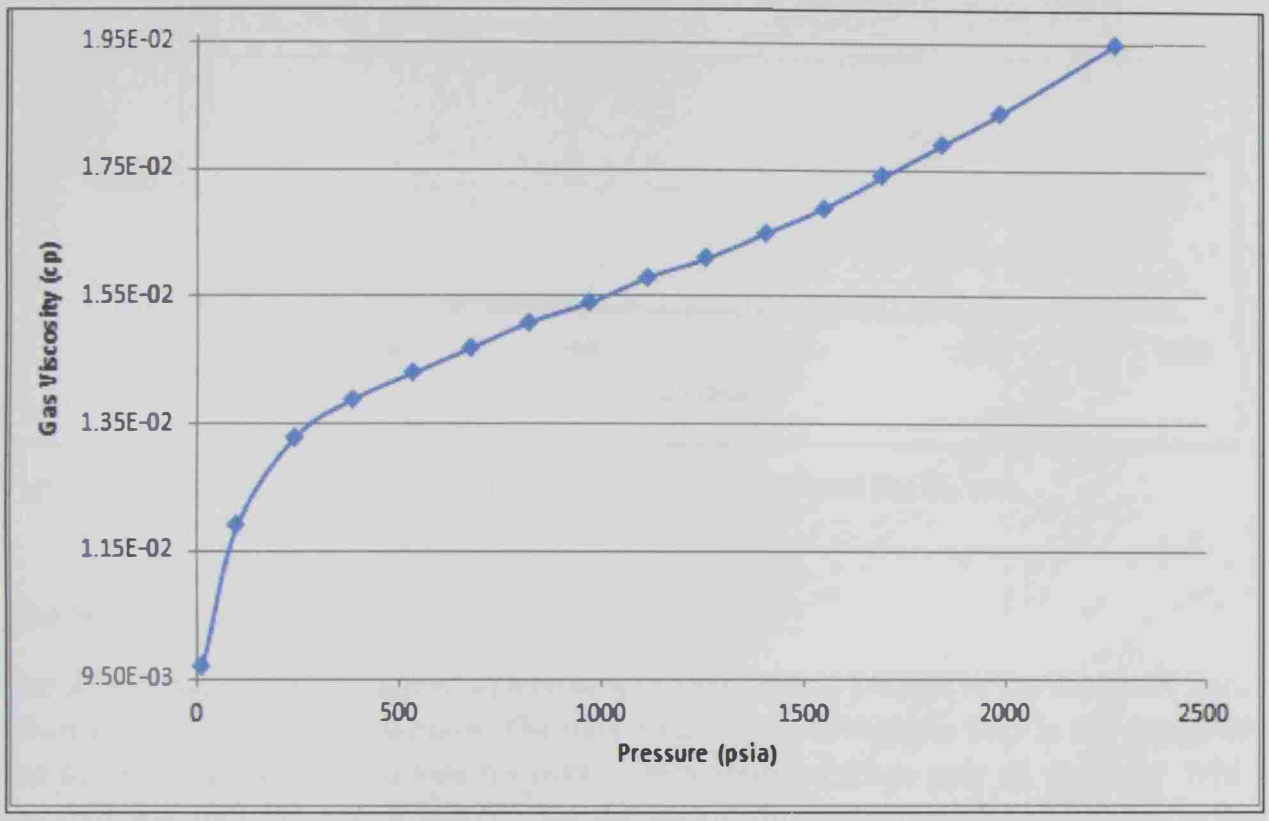

Figure B.25: Gas viscosity vs. pressure at 235 °F for well A#22 from the DL test.

Gas Formation Volume Factor (FVF_g)

The formation volume factor for a gas is defined as the volume occupied by the gas at the reservoir temperature and pressure (V_{res}) divided by the volume occupied by the same mass of gas at standard conditions (V_{st}):

$$FVF_g = \frac{V_{res}}{V_{st}} \quad \text{where } V_{res} = \frac{nZRT}{P} \tag{B.8}$$

Since the gas is compressible, as the pressure is decreased V_{res} defined in Eq. (B.6) will increase as a result of the decrease in pressure and the increase in both n and Z. Since V_{st} is constant; the result will be an increase in FVF_g as illustrated in Figure B.26.

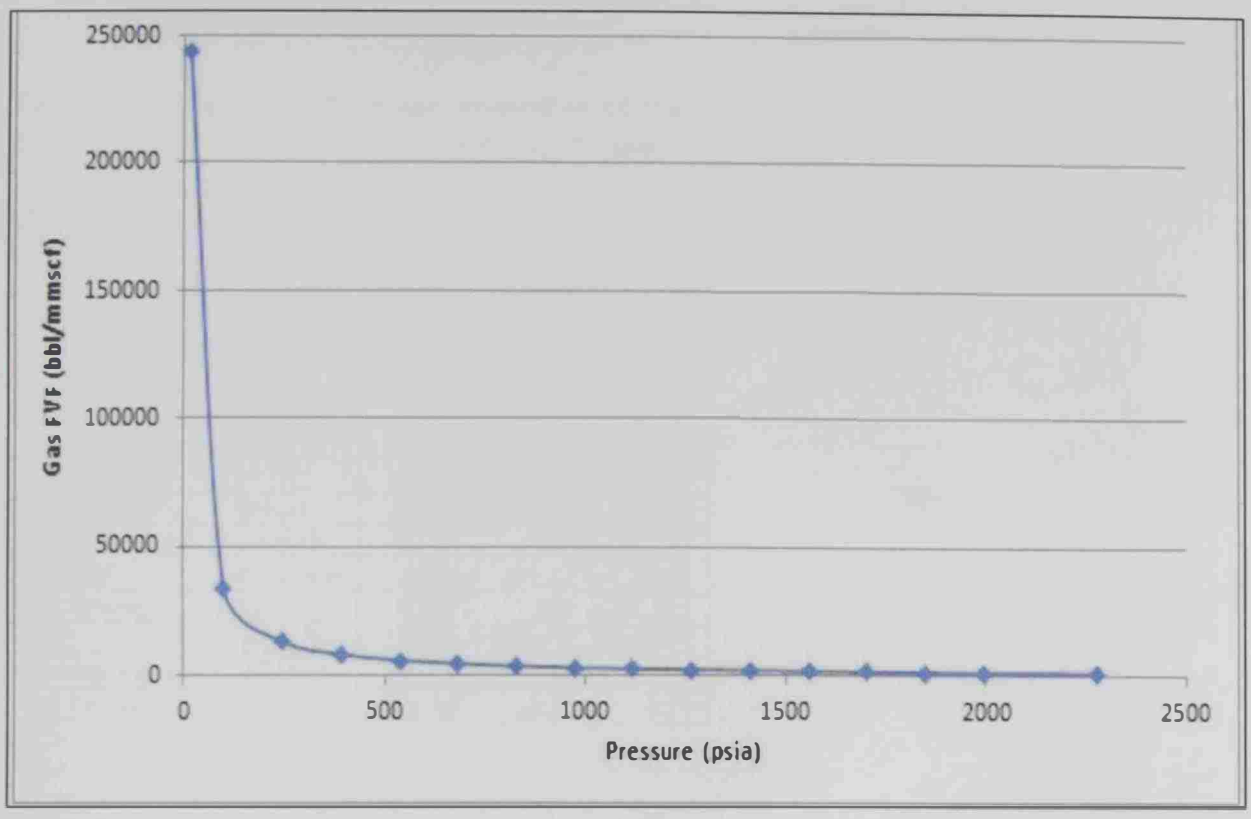

Figure B.26: Gas FVT vs. pressure at 235 °F for well A#22 from the DL test.

The Separation Test (ST)

The separation test is performed to simulate the separation process of the reservoir fluid when it is produced at the surface. The data obtained from this test help in the design of the optimal separator conditions for maximum amount of stock-tank oil recovery. With the Oilphase-DBR PVT cell, the procedure for performing the separation test is similar to that for the DL test except that the temperature in the separation test may vary from stage to stage.

A sample of the reservoir fluid measured for volume at the reservoir temperature and saturation pressure is charged into the PVT cell. Then the cell pressure and temperature are set to the first specified stage conditions, at which the sample is equilibrated. After the vapor and liquid volumes are quantified, the vapor is completely pushed out from the cell for composition and volumetric measurements. The remaining liquid in the cell is then flashed to the next specified separator conditions and the measurements and analyses are repeated till the last stage, typically at atmospheric pressure.

Tables B.7 and B.8 present the multistage separation test data and the results obtained for wells A#22 and A#33, respectively. The definitions for GOR and oil formation volume factor are the same as those mentioned in the DL test. Table B.7: Separator after-stage properties of the gas and liquid phases for well A#22.

Table B.7: Separator after-stage properties of the gas and liquid phases for well A#22 (at saturation pressure: total GOR = 494.6 scf/STB and FVF = 1.311)

Property	Units	Stage 1	Stage 2	Stage 3
Pressure	psia	265	60	14.7
Temperature	°F	100	100	60
GOR	scf/STB	400.0	71.7	22.9
Liquid Density	lb/ft³	51.0	51.8	52.6
Liquid Viscosity	cP	1.275	1.545	2.461
Oil FVF	bbl/STB	1.059	1.024	1.000
Gas Viscosity	cP	0.012	0.011	0.009
Gas Z-Factor	PV/RT	0.946	0.976	0.987
Gas FVF	ft³/scf	0.057	0.259	0.980
Separator GOR	scf/STB	377.8	70.0	22.9
Gas MW	lb/lb-mol	21.36	29.17	37.43
Gas Gravity	Air = 1	0.737	1.007	1.292
IFT	dyne/cm	18.606	20.692	22.291
Heating Value	BTU/scf	1192.9	1596.8	2064.6
Gas Density	lb/ft³	1.00	0.30	0.10

Table B.8: Separator after-stage properties of the gas and liquid phases for well A#33 (at saturation pressure: total GOR = 545.1 scf/STB and FVF = 1.364).

Property	Units	Stage 1	Stage 2	Stage 3
Pressure	psia	265	60	14.7
Temperature	°F	100	100	60
GOR	scf/STB	437.4	80.2	27.5
Liquid Density	lb/ft³	50.4	51.2	52.1
Liquid Viscosity	cP	1.157	1.402	2.199
Oil FVF	bbl/STB	1.067	1.028	1.000
Gas Viscosity	cP	0.012	0.011	0.009
Gas Z-Factor	PV/RT	0.943	0.974	0.986
Gas FVF	ft³/scf	0.057	0.259	1.000
Separator GOR	scf/STB	409.9	78.1	27.5
Gas MW	lb/lb-mol	22.17	30.74	39.54
Gas Gravity	Air = 1	0.765	1.061	1.365
IFT	dyne/cm	17.908	19.998	21.640
Heating Value	BTU/scf	1199.8	1642.9	2158.3
Gas Density	lb/ft³	1.0	0.3	0.1

Gas Heating Value

The heating value of the gas is the quantity of heat produced when the gas is burned completely; usually expressed as kJ/m³ or (BTU/scf). Although the volume of the gas increases with the decrease in pressure, the net result will be an increase in the heating value of the gas. The increase in the heating value may be due to the release of heavier hydrocarbons from the liquid phase to the gas phase. Figure B.27 shows the resultant heating value vs. pressure.

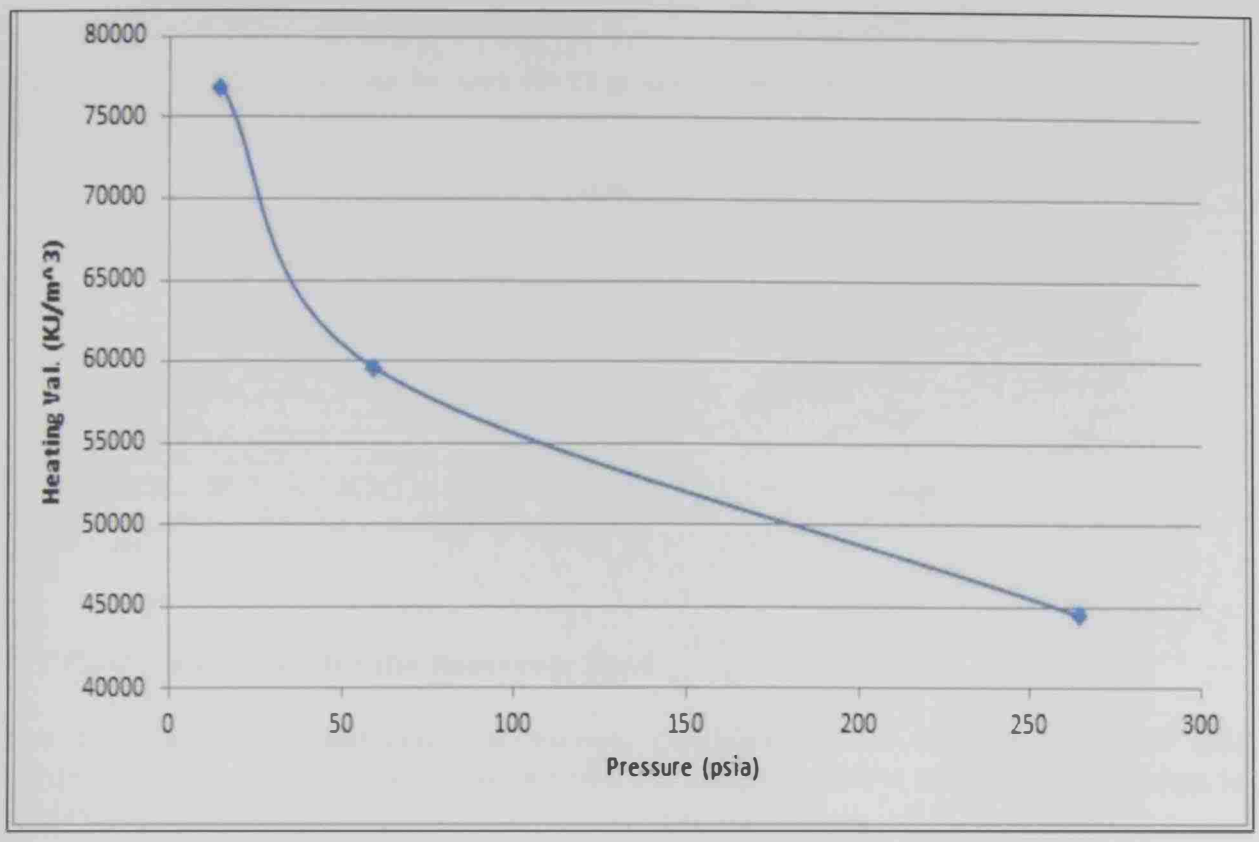

Figure B.27: Heating value vs. pressure at 235 °F for well A#22 from the separation test.

VLE Details

The fluid equilibrium properties obtained from the PVTpro simulator at the bubble point conditions were compared with the experimental data as shown in Tables B.9 and B.10 for wells A#22 and A#33, respectively. The results of the VLE are discussed in Chapter 6.

Table B.9: Fluid properties for well A#22 at saturation condition (T = 235 °F & P = 2277 psia) from VLE calculations

Property	Unit	Liquid	Vapor
Z-Factor	Z = PV/RT	0.7652	0.8685
Viscosity	cP	0.3778	0.0195
MW	lb/lb-mol	110.96	23.03
Volume	ft^3/lb-mol	2.51	2.84
Density	lb/ft^3	44.29	8.10
Volume %		100	0
Mole %		100	0
Light	$T_c \leq 88$ °F	0.3367	0.8244
Intermediate	88 °F < $T_c \leq 460$ °F	0.2351	0.1601
Heavy	$T_c > 460$ °F	0.4283	0.0155

Table B.10: Fluid properties for well A#33 at saturation condition (T = 257 °F & P = 2377 psia) from VLE calculations.

Property	Unit	Liquid	Vapor
Z-Factor	Z = PV/RT	0.7482	0.8559
Viscosity	cP	0.3033	0.021
MW	lb/lb-mol	102.93	25.43
Volume	ft^3/lb-mol	2.42	2.77
Density	kg/m^3	42.81	9.12
Volume %		100	0
Mole %		100	0
Light	$T_c \leq 88$ °F	0.346	0.7864
Intermediate	88 °F < $T_c \leq$ 460 °F	0.2638	0.1895
Heavy	$T_c >$ 460 °F	0.3903	0.0241

P-T Flash Calculation for the Reservoir Fluid

The P-T flash was performed at various combinations of constant pressure and temperature. The fluid properties obtained from PVTpro at these conditions are shown in Tables B.11 and B.12

Table B.11: Results of *P-T* flash calculation for reservoir fluid of well A#22.

P, psia	T, °F	Liquid Volume, %	Liquid Density, lb/ft^3	Liquid Viscosity, cP	Liquid Z-Factor	Vapor Volume, %	Vapor Density, lb/ft^3	Vapor Viscosity, cP	Vapor Z-Factor
4687	235	100	45.8	0.465	1.5244	-	-	-	-
3650	235	100	45.2	0.428	1.2019	-	-	-	-
2277	235	100	44.3	0.378	0.7652	-	8.1	1.95E-02	0.8685
1800	235	85.85	45.4	0.430	0.6478	14.15	6.3	1.77E-02	0.8745
700	235	39.09	48.1	0.593	0.3042	60.91	2.5	1.48E-02	0.9205
265	100	20.76	51.0	1.275	0.1396	79.24	1.0	1.19E-02	0.9456
60	100	4.03	52.2	1.744	0.0353	95.97	0.3	1.12E-02	0.9824
14.7	60	0.97	53.2	3.081	0.0096	99.03	0.071	1.02E-02	0.9938

Table B.12: Results of *P-T* flash calculation for reservoir fluid of well A#33.

P, psia	T, °F	Liquid Volume, %	Liquid Density, lb/ft^3	Liquid Viscosity, cP	Liquid Z-Factor	Vapor Volume, %	Vapor Density, lb/ft^3	Vapor Viscosity, cP	Vapor Z-Factor
2820	257	100	43.2	0.333	0.8880	-	-	-	-
2500	257	100	42.9	0.323	0.7922	-	-	-	-
2377	257	100	42.8	0.319	0.7551	-	-	-	-
1600	257	74.74	44.7	0.395	0.5685	25.26	5.9	1.76E-02	0.8728
700	257	34.95	47.1	0.531	0.2916	65.05	2.6	1.51E-02	0.9148
265	100	19.49	50.4	1.157	0.1337	80.51	1.0	1.19E-02	0.9431
60	100	3.65	51.8	1.602	0.0340	96.35	0.3	1.12E-02	0.9812
14.7	60	0.89	52.8	2.798	0.0095	99.11	0.076	1.02E-02	0.9933

The Swelling Test

CO_2 is injected in the recombined fluid (Oil from stock-tank oil and gas from first-stage separator) to investigate how much oil is going to swell by CO_2. This process helps in enhanced oil recovery in the heavy oil reservoirs. The following table B.13 was obtained from PVTpro while performing swelling test for well A#22 and A#33.

Table B.13. Results of the simulated swelling test (using PVTpro) for wells A#22 and A#33.

A#22 Fluid at 235 °F		
ω_{CO2} injected	$P_{bub,}$, psia	P_{dew}, psia
0.00	2277.0	
0.05	2410.4	
0.10	2553.6	
0.15	2708.5	
0.20	2877.9	
0.25	3065.7	
0.30	3277.9	
0.35	3522.7	
0.40	3812.0	
0.45	4160.2	
0.50	4582.5	
0.55	5094.0	
0.60	5713.8	
0.65	6572.2	
0.70	7422.1	
0.75		8666.1

A#33 Fluid at 257 °F		
ω_{CO2} injected	$P_{bub,}$, psia	P_{dew}, psia
0.00	2377.0	
0.05	2522.2	
0.10	2678.3	
0.15	2848.0	
0.20	3034.6	
0.25	3243.5	
0.30	3482.1	
0.35	3760.8	
0.40	4090.7	
0.45	4481.2	
0.50	4939.5	
0.55	5474.7	
0.60	6101.4	
0.65		6843.0
0.70		7738.3
0.75		8853.6

Nomenclature

B_{HP}	Stable bottom hole pressure
B_o	Oil formation volume factor, bbl/STB
C	Critical point
c_i	The shift parameter
K_i	Vapor-liquid equilibrium ratio
M_o	Molecular weight of the oil sample, g/g-mol
m^0	Displaced CO_2 mass, defined in swelling test
n_g	Number of moles in the gas sample
n_o	Number of moles in the oil sample
P_c	Critical pressure
P_{pr}	Pseudo-reduced pressure, dimensionless
P_r	Reduced pressure, dimensionless
P^{sat}	Saturation pressure
P_{st}	Pressure at standard condition
T_c	Critical temperature
T_{ct}	Cricondentherm temperature
T_{HP}	Stable top hole temperature
T_{pr}	Pseudo-reduced temperature, dimensionless
T_{res}	Reservoir temperature
T_r	Reduced temperature, dimensionless
T_{st}	Temperature at standard condition
T_{WH}	Stable wellhead temperature
V_c	Specific critical volume
V_i	Initial volume in swelling test, ml
V_f	Final volume in swelling test, ml
V_g	Specific volume of gas in stock tank
V_o	Specific volume of oil in stock tank
V_{gm}	Molar volume of gas in stock tank, m^3/g-mol
V_{om}	Molar volume of oil in stock tank, m^3/g-mol
V^{s0}	Displaced volume inside the syringe pump, ml
V^{c0}	Volume at backside of the piston, ml
V^0	Volume of saturated live oil, ml
V_i	Valve number *i* in the PVT Cell
V_{rel}	Relative volume
V_{sw}	Swelling volume or Swelling factor
w_{CO2}	Mass fraction of CO_2
w_{gi}	Normalized weight fraction of the gas sample in the stock tank
w_{oi}	Normalized weight fraction of the oil sample in the stock tank
x_i	Liquid mole fraction of component *i*
y_i	Vapor mole fraction of component *i*
Z	Gas compressibility factor

Greek Symbols:

B	Vapor molar ratio
Γ	Specific gravity
k_{ij}	Binary interaction parameter between components i and j
ρ_{BH}	Stable bottom hole density
ρ_o	Oil sample density
Ω	Acentric factor

Subscripts:

C	Critical
F	Final
G	Gas
i, j	Component i or j
I	Initial
O	Oil
R	Reduced
Res	Reservoir
St	Standard conditions

Abbreviations:

ARE	Absolute Relative Error
CCE	Constant Composition Expansion
CME	Constant Mass Expansion
EC	Equilibrium Cell
EOR	Enhanced Oil Recovery
FID	Flame Ionization Detector
FPE	Fluid Properties Estimation
FVF	Formation Volume Factor
GC	Gas Chromatograph
GOR	Gas-to-Oil Ratio
PR	Peng-Robinson
SAFT	Statistical Associating Fluid Theory
SRK	Soave-Redlich-Kwong
STB	Stock Tank Barrel
TCD	Thermal Conductivity Detector

الملخص باللغة العربية

تشمل نمذجة سلوك الحالة في النفط الخام استنباط عدد من خصائص الحركية الحرارية (مثل ضغط التشبع، الكثافة، اللزوجة، الموصلية الحرارية، الخ...) لأطوار البخار والسائل. هذه الخصائص هي المعايير الأساسية لحسابات انخفاض الضغط في محيط فتحات آبار النفط. الهدف من وضع نماذج سلوك الحالة هو تحديد دقة وموثوقية معادلات الحالة المطورة للتنبؤ بمختلف خصائص سلوك الموائع الأخرى تحت ظروف ضغط ودرجات حرارة مرتفعة.

في الجزء الأول من هذا العمل، تم تصميم جهاز سلوك طور جديد، ويمكن الاعتماد عليه، لقياس عملية إعادة الجمع ذات المرحلتين وكذلك سلوك الطور. وتم استخدام إعادة جمع عينة الموائع السطحية (غاز فاصل المرحلة الأولى ونفط مخزون الخزان) في هذا العمل بغية إعادة تكوين الزيت الأصلي. في البداية، يتم إدخال كمية محددة من نفط مخزون الخزان في خلية (ضغط – حجم - درجة حرارة) (PVT) ، ثم تم حقن كمية محسوبة مسبقاً من الغاز مأخوذة من فاصل المرحلة الأولى للخلية. بدأ الاختبار عند ضغط أعلى نقطة الفقاعة حتى الحصول على سائل أحادي الطور، ومن ثم خفضت stepwise حتى لوحظت الفقاعة الأولى. وكان ضغط نقطة فقاعة الملاحظ يساوي ضغط المكمن الحقل تقريبا (2277 باوند/إنش^2 للحقل أ#22 و2377 باوند/إنش^2 للحقل أ#33، الإمارات العربية المتحدة).

ولكن تبين أن تركيبة السائل المعاد تكوينه بعيد قليلاً عن تركيبة سائل المكمن المطلوبة؛ ولذلك فقد تم تعديل نسبة البخار المولي حتى تم الحصول على مائع أحادي الطور ذو تركيبة مماثلة تقريبا (ضمن الحد الأدنى من الانحراف) لتركيبة الموائع المكمنية تحت الاختبار. وكانت نسبة البخار المولي الأمثل هي 0.5183 و 0.5603 للآبار أ#22 و أ#33، على التوالي، وهي تقريبا نفس القيم التي قدمها موفر الخدمة. كما وجد في هذا العمل قيمة نسبة البخار المولي (مع الحد الأدنى من الانحراف في تركيز الميثان) عند مقارنتة بتلك في غاز ميثان مائع المكمن؛ وكان ذلك حوالي 0.42 لكل حقل.

في الجزء الثاني من هذا العمل، تم وصف تجربة معملية جديدة لقياسات المائع المعاد تكوينه وسلوك الطور في حال حقن ثاني أوكسيد الكربون CO_2. بعد عملية إعادة التكوين، تم حقن كمية دقيقة من CO_2 في الخلية PVT ومن ثم تم قياس ضغط تشبع المزيج وعامل التورم. وتم دراسة تأثير إضافة CO_2 في خصائص النفط الخام عن طريق استخدام عدة نسب مولية للنفط الخام/CO_2 في ظروف قريبة من ظروف مزيج آبار النفط. واستخدم أسلوب المبادئ الثابتة-الاصطناعية، التي تتألف من إعداد مزيج ذو تركيب شامل معروف، لمراقبة سلوك طور الموائع عن طريق تغيير ضغط الخلية PVT على درجة حرارة ثابتة. لوحظ تكون طور انتقالي مؤلف من بخار - سائل - سائل عند تركيز (كسر كتلة) CO_2 أعلى من 0.3. وقد تراوح

معامل التورم بين 1.0 إلى 1.74 لكسور كتلة CO_2 بين 0.0 و 0.6. أجريت جميع القياسات في التجارب المشار إليها أعلاه باستخدام جهاز الأشعة تحت الحمراء الذي يسمح بكشف مرحلة الانتقال بدقة (أقل من 1 بار ضغط وخطأ 3من إلى 4%).

وأخيراً، أجريت نمذجة سلوك الطور باستخدام برامج المحاكاة PVTi [1] وPVTpro [2] المتوفرة من محاكي تجاري (Schlumberger Simulators). تمت محاكاة عملية إعادة التكوين باستخدام معادلات الحالة ل: سواف - ردليك – كوانج Soave-Redlich-Kwong (SRK) و بنج - روبنسون Peng-Robinson (PR) واشتمل ذلك على استخدام معامل التداخل الثنائي وتصويبات حجم التحول. وكانت المدخلات الرئيسية لمحاكاة سلوك المرحلة هي تركيب الموائع وضغط تشبع خزان النفط ودرجة حرارته.

تم تنفيذ مهمة المحاكاة للتحليل التركيبي ومقارنة النتائج ببيانات الحقل المتوفرة. بعد الوصول إلى ضغط التشبع (نقطة الفقاعة) (نفس ضغط بيانات الحقل)، وبمقارنة نتائج معادلتي الحالة المستخدمة تم اختيار معادلة PR كونها تعطي نتائج أكثر دقة عند مقارنتها بالنتائج المعملية وبيانات الحقل. وقد وجد تطابق شبه تام مع البيانات التجريبية والحقلية لعدد من خصائص السوائل مثل معامل الانضغاط، محدد الحجم، الكثافة، اللزوجة، معامل الحجم لتشكيل النفط ، إلخ، ، فيما عدا الكثافة المولية للسائل المشبع، لذا فقد استخدمت معادلة راكيت Rackett لتقدير الكثافة المولية السائل المشبع وأعطت قيما قريبة جداً إذا ما قورنت بقيم الحقل المقابل.

واستخدمت أيضا محاكاة PVTpro لإعادة تجميع السوائل السطحية (الغاز من فاصل المرحلة الأولى و النفط من مخزون الخزان) في الظروف المكمنية. وقد وجد أن تركيب المائع المعاد تكوينه والمستنبط من PVTpro يتفق إلى حد بعيد مع تركيب حقل المكمن؛ مع خطأ مطلق يتراوح بين 0.17 في المائة و 3.11 في المائة للآبار أ#22 و أ#33، على التوالي. كما استخدمت محاكاة PVTpro لتنفيذ اختبار التضخم عن طريق حقن غاز CO_2 في المائع المعاد تكوينه (للتحقق من مقدار التضخم في النفط وإقامة العلاقة بين ضغط التشبع والكسر الجزئي لغاز CO_2 المحقون)، وكان مقدار الخطأ النسبي في ضغط التشبع المستنبط بالنسبة إلى القيم التجريبية هو 8.4 في المائة و 6.3 في المائة للحقل أ#22 و أ#33، على الترتيب.

UAEU College of Engineering

جامعة الإمارات العربية المتحدة
United Arab Emirates University

دراسة ضغط – حجم - درجة حرارة السوائل المختارة من خزان الامارات العربية المتحدة

إعداد

راشـد شـير محـمد

قسم الهندسة الكميائية و البترول

كلـية الهنـدسـة

جامعة الإمارات العربية المتحدة

رسـالة مقدمة لإستكمال متطلبات الحصول على درجة

ماجستـير العلوم في الهنـدسة البتـرولية

برنامج ماجستـير الهنـدسة البتـرولية

قسم الهنـدسـة الكميائية والبتـرول

كليـة الهنـدسـة

جامعـة الإمارات العربيـة المتـحدة

ديسمـبر 2012